TERRAIN ANALYSIS FOR LANDSLIDE HAZARD ZONATION IN TEHRI RESERVOIR RIM REGION USING GIS

Ph. D. THESIS

by
ROHAN KUMAR

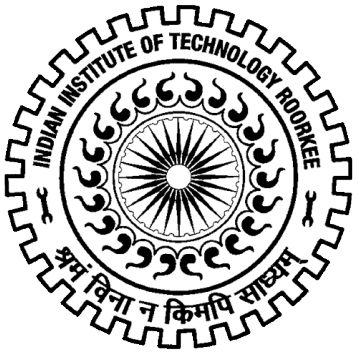

DEPARTMENT OF EARTH SCIENCES
INDIAN INSTITUTE OF TECHNOLOGY ROORKEE
ROORKEE-247 667 (INDIA)

JUNE, 2014

TERRAIN ANALYSIS FOR LANDSLIDE HAZARD ZONATION IN TEHRI RESERVOIR RIM REGION USING GIS

A THESIS

Submitted in partial fulfilment of the requirements for the award of the degree of

DOCTOR OF PHILOSOPHY

in

EARTH SCIENCES

by

ROHAN KUMAR

DEPARTMENT OF EARTH SCIENCES
INDIAN INSTITUTE OF TECHNOLOGY ROORKEE
ROORKEE-247 667 (INDIA)

JUNE, 2014

INDIAN INSTITUTE OF TECHNOLOGY ROORKEE
ROORKEE

CANDIDATE'S DECLARATION

I hereby certify that the work which is being presented in this thesis entitled **"TERRAIN ANALYSIS FOR LANDSLIDE HAZARD ZONATION IN TEHRI RESERVOIR RIM REGION USING GIS"** in partial fulfilment of the requirements for the award of the Degree of Doctor of Philosophy and submitted in the Department of Earth Sciences of the Indian Institute of Technology Roorkee, Roorkee is an authentic record of my own work carried out during the period from December, 2009 to June, 2014 under the supervision of Dr. R. Anbalagan, Professor, and Dr. V. N. Singh, Professor, Department of Earth Sciences, Indian Institute of Technology Roorkee, Roorkee.

The matter presented in the thesis has not been submitted by me for the award of any other degree of this or any other Institute.

(ROHAN KUMAR)

This is to certify that the above statement made by the candidate is correct to the best of our knowledge.

(R. ANBALAGAN)
Supervisor

(V. N. SINGH)
Supervisor

Date: June , 2014

The Ph.D. Viva-Voce Examination of **Mr. Rohan Kumar**, Research Scholar, has been held on _____.

Signature of Supervisor (s) Signature of Chairman, SRC Signature of External Examiner

Head of the Department/Chairman, ODC

ABSTRACT

The advent of frequent natural disasters necessitates a sustained management and mitigation strategy. Landslides are the most frequent disaster in the Uttarakhand Himalaya. Construction of major infrastructures such as dams, tunnels, roads and industries complicates the impact of disaster and mitigation measures. The present study area is situated around a huge reservoir (67 km), which was developed because of the construction of the Tehri dam. Landslide hazard zonation mapping around the reservoir rim area is a prerequisite for the health of the reservoir and settlements situated in the surrounding region of the reservoir.

Landslide hazard zonation mapping is practiced to facilitate the planners for mitigation strategies in the wake up of any landslide related disaster. To carry out landslide hazard zonation mapping, a number of causal parameters belonging to the geo-environment are assumed. In the present research, thirteen terrain factors namely, lithology, soil cover, land use/land cover, photo-lineament, slope, relative relief, aspect, profile curvature, topographic wetness index, stream power index, drainage buffer, road buffer and reservoir buffer are considered. Along with the terrain factors, landslide inventory map is also prepared on the basis of remote sensing data, field observations past landslide information.

Using remote sensing data, important terrain factors such as land use/land cover, drainage, photo-lineaments, slope, aspect, relative relief, profile curvature, topographic wetness index and stream power index were derived. Remote sensing imageries of varying spatial, spectral and temporal resolution were also used to generate credible data of the terrain factors. Digital elevation models of varying spatial resolution were used to extract primary and secondary topographic parameters. Data management was done in the GIS platform.

Several digital image processing techniques such as topographic correction, NDVI, supervised classification, band ratioing and edge detection were extensively used in the process of terrain factor extraction. Visual interpretation based on colour, tone, texture, shape, size, pattern and shadow were also performed on the remote sensing multispectral data for the delineation of important causative factors.

A comprehensive landslide inventory for the study area was generated using combination of the remote sensing data, field data and historical information about the landslides. Total 195 landslide incidences of dimension varying from 25 m^2 to 3000 m^2

were covered in the point vector format. Majority of the landslide incidences were found to be belonging to rotational and talus slope failure categories. Few landslides were found to be of plane failure categories observed within the region.

An attempt was made to analyse the feasibility of the causal factors considered in the present study. Landslide frequency ratio analysis and weights of evidence analysis were performed to determine the relationship between landslide incidences and the terrain factor classes. Landslide frequency ratio values were used to identify the association between the landslide incidences and terrain factors/classes. Contrast between positive weights and negative weights derived from the weights of evidence analysis was used to determine the relationship between terrain factor classes and landslide incidences.

A number of methods are available for the delineation of landslide hazard zones. Here, it is made very clear that the term 'landslide hazard zonation' was adopted according to the guidelines of the Bureau of Indian Standards (1998). These guidelines do not consider temporal factors such as rainfall, seismicity, temperature variation for landslide hazard zonation mapping. So this term best resembles with the term 'landslide susceptibility zonation' mapping. In the Uttarakhand Himalaya, several methods of landslide hazard zonation mapping belonging to heuristic, semi-quantitative and quantitative approaches have been extensively applied. But a suitable method in accordance with ground physical conditions needs a comparative study of several important landslide hazard zonation methods. Accordingly, seven different landslide hazard zonation methods were used to compute five relative landslide hazard zones namely, very low hazard, low hazard, moderate hazard, high hazard and very high hazard and validated on the basis of cumulative percentage curve/cumulative frequency diagram technique along with a bar diagram technique showing frequency of landslides in each identified hazard zone. A comparison between them was carried out to find the suitable method for the Tehri reservoir rim region.

Among the heuristic methods, a GIS based weighted overlay method and a modified BIS (LHEF) method was used. In case of GIS based weighted overlay method, weights/ratings of the factors/classes were awarded by considering landslide density in the factor classes. Landslide frequency ratio assumes landslide densities in the factor classes and hence was considered in awarding the ratings of the factor classes. A methodology was evolved to subjectively scale the landslide frequency ratio value and award the ratings to the factor classes. Arithmetic weighted overlay of factors/classes was performed to

generate landslide hazard index map, which was further classified into five relative hazard zones with an accuracy of 74 %. In case of the modified BIS approach, six inherent factor along with the external factors, seismicity and rainfall were rated according to the guidelines of BIS. Slope facets were prepared on the basis of the digital elevation model. Density of the photo-lineaments in each facet was incorporated at the place of structural discontinuity. Total estimated hazard was calculated for each slope facet and the whole area (covering 126 slope facets) was classified into five landslide hazard zones using BIS guidelines. A methodology was evolved to validate this method using cumulative percentage curve which resulted in an accuracy of 62 %.

Two semi - quantitative methods, namely, combined fuzzy logic and frequency ratio method and AHP method were used for the landslide hazard zonation mapping. In the first method, fuzzy membership was derived by incorporating normalized landslide frequency ratio value and fuzzy integration was performed by applying fuzzy OR operator and fuzzy gamma operator. Six different fuzzy gamma values were used to compute six landslide hazard index maps. Among the fuzzy OR integration and fuzzy gamma integration, fuzzy gamma (gamma = 0.95) was found to be most suitable for the landslide hazard zonation mapping with an accuracy of 78.2 %. A comprehensive analytical hierarchy process resulted in delineation of landslide hazard zones with an accuracy of 80%.

Three different landslide inventory driven methods namely, landslide frequency ratio, weights of evidence and logistic regression method was used to delineate landslide hazard zones. In the case of landslide frequency ratio method, the normalized frequency ratio values (0-1) of the terrain factors were used for the ratings of the factors. Rated factor classes were integrated in the GIS domain using fuzzy SUM overlay. Fuzzy SUM overlay can be used not only with the fuzzy membership values but also in the case of raster data having a range of 0 to 1. This method successfully resulted in delineation of landslide hazard zones with a prediction accuracy of 72%. In the case of weights of evidence method, a landslide posterior probability map was generated using weight positive (W^+), weight negative (W^-) and contrast (C) values. A total of 134 landside incidences were used for the calculation of W^+, W^-, C and other parameters. The posterior probability map was classified into five landslide hazard zones and it gave a prediction accuracy of 82%.

In the case of binary logistic regression method, correlation between factor classes and landslides were computed using binary logistic regression method and a probability

estimate of landslide occurrence on cell by cell basis for entire study area was obtained. Probability map was further classified into five landslide hazard zones using statistical class break technique. Accuracy assessment of the model was performed using cumulative frequency diagram technique along with ROC curve technique which in turn gave accuracies of 83.5% and 82.65%.

A comparison between the seven different landslide hazard zonation methods used in this study was performed on the basis of landslide density method and cumulative percentage curve method. Results of the landslide density method have indicated the consistency of the landslide hazard map produced from different models. Comparison of the prediction rate curves have reflected the different accuracy estimates calculated from the LHZ mapping method. Least accuracy was achieved in the case of heuristic models, where as peak accuracy was achieved from the multivariate logistic regression mapping method.

On the basis of comparisons between landslide hazard maps computed from different methods, it was observed that quantitative methods such as weights of evidence and binary logistic regression method are most suitable techniques for the study area. Heuristic methods also have good prediction capability for landslides and can be utilized in the study area. AHP and fuzzy logic approaches have resulted in better prediction accuracy than the heuristic methods. On the basis of this analysis, the multivariate quantitative method -binary logistic regression-has been found to be the most suitable method for landslide hazard zonation mapping in the Tehri reservoir rim region.

ACKNOWLEDGEMENTS

Apart from my efforts, the success of this study depended mainly on the encouragement and guidelines of many others. At this juncture, I would like to take an opportunity to thank all those who have directly or indirectly helped me in the completion of my research work.

First and foremost, I would like to express my profound gratitude to my supervisors, **Prof. R. Anbalagan** and **Prof. V. N. Singh** for their precious guidance and productive criticism during the tenure of my research work. Professional expertise, open discussions, endless advices and constant unflinching support rendered by **Prof. R. Anbalagan** have shaped this thesis to its present form. I'm immensely thankful to him for his patience, motivation, enthusiasm, and immense knowledge. His guidance helped me in all the time of research and writing of this thesis. To him, I remain, professionally and emotionally indebted. I could not have imagined having a better advisor and mentor for my Ph.D study.

I'm grateful to the committee members **Prof. G. J. Chakrapani, Prof. Ashish Pandey** and **Prof. Krishnamurthy** for sparing their valuable time in monitoring the work progress and providing useful tips, critical comments and precious suggestions from time to time.

Prof. A. K. Saraf (Head, Department of Earth Sciences) is gratefully acknowledged for providing me the necessary research facilities to complete this work.

I express my special gratitude to **Prof. R. P. Gupta** for his immense interest in my work, for encouragement and moral support. He is a great teacher, educator and advisor.

I'm thankful to **THDC Ltd.** (Rishikesh, Uttarakhand) for providing me accommodation and other facilities during my field work.

I would like to thank my wife, **Mugdha** for her unconditional support during my research work. I am deeply thankful to my her for her love, support, and sacrifices. Without her help and co-operation I would never have reached this mile-stone.

It's my fortune to gratefully acknowledge the support of some special individuals- **Ms. Varinder Saini, Reet Kamal Tiwari** and **Madan Mohan Rout.** This thesis is the result of their advices and support and who were always there when I really needed.

I feel lucky to be blessed by the company of wonderful friends who have shared my failures and triumphs. For help at various stages, special thanks goes to **Laxamanan, Sujata, Neethu, Gaurav** and **Bipin.**

I thank my **parents** for their faith in me and allowing me to be as ambitious as I wanted and shared their support, morally and physically.

There's another person without whose help the journey to this thesis would have been very difficult. I specially thank **Nair Ji** for being always there and helping me with all the paperwork and other formalities for completion of this thesis.

Above all, to the **Great Almighty**, the author of knowledge and wisdom, for His countless love and strength that He bestowed upon me throughout this journey.

ROHAN KUMAR

Contents

LIST OF FIGURES

LIST OF TABLES

LIST OF PUBLICATIONS

Papers publication in International Journals

1. R Anbalagan, Rohan Kumar, K Lakshmanan, Sujata Parida, S Neethu, "Remote Sensing and GIS Based Landslide Susceptibility Mapping Using Frequency Ratio and Fuzzy Logic Approach" *International Journal of Emerging Technology and Advanced Engineering*, 4(1), 2014.

2. Rohan Kumar, R Anbalagan "Landslide Susceptibility Mapping Using Analytical Hierarchy Process in Tehri Reservoir Rim Region, Uttarakhand, India' status – *status- Accepted for publication* in *Journal of Geological Society of India*

3. Rohan Kumar, R.Anbalagan, "Landslide Susceptibility Zonation In Part of Tehri Reservoir Region Using Frequency Ratio, Fuzzy Logic and GIS" Status – under review in *Journal of Earth System Sciences*

4. Rohan Kumar, R Anbalagan "Landslide Susceptibility Zonation of Tehri Reservoir Rim Region Using Binary Logistic Regression Model" Status – Under review in *Current Sciences*

5. R Anbalagan, Rohan Kumar "Landslide Hazard Zonation Mapping Using Frequency Ratio and Fuzzy Logic Approach, A Case Study of Lachung Valley, Sikkim" Status – Under review in *Geoenvironmental Disasters (at very advance stage)*

6. Rohan Kumar, R Anbalagan " Landslide Hazard Zonation mapping using a heuristic method" – Status – Manuscript preparation in advanced stage

7. Rohan Kumar, R Anbalagan " Landslide Hazard Zonation mapping using a modified Bureau of Indian Standard (BIS) approach" Status - Manuscript preparation in advance stage

Papers publication in International Conferences

1. R. Mani Murali , K. R. Divyalaxmi, Shyama Narayanan, Rohan kumar, P. Vethamony and A. Unnikrishnan "Estimation of inundation areas at Cochin, South west coast of India due to global climate change and natural disasters" AOGS 2009, Singapore, 11-15 Aug,2009

2. R. Mani Murali, Rohan Kumar, P. Vethamony "Taluka level environmental sensitivity index (ESI) and vulnerability mapping for oil spills: A pilot study from Goa state, India" In "Second International Conference on Coastal Zone Engineering and Management (Arabian Coast 2010)"., Muscat; Sultanate of Oman, November 1-3, 2010

3. Rohan Kumar "Terrain analysis using satellite imageries & Landslide Hazard Zonation (LHZ) mapping in Tehri reservoir region, Uttarakhand" International Conference on Challenges in Disaster Mitigation and Management IIT Roorkee, 15-17 February 2013

4. Rohan Kumar R. Anbalagan "Pixel based terrain analysis for landslide hazard zonation, a case study of Tehri reservoir region, Uttarakhand, India" IEEE International Geoscience and Remote Sensing Symposium, Melbourne, Australia, 21-26 July 2013

5. Rohan Kumar, R Anbalagan "Geotechnical evaluation of landslides along the pathways of Shri Mata Vaishnao Devi Shrine" The 11th International Symposium on Mitigation of Geo-disasters in Asia, Kathmandu & Pokhara, 22-28, Nepal October 2013

Papers publication in National Conferences

1. R. Mani Murali, Rohan Kumar, "Mapping of Environmental Sensitive Index (ESI) for the oil spills at Goa coast, India" Proceedings of Geomatrix 2009, IIT; Bombay; India, 27 Feb - 2 March 2009

CHAPTER 1
INTRODUCTION

Scientific research regarding processes involved, prior planning and mitigation strategies for natural hazard phenomenon have been given greater emphasis lately. This can be attributed to the fact that there is a substantial increase in the frequency of natural hazards and consequent fatalities. Fatalities due to natural hazards are often related to the human interference in natural processes leading to unsustainable environment. Some glaring examples of the same are 2011 Japan tsunami (Fritz et al. 2012) and 2013 Kedarnath floods, Uttarakhand, India (Dobhal et al. 2013). Out of different types of natural hazards such as landslides, earthquakes, tsunamis, flash floods, hurricanes, volcanoes, and typhoons, landslides are the most dominant and frequently occurring hazardous phenomenon in the mountainous region.

Disaster studies on global scale indicate that developing countries like India, China, Nepal and have suffered much destruction and fatalities due to the landslide hazard in the last decade (OFDA/CERD, 2010). Estimates suggest that out of 80% landslides related fatalities reported from the developed countries, India accounts for 8% of landslide fatalities (Kirschbaum et al. 2010; Ghosh 2011). About 15% of the geographical area of India (nearly 0.49 million km^2) including the mountain areas of Himalaya, the Meghalaya plateau and the Western Ghats are landslide prone (NDMA, 2009; Ghosh 2011; Kundu et al. 2013). The higher incidences of landslides can be related to high precipitation, seismic activity and adverse anthropogenic activities in these regions.

A number of government organisations at central and state level such as NDMA, NDRC and DMMC are engaged in disaster awareness and mitigation programmes. Policies of these organisations emanate from the perception that investment in disaster preparedness and mitigation are much more cost effective than expenditures on relief and rehabilitation (NDMA 2009). Apart from Government Authorities, a number of corporate organisation, who have interest in dams, tunnels and hydroelectricity, are also participating

in disaster preparedness and mitigation programmes. Corporate sectors like THDC, NHPC and NTPC are well known examples, who are actively engaged in such activities in the hilly regions. Inspite of efforts by various organizations, a spate of fatalities and financial losses are perennially occurring every year during monsoons.

1.1 Landslides in Himalaya

The Himalaya has a very conspicuous landscape consisting of steep slopes, high ridges/spurs, deep valleys and a complex network of streams. Terrain conditions of Himalaya combined with increasing anthropogenic activities are largely responsible for the landslide incidences (Gupta and Anbalagan 1997). Above all, the Himalaya is a young mountain, which is witnessing various geodynamic activities such as folding, faulting, shearing and earthquakes. Successive phases of orogeny have produced structurally deformed rocks, which are subjected to severe erosion by toe cutting of deeply dissecting rivers and streams. All these adverse phenomena of the Himalayan terrain contribute to the landslide susceptibility. The Himalaya is receiving high precipitation during monsoon season and most of the landslides are triggered during this period.

Most of the Indian Himalaya falls under high seismic hazard zone (Zone-IV & Zone-V, BIS 2002) owing to the high level geodynamic activities in this region (Valdiya 2001). A number of landslides were reported due to earthquakes namely, Uttarkashi earthquake (1991), Chamoli earthquake (1999) and Sikkim earthquake (2011). In last two decades, several hydro-electric projects, roads, towers, ropeways and other public utility works as well as indiscriminate mining and quarrying had further aggravated the landslide problems. Moreover, deforestation on steep slopes and excavation of agricultural terraces led to rapid acceleration in gullying, landslide incidences and soil erosion (Ives and Messerli 1989; Sarkar 1996).

The Indian Himalaya, particularly Uttarakhand and Himachal is home to a number of religious places and recreational places, which attracts thousands of tourists every year. To cater to the needs of the surging tourists, unplanned constructions like hotels, shops and other infrastructures have increased the degree of hazard. Financial prosperity among the population of hilly region has changed the traditional approach of construction and cultivation pattern, which is increasingly resulting in frequent slope instability problems.

Table 1.1 refers to the major landslide incidence and related fatalities in the Indian Himalayan region

Table 1.1: Landslide occurrences in the Himalaya in last two decades

Year	Place	Nature of Damage
August 1993	Kalimpong, West Bengal	40 people killed, heavy loss of property
January 1994	Kashmir	National Highway 1A severely damaged
June 1995	Malori Jammu	6 persons killed, NH 1A damaged
September 1995	Kullu, HP	22 persons killed and several injured about 1 km road destroyed
14 August 1998	Okhimath	69 people killed
18 August 1998	Malpa,Kali river	205 people killed road network to Mansarovar disrupted
29 march 1999	Chamoli, earthquake induced landslides	150 lives lost
August 2003	Uttarkashi	Heavy loss of infrastructures
July 2004	Joshimath - Badrinath	Heavy landslides hit Lambagarh areawashed away nearly 300 meter long road between Joshimath and Badrinath, 17 killed
03 August 2004	Landslide at Tehri dam project;	9 killed
8 August 2009	Kuity village in Pithoragarh	43 lives lost
Monsoon 2010	Entire Uttarakhand	220 lives lost
16 July 2013	Entire Uttarakhand	Thousands lives lost

(Source: Kanungo et al. 2009; Dobhal et al. 2013)

1.2 Need for Landslide Hazard Zonation

Present global scenario necessitates identification of the degree of vulnerability of natural disasters in an area. Susceptibility/hazard study of natural disasters of a region makes it easier to execute a planned infrastructure development. Present study area forms a part of rugged Lesser Himalayan terrain, where construction of Tehri dam and consequent development of a huge reservoir (67 km long) has substantially changed the nature of the terrain in the region. After the impoundment of water in the reservoir, increased incidences of landslides have been reported from the rim region (Joint Expert committee report 2011). Steep topography, unfavourable lithology, structural discontinuities in addition to nature of soil in some areas are the major reasons for the instability in the region. (Gupta and Anbalagan 1997; Kumar and Anbalagan 2013). The reservoir draw-down conditions, in addition to inherent causative factors of the terrain have been responsible for inducing many landslides in the rim area. This generally leads to reservoir side slope settlement process and subsequent flattening of the slope gradient.

The landslide hazards in general cannot be completely prevented; however, the intensity and severity of their impacts can be minimized by taking effective measures and by planning for disaster preparedness (Sarkar 1996). Hence, it is a prerequisite to characterize terrain condition of a region so as to minimize landslide related damages. A landslide hazard zonation (LHZ) map can be prepared to facilitate mitigation strategies in the wake of any future landslide hazard. It provides a prior knowledge of landslide prone zones on the basis of a set of geo-environmental factors.

1.3 Review of Literature

Varnes (1984) and Hutchinson (1995) discussed in detail about various combination of geo-environmental factors leading to landslides. According to them, most important inherent factors are bedrock geology (lithology, structure, degree of weathering), geomorphology (slope gradient, aspect, and relative relief), soil (depth, structure, permeability, and porosity), land-use/land-cover (LULC), and hydrologic conditions. Landslides are often triggered by many extrinsic causative factors such as rainfall, earthquake, blasting and drilling, cloudburst and flash-floods. Gupta and Anbalagan (1997) used a set of inherent landslide causative factors namely: lithology, structural discontinuity,

hydrogeology, slope morphometry, and LULC along with external factors like seismicity and rainfall for LHZ study in Tehri reservoir region. Identification of the landslide hazard zones are based on the assumption that landslide in the future will be more likely to occur under those conditions which led to the past and present instability (Varnes 1984; Carrara et al. 1995; Guzzetti et al. 1999; Kanungo et al. 2009). Varnes (1984) defined zonation as division of the land surface into areas and ranking these areas according to degree of actual or potential hazard from landslides or other mass movements on the slopes. On the other hand, Brabb (1984) introduced the term 'landslide susceptibility', which is the spatial probability of occurrence of landslide based on a set of geo-environmental factors. Both terminologies have been extensively used in landslide hazard study (Anbalagan 1992; Pachauri and Pant 1992; Gupta and Anbalagan 1997; Nagarajan et al. 1998; Gupta et al. 1999; Saha et al. 2002; Arora *e*t al. 2004; Anbalagan et al. 2008; Kumar and Anbalagan 2013; Lee et al. 2002; Sarkar and Kanungo 2004; Ayalew et al. 2005; Lee 2005; Akgun et al. 2008; Yilmaz 2009; Das et al. 2010; Kayastha et al. 2013).

A vast group of authors have been using the term 'landslide hazard mapping' in which they consider landslide with respect to the definition of natural hazard given by UNESCO (1984) and accordingly probability of occurrence of a landslide within a given space and time is considered. Therefore, constraints related to rainfall, earthquake and temperature variation, are incorporated as an input to predict landslide hazard (Guzzetti et al. 1999; Chung and Fabbiri 1999; Van Westen et al. 2003; Ohlmacher and Davis 2003; Chung and Fabbiri 2003; Guzetti et al. 2005; Lee and Pradhan 2007; Dahal et al. 2008; Ghosh et al. 2009). A group of authors perceived time constraint as temporal factor and hence a compromise term 'landslide susceptibility zonation'(LSZ) was introduced for the prediction of landslide probable zones (Clerici et al. 2002; Saha et al. 2005; Kanungo et al. 2006; Gupta et al. 2008; Kanungo et al. 2009a; Mathew et al. 2009; Chauhan et al. 2010). Landslide susceptibility mapping (LSM) is also practiced for the delineation of the landslide probable areas and it does not consider the temporal factor either (Gokceoglu and Aksoy 1996; Lee and Choi 2004; Ayalew et al. 2005; Yesilnacar and Topal 2005; Lee and Sambath 2006; Mathew et al. 2007; Yalcin 2008; Yilmaz 2009; Ramani et al. 2011; Kayastha et al. 2012; Kundu et al. 2013). In the present study, LSZ, LSM and LHZ are considered to convey nearly same meaning and hence are synonymous in nature. Landslide

hazard mapping is perceived differently because it considers temporal factors along with other terrain factors to identify the degree of landslide hazard of an area (Guzzetti et al. 2005; Fell et al. 2008). Also, landslide hazard zonation (LHZ) mapping is defined comprehensively in the Bureau of Indian Standards (BIS) 1998 code which assumes inherent and external causative factors to identify relative landslide hazard zones and excludes time and space constraints.

A number of methods are available to prepare LHZ maps. Several authors attempted to classify the available landslide hazard zonation technique (Guzzetti et al. 1999; Aleotti and Chowdhury 1999; Guzzetti et al. 2005; Kanungo et al. 2009a; Pardeshi et al. 2013). In general, LHZ mapping techniques can be grouped into the following three broad categories: - quantitative, semi-quantitative and qualitative methods. Qualitative methods involve geomorphologic mapping approach, heuristic approach and other subjective judgement approach (Zimmerman et al. 1986; Anbalagan 1992; Nagarajan et al. 1998; Gupta et al.1999; Saha et al. 2002). Geomorphological mapping approach is a direct mapping approach and it results in hazard zones in descriptive terms (Guzzetti et al. 1999). Geomorphological parameters associated with landslide incidents are mapped and a descriptive hazard zonation map is produced. This approach of LHZ mapping is found to be suitable for the regional analysis (van Westen et al. 2003; Guzzetti et al. 2005).

Semi-quantitative methods are based on weighing and rating based on logical tools such as AHP (Analytical hierarchy process) approach, fuzzy logic approach, combined landslide frequency ratio & fuzzy logic approach and weighted linear combination (WLC) approach (Ercanoglu and Gokceoglu 2004; Kanungo et al. 2006; Champatiray et al. 2007; Yalcin 2008; Pradhan and Lee 2009; Mondal and Maiti 2012; Kayastha et al. 2013). These approaches are also mostly found to be suitable for regional scale and medium scale LHZ mapping. These approaches are robust with all kind of terrain units such as grid-cell, unique-condition units; slope facets and other terrain units. Logical tools such as AHP or fuzzy logic are based on some kind of mathematical analogy and based on those analogy and professional experiences, weighting and ratings of terrain factors and their classes are determined. Logical analogy brings objectivity to the LHZ model.

Quantitative landslide susceptibility methods produce numerical estimates (probabilities) of the occurrence of landslide phenomena in a region (Guzzetti et al. 1999). Quantitative methods are landslide inventory driven methods, which predict landslide probability based on assumption that landslide conditioning factors and landslides are uniformally distributed in an area. Quantitative methods are further divided into bivariate and multivariate classes. Bivariate landslide susceptibility method is based on link between historical landslide data and landslide density in the terrain factors (Dai and Lee 2002; Lee and Pradhan 2007; Mathew et al. 2007; Dahal et al. 2008; Pradhan and Lee 2010; Ghosh et al. 2011; Kumar and Anbalagan 2013). It considers landslide as dependent variable whereas independent variables (factors) are considered individually for the hazard assessment. Landslide frequency ratio model, weights of evidence model, maximum likelihood approach, nominal scale approach etc., are the examples of bivariate LHZ mapping approach (Gupta and Joshi 1990; Lee and Sambath 2006; Pradhan et al. 2010; Dahal et al. 2008; Akgun et al. 2008).

Multivariate techniques are also a data driven but in this case, combined influence of factors on dependent variables are mathematically synthesized and influence of individual factors can also be acquired in numerical form (Lee 2005; Yesilnacar and Topal 2005; Lee and Pradhan 2007; Mathew et al. 2007; Pradhan and Lee 2010; Das et al. 2010; Das et al. 2012; Kundu et al. 2013). Examples of multivariate approaches are logistic regression analysis, linear regression analysis, discriminant analysis etc (Ayalew and Yamagishi 2005; Guzzetti et al. 2006). All the mentioned multivariate models are based on landslide density in each factor class and it considers landslide as a dependant variable and factor classes as independent variable. Rigorous mathematical functions are used to determine LHZ in terms of probability values on cell by cell basis. Overall quantitative methods are robust with grid-cells. Another type of quantitative method is the deterministic model, which is a site specific model. Deterministic model is based on geometric properties of slope, structural discontinuity, moisture content etc. This gives result in the form of factor of safety of a particular slope (Sharma et al. 1994; Singh et al. 2008; Anbalagan et al. 2008). It is a site specific approach which requires detailed physical analysis of the slope.

A quantum of literature is available on landslide susceptibility mapping for the Uttarakhand Himalaya. Many researchers applied different techniques of susceptibility mapping of the Uttarakhand region (Gupta and Joshi 1990; Anbalagan 1992; Pachauri and Pant 1992; Gupta et al. 1999; Saha et al. 2002; Arora et al. 2004; Kanungo et al. 2006; Champatiray et al. 2007; Mathew et al. 2007; Anbalagan et al. 2008; Das et al. 2010; Kundu et al. 2013). Some researchers found multivariate statistical method more suitable (Das et al. 2012; Kundu et al. 2013) where as others have found bivariate statistical method suitable (Saha et al. 2005). Heuristic methods such as LHEF (landslide hazard evaluation factor) based landslide hazard zonation (which is also a Bureau of Indian Standard code) and GIS based weighted overlay approach were extensively applied in the Uttarakhand Himalaya region (Anbalagan 1992; Pachauri and Pant 1992; Gupta et al. 1999; Sarkar and Kanungo 2004). But still a best suitable technique for the Uttarakhand region seems to be eluding. However, heuristic model based on empirical method had been adopted and recommended by BIS and the same is being used to cover various parts of the country in terms of LHZ.

1.4 Detailed Review of LHZ Mapping in Indian Himalaya

In the previous paragraph, glimpses of LHZ studies in Indian Himalaya by several authors are reflected. In this section, more elaborate review of LHZ study in Indian Himalaya is presented. All approaches available for LHZ mapping have been adopted by the authors in the Indian Himalaya.

1.4.1 Qualitative methods

Since early 1990s, bulk importance was given towards landslide preparedness programme in India. Initial approaches were mostly heuristic in nature. Anbalagan (1992) authored a landmark paper about LHZ mapping in mountainous region based on landslide evaluation factor rating (LHEF) approach. This work is based on a homogeneous terrain unit called slope facet as the mapping unit. The entire study area was divided into slope facets. For each slope facet, six inherent landslide causative factors namely, lithology, structural discontinuity, slope morphometry, relative relief, LULC and ground water condition were awarded maximum ratings of 2, 2, 2, 1, 2, 1 respectively (Total contribution

– 10). If more than 1 sub-categories of landslide factors are present in a facet, their fraction value with respect to the facet area were accounted. Total estimated hazard (TEHD) was calculated by adding all the ratings and a facet wise TEHD value was calculated. Further, TEHD values were categorised to generate relative hazard zones. The author proposed ratings for the each inherent causative factor and their sub-categories (classes). This is an index based approach and highly subjective in nature.

Another remarkable paper regarding the LHZ mapping based on the geological attributes was authored by Pachauri and Pant (1992). This paper was also based on homogeneous terrain unit called facet. But in this case, facet was defined according to the slope angle such as ridge top escarpment, very steep slope, steep slope, moderately steep slope, less steep slope, moderately gentle slope, gentle slope and very gentle slope. The entire study area (Part of Garhwal Himalaya) was divided into the facet categories. Total nine casual terrain parameters were chosen for the weighting and rating. Remote sensing data such as aerial photographs, and satellite images were used to delineate landslides, LULC and other important terrain factors. Terrain factors and their classes were weighted and rated on the basis of their association with the past and present landslide occurrences. GIS overlay of the factors was performed and a landslide hazard map was produced. In this paper, a method for reducing the subjectivity in weighting/rating by mathematically interpreting association of landslides with terrain factors has been proposed. Gupta and Anbalagan (1997) carried out LHZ mapping based on the LHEF rating scheme for the slope stability analysis of a part of Tehri reservoir area. An attempt was made to identify unstable slopes facets on the basis of LHEF method earlier proposed by Anbalagan (1992). Gupta et al. (1999) in their paper carried out integrated remote sensing-GIS for LHZ in a part of the Bhagirathi valley, Garhwal Himalaya. This work was intended to utilize the capabilities of remote sensing and GIS derived landslide factors along with ancillary data to delineate landslide hazard zones of the part of the Bhagirathi valley. The weights and ratings were subjectively awarded to the factors and their attributes. Factor maps were reclassified according to the ratings of their attributes and GIS based arithmetic weighted overlay was carried out. Landslide hazard index (LHI) map was produced from the overlaying which was further divided into five relative hazard zones. Apart from subjective weighting, this work was able to reflect the ability of integrated remote sensing and GIS in

depicting landslide probable zones of a part of Bhagirathi valley. A similar work was carried out in a part of the Garhwal Himalaya by Pachauri et al. (1998). Other important works of LHZ mapping in the Himalayan region were of Saha et al. (2002) and Sarkar and Kanungo (2004). Both works are more or less similar to the work of Gupta et al. (1999).

1.4.2 Semi-quantitative methods

Three noticeable semi-quantitative landslide susceptibility mapping approaches can be found in the works of Champatiray et al. (2007), Kanungo et al. (2009) and Mandal and Maiti (2013). Champatiray et al. (2007) attempted fuzzy logic technique using multi-temporal remote sensing data for landslide hazard assessment in Uttarkashi region (an active seismic zone) of Himalaya. Subjective weighting technique was adopted for the fuzzy membership characterization, whereas fuzzy-gamma operation was considered for the data integration. Based on the LHZ, authors suggested about the influence of the individual factor can be attributed to landslide incidences. Kanungo et al. (2009b) carried out fuzzy set based approach for integration of thematic maps for LSZ. This study was based on the application of remote sensing, GIS and fuzzy logic for the Darjeeling Himalaya. A cosine amplitude fuzzy similarity method was used for fuzzy membership determination and later fuzzy gamma operation using different gamma values for the factor integration. Landslide susceptibility index (LSI) maps were reclassified on the basis of statistical method proposed by Saha et al. (2005) to produce LSZ map. Mandal and Maiti (2013) used frequency ratio and AHP method to assign weights and ratings to the causative factors and their classes and produced LSZ map for the part of Darjeeling Himalaya.

1.4.3 Quantitative methods

A number of papers based on quantitative approaches such as frequency ratio, weights of evidence (WofE), logistic regression and deterministic approaches are available for the Indian Himalayan region (Anbalagan et al. 2008; Chauhan et al. 2010; Das et al. 2010; Das et al. 2012; Ghosh et al. 2009; Kundu et al. 2013; Mathew et al. 2007; Mathew et al. 2009; Sharma and Kumar 2008; Singh et al. 2008). Mathew et al. (2007) mapped LSZ in a part of Bhagirathi valley, Uttarakhand by applying quantitative modeling. WofE method was used to deduce negative and positive weights for the landslide causative factor classes. Prior probability of landslides was used to acquire posterior probability of

landslides based on evidential teams (factors/classes). Authors used remote sensing data to extract some important evidential themes and GIS for the data integration and validated the model using cumulative percentage curve technique as well as ROC curve technique. Sharma et al. (2008) also employed Bayesian probability model (also called WofE model) for the mapping of LHZ in parts of Himachal Himalaya in the GIS domain. Authors extracted positive weights (W^+) and negative weights (W^-) for the factor classes and their sum was used as ratings to map LHZ.

A quantitative approach for improving the BIS (Indian) Method of Medium-scale Landslide Susceptibility was given by Ghosh et al. (2009). WofE method was used to bring subjectivity in the factor rating scheme of the BIS approach for a part of Darjeeling Himalaya. For this, remote sensing data was used to delineate slope facets and W^+ and W^- were aquired for the factor classes on the basis of landslide inventory. A comparison of LHZ maps computed from the BIS based rating approach and adjusted BIS rating (based on WofE) approach using success rate curves was carried out. They recommended the adjustments in the BIS ratings based on WofE method. Mathew et al. (2009) attempted logistic regression model for LSZ in parts of Garhwal Himalaya. The authors subjected evidential layers and landslide inventory to logistic regression which resulted in rejection of insignificant evidences and retained best predictors and it also computed corresponding coefficients. Based on those coefficients, a landslide probability map was created and divided into relative hazard zones. Receiver operating characteristic (ROC) curves were used to analyze the validation capability of the model. A similar type of the work was carried out by Chauhan et al. (2010) in part of Chamoli region, Garhwal Himalaya and by Kundu et al. (2013) for a part of Ganeshganga watershed, Himalaya. Das et al. (2010) carried out landslide susceptibility assessment using logistic regression and its comparison with a rock mass classification system. They used the same principals of logistic regression as mentioned above along with its comparison with the deterministic model for the upper Himalayas. The authors utilized geotechnical-based slope stability probability classification (SSPC) methodology for the deterministic landslide susceptibility assessment and validated the model using ROC curve technique. Das et al. (2012) attempted Bayesian logistic model for the LSM of the road corridor of upper Himalaya. Bayesian logistic regression model is a weighted regression model which allows inclusion of prior information in the model,

which is absent in the common binary logistic regression model. Two prominent works regarding the usage of deterministic model for carrying out slope stability assessment have been carried out by Anbalagan et al. (2008) and Singh et al. (2008). Anbalagan et al. (2008) analyzed the slope instability condition of a peculiar landslide prone slope along a road corridor in northern Himalaya. They utilized circular failure charts (CFC) of Hoek and Bray for the computation of factor of safety (FOS) on the basis of the site specific geotechnical parameters. Singh et al. (2008) carried out slope stability characterization of cut slopes along a road corridor in Rudraprayag (Uttarakhand, India) using advanced 3D modeling of cut slopes on the basis of the physio-mechanical conditions, which further resulted in FOS values of the slopes.

1.5 Area of Study

1.5.1 Location and accessibility

The Tehri reservoir rim area is situated in the Lesser Himalaya of Garhwal hills having central latitude/longitude of 30° 22′ 40″ N/ 78° 28′ 50.4″ E and is located within the administrative limits of Tehri Garhwal districts of Uttarakhand (Figure 1.1). The area of study falls in the Survey of India toposheet no. 53J/7NW (1:25000) and covers about 550 sq km area. Bhagirathipuram, New Tehri, Chamba, Chham, Ghansali and Chinyalisod are on the right bank of Bhagirathi river and Khand, Madannegi, Baldogi and Hadiyari on the left bank of the river are the prominent settlements. The National Highway-94, off-taking from Rishikesh and passes through Chamba, Tehri and further extends upto Gangotri. The Dehradun-Mussoorie-Chamba road provides access to western parts of the study area. A 260.5 m high Tehri dam, which became operational in the first decade of this century, is one of the biggest dams of the world. The construction of the dam has resulted in the formation of a huge reservoir (67 km) in Bhagirathi and Bhilangana valley. Full reservoir level (FRL) is 830 m and dead storage level (DSL) is 740 m. The reservoir water fluctuates between FRL and DSL during the draw down conditions.

1.5.2 Physiography and drainage pattern

Physiographically, the study area (Figure 1.2), falling in the Lesser Himalaya is highly rugged due to high mountains, steep slopes and deep valleys. There are two major ridges in the study area namely the Pratapnagar-Banali-Gwar and Taru-Kanatal Dhar-

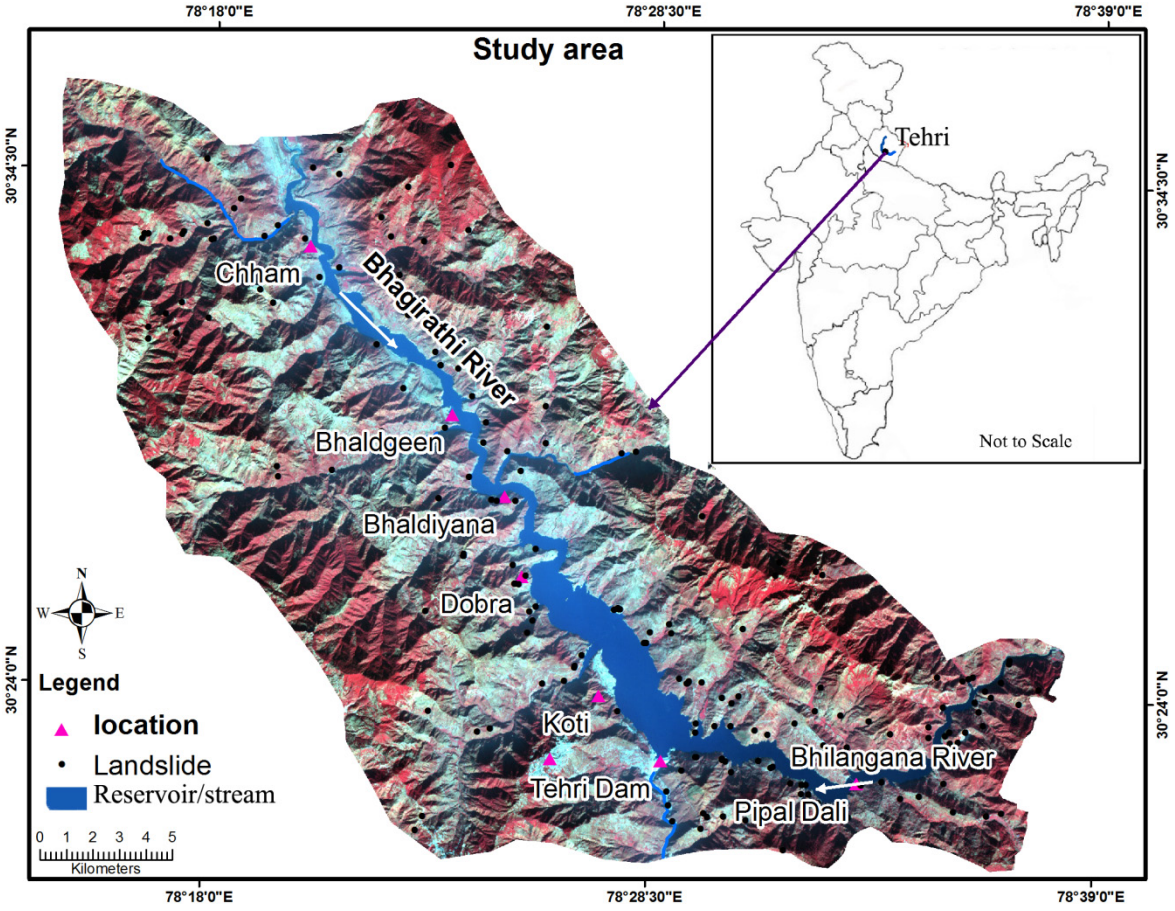

Figure 1.1 Location and landslide inventory map of the study area

Chamba ridge trending north west-south east. The study area falls in a part of Bhagirathi and Bhilangna river basins. The river Bhagirathi flows roughly in a southerly direction on the eastern part of the area. The East flowing Bhilangna river joins the Bhagirathi river at Tehri. In addition, the region is well drained by numerous streams, which are mostly first and second order in nature. Dendritic and subdendritic pattern are commonly seen in major part of the region. Subparallel pattern is also found at one or two places in the northeast and southwest region. Moreover, radial patterns are developed locally around the hill of Pratapnagar and Surkanda. A number of springs are also seen in the region and majority of them are located in the southeastern part of the study area.

1.5.3 Seismicity

The study area is a part of Garhwal Himalaya and lies within zone IV of the seismic zoning map of India, prepared by the Bureau of Indian Standards (BIS 2002). In historical

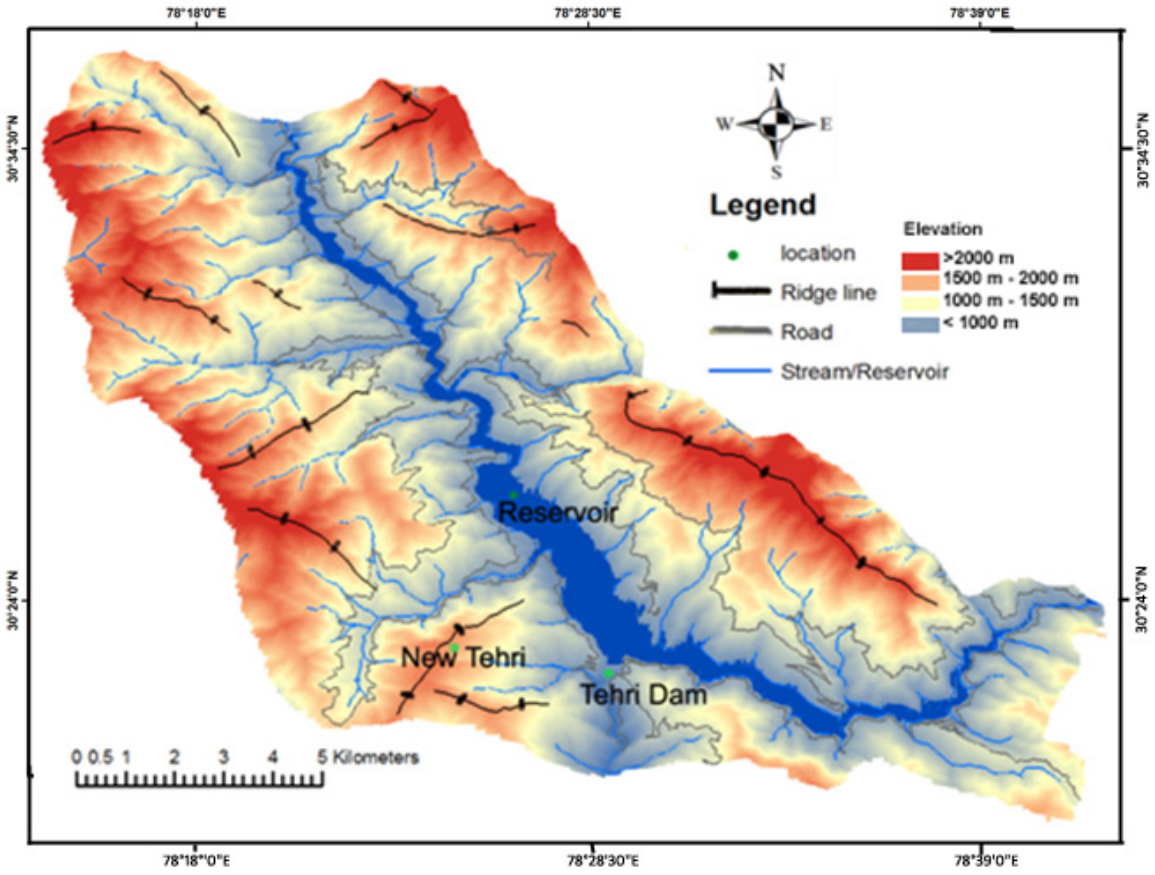

Figure 1.2 Physiographic map of the Tehri reservoir rim area

records of seismicity of Garhwal Himalaya, a violent earthquake of more than VIII occurred on September 1803 in the central portion of the Himalayan range (31.3^{o} -78.8^{o}). This earthquake was highly destructive and a large part of the population was perished in widespread landslides. In this earthquake, Badrinath temple was severely damaged and the upper portion of Kutub Minar in Delhi was also damaged. Earthquake shocks of magnitude 5 to 6 were recorded for Garhwal region in 1809, 1816, 1966, 1967, 1968, 1969, 1976, 1979 and 1986 (Thakur and Kumar 1995). The most recent event was the Uttarkashi (magnitude 6.6) earthquake, which struck the Garhwal region for 45 seconds in the early hours (02.53) of 20th October, 1991. Besides these strong events, many small magnitude earthquakes also occurred in this region.

1.5.4 Vegetation

The study area has a good forest cover in many parts. The natural vegetation follows climatic altitudinal zonation in the generally mountainous region, because of the temperature variations. The development processes such as, urbanization, road construction, hydroelectric projects and other civil structures have been largely responsible for putting additional pressure on the vegetation, wildlife and pastoral lands. In this context, Garhwal Himalaya was greatly subjected to this type of pressure, in addition to intensive cultivation, overgrazing, ruthless felling of trees, new human settlements and population influx which resulted in the reduction of forest cover of this region.

The important plants in the study area are chir pine *(Pinus roxburghii)*, Buras (*Rhododendron arboreum)*, Oak (*Quercus incana*), Kilmore (*Berberis spp.*), Dhaula (*Woodflorida fruiticosa*), Hinselu (*Rubus ellipticus)*, Deodar (*Cedrus deodara*), Pipal (*Fias religrose*), Neem (*Azardirachta indica*), Barh (*Ficus benghalensis*) etc. A variety of wild animals have been reported in this region. The important ones are tiger, panther, leopard, hyena, jackal, fox, bear, wild got, rabbit, monkey, langur and several types of birds.

1.6 Research Gaps

The review of the literature reveals that a large number of methods are being used for LHZ mapping in the Himalayan region. Some authors found multivariate statistical method more suitable (Das et al. 2012; Kundu et al. 2013) where as others found bivariate statistical method suitable (Saha et al. 2005). Heuristic methods such as LHEF (landslide hazard evaluation factor) based LHZ (which is also a Bureau of Indian Standards code) and GIS based weighted overlay approach are extensively applied in the Uttarakhand Himalayan region (Anbalagan 1992; Pachauri and Pant 1992; Gupta et al. 1999; Sarkar and Kanungo 2004). Varnes (1984) and Guzzetti et al. (1999) emphasised the use of heuristic models for the regional scale hazard zonation mapping. The highly rugged Himalayan terrain inherit steep spatial variation in lithology, structure, slope morphometry and drainage pattern. The suitability of any one of are the techniques in such terrain cannot be decided. However, literature review has reflected a few research gaps which are summarized as follows:

- A number of LHZ methods have been proposed for Himalayan terrain but least consideration was given to the feasibility of terrain factors applied in the process. No substantial work has been done for the characterization of terrain factors responsible for landslides on the basis of field observations and landslide inventory.

- None of the proposed methods of LHZ mapping in the Lesser Himalayan terrain (Indian part) has incorporated secondary topographic attributes such as Topographic Wetness Index and Stream Power Index. A study of secondary topographic features and their association with landslides was found to be lacking.

- Impoundment of huge amount of water in Tehri reservoir has itself changed the terrain conditions of the area. Understanding of reservoir induced landslide process and its impacts on the surrounding areas are also found to be a major aspect.

- A comprehensive approach for the identification of landslide hazard zones would be the identification of the best fit method, which can be carried out by applying some important method of LHZ mapping and choosing the best fit on the basis of detailed comparison. Complying with the field conditions, application of important LHZ mapping techniques and their detailed comparison for the Indian Himalayan region was also found to be lacking.

1.7 Objectives

The Tehri reservoir rim area received special attention of the researchers because of the large scale slope instability manifestation during the functioning of the Tehri reservoir. It is a major concern as it affects the existing geo-environmental conditions of the region in addition to damaging land and properties of the region. Since it's an important region where the existing geo-environment is affected by the anthropogenic activities, this area has been studied by focussing on the important parameters which may be responsible for the slope instability.

In order to achieve this main objective, high resolution satellite data was used for the delineation of terrain factors. The following are the main objectives of the study:

- Delineation of landslide hazard prone areas around the rim of reservoir.
- Identification of terrain factors responsible for landslides in Tehri reservoir region

- Detailed analysis of terrain factors selected for the study.
- Landslide hazard zonation mapping using different approaches
- Comparison and validation of different LHZ approaches and finding best-fit method acceptable for the Tehri reservoir region

1.8 Thesis Outline

Based on the data obtained, analysis and various inferences arrived related to the these, the existing work has been divided into a number of chapters and sub-chapters which are given below. Chapter 1 provides an overview of the perceived problem, in addition to indicating various approaches to tackle the problems and also a general introduction of the study. Chapter 2 provides improvement related to geological setting, data used and description of types of landslides and their mapping. Detailed discussion of terrain factors responsible for landslides and characterization of these factors on the basis of landslide frequency ratio and weights of evidence methods are presented in the chapter 3. Chapter 4 deals with LHZ mapping of Tehri reservoir rim region based on heuristic approaches namely, GIS based weighted overlay method and modified BIS approach. LHZ mapping based on semi-quantitative approaches namely, AHP approach and fuzzy logic approach is presented in chapter 5. In chapter 6, three data driven approaches namely, landslide frequency approach, weights of evidence approach and logistic regression approach of LHZ mapping for Tehri reservoir rim region is presented. A comparative study of all the methods adopted for the LHZ mapping and conclusions are presented in the chapter 7.

CHAPTER 2
GEOLOGICAL SETTING, LANDSLIDE INVENTORY AND DATA USED

2.1 Geological Setting

The crescent shaped Himalaya crowned by Mount Everest is the world's highest and youngest belt of mountains. The landscape of the Himalaya presents the snow-clad peaks, large valley glaciers, deep gorges, roaring waterfalls in addition to dense forest cover. The Himalaya is sub-divided into four longitudinal tectonic-geomorphic zones namely, the Outer Himalaya or the Shivaliks, the Lesser Himalaya or the lower Himalaya, the Higher Himalaya or the Greater Himalaya and the Tethyan Himalayan or the Tibetan Himalaya. The present area of study lies in the Lesser Himalaya of Uttarakhand. The Uttarakhand Himalaya includes eight districts namely Pithoragarh, Almora, Nainital, Pauri, Chamoli, Uttarkashi, Tehri and Dehradun. The former three districts constitute the administrative division of Kumaon and latter five of Garhwal. The Lesser Himalaya domain is demarcated by thrust such as main boundary thrust (MBT) and main central thrust (MCT). In addition, the area is characterized by multiple thrusting, repetition of rock units showing mylonitization. In north, the MCT has brought up the basement rocks comprising high grade metamorphic to soaring heights of great Himalaya, the vertical stratigraphy through being of the order of 20 km (Valdiya 1983). The MBT in the south seems to be still geodynamically active, being under thrusting of the Indian plate under the Himalaya (Valdiya 1983).

2.2. Regional Geology

Four major litho-tectonic units, each characterized by distinct lithological composition, stratigraphic succession, structural pattern and magmatic history have been recognized in the study area (Figure 2.1) by Valdiya (1980) which is being discussed below. They are:

i) Autochthonous unit of Damtha and Tejam Groups, exposed in the inner belt of the Lesser Himalaya
ii) The Krol Nappe of the outer Lesser Himalaya constituted of Jaunsar and Mussorie Groups whose equivalent n inner Lesser Himalaya being represented by Berinag Nappe
iii) The Ramgarh Nappe and its extension
iv) The Almora Nappe made up of medium grade metamorphics and intruded by syntectonic and highly deformed granitic suites

The Inner Lesser Himalaya reveals the autochthonous Precambrian sedimentary Groups. The lower Damtha Group at its best consists of the Chakrata Formation of tubidite flysch. The Formation is gradually succeeded by an assemblage of slate-quartzite of Rautgara Formation. The Rautgara included a vast proportion of intrusive of dolerites and basalts. The Damtha is conformably succeeded by Tejam Group, comprising the Deoban and Mandhali Formations. The Deoban Formation is characterized predominantly by dolomites with prolifically developed branching stromatolites. This Formation grades upwards into the pyritous-carbonaceous slates, marl and interbedded calcite, marbles of the Mandhali Formation.

The Tejam Group has been thrusted over by huge pile of quartzite and basic volcanics of the bearing Formation in the inner Lesser Himalaya. Across the Tons river in the west, the Berinag joins with the Nagthat Formation of the Jaunsar Group.

In the Outer Lesser Himalaya, the autochthonous Damtha in the north and Shivalik in the south have been thrusted over by 6000 m thick sedimentary successions forming the Krol Nappe. The litho-stratigraphic units involved in the Krol Nappe include the impersistently occuring Mandhali Formation at the base, Chandpur and the Nagthat Formations of the Jaunsar Groups; Blaini, Krol and Tal Formations of the Mussoorie Group constituting the top. The Mandhali consists of black and green phyllites, plastically deformed marble and a variety of quartzites at its base. The Chandpur is a metaflysch Formation made-up of olive green and grey phyllite and metasiltstones. The Nagthat Formations consists of quartzites with subordibnate slates and includes synsedimentary basic volcanics. The Blaini Formation begins with a persistent horizon of conglomerate intercalated with greywacks and siltstones which pass into carbonaceous slates and

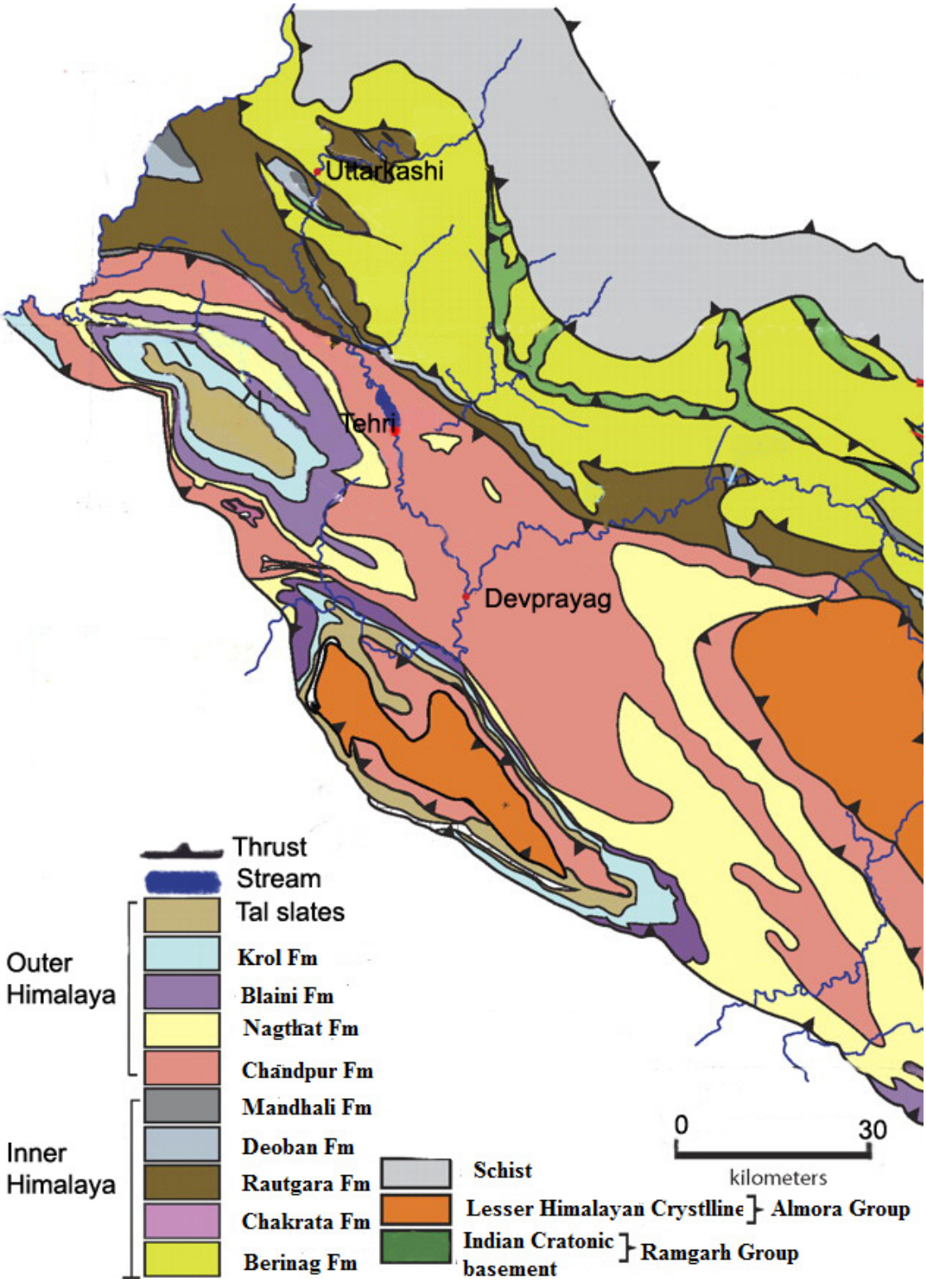

Figure 2.1 Regional geological map of the Garhwal Himalaya (After Valdiya (1980))

varicoloured limestone. The succeeding Krol Formation consists predominantly of carbonates; limestones, marls and slates in the lower parts and dolomites in the upper parts. The Tal Formation is fossiliferous at the top. The Bryozoa bearing profusely oolitic and sandy limestone, unconformably overlying the Tal Formation constitute the Singtali Formation. This Formation is covered with the veneer of slates, limestones and greywackes of Subathu Formation

The third litho-tectonic unit comprises the Ramgarh Group which is constituted of two lithological units, the Nathuakhan Formation and Debguru Porphyroid. The Nathuakhan Formation is invaded at the base by Devguru Porphyroid which is a vast and thick suit of spectacularly porphyritic granite grading into quartz-porphyry. The upper unit, Nathuakhan Formation is constituted of olive green and grey phyllites interbedded with quartzwacke.

The fourth and the uppermost litho-tectonic unit consists of a vast sheet of medium grade metamorphics intruded by syntectonic granodiorite-granite suite. This is the Almora Nappe which builds the upper part of Nag Tibba range extending from the Kali valley through Champawat and Ranikhet to Dudhatoli in Pauri-Garhwal. The basal Saryu Formation consist of phylonnites, chlorite-sericite-biotite schists, garnetiferous sericite schist and flaggy quartzites. This unit has been intruded by the Champawat Granodiorite or its equivalents such as the Almora and Dudhatoli granites. The upper unit Gumalikhet Formation is composed of carbonaceous phyllites, generally grading into graphite schists. The root of the Almora Nappe is the Munsiari Formation constituting the base of the Great Himalaya.

2.3 Geology of Tehri Area

A number of researchers carried out geological studies in the study area and its vicinity. Kumar and Dhaundiyal (1976) worked on the stratigraphy and structure of "Garhwal Synform" in the Garhwal and Tehri Garhwal regions of Uttarakhand. Saklani study in south eastern Uttarkashi between the Jajkur and Bhilangna rivers. The geology of the study area described here is mainly based on the work of Valdiya (1980).

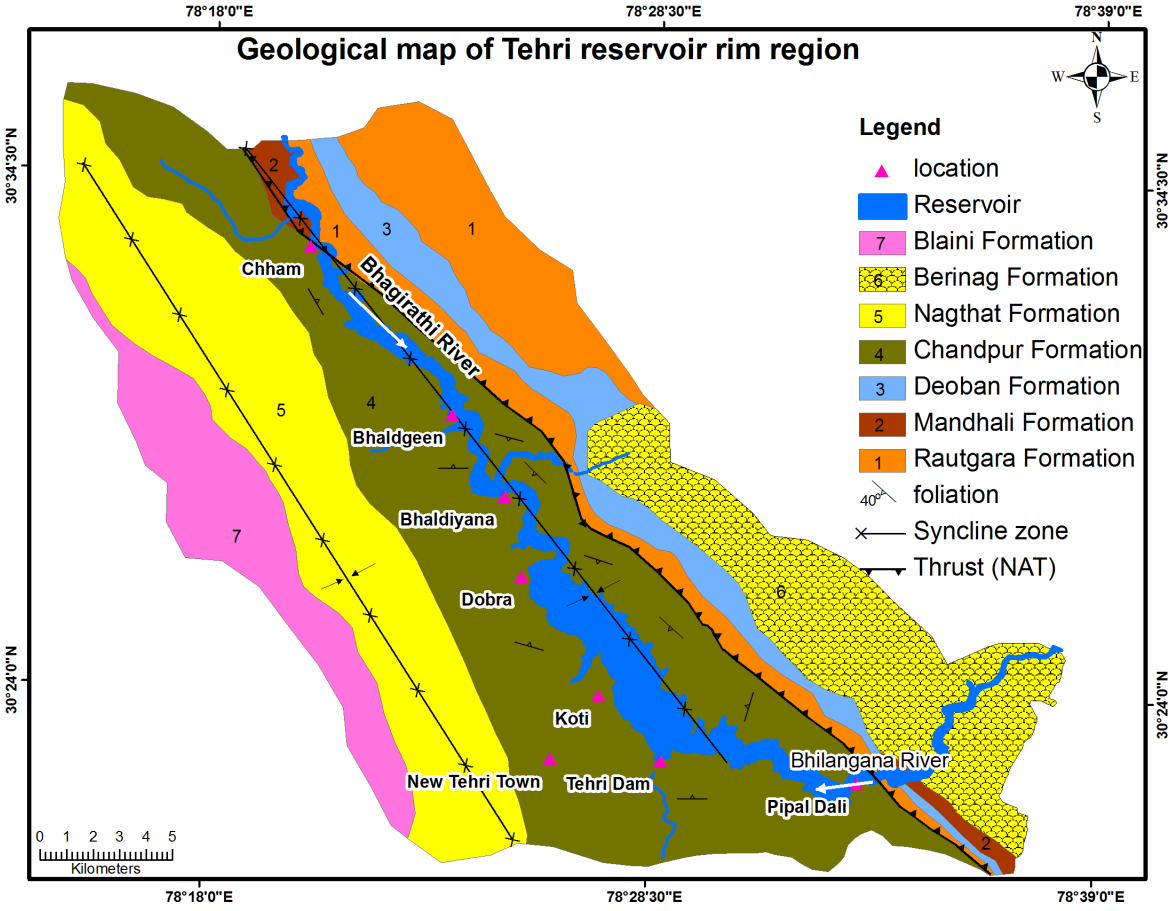

Figure 2.2 Geological map of the Tehri area

Table 2.1 Stratigraphic succession of the study area

Group	Inner Lesser Himalaya	Outer Lesser Himalaya	Age	Rock type
	Formations			
Mussoorie		Krol	Cambrian	Limestone intercalated with slates and siltstone
		Blaini	Neoproterozoic	Quartzite, limestone, slates, phyllites and conglomerate
Jaunsar	Berinag	Nagthat	Mesoproterozoic	Weathered quartzite intercalated with slate
		Chandpur	Mesoproterozoic	Low grade lustrous phyllites
Tejam	Deoban	Mandhali	Mesoproterozoic	Dolomitic limestone with phyllitic intercalations
Damtha	Rautgara		Mesoproterozoic (>1300my)	Quartzite, slate, metavolcanic rocks

The rocks exposed in the study area belonging to the inner as well as the outer Lesser Himalaya. The Inner Lesser Himalaya, in the study area is represented by the rocks of Rautgara Formation of Damtha Group, Deoban Formation of Tejam Group and Berinag Formation of Jaunsar Group. On the other hand, the rocks exposed in the outer Lesser Himalaya belong to the Chandpur and Nagthat Formation of Jaunsar Group and Blaini, Krol and Tal Formations of Mussoorie Group. The stratigraphy succession of the study area is shown in Table 2.1 and the distribution of different Formations belonging to the various Groups is shown in Figure 2.2

a) Rautgara Formation

The Rautgara Formation is exposed in two places in the north eastern region of the study area. In the extreme northeast, it is separated by Berinag thrust from the bearing Formation, while its southern contact is marked by north Almora thrust (NAT), separating it from the Chandpur Formation. The Rautgara Formation comprises purple, pink and white colour, well jointed, medium grain quartzites interbedded with medium grained, grey and dark green sublitharenites and minor slates as well as metavocalnics. Some lithounits of the Rautgara Formation show ripple marks indicating deposition under the shallow water conditions (Valdiya 1980).

b) Mandhali Formation

The Mandhali Formation is exposed in northern most and southern region of the study area and comprises mostly greyish-green and black carbonaceous pyritic phyllites, slates and interbedded blue limestone .

c) Deoban Formation

The Deoban Formation is also exposed in the north-eastern region of the study area. This is sandwiched between the Rautgara and Blaini Formations having a thrusted contact (Berinag thrust) with the Berinag Formation. The Deoban Formation occupies topographically higher ridges and consists of dense, fine grained dolomitic limestone which is white, light pink and blue-grey in colour with minor phyllitic intercalations.

d) Chandpur Formation

The Chandpur Formation is delimited towards north by a well defined thrust called NAT trending roughly north west - south east and dipping south west. The rocks of the Chandpur Formation are low grade metamorphose lustrous and shiny phyllites. These phyllites are olive green and grey in colour interbedded and finely interbanded with metasiltstone and fine grained wackes. The Chandpur Formation occupies the valley all along the Bhagirathi river.

e) Nagthat Formation

The Nagthat Formation is exposed roughly at the central and western regions of the study area. The north end of this Formation is restricted by the Chandpur Formation. As a result of folding, the same Formation once again appears in the western region bounded by Blaini Formation. The same Formation exposed in the western region is restricted by the Blaini Formation of its north and south ends. The rocks of the Nagthat Formation is characterized by white, purple and green coloured quartzites with subordinate intercalations of grey and olive green slates with siltstones.

f) Berinag Formation

The rocks of the Berinag Formation are exposed in the north-eastern part of the study area (Figure 2.2). The Berinag Formation is separated by the Berinag thrust at its base. The Berinag Formation consist of white, purple and green coloured quartzites.

g) Blaini Formation

The rocks of the Blaini Formation are also exposed in the study area. The Formation consists of quartzites, limestones, slates, phyllites and conglomerates with subrounded to well rounded clasts (cobbled to pebble size).

2.4 Structure

Major as well as minor structures have been observed in the area of study. The major structural features include the NAT, exposed in the north-eastern region. The south-easterly dipping NAT separates the Chandpur phyllites from the Rautgara Formation towards north (Figure 2.2). A number of antiforms and synforms in the central and south-western regions, which together form a part of the Mussoorie syncline (Valdiya 1980) have

been observed. A number of shear zone of varying shape and size were observed during field work.

2.5 Landslide Inventory of the Tehri Reservoir Rim Region

A total of 195 landslide locations (varying more or less between 25 m^2 to 3000 m^2) were mapped through field observations, image interpretation and historical information. Out of these, substantial number of landslides were found to be related to reservoir drawdown phenomenon, which makes a typical actuate shaped scar (Figure 2.3a). These kinds of landslides were found to be occurring predominantly in talus slopes, (which are in contact with reservoir. In addition, terraces occupied by debris or river borne materials (RBM) are also affected causing a series of landslides (Figure 2.3b).

Progressive nature of these landslides has become major threat to the population settled at upper reaches of slopes (Figure 2.3b-d). Sizable number of landslides was observed all along the road networks present in the area. Roads are present all along the reservoir rim boundary but some section of road sunk into reservoir. Roads were made by cutting the slope faces and were left untreated after construction. During monsoon season, these cut slopes fail and disrupts logistic operations and sometimes they cause fatalities. They were found to be occurring in rocks as well as debris (Figure 2.3e-f). Most part of the reservoir rim area is represented by weathered phyllites and quartzite. Typical plane failures were observed in those rocks (Figure 2.3h).

Another group of landslides were observed associated with photo-lineaments such as faults, thrusts, joints, ridges and spars (Figure 2.3g). Photo-lineaments are type of linear discontinuities observed in imageries (Gupta et al. 1999; Saha et al. 2002). The area is represented by a complex network of streams, which are deeply dissecting and are major cause of landslides. It affects terrain made up of rocks and overburdens. During rainy season, when stream (owing to steep gradients) flows are at peak, they erode its banks rapidly. Irrespective of slope materials, eroded section of the river bank becomes a site of progressive landslide (Figure 2.3i). Apart from these, a number of landslides were observed at less vegetated places, settlement areas and barren lands.

In general, the landslide in the Tehri reservoir rim region belongs to three categories namely, rotational failure, plane failure and talus failure. More than 80% of the landslides are rotational failures and are observed along the reservoir boundary, road networks and ridges/cliffs. Talus slope failure are also prominent landslide in this region, and are mostly observed along the reservoir boundary. Talus failures are shallow failures affecting debris materials lying above the rock surface. They generally affect debris of thickness less than 5 m and slide down along the slope direction deforming the rock surface. Plane failure are mostly observed in the phyllitic rocks and it occurs along the foliation and joint planes.


b


c


d


e

f

g

Figure 2.3. Field photographs a) Typical arcuate shape scar of the reservoir induced landslide, b) settlement at risk due to the reservoir induced failures, c) talus slope failure advancing to the upper reaches, d) talus slope failures along the side slopes of the reservoir, e) rotational failure along the road network, f) rotational failure in debris along the road g) a natural slope failure at the ridge, h) slope form of phyllite is subjected to plain failure, i) drainage induced landslide.

2.6 Data Used

Remote sensing data from several satellite sensors was used in this study. Different remote sensing data used in this study is listed in Table 2.2. Furthermore, ancillary data in the form of SOI (Survey of India) Toposheets, geological map, soil map and field data has also been used during processing and interpretations and listed along with the remote sensing data in Table 2.2.

2.6.1 ASTER multispectral data

ASTER multispectral images have coarse to moderate resolution in three different bandwidth: VNIR, SWIR and TIR belonging to different spectral ranges. Out of the three bandwidths, VNIR bandwidth was used for the study which has green (B1), red (B2), and NIR (3N & 3B) bands with a spatial resolution of 15 m. NIR bands 3N and 3B are used for stereo viewing and DEM generation. Two scenes of ASTER images were acquired from NASA free data privilege programmed. One of the scene was of October 2003 and other

Table 2.2: List of datasets used in this study

Data Type	Sensor	Resolution/Scale	Data Derivative
Multispectral Data	ASTER Landsat series IRS - LISS III World view - 2	15 m 30 m 23.5 m 0.5 m	LULC Photo-lineament Landslide inventory
DEM	Cartosat 1 DEM ASTER GDEM	2.5 m 30 m	Slope Aspect Relative Relief Curvature TWI SPI Drainage
Ancillary Data	Published geology map	1:250000	Digitized Geology map
	Published report on soils of Uttarakhand	1:250000	Digitized Soil map
	Survey of India Toposheet 53 J/7 NW	1:25000	Digitized base map

was of November 2007. These data were used for LULC generation, photo-lineament mapping and landslide inventory mapping (Figure 2.4b, 2.5b).

2.6.2 Landsat series data

Ten scenes (1999 to 2013, Table 2.4) of Landsat belonging to thematic mapper (TM) sensor of Landsat -5, enhanced thematic mapper plus (ETM+) sensor of Landsat -7 and Operational Land Imager (OLI) sensor of Landsat -8 were acquired from the USGS website which comes under free data privilege program. TM sensor has a spatial resolution of 30 m for seven different bands: B1 (blue), B2 (green), B3 (red), B4 (near infrared), B5 (shortwave infrared), B6 (thermal infrared) and B7 (reflective infrared). Out of these bands B1, B2, B3, B4, B5 were used to prepare false colour composites (FCC) which were further used in the study. ETM+ sensor have 8 bands of which seven are consistent with the TM and 8th band is a panchromatic band of 15 m spatial resolution. FCC images were papered using the same combination as of TM, along with that panchromatic band was also taken into consideration. OLI sensor has 9 bands out of which 7 bands are consistent with TM and ETM+ in addition to two new spectral bands, a deep blue coastal / aerosol band and a shortwave-infrared cirrus band. FCCs were prepared using B1, B2, B3, B4, B5 and B9 bands. Landsat series data were used for the landslide inventory mapping, vegetation cover mapping and the Tehri reservoir boundary mapping.

2.6.3 IRS LISS III data

The Linear Imaging Self Scanning Sensor (LISS-III) is a multi-spectral sensor operating in four spectral bands (B1 to B4), three in the visible and near infrared and one in the SWIR region. One scene of November 2005 was acquired from the Bhuvan free data resource and FCC was prepared using B1, B2 and B3 bands.

2.6.4 Worldview -2 data

Worldview-2 image is high-spatial resolution data having eight multispectral bands (2.5 m spatial resolution) and a panchromatic band (0.5 m spatial resolution). One scene of March 2010 which covers 40% of the study area was procured (Source -DigitalGlobe 8-

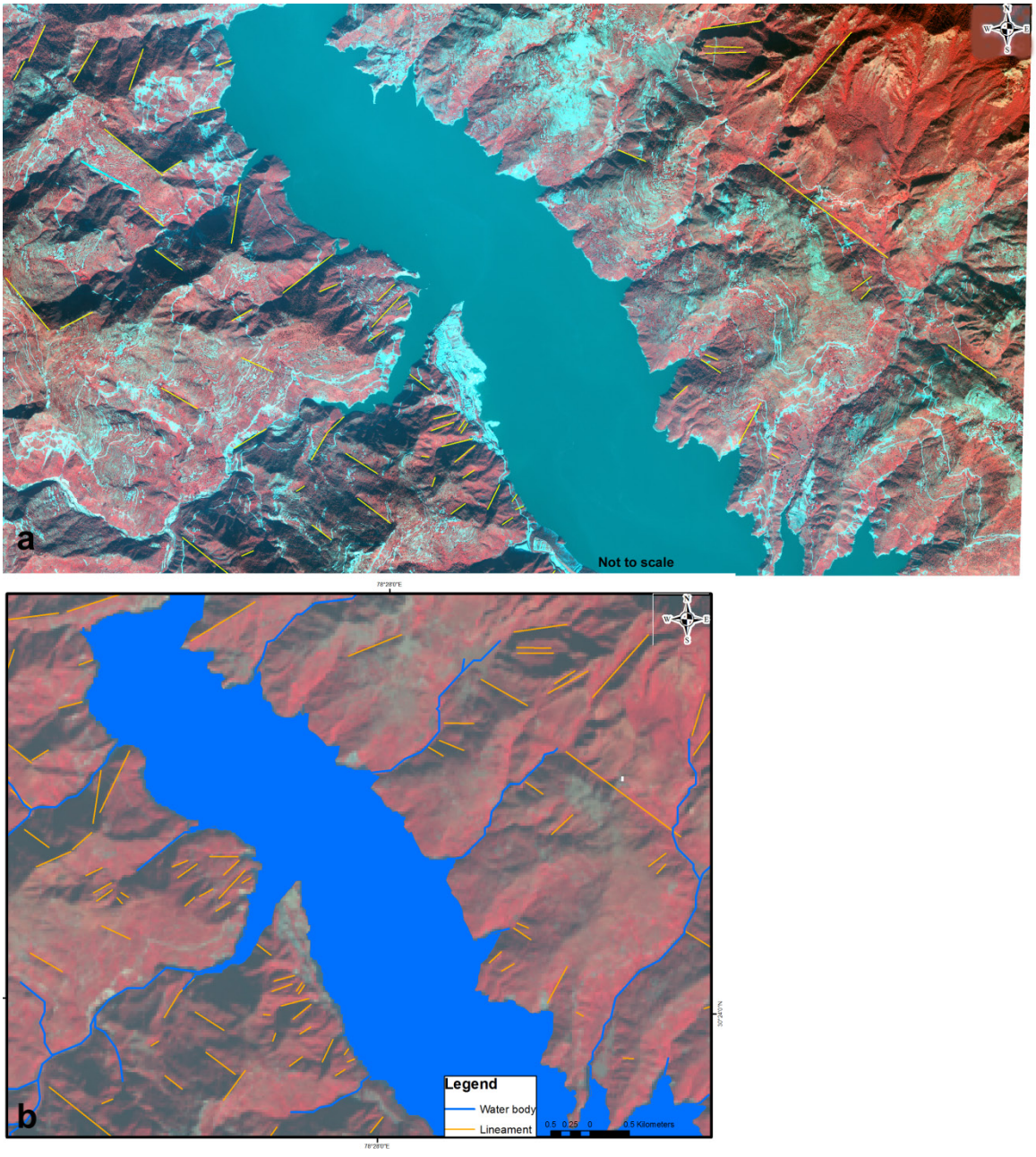

Figure 2.4 Remote sensing multispectral images used for lineament extraction a) Worldview-2 data, b) ASTER data

Band Challenge**).** This data was found suitable for large scale mapping of the landslide inventory, structural and geomorphic features. Due to the higher resolution of the image, it helped in the mapping of the extent of landslides, lineaments and other important terrain features (Figure 2.4a, 2.5c).

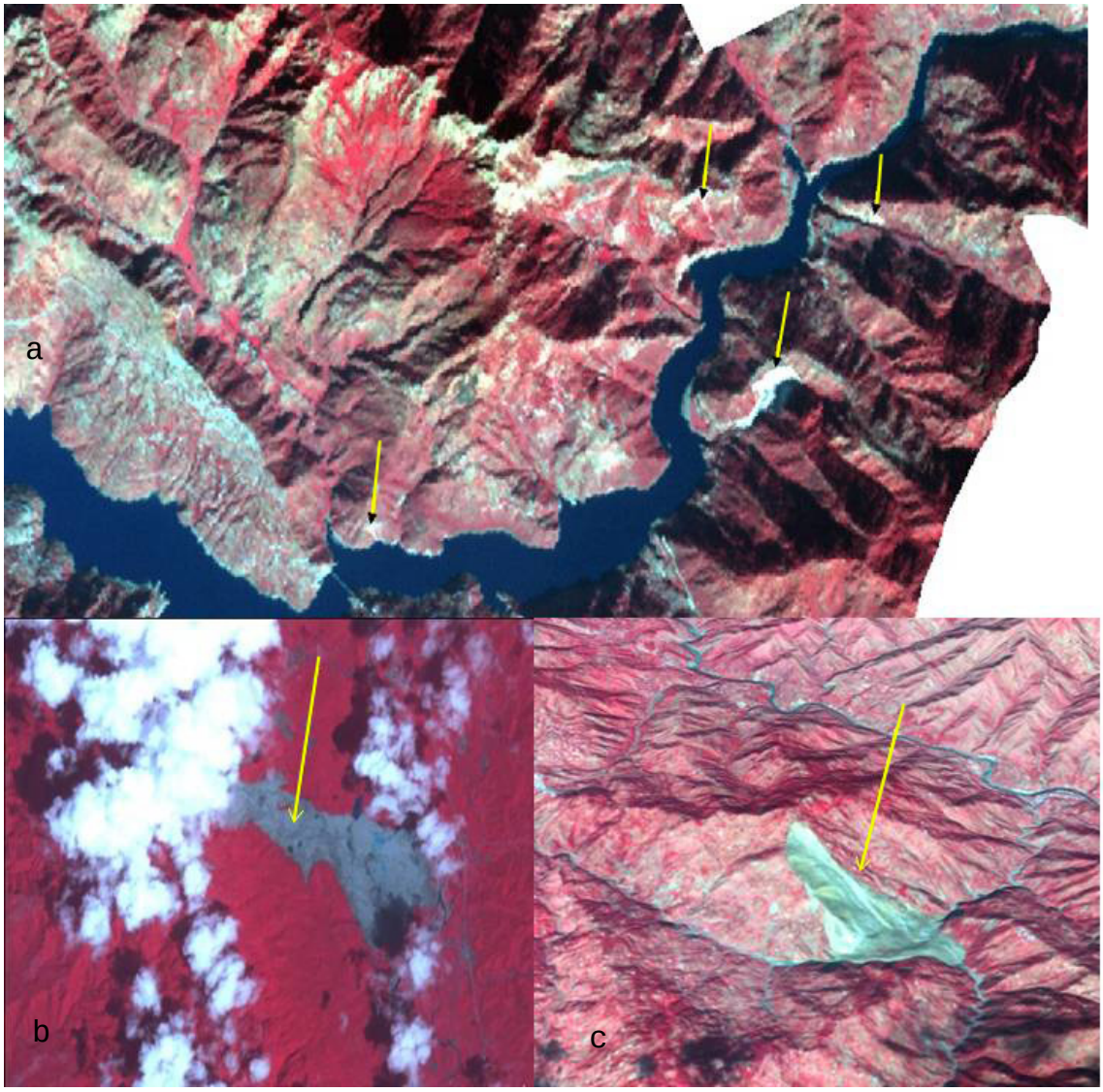

Figure 2.5 Remote sensing data for landslide inventory mapping (Arrow shows the location of landslides) *(Source: USGS Report, 2006)*

2.6.5 Digital Elevation Models (DEM)

ASTER GDEM (30 m spatial resolution, version -2, 2011 release) and Cartosat-1 DEM (2.5 m) were subjected to DEM enhancement techniques such as DEM fill and sink removal for further analysis.

2.6.6 Ancillary data

Ancillary data included geological map, soil map and toposheets, acquired from the websites of the relevant government organizations. General geological map of the

Uttarakhand state was acquired from the government of Uttarakhand website. Soil map was acquired from the published report of Watershed Management Directorate, Dehradun. Survey of India toposheets of 1:25000 scale and 1:50000 scale were available in the department (Department of Earth Sciences, IIT Roorkee). Along with them, field data related to landslide locations, types of landslides, slope materials and geological discontinuities were acquired through extensive field works.

CHAPTER 3
CHARACTERIZATION OF TERRAIN FACTORS

3.1 Terrain Parameters

Landslides result due to the contribution of a number of terrain factors. These factors can be natural such as geology, lineaments, slope, aspect, relative relief and drainage as well as artificial terrain conditions such as road cut slopes, reservoir impoundment and other such factors. In this study, a total of 13 terrain factors belonging to natural and artificial terrain categories were used for the LHZ mapping (using different techniques) in a raster grid form of 25 m x 25 m. These factors were subjected to frequency ratio and weights of evidence (WofE) analysis to determine their relationship with landslide occurrences. The characteristics of these factors and their association with the landslides have been discussed in the following sections.

3.1.1 Lithology

Several geological studies were carried out in the study area. A geological map (Figure 3.1) of the study area was prepared on the basis of extensive field works and by following the work of Valdiya (1980). The whole study area is a part of the broader physiographic entity called Lesser Himalaya. Rocks of the study area belong to the following Formations – Rautgara, Mandhali, Deoban, Chandpur, Nagthat, Berinag, and Blaini. Table 2.1 shows the stratigraphic succession of the geological Groups and Formations of Tehri area. Central part of the area is represented by Chandpur Formation. Rocks of Chandpur Formation are low grade metamorphosed lustrous phyllites and highly weathered quartzites. These rocks are highly vulnerable to sliding because of the presence of well developed foliation plains and joints. Nagthat Formation is found in the western part of the study area. Rocks of Nagthat Formation are characterized by white, purple and

green coloured quartzites with subordinate intercalation of grey and olive green slates with siltstones. Different pattern of weathering was observed in quartzites belonging to Nagthat Formation. Shearing was found to be common discontinuity in those rocks. In eastern part of the study area, North Almora Thrust (NAT) separates Jaunsar Group of rocks from Damtha Group (Rautgara Formation). Rocks of Rautgara Formation comprises of purple, pink and white coloured, well jointed, medium grained quartzites, minor slates and metavolcanics. Deoban Formation is found in eastern and north-eastern part of the study area. It is sandwiched between Rautgara Formation and Berinag Formation in the southern part of the study area. Deoban Formation consists of fine grained dolomitic limestone with minor phyllitic intercalations. These rocks are mainly found at the higher ridges. Rocks of Berinag Formations are exposed in the eastern part of the area. It is separated by Berinag thrust at its base. These rocks are mostly quartzites. Bliani Formations are found in the western part of the study area. This Formation comprises of quartzites, slates and carbonate rocks. Two major synclines and NAT are the major structural features present in the area.

3.1.2 Land use/Land cover (LULC)

The LULC pattern of the terrain has huge influence on landslide hazard study. Five categories of LULC namely dense forest, scrub forest, agricultural land, settlement/barren land and water body were derived from the combination of topographic map and satellite imageries (Figure. 3.2). The LULC categories were prepared from different multispectral data of varying spatial resolution (Table 2.2) by performing NDVI (Normalized Difference Vegetation Index) and supervised classification. Vegetation thresholds were obtained from NDVI and other classes from supervised classification. Reasonable accuracy (78%) was achieved for the LULC mapping. Most of the landslide incidences were found to be associated with settlement/barren land class and agricultural land class.

3.1.3 Soil cover

Soil categories of the Tehri reservoir rim area consist of alluvial/sandy loam, sandy loam, forest/ black clay soil (Figure 3.3). Soil type varies with the relief/elevation and annual rainfall. Elevation in the present area varies roughly from 500 m to 2600 m where as rainfall varies according to the aspect of slope faces (Source – Published report of

Watershed Management Directorate, Dehradun.). At lower elevations (600–1000 m) mainly alluvial mixed with boulders are present. In 1000–1500 m range, sandy loamy soils are present. Above 1500 m, red/black forest soils are present. Each category of soil has certain influence on the landslides. Forest soil is relatively less prone to slope failures because of thick vegetation support. Recent alluvium and loose boulders are more prone to mass movement owing to less compaction and high moisture. Old alluvial deposits seen as terraces in different levels adjoining the river courses on either side particularly on left side are more stable because of high compaction and high friction. Sandy loamy soil is also weathering prone due to less cementation and compaction. Several cones of debris which were formed because of older landslides consists of assorted size of material ranging from clay to boulder size. They are seen at a number of places mainly adjoining the river course due to past landslides.

3.1.4 Structure and photo-lineament

The area falls under Lesser Himalayan terrain. A number of geological discontinuities like Faults, thrusts, folds and joints of varying shape and size can be seen in large numbers in the area. Two major synclines and North Almora Thrust (NAT) are the major regional structural features present in the area (Figure 3.1) Minor to major depressions are seen along the axial zone of synclines in the area. NAT crosses through eastern and north eastern side of the area and crossing the reservoir at Chham where it crosses reservoir the NAT forms visible scrap faces on the left bank adjoining the river course. Moreover, since the trend of NAT is nearly parallel to the river course, where it crosses the reservoir, the scrap face extend over a long distance. Linear geological discontinuities can be delineated from multispectral image and DEM, accordingly a photo-lineament map of the area was prepared. Landslides are associated with the proximity to lineament (Gupta et al.1999). A distance to lineament map (also called lineament buffer map) covering 50 m, 100 m, 150 m and 200 m distances was prepared complying with field evidences of landslides (Figure 3.4). More landslides were observed in areas nearer to the photo-lineaments.

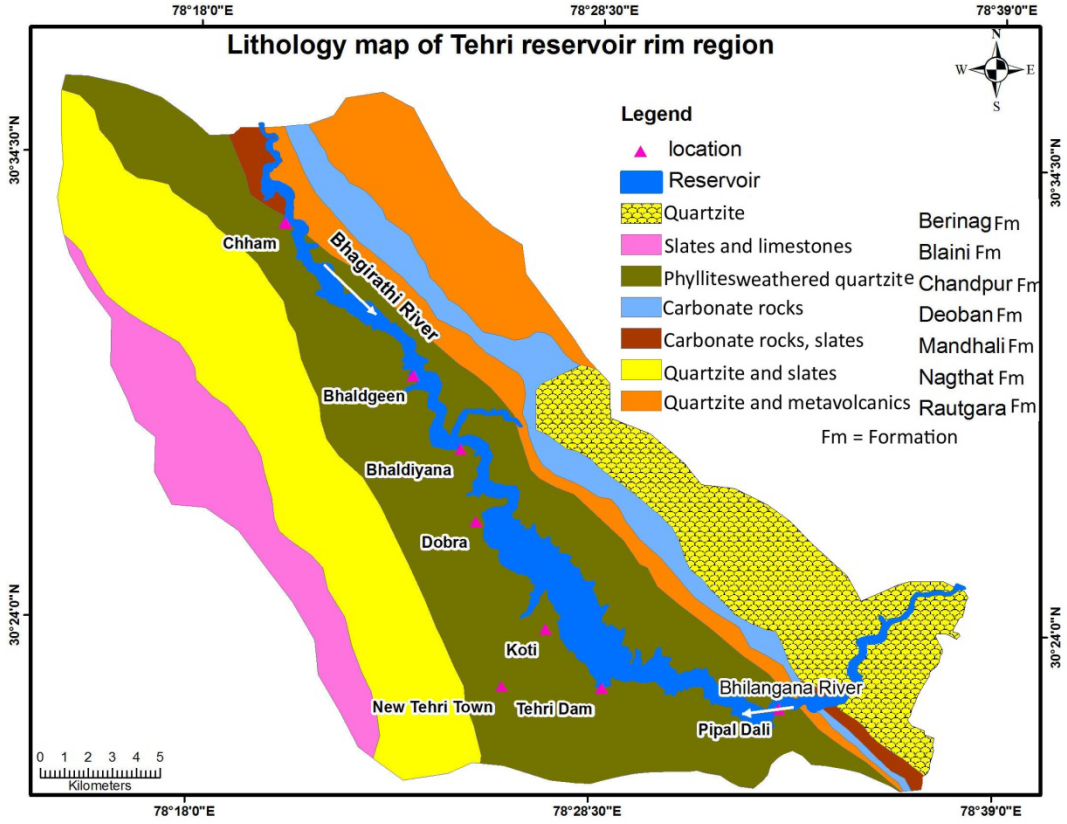

Figure 3.1 Lithological map of the Tehri reservoir rim area

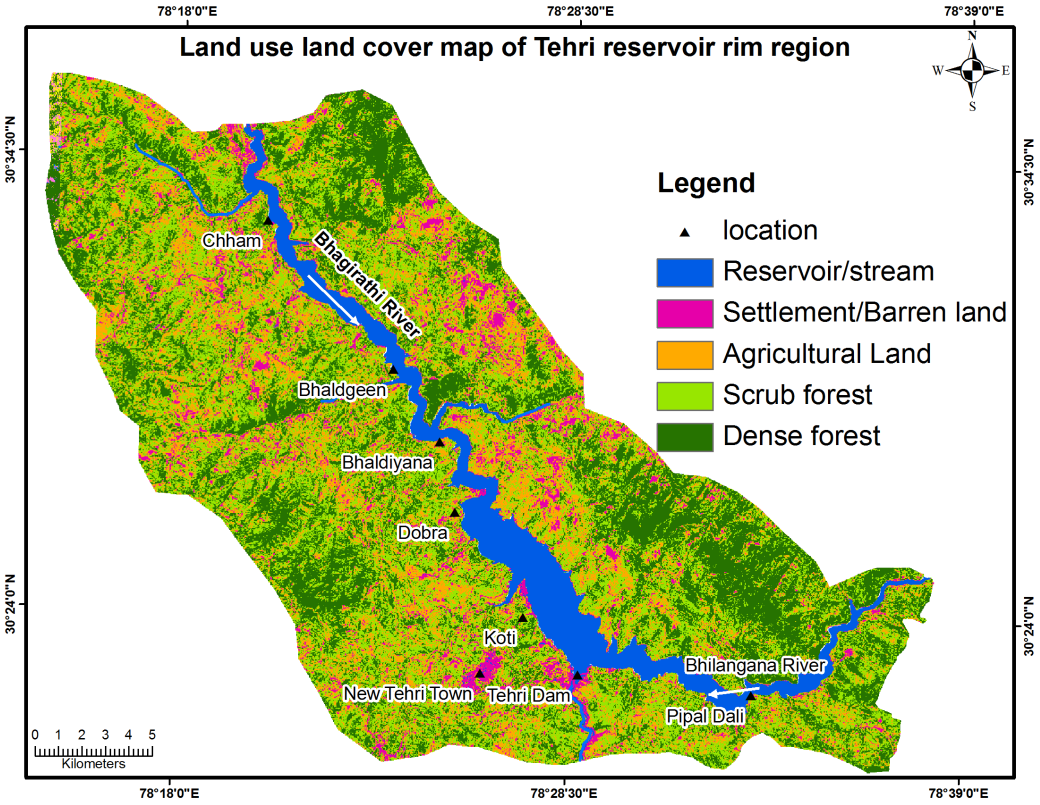

Figure 3.2 Land use/land cover map of the Tehri reservoir rim area

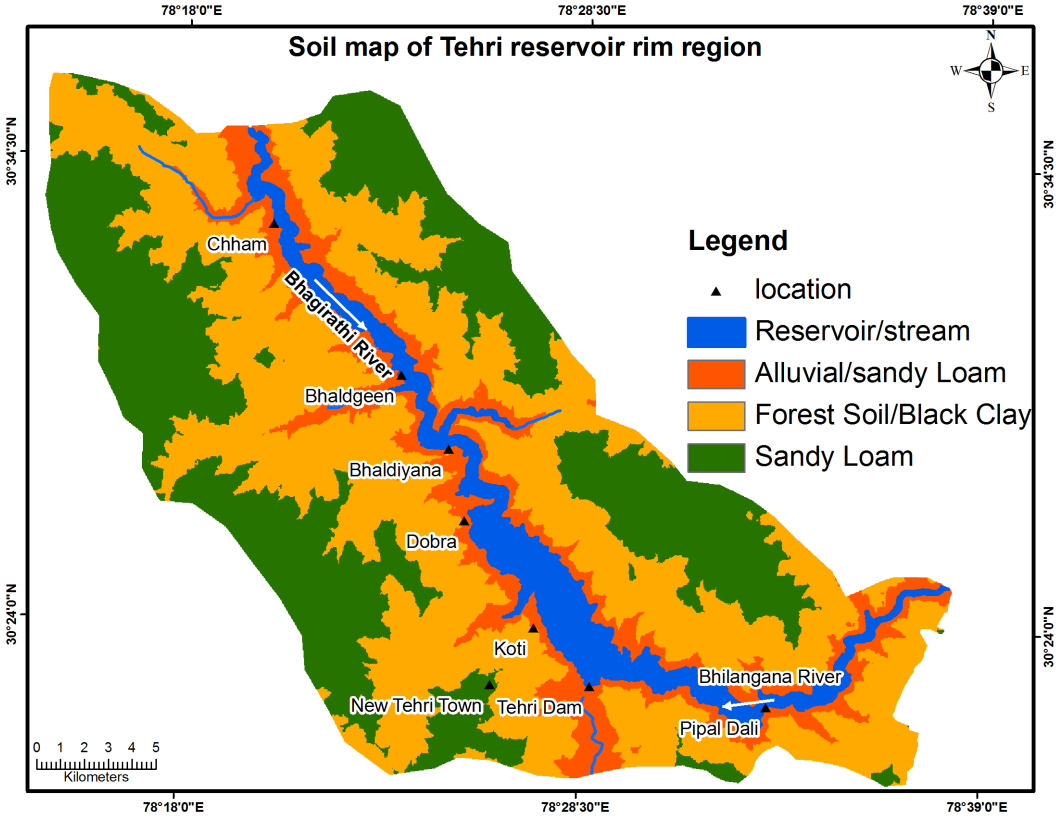

Figure 3.3 Soil cover map of the Tehri reservoir rim area

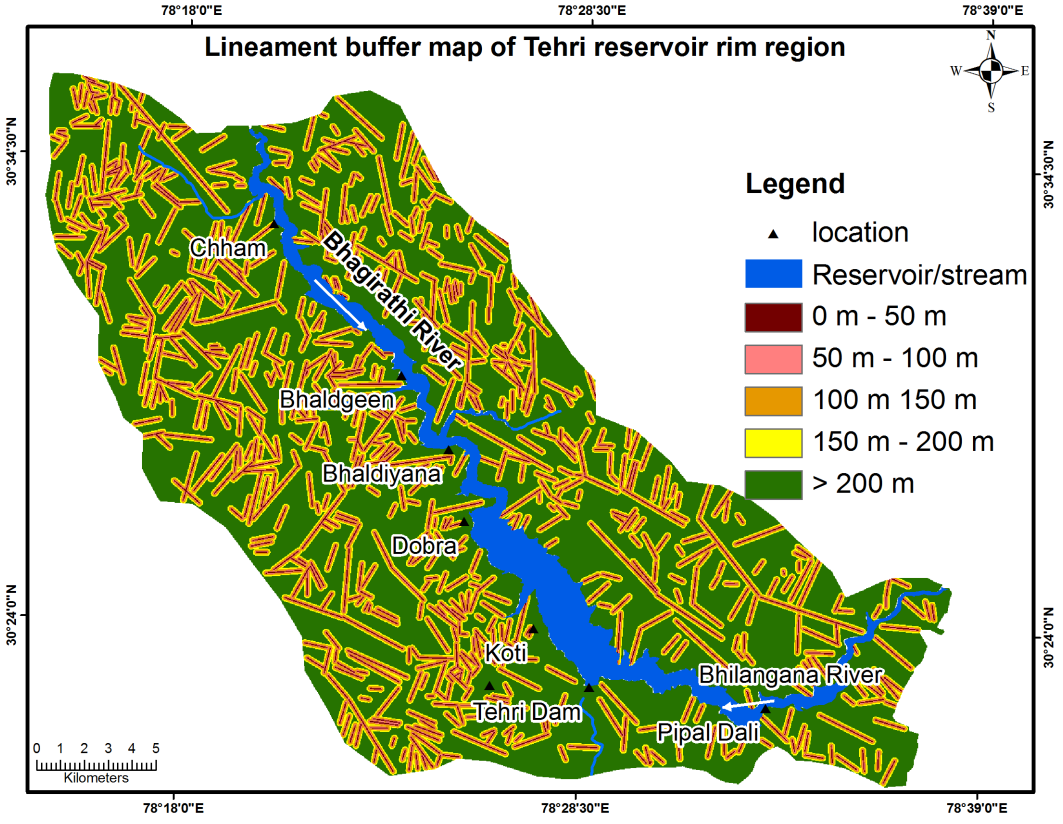

Figure 3.4 Lineament buffer (or distance to lineament) map of the Tehri reservoir rim area

3.1.5 DEM derivatives

Primary topographic attributes such as slope, aspect, relative relief, and slope curvature, were derived with the help of topographic map (1:25000) and DEM data. Secondary topographic attributes can be computed from two or more primary attributes, and are important because it gives an idea about the role of topography in distribution of water and solar radiation, which further has a great importance in vegetation and mass movement process (Wilson 2011).

3.1.6 Primary topographic attributes

Topographic slope, aspect, relative relief, and curvature were derived from DEM by using Arc GIS 9.3 software. Slope angle was found to be varying in range of 0° to 70°. Slope angle was divided into five classes according to its inherent influence on the landslide (Figure 3.5). It has been widely perceived that area with higher slope gradient is more prone to landslides, whereas area having low slope gradient is less prone (Anbalagan 1992; Gupta et al. 1999; Saha et al. 2005; Kayastha et al. 2013). Five slope categories namely very low (0°-8°), low (8°-18°), moderate (18°-30°), high (30°-42°) and very high (>42°) were categorised from the DEM. Topographic aspect often influences the landslide susceptibility. Aspect of a slope face determines concentration of sun rays which is associated with temperature and related climatic condition. In the Himalayan region, influence of aspect on the terrain can be seen, with south-facing slopes being warm, wet and forested, whereas north-facing slopes are cold, dry and glaciated. South facing slopes of Himalayan terrain are more susceptible to landslides. In the present study, aspect was divided into nine classes (Figure 3.6). Another important DEM derivative is relative relief, which is the difference between maximum and minimum elevation point within a facet or area (Gupta et al. 1999). In the present study, relative relief was found to be varying between 0 to 367 m. Following five classes of relative relief: very low relief (0-30 m), low relief (30 m-60 m), moderate relief (60 m-100 m), high relief (100 m – 150 m) and very high relief (>150 m) were considered for the LHZ (Figure 3.7). Field observations suggest that terrains having high relative relief are more prone to landslides compared to low relative relief. Together with other factors, slope curvatures control the flow of water in and out of slopes and are therefore, important in the study of landslides (Ayalew and

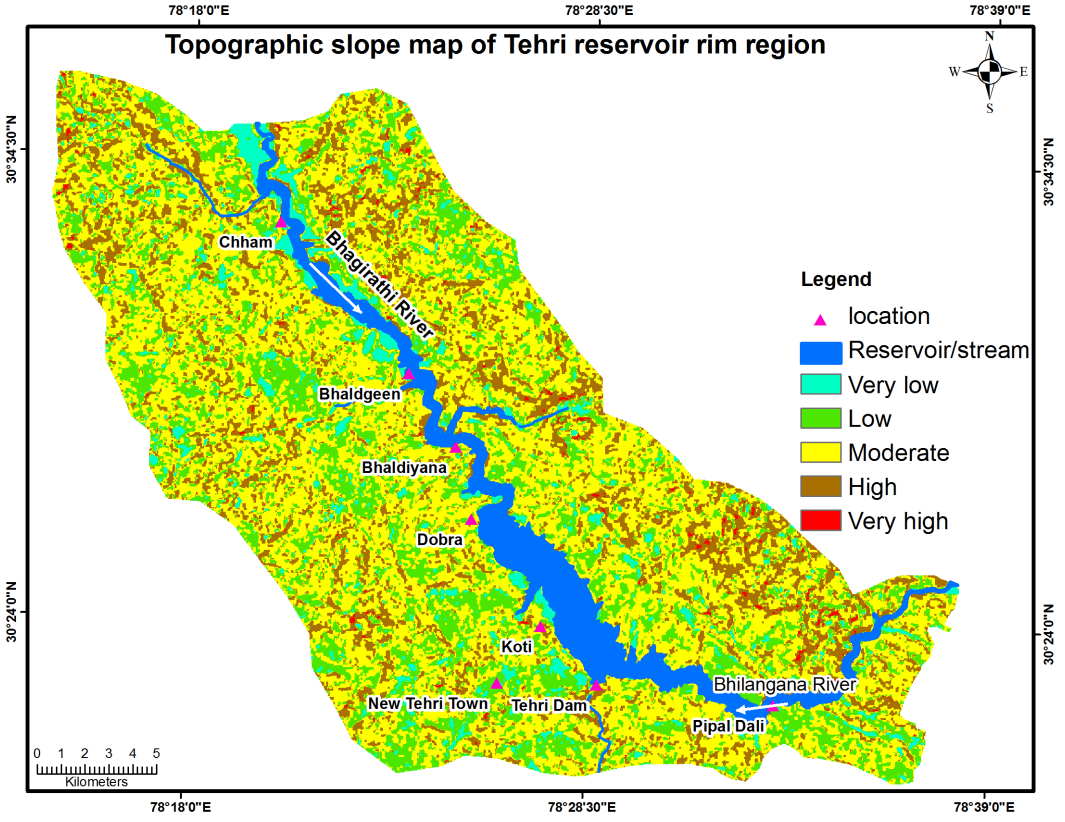

Figure 3.5 Topographic slope (angle) map of the Tehri reservoir rim area

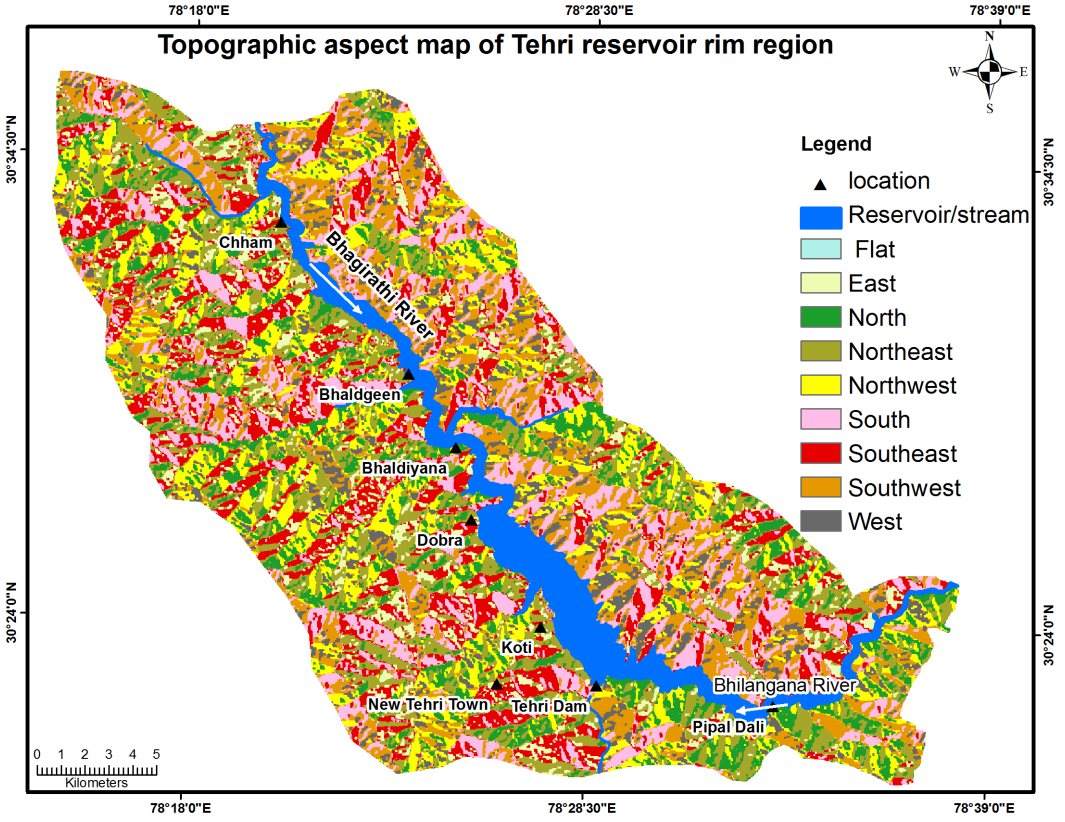

Figure 3.6 Topographic aspect map of the Tehri reservoir rim area

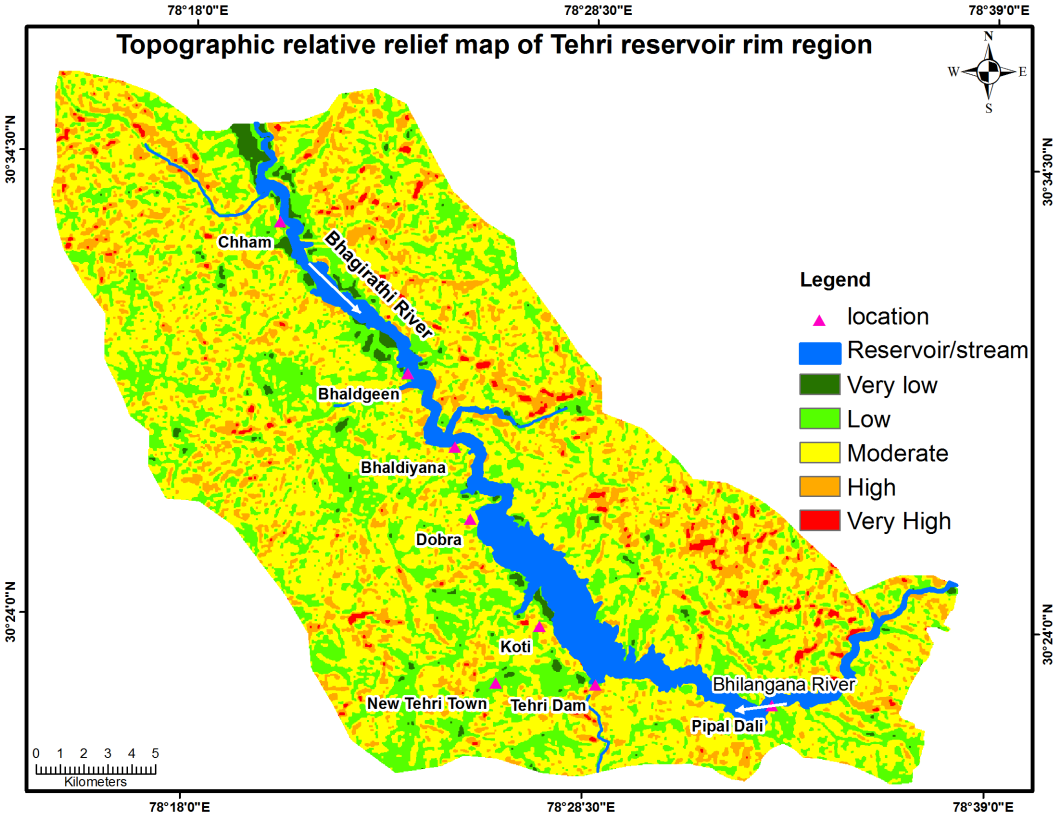

Figure 3.7 Topographic relative relief map of the Tehri reservoir rim area

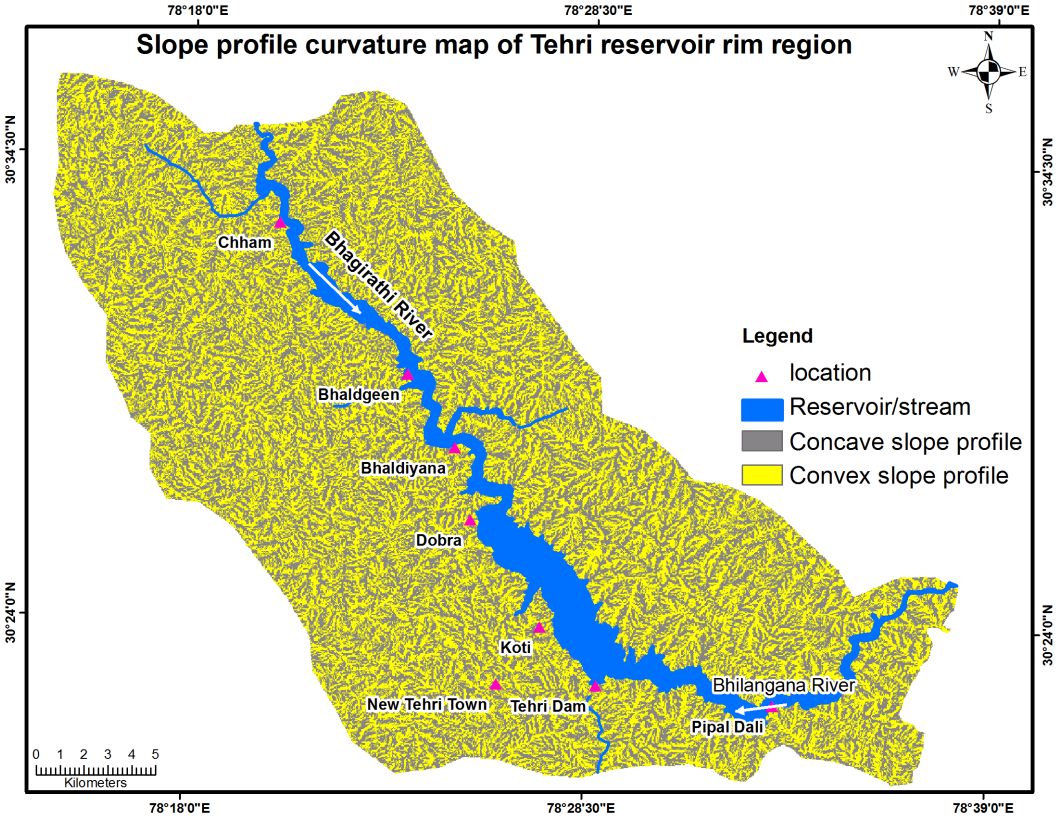

Figure 3.8 Slope profile curvature map of the Tehri reservoir rim area

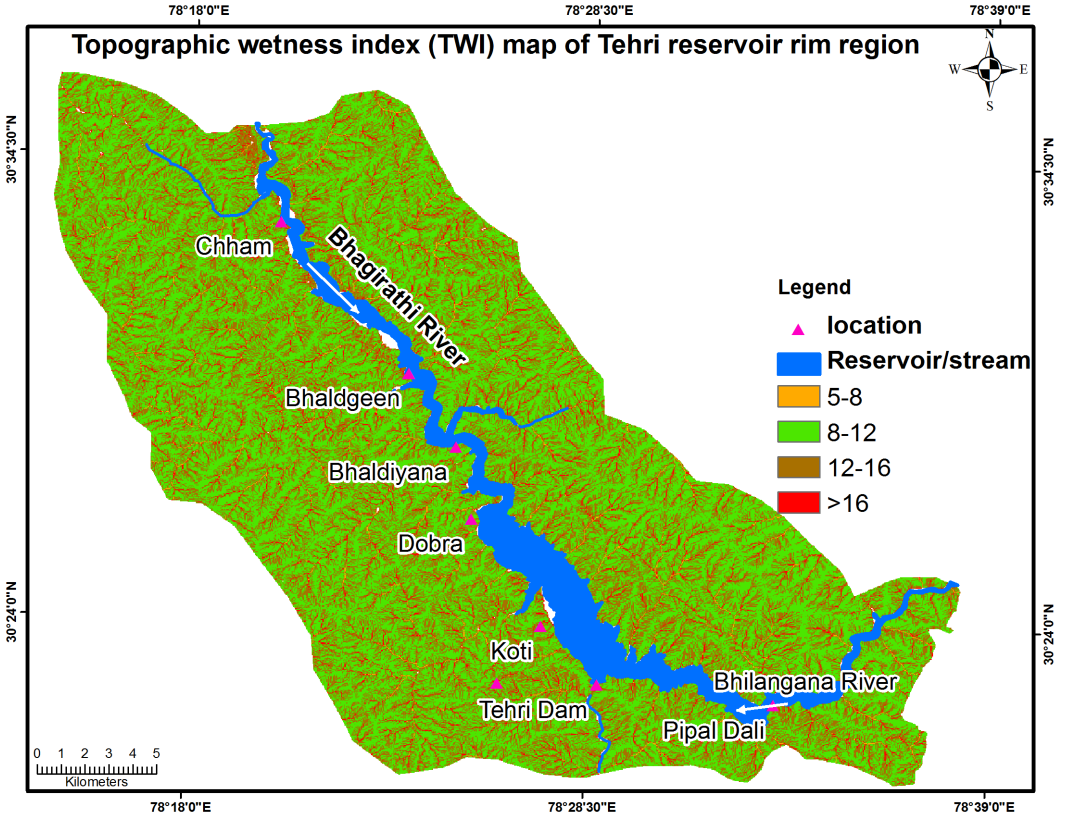

Figure 3.9 Topographic wetness index map of the Tehri reservoir rim area

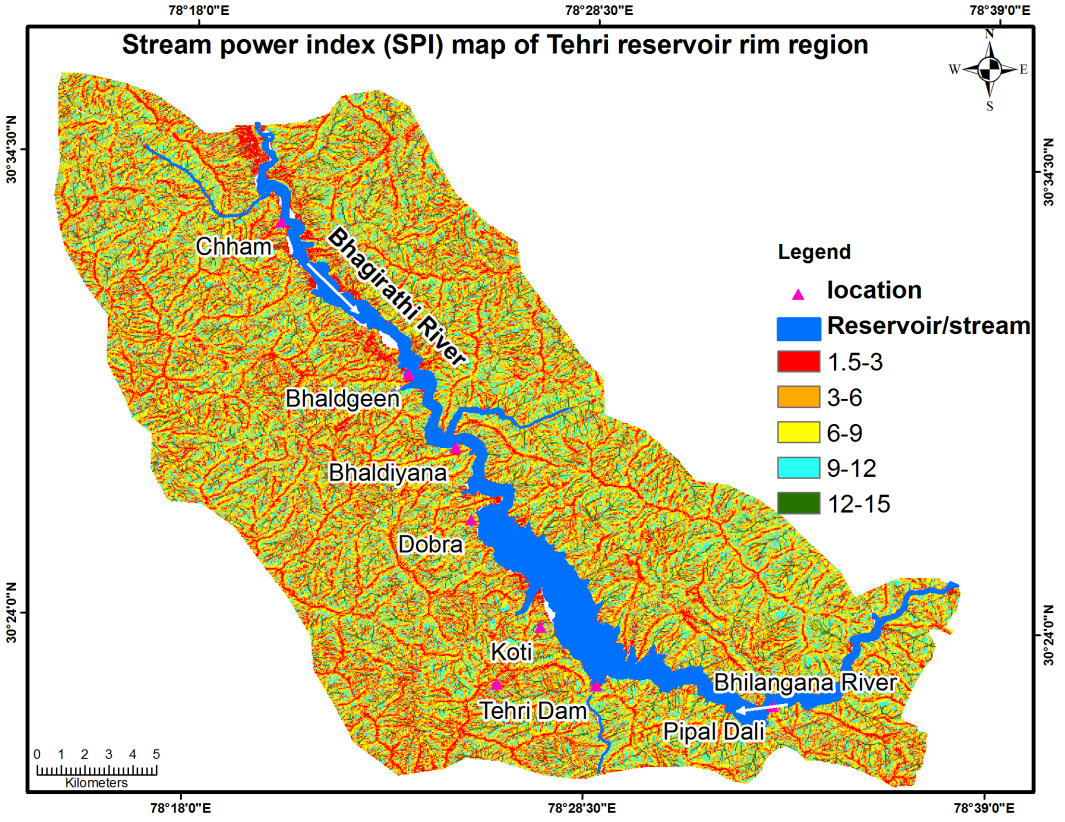

Figure 3.10 Stream power index map of the Tehri reservoir rim area

Yamagishi 2005). Profile curvature was considered in the study. Profile curvature is computed parallel to the direction of the maximum slope in which, a negative value indicates that the surface is upwardly convex; a positive profile indicates that the surface is upwardly concave and a value of zero indicates that the surface is linear (ESRI, 2012). Profile curvature affects the acceleration or deceleration of flow across the surface and it may be associated with mass movement/erosion processes. Accordingly, a profile curvature map was prepared, showing concave and convex profiles (Figure 3.8).

3.1.7 Secondary topographic attributes

Topographic wetness index (TWI) and stream power index (SPI) are the two secondary topographic units considered for the landslide susceptibility study. TWI considers catchment area and slope gradient (Wilson 2011). It can be calculated from following formula:

$$\text{TWI} = \ln \frac{CA}{\tan slp} \tag{3.1}$$

where CA stands for catchment area and *slp* for slope gradient of the area. TWI is associated with flow accumulation at the given terrain. It is effectively used to understand the soil moisture condition and other related phenomenon. With the increase of catchment area and decrease of slope gradient, soil moisture content and TWI of a terrain increases. Flow accumulation in a terrain is controlled by TWI. Other parameters such as distribution of water saturation zones, evapotranspiration, silt and sand content and vegetation are associated with TWI. In a reservoir rim environment, fluctuation of reservoir water between MRL and DSL induces water saturation in side slopes which reduces its stability. Determination of TWI is helpful in delineating saturation zone and water table conditions. TWI values (on natural log scale) were found to vary in a range of 5 to 19, which were further classified into four classes as shown in the Figure 3.9

SPI also takes into account catchment area and slope gradient. It indicates the erosive power of the stream. It can be calculated by using the following formula:

$$\text{SPI} = \ln(CA \times \tan slp) \tag{3.2}$$

SPI is directly proportional to catchment area and slope gradient. Increase in catchment area and slope gradient increases the erosion potential of a stream. The Tehri reservoir rim area has very high stream density, which triggers a number of landslides during monsoon season. SPI resulted in determining the erosive power of the streams of the area. SPI was found to range between 1.5 and 15. Higher values are associated with more number of landslides. SPI values have been divided into five categories by applying natural break classifier (Figure 3.10) (ESRI, 2012).

3.1.8 Distance/Buffer layers

Apart from lineament, reservoir, road and drainage buffer maps were prepared in view of their proximity to landslides. Reservoir water fluctuation (up to 50 m) saturates the side slopes (banks) leading to landslides. A number of landslides are reported from the adjoining areas also. Field observations give an indication of the frequency of landslides along the reservoir rim region (Figure 2.3 (a-d)), accordingly reservoir multi-buffer map (100 m, 200 m, 300 m, 400 m and 500 m) was prepared (Figure 3.11). Very high number of landslides were observed along the roads which have been constructed by cutting the slopes randomly. Cut slopes along the road network were found to be standing steeply and sometimes making overhangs. Most of the cut slopes observed were untreated. During monsoon, these cut slopes fail frequently and obstruct transportation. Most of the failed slopes are progressive in nature as observed in the field. Road multi buffer (50 m, 100 m, 200 m) layer was prepared in view of its proximity to landslides (Figure 3.12).

3.1.9 Drainage

Drainage map was derived from the DEM in Archydro tool of ESRI GIS package. High drainage density was observed from DEM analysis with up to 5^{th} order stream present. Highly undulating terrain of the area supports a network of dissected drainages. Drainage network has compelling relation with the landslides. In hilly regions, streams continuously erode its banks and create steep side slopes which are very prone to failures. A number of such failures were observed during field investigation (Figure 2.3 (i)). These failures are also progressive in nature. More landslides were observed closer to streams.

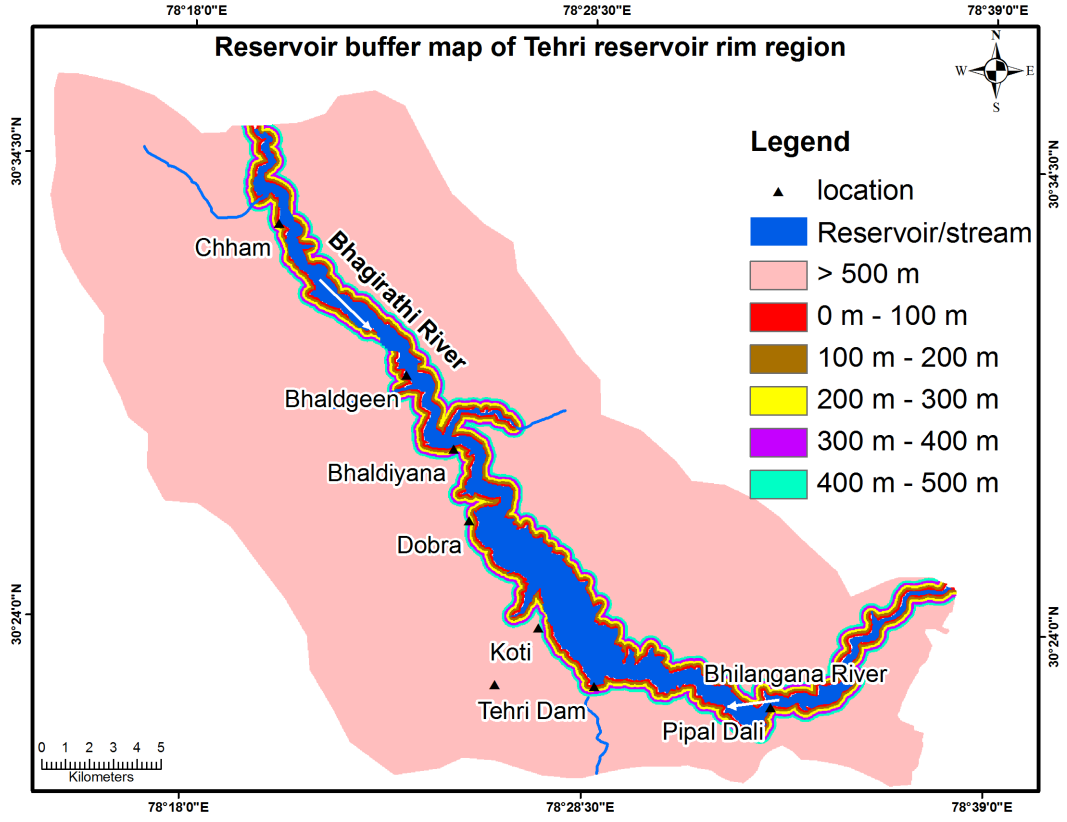

Figure 3.11 Reservoir buffer map of the Tehri reservoir rim area

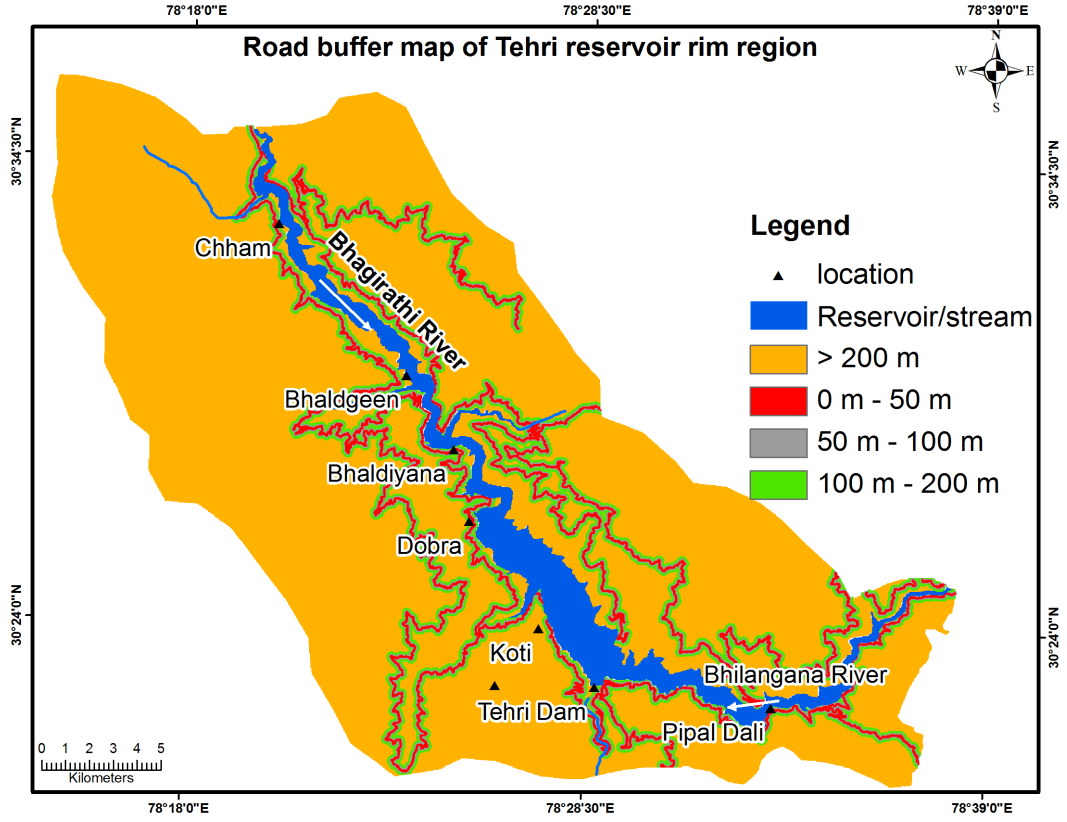

Figure 3.12 Road buffer map of the Tehri reservoir rim area

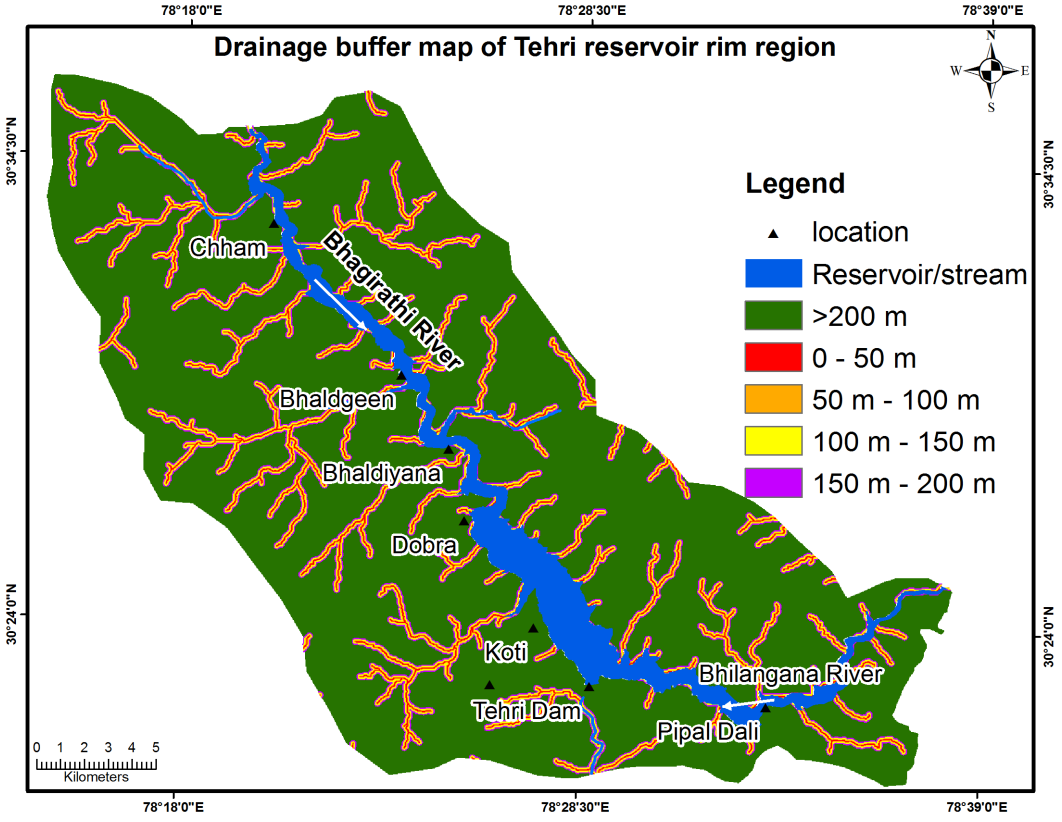

Figure 3.13 Drainage buffer map of the Tehri reservoir rim area

For the assessment of landslide hazard, drainage buffer maps (50 m, 100 m, 150 m and 200 m) were prepared complying with field evidences (Figure 3.13).

3.2 Relationship of Terrain Conditions with Landslide Occurrences

Relationship and significance of terrain factors for landslide occurrences were determined by subjecting landslide inventory to landslide frequency ratio and weights of evidence analysis. A total of 195 landslide incidences were covered in point vector format throughout the area out of which 116 (60%) landslide incidences were subjected to the landslide frequency ratio analysis and 134 (almost 70%) landslide incidences were subjected to WofE analysis. Random landslide training data were selected for the two different methods to induce robustness. landslide frequency ration and WofE methods depend upon landslide densities in terrain factors and also both follows the principle of conditional probabilities (Lee and Talib 2005; Lee and Sambath 2006). In view to these facts separate training data were considered.

3.2.1 Landslide frequency ratio approach

It is very common to assume terrain factors to predict landslide occurrences. The assumption behind this is that future landslides will occur under similar conditions as past and present landslides (Lee and Talib 2005). Following the same assumption, a relationship can be determined between landslide related terrain factors with landslide occurrences and non-occurrences spatially. This relationship can be quantified using frequency ratio. Landslide frequency ratio can be calculated by ratio of percent domain of a factor class and percent landslide in that class (Lee and Talib 2005; Lee and Sambath 2006; Poudyal et al. 2010; Pradhan 2010; Pourghasemi et al. 2013). It follows the principle of conditional probability, in which if the ratio is >1 then there is a strong relationship between landslides and factor classes whereas ratio <1 represents weak relationship. Calculation of frequency ratio was performed as per the following steps. In the first step, percentage domains of factor classes (a_i) were calculated, then percentage of landslides (l_i) in corresponding classes was calculated and finally ratios between l_i and a_i (frequency ratio, Fr_i) were calculated.

Analysis of landslide frequency ratio suggests importance of terrain factors and their classes on the landslides. Primary topographic attributes are found to be important landslide causative factors. Among the slope categories, high landslide frequency ratios ranging between 3.99 and 2.58 were observed in high slope (30°-42°) and very high slope categories (>42°) respectively (Table 3.1). Table 3.1 indicates that frequency ratio value increases as the slope angle increases, which further suggests that landslide probability increases. In steep slopes, the weight of the possible mobilized material under gravity will be more as compared to a moderate slope. Shear strength being same in both the cases, a steep slope with more mobilizing force may fail early.

High and very high relative relief categories have resulted in high frequency values of 3.164 and 2.95 respectively. Frequency ratio of the relative relief categories also indicates the increasing tendency in very low relief to very high relative relief classes. High relative reliefs are surface manifestation of cliffs and ridges, which are often rendered unstable by the influence of triggering factors such as rainfall and earthquakes.

Topographic aspect is also found to be an important landslide conditioning factor in the present area. Southern aspect of the study area, which is receiving excessive sun radiation and high rainfall, are more prone to landslides (Gupta 1996). Incidentally, in the area of study, major number of agricultural terraces are present on the southwest facing slopes leading to more instability. Very high frequency ratios - 0.9, 2.6 and 1.34 are found for southwest, south and southeast aspect respectively. Secondary topographic attributes are also found to be important causative factors.

High frequency ratio is found in the case of higher ranges (8-12, 12-16, 16-19) of TWI (Table 3.1). Higher TWI ranges indicates increasing water infiltration which leads to increase in the pore water pressure and further reduces the soil strength, hence making the terrain prone to slope failures. In case of SPI, high frequency value is found in the range of: 3-6 and 6-9 (Table 3.1). SPI indicates the erosive power of the streams and lower ranges of SPI is related to the low erosive power of the streams.

In view of LHZ mapping, drainage and lineaments distance maps (buffer maps) of 0-50 m, 50 -100 m, 100 -150 m, 150-200 m and >200 m distances were prepared. Frequency ratio for the range: 0-50 m, 50-100 m and 100 -150 m are found to be high in case of distance to drainage classes (Table 3.1) and it can be attributed to the stream bank erosion due to the river flow such as gulling, toe cutting which further leads to landslides.

Distance to lineament category indicates varying degree of frequency ratio and it does not follow any pattern. Lithology of the area belongs to different Formations as mentioned in the previous section 3.1.1. Each Formation is represented by a characteristic rock type, which might govern landslide incidences. Frequency ratio results of geology layer has reflected that rocks of Chandpur and Nagthat Formation are more prone to landslides as they have resulted in high frequency ratio values (Table 3.1). Blaini, Mandhali, and Deoban Formations constitute of slate, quartzite, siltstone and carbonate rocks, which have resulted in low frequency ratio value.

Among the soil categories, alluvial/sandy loam have resulted in high frequency value. Alluvial soil has been observed at lower elevations along the drainage network and are not well compacted which leads to slope failures. Forest soil and sandy loam resulted in

low frequency ratio values (Table 3.1). These soils are compacted and are under the influence of scrub to dense vegetation, which makes them relatively stable.

Reservoir buffer area is mainly formed of different grade of phyllite rocks. Distance to reservoir has reflected progressive decrease of frequency ratio value from 100-500 m distance (Table 3.1) which can be attributed to the reservoir induced slope failures discussed in section 3.1.8.

Road buffer layers have also shown substantial decrease in frequency ratio value from 0-50 m buffer to 200 m buffer (Table 3.1). It is often seen in the area that steep cut slopes are left untreated after the road construction and they often fail under the influence of triggering factors. Progressive nature of these failures makes the overall terrain condition very unstable.

Within the LULC classes, high landslide frequency value is observed in scrub forest, agricultural land, and settlement/fallow land classes (Table 3.1) and can be attributed to the inherent physical properties of the LULC classes. Relationship between landslide incidences and slope curvature could not be achieved because frequency ratio value in both the cases (convex profile, concave profile) is more or less equal.

3.2.2 Terrain characterization for the LHZ using WofE approach

WofE model is based on Bayesian probability model and is capable of analyzing association between the terrain conditions of the region affected by landslides and the casual factors responsible for the landslides with the help of known landslide locations and it leads to portray the degree of impact of each causal factor towards the landslide incidences. WofE method is used to calculate the probability of landslide on the basis of a set of causal factors and providing a statistical measure in numerical form thus avoiding subjectivity. This model is also helpful in identifying the effect of landslide factors and their combination on model susceptibility.

Table 3.1: Landslide frequency ratio occurrence factors

Factors & attributes	Percentage of domain (a_i)	No. of landslides	Percentage of landslides (l_i)	Frequency Ratio (f_i)
Geology				
Blaini Formation	8.69	3	2.58	0.297
Nagthat Formation	21.8	20	17.241	0.790
Chandpur Formation	35.47	72	62.058	1.74
Berinag Formation	13.87	11	9.48	0.683
Deoban Formation	6.84	3	2.58	0.378
Mandhali Formation	0.135	0	0	0
Rautgara Formation	5.72	7	5.2	0.87
Soil type				
Alluvial/sandy Loam	19.685	72	62.068	3.152
Forest Soil/Black Clay	47.827	6	32.758	1.008
Sandy Loam	32.486	38	5.172	0.108
Relative relief				
Very low	4.747	0	0	0
Low	28.426	3	2.586	0.09
Moderate	49.817	51	43.965	0.882
High	15.256	56	48.275	3.164
Very high	1.751	6	5.172	2.953
Slope category				
0°-8°	13.818	0	0	0
8°-18°	27.442	2	1.724	0.062
18°-30°	40.383	30	25.862	0.64
30°-42°	17.687	82	70.689	3.996
>42°	0.667	2	1.724	2.581
Lineament buffer				
0 – 50m	6.082	2	1.724	0.283
50 – 100m	6.532	5	4.31	0.66
100 – 150m	13.435	11	9.482	0.705
150 – 200m	12.652	34	29.31	2.316
>200m	61.297	64	55.172	0.9
Drainage buffer				
0 – 50m	3.17	10	8.62	2.718
50 – 100m	3.217	8	6.896	2.143
100 – 150m	6.351	12	10.344	1.628
150 – 200m	6.183	30	25.862	4.182
>200m	81.077	56	48.275	0.595

LULC Type				
Dense forest/vegetation	5.854	0	0	0
Scrub/open forest	7.476	19	16.379	2.19
Agricultural land	33.044	67	57.758	1.747
Settlement/ barren Land	24.498	30	24.137	0.985
Water Body	29.126	0	0	0
Aspect				
North	14.783	14	12.068	0.816
Northwest	11.47	4	3.448	0.3
West	9.593	7	6.034	0.629
Southwest	12.702	14	12.068	0.95
South	12.874	40	34.482	2.678
Southeast	12.771	20	17.241	1.349
East	10.26	10	8.62	0.84
Northeast	12.667	7	6.034	0.476
Flat	2.876	0	0	0
TWI				
5-8	61.907	39	33.62	0.543
8-12	35.035	55	47.413	1.353
12-16	2.612	20	17.241	6.6
16-19	0.444	2	1.724	3.882
SPI				
1.5-3	67.143	47	40.517	0.603
3-6	28.043	59	50.103	1.813
6-9	4.434	10	8.62	1.944
9-12	0.215	0	0	0
12-15	0.163	0	0	0
Profile Curvature				
Concave	51	56	48.27	0.946
Convex	49	60	51.73	1.055
Road Buffer				
0 -50m	4.2	32	27.58	6.56
50 -100m	5	24	20.68	4.136
100-200m	10.8	16	13.79	1.27
>200m	80	44	37.93	0.47
Reservoir buffer				
0 - 100m	3.24	30	20	6.17
100 - 200m	3.78	30	20	5.29
200 - 300m	4.47	15	10	2.23
300 - 400m	5.22	5	3.3	0.63
400 - 500m	6.14	10	6.6	1.07
>500m	77.15	60	40	0.51

Basic assumption of the WofE method is that if a fraction of area is affected by landslides (L), the prior probability of having a landslide in the total study area (S) is:

$$P(L) = L/S \tag{3.3}$$

And the probability of having one of the factor classes in the study area is:

$$P(F) = S_f/S \tag{3.4}$$

Where S_f is the area occupied by a certain factor class (such as forest cover, agricultural land etc). Based on this assumption, Bonham carter (1994) synthesised the formula of positive weight evidence (W^+) and negative weight evidence (W^-) of the factor classes with landslides and can be given as:

$$W^+ = \ln \frac{P(S_f|L)}{P(S_f|\bar{L})} \tag{3.5}$$

$$W^- = \ln \frac{P(\overline{S_f}/L)}{P(\overline{S_f}/\bar{L})} \tag{3.6}$$

$$C = W^+ - W^- \tag{3.7}$$

W^+ reflects the positive association between the factor class and landslide where as W^- reflects the negative association. The contrast (C) between W^+ and W^- is a measure of the spatial association between landslides and the factor classes. C is positive for a positive spatial association, and negative for a negative spatial association. By applying formulas mentioned above W^+, W^- and C were calculated along with the variance of the W^+ [S^2 (W^+)], variance of W^- [S^2 (W^-)], standard devotion of contrast (S(C)) and the student zed contrast value (C/S(C)). The calculation result is presented in the Table 3.2.

3.2.3 Analysis of the terrain factors

The contrast (C) between W^+ and W^- is a measure of the spatial association between landslides and the terrain variables and the magnitude of the contrast reflects the overall spatial association between the terrain variables and the landslides (Lee and Choi 2004; Dahal et al. 2008; Kayastha et al. 2012). On the basis of the contrast values, terrain factor classes were analyzed for their relationship with the landslide occurrences.

Within the geological category, high contrast values were observed for Chandpur Formation and Berinag Formation. It reflects the association between the inherent properties of the rock types belonging to these Formations. Rock types belonging to Chandpur Formation are largely low grade phyllites and highly jointed quartzites which are prone to weathering. Berinag Formation is also represented by well jointed quartzite, shiny phyllite and meta-sedimentry rocks, which show instability in many locations. Other geologic Formations resulted in negative contrast values, which reflect that rock types belonging to those Formations may not influence landsliding. Among the soil categories contrast value of the recent alluvial sandy loam soil was found to be very high whereas other two categories resulted in a negative contrast value (Table 3.2). Older alluvial soils which show good thickness of more than 100 m have steep to nearly vertical slopes adjoining the reservoir course. The toe erosion due to fluctuating reservoir often leads to unstable slopes affecting the entire slope. Other soil categories, sandy loam and forest black soil supports thick vegetation covered are generally stable. Among the LULC categories, positive contrast value was observed in the case of settlement with barren land class and agricultural land class. During field investigations, it was found that settlements were built on moderate to steep slopes or just adjoining them without treating those slopes, which leads to slope failures. Agricultural practices in this region are very typical. Dry random stone walls generally support the valley side slopes of the terraces used for agriculture. Since the terraces are subjected to repeated inundation for crops, the dry masonry stone wall often fail leading to landslides. Other LULC classes such as sparse forest and dense vegetation are less prone to landslides.

Topographic features such as slope, aspect, relative relief, profile curvature etc. are important factors for landsliding. In case of slope categories, peak contrast value was observed for high slope angle class (30 -42˚) (Table 3.2). Very high slope angle class (>42˚) resulted in high positive contrast value whereas moderate slope angle class resulted in low negative contrast value. Low and very low slope classes resulted in negative contrast values. In general, the calculated contrast values of the slope categories reflect universal assumption that landslides are mostly associated with terrain made up of steeper slopes. Positive contrast values were observed for the high, very high and moderate relative

Table 3.2: Computed weights for classes of various data layers based on landslide occurrence

CLASS	A (km^2)	Area %	L	W^+	W^-	C
Geology						
Bliani Formation	48.302	8.694	0	0.000	0.000	0.000
Nagthat Formation	121.080	21.793	27	-0.096	0.026	-0.122
Chandpur Formation	197.076	35.471	75	0.605	-0.456	1.060
Berinag Formation	76.817	13.826	19	0.031	-0.005	0.036
Deoban Formation	34.641	6.235	4	-0.854	0.042	-0.896
Mandhali Formation	7.025	1.264	0	0.000	0.000	0.000
Rautgara Formation	29.047	5.228	9	-0.404	0.020	-0.423
Soil						
Alluvial/sandy Loam	84.092	15.003	75	2.354	-0.766	3.120
Forest soil/Black Clay	283.808	50.634	48	-0.413	0.336	-0.749
Sandy Loam	192.603	34.363	11	-1.597	0.434	-2.032
LULC						
Water body	6.570	1.182	2	0.298	-0.004	0.302
Settlement/barren Land	37.142	6.683	23	1.413	-0.146	1.559
Agricultural land	123.805	22.276	38	0.309	-0.100	0.409
Scrub/open forest	209.616	37.715	50	-0.013	0.008	-0.021
Dense forest/vegetation	178.648	32.144	21	-0.834	0.277	-1.111
Lineament Buffer						
0 – 50m	36.103	6.441	8	-0.093	0.006	-0.099
50 – 100m	38.707	6.906	3	-1.275	0.061	-1.336
100 – 150m	79.273	14.143	8	-0.991	0.114	-1.104
150 – 200m	73.983	13.199	11	-0.561	0.070	-0.630
>200m	332.439	59.311	104	0.345	-0.699	1.043
Slope Category						
0°-8°	27.684	4.939	5	-0.337	0.016	-0.352
8°-18°	136.630	24.374	10	-1.336	0.256	-1.592
18°-30°	288.293	51.429	63	-0.110	0.109	-0.219
30°-42°	104.875	18.709	55	1.117	-0.384	1.502
>42°	3.081	0.550	1	0.395	-0.002	0.397
Relative Relief						
Very low	8.405	1.499	2	-0.006	0.000	-0.006
Low	145.779	26.005	11	-1.303	0.274	-1.577
Moderate	316.705	56.496	79	0.053	-0.072	0.124
High	81.805	14.593	39	0.958	-0.226	1.184
Very high	7.888	1.407	3	0.615	-0.011	0.625
Aspect						

Flat	0.046	0.008	0	0.000	0.000	0.000
North	18.859	3.366	5	0.129	-0.005	0.134
Northeast	98.793	17.633	12	-0.788	0.125	-0.913
East	36.655	6.542	8	-0.112	0.008	-0.120
South east	87.373	15.594	34	0.647	-0.150	0.798
South	83.952	14.984	37	0.834	-0.195	1.029
Southwest	81.435	14.534	13	-0.480	0.069	-0.548
West	37.120	6.625	2	-1.659	0.067	-1.725
North west	75.934	13.553	12	-0.492	0.065	-0.556
North	40.123	7.161	11	0.172	-0.014	0.186
Slope Profile Curvature						
Concave	275.544	55.240	63	-0.061	0.057	-0.118
Convex	282.263	56.588	71	0.057	-0.061	0.118
TWI						
5-8	337.784	60.586	89	0.124	-0.212	0.337
8-12	189.305	33.954	43	-0.060	0.030	-0.090
12-16	25.748	4.618	1	-1.995	0.049	-2.045
16-19	4.693	0.842	0	0.000	0.000	0.000
SPI						
1.5-3	2.526	0.453	1	0.676	-0.004	0.679
3-6	209.757	37.623	42	-0.212	0.116	-0.328
6-9	255.445	45.817	71	0.193	-0.183	0.375
9-12	82.825	14.856	19	-0.048	0.008	-0.056
12-15	6.978	1.252	0	0.000	0.000	0.000
Drainage Buffer						
0 – 50m	14.983	2.684	7	1.32	-0.156	1.417
50 – 100m	15.537	2.783	4	0.087	-0.003	0.090
100 – 150m	31.330	5.613	10	1.172	-0.096	1.267
150 – 200m	31.722	5.683	10	0.350	-0.024	0.373
>200m	464.636	83.237	103	-0.098	0.417	-0.515
Road Buffer						
0 -50m	32.301	5.785	52	1.904	-0.432	2.336
50 -100m	27.960	5.008	7	0.042	-0.002	0.045
100-200m	46.575	8.342	8	-0.335	0.026	-0.360
>200m	451.489	80.865	67	-0.481	0.961	-1.442
Reservoir buffer						
0 - 100m	13.776	2.458	20	1.805	-0.137	1.942
100 - 200m	12.904	2.302	36	2.459	-0.290	2.749
200 - 300m	12.256	2.187	11	1.323	-0.064	1.387
300 - 400m	11.620	2.073	1	-1.022	0.014	-1.035
400 - 500m	11.141	1.988	5	0.630	-0.018	0.648
>500m	498.807	88.993	61	-0.670	1.600	-2.270

relief classes in the decreasing order respectively. Whereas negative contrast was observed for low and very low relative relief classes. These results also fit according to the universal assumption that high relief areas are more prone to the landslides. South, southeast and north aspects gave positive contrast values (in decreasing order, Table 3.2) among the aspect classes. Other aspect classes resulted in negative contrast values. Southern aspect of the study area, which is receiving excessive sun radiation and high rainfall, is more prone to landslides (Gupta 1996). Incidentally, in the study area, major number of agricultural terraces are present on the southwest facing slopes leading to more instability. Among the profile curvature categories, low positive contrast value was observed for the convex profile and low negative contrast value was observed for the concave slope profile. Concave profile of the slopes make overhangs and are normally more prone to landslides. Flat slope profile constituted a very small part of the area, hence it was not considered in the study.

Secondary topographic attributes such as TWI and SPI are also important factors for the landsliding. In case of TWI, positive contrast values were observed for the range 5-8 while negative contrast values were observed for the ranges, 8-12 and 12-16. The range 16-19 gave null value because no landslide was observed in that range. Positive contrast values were observed in the ranges 1.5-3 and 6-9 for the SPI categories whereas negative ranges were observed for the ranges 3-6 and 9-12 (Table 3.2). In the range 12-15, no landslide was observed hence the null contrast value was observed.

Among the distance to lineament (lineament buffer) classes except >200 m distance category, all the classes resulted in negative values. This result indicates that photo-lineament categories do not show any pattern. In general, landslides are observed in lesser proximity to the lineaments such as joints, faults, foliations, shear zones etc. Among the drainage buffer categories, positive contrast values were observed in case of 0-50 m, 50-100 m, 100-150 m and 150-200 m distances. The area is represented by a complex network of streams which are deeply dissecting and are major cause of landslides. During the rainy season, when stream (owing to steep gradients) flows are at peak, they erode its banks rapidly and landslides occur which may advance gradually. Negative contrast value was observed for >200m distance and it complies with the ground physical situation.

In the case of road buffer categories, positive contrast values were observed for 0-50 m and 50-100 m distances, whereas 100-200 m and >200 m distance resulted in negative contrast values. As mentioned in the Section 3.1.8, a large number of landslides were observed along the roads which were constructed by cutting the slopes randomly. Most of the cut slopes observed were found untreated (Figure 2.3 (e-f)). During monsoon, these cut slopes fail frequently and obstruct transportation. Most of the failed slopes are progressive in nature as observed in the field. High positive contrast values were observed for 0-100 m, 100-200 m and 200-300 m distance categories of reservoir buffer class. Reservoir water fluctuation (between El 750 to El 830 m saturates side slopes (banks) which cause landslides owing to the increased pore water pressure. These landslides progress to the upper reaches of the side slopes as observed in the field (Figure 2.3 (b-c)). Hence, these positive contrast values justifies the existing field conditions. Negative contrast values were observed for the higher distances to reservoir categories. As the distance increases, impact of the reservoir induced slope material saturation decreases hence failure probability decreases.

CHAPTER 4
LHZ MAPPING BASED ON HEURISTIC METHODS

4.1 Heuristic Method

Heuristic method is a qualitative method which is based on prior knowledge, field experiences, and expert judgement and it uses spatial information in explaining landslide prediction (Nilsen and Brabb 1977; Anbalagan 1992; Pachauri and Pant 1992; Sarkar et al. 1995; Gupta and Anbalagan 1997; Pachauri et al. 1998; Nagarajan et al. 2000; Lee et al. 2002; Saha et al. 2003; Sarkar et al. 2004; Anbalagan et al. 2014). Generally, a spatial information for the analysis includes topographic, geologic, geomorphic factors and land use/land cover (LULC). The data on spatial factors is collected using aerial photographs/satellite images in addition to field investigations. Ideally, experts identify set of field conditions for the geo-environmental changes. These factors are ranked based on their influence on the instability, then these qualitative conditions can be assigned suitable rating. Subjective weightings largely bank on the knowledge of a person or professional group responsible for landslide hazard analysis. Parameters chosen for LHZ analysis by a person or professional group are often not recognised by others, which is a major drawback of the heuristic approach. To limit the subjectivity in the heuristic model, Pachauri et al. (1998) and Nagrajan et al. (2000) suggested objective inputs namely, landslide density in each factor and regression analysis respectively. In Uttarakhand Himalayan region, a number of heuristic LHZ techniques have been adopted to delineate landslide probable zones (Anbalagan 1992; Gupta and Anbalagan 1997; Pachauri et al. 1998; Gupta et al. 1999; Saha et al. 2002; Sarkar et al. 2004; Anbalagan et al. 2008). In the present study two heuristic methods: a) GIS based weighted overlay method, and b) A modified landslide hazard evaluation factor (LHEF) based LHZ mapping method have been used for delineation of landslide probable zone.

4.2 Weighted GIS Overlay Method

This method is based on arithmetic overlay of weighted/ranked landslide factor maps in GIS domain. As suggested in the previous section, weight/rank is assigned

subjectively. In this study, weights and ratings of landslide factors and their classes were determined by considering landslide frequency ratio values. In general, landslide frequency ratio method of LHZ mapping comes under quantitative LHZ mapping approach (bivariate statistical). In those cases, frequency ratio values are directly used for ratings of the factor classes and rated factor classes are arithmetically overlaid to acquire LHZ map. In the present study, frequency ratio values are considered to subjectively rate the factor classes. Furthermore, some authors already considered landslide density to rate the factor class in heuristic models (Pachauri et al. 1998; Nagrajan et al. 1998; Nagrajan et al. 2000) and landslide frequency ratio also considers landslide density in factor classes. Thirteen terrain factors described in the data preparation section namely, geology, soil, LULC, Photo-lineament buffer, drainage buffer, road buffer, reservoir buffer, slope, aspect, relative relief, profile curvature, TWI and SPI were subjected to landslide frequency ratio. These factors are described in detail in section 3.1. Exhaustive field studies of the area resulted in the evaluation of factors with respect to the landslides. A general perception about the influence of factors on the landslides was made through the field evaluation. A certain degree of objectivity was introduced into this heuristic model by adopting landslide frequency ratio values to determine the ratings of each factor class. A simple scaling approach was adopted for the determination of ratings of the factor classes on an ordinal scale of 1 to 10 along with them, influence/weight of a particular factor towards the degree of landslide hazard was also awarded. Arithmetic overlay of terrain factors was performed in GIS domain which resulted in a landslide hazard index/landslide susceptibility index (LHI/LSI) map containing information about propensity to landslide of each pixel. LHI map was further divided into five relative hazard zone categories namely, very low hazard, low hazard, moderate hazard, high hazard and very high hazard zones by using Jenk's Natural Break classifier (ESRI, 2012). Validation of the model was performed on the basis of cumulative percentage/success rate curve and area under curve (AUC) technique. Further, a traditional method, comparison of landslide incidences with the computed hazard zones was also adopted to reflect the prediction capability of this heuristic model. (Figure 4.1)

4.2.1. Weights and ratings

Ratings of the each terrain factor classes were determined by considering landslide frequency ratio values. The frequency ratio is the ratio of the probability of an occurrence to the probability of a non-occurrence for given attributes (Bonham-Carter 1994). In the

case of landslides, it is defined as the ratio between the percentage of landslides in a factor class and percentage domain of that class. It works on the line of conditional probability in which frequency ratio > 1 reflects that relationship between landslide occurrence and the factor class is strong. Similarly, if the frequency ratio is < 1, then the relationship between the landslide occurrence and the factor class is weak (Lee and Sambath 2006). Frequency ratio of each factor class was calculated and is presented in Table 4.1. Further, percentage of frequency ratio (Fr) value of factor class with respect to the sum total Fr value of that factor was calculated. A methodology was then evolved to assign ratings to the factor class. Table 4.2 reflects the criteria adopted for the assignment of ratings. For a factor 'B', percentage of frequency ratio of their classes b_i ...b_n was matched with an ordinal scale, subjectively adopted to define ratings of the factor class (Table 4.2). The ordinal scale of 1 to 10 was assumed on the basis of an adopted range of b_{i-n} values (Table 4.2). According to the match of b_i to the adopted range, ratings (b_{ir}) were awarded. As Table 4.2 suggests, if b_i falls under 0 -5% range, rating 1 can be awarded and this evaluation was followed for each factor class. Weights were determined on the basis of sum of the Fr value of the factor classes. Suppose factors are B1, B2,..B13 and the Fr value of their classes are $B1_i$ .. $B1_n$, $B2_i$...$B2_n$,.... $B13_{i...}B13_n$ respectively then $\sum B1_{i\ to\ n}$ would be $B1_{SUM.}$ Following the same criteria, $B2_{SUM}$ to $B13_{SUM}$ were calculated. Percentage of $B1_{SUM}$ with respect to the $\sum(B1_{\ SUM} to\ B13_{SUM})$ was adopted as the weight/influence criteria '$B1_w$' for factor B1. Figure 4.1 refers to the flowchart of the general methodology adopted for LHZ mapping.

4.2.2. LHZ mapping

Landslides are influenced by the combined impact of a number of geo-environmental processes even though exact mechanism of landslides is yet to be explained. There is high degree of uncertainty involved in the prediction of the landslides. In the present case, the ordinal scale (subjective) rating system and Fr induced weighting system was adopted for LHZ mapping. Factor classes were assigned the associated rating values in the GIS domain and reclassified factor map representing rating value was generated for each factor. These reclassified maps were further multiplied by the corresponding weights and then summed up to compute the LHI map representing hazard information on cell by cell basis. The weighted overlay capabilities of Arc GIS 9.3 software were used to compute LHI.

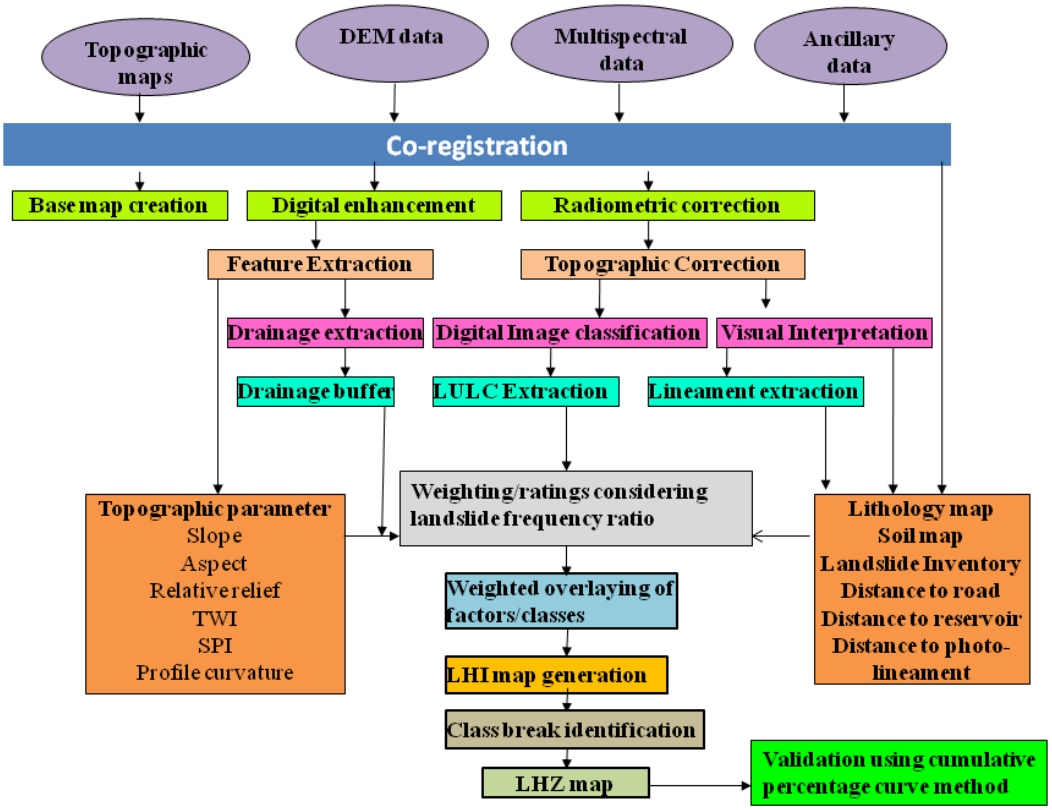

Figure 4.1 Methodology flowchart for LHZ mapping using GIS based weighted overlay method

The LHI is computed using the formula given below:

$$\text{LHI} = \sum(Factor\ Weights\ \times class\ ratings) \tag{4.1}$$

LHI map was then subjected to Jenk's Natural Break classification for producing a LHZ map (Figure 4.2) containing very low hazard, low hazard, moderate hazard, high hazard and very high hazard zones. Figure 4.3 refers to the heuristic model generated percent domain of LHZ represented in the area.

Table 4.1: Frequency ratio of terrain factor classes and influence of factors based on landslide inventory

Factors and classes	Frequency	Percentage	Weight (%)	Rating
Geology				
Blaini Formation	**0.297**	6.18	5	2
Nagthat Formation	0.79	16.45		3
Chandpur Formation	1.74	36.25		5
Berinag Formation	0.683	14.229		2
Deoban formation	0.378	7.875		2
Mandhali formation	0	0		1
Rautgara formation	0.87	9.416		2
Soil cover				
Alluvial/sandy Loam	3.152	73.851	4.6	8
Forest Soil/Black Clay	1.008	23.617		3
Sandy Loam	0.108	2.530		1
Relative Relief				
Very low	0	0	7.15	1
Low	0.09	1.269		1
Moderate	0.882	12.44		2
High	3.164	44.632		5
Very high	2.953	41.65		5
Slope angle				
0°-8°	0	0	7.5	1
8°-18°	0.062	0.851765		1
18°-30°	0.64	8.792417		2
30°-42°	3.996	54.89765		6
>42°	2.581	35.45817		5
Photo lineament buffer				
0 – 50 m	0.283	5.818257	5.1	2
50 – 100 m	0.66	13.56908		2
100 – 150 m	0.705	14.49424		2
150 – 200 m	2.316	47.61513		5
>200 m	0.9	18.50329		3
Drainage Buffer				
0 – 50 m	2.718	24.12569	11	3
50 – 100 m	2.143	19.02184		3
100 – 150 m	1.628	14.45056		2
150 – 200 m	4.182	37.12054		5
>200 m	0.595	5.281378		2
Land Use/ Land Cover				
Dense forest/Vegetation	0	0	5.1	1
Scrub/Open forest	2.19	44.49411		5
Agricultural land	1.747	35.4937		5
Settlement/ Barren Land	0.985	20.01219		3
Water Body	0	0		0
Topographic Aspect				
North	0.816	10.15178		2
Northwest	0.3	3.732272		1

West	0.629	7.82533	8	2
Southwest	0.95	11.81886		2
South	2.678	33.31675		4
Southeast	1.349	16.78278		3
East	0.84	10.45036		2
Northeast	0.476	5.921871		2
Flat	0	0		1
TWI				
5 - 8	0.543	4.386815	12	1
8- 12	1.353	10.93068		2
12 - 16	6.6	53.32041		6
16-19	3.882	31.36209		4
SPI				
1.5 - 3	0.603	13.83028	4	2
3 - 6	1.813	41.58257		5
6 - 9	1.944	44.58716		5
9 - 12	0	0		1
12 - 15	0	0		1
Slope profile curvature				
Concave	0.946	47.27636	2	5
Convex	1.055	52.72364		6
Road Buffer				
0 -50 m	6.56	52.75008	12	6
50 -100 m	4.136	33.25828		4
100-200 m	1.27	10.21229		2
>200 m	0.47	3.77935		1
Reservoir Buffer				
0- 100 m	6.17	38.80503	15	5
100- 200 m	5.29	33.27044		4
200- 300 m	2.23	14.02516		2
300- 400 m	0.63	3.962264		1
400- 500 m	1.07	6.72956		2
>500 m	0.51	3.207547		1

Table 4.2: Criteria adopted for assignment of ratings of the factor classes

Percentage domain of Fr in each factor	Ordinal rating
0 - 5%	1
5 - 15%	2
15 - 25%	3
25 - 35%	4
35 - 50%	5
50 - 60%	6
60 - 70%	7
70 - 80%	8
80 - 90%	9
90 - 100%	10

4.2.3. Validation

Validation was performed to obtain the accuracy of the LHZ map. Accuracy of LHZ method is the capability of a map to delineate landslide free and landslide prone areas. Comparison of different models and model parameter variables can also be done from validation (Begueria 2006). Accuracy and objectivity depend on the model accuracy, input data, size of the study area and experience of the earth scientist (Soeters and Van Westen 1996). In the present study, cumulative percentage curve/success rate curve technique was used to validate the LHZ map. Cumulative percentage curve is achieved by plotting cumulative percent of LHI in descending order against the cumulative percentage of landslide (on all 195 locations) on X and Y axis respectively. Figure 4.4 indicates that 43% of the landslides fall under first 20% of the high LHI value pixels whereas 22% landslides fall under next 20% of LHI owing to relatively lower values and indicates that 43% of the landslides fall under first 20% of the high LHI value pixels whereas 22% landslides fall under next 20% of LHI owing to relatively lower values and accordingly other values follow. In this way, percentage cumulative curve clearly state the accuracy of the LHZ. Further, AUC value of the accuracy curves were calculated by simple trapezium method. AUC value of 0.71 was computed from the cumulative curve, and it can be said that 71% accuracy was achieved in this case. Apart from this, comparison of landslide incidences with the computed hazard zones was also adopted to reflect the prediction capability of this heuristic model (Figure 4.5). This comparison reflects that very high and high hazard zones occupy 5.4% of the total area and almost 55% landslides observed in these areas. Very low and low landslide hazard zones occupy almost 52% of the area with 28% landslides. From this comparison, it can be said that this LHZ mapping method has good success in predicting landslide incidences.

4.2.4. Discussion

LHZ map adequately reflected landslide probable zones present in the area along with the relationship of terrain factor with the landslides. The very low hazard zones are found to be present at flatter terrains such as terraces, build-up areas etc. They are also found in terrains supporting thick vegetation cover. Thick vegetation cover was observed mostly in north-western and south-eastern part of area and are associated with inhabited high ridges. Low to very low hazard zones are reflected at talus slopes which are made relatively flatter for agricultural practices.

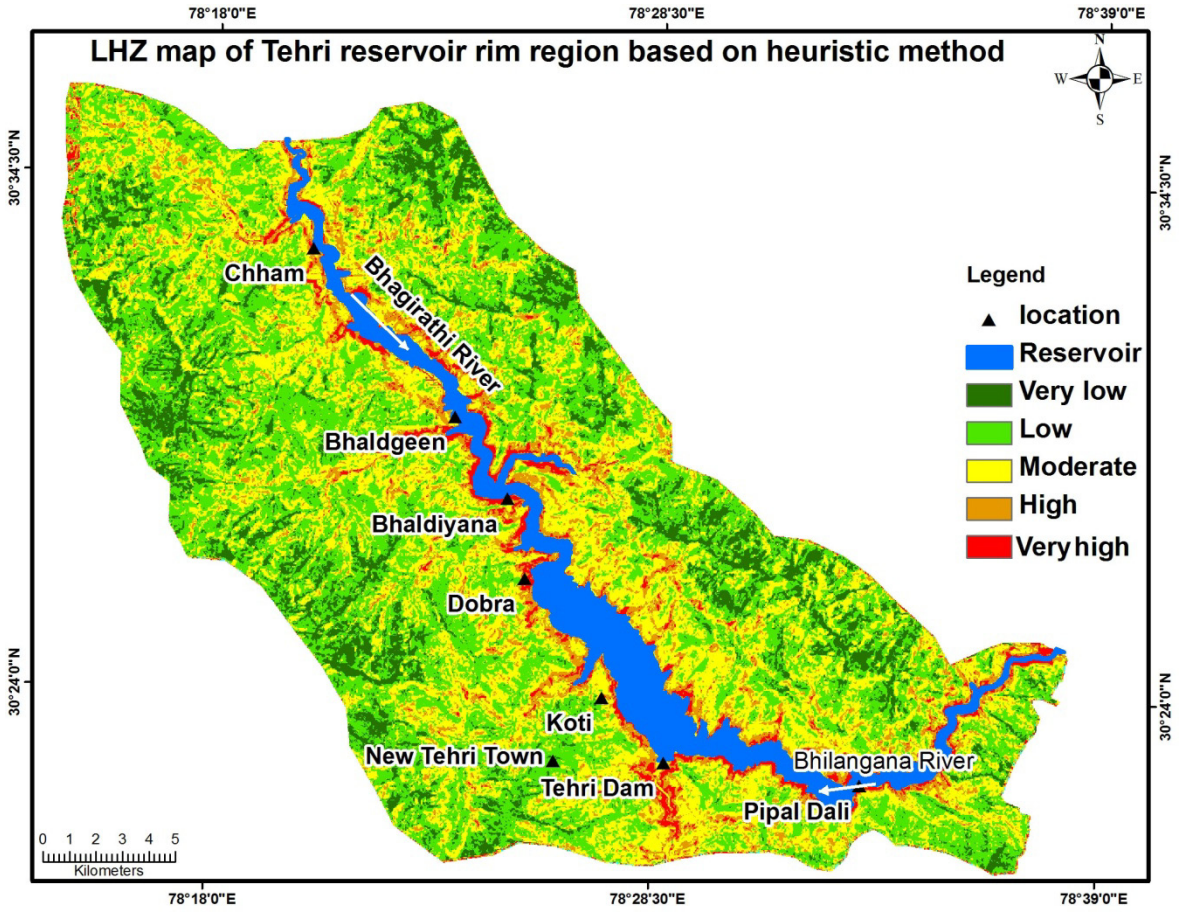

Figure 4.2 LHZ map of Tehri reservoir rim region based on GIS based weighted overlay method

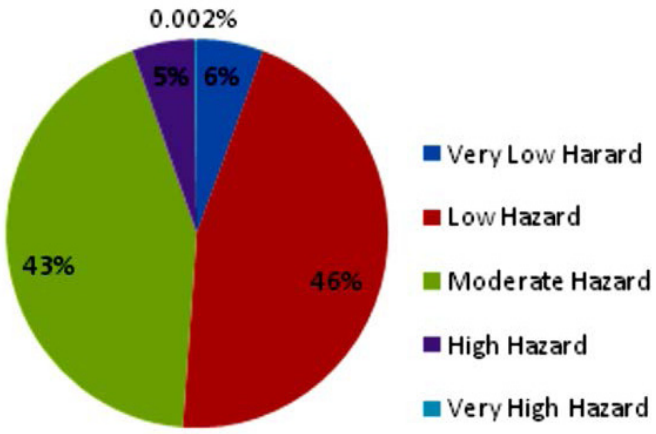

Figure 4.3 Distribution of relative landslide hazard zones computed on the basis of GIS based weighted overlay method

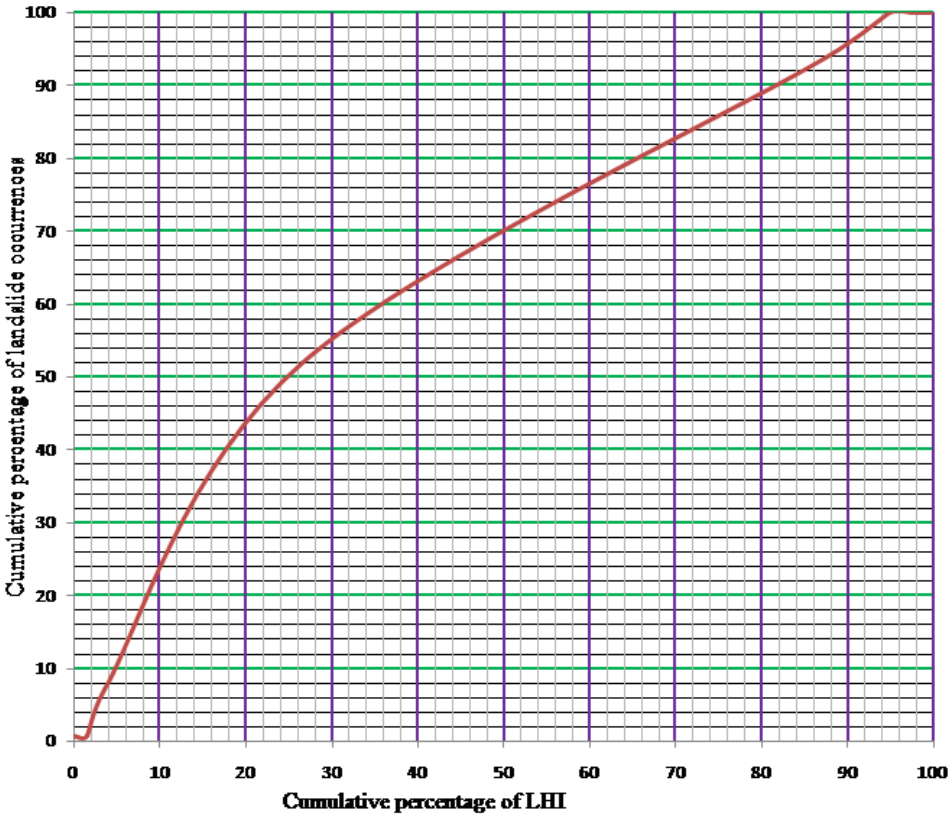

Figure 4.4 Cumulative percentage curve representing variation of landslide occurrence with respect to LHI. Note: The values are set in descending order which means 0-10 represents initial 10% of high LHI values.

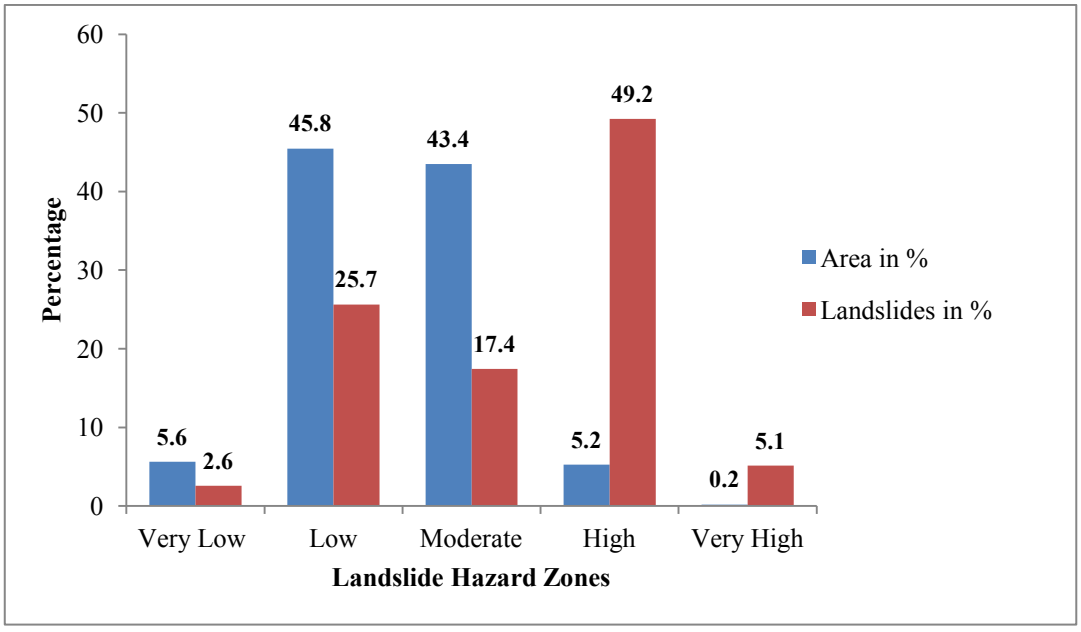

Figure 4.5 Bar diagram representing area of relative hazard zone with respect to associated number of landslide occurrences

Moderate hazard zones reflected in the LHZ map are those terrains, which are made up of gentle slope angles. A number of villages are present in these kind of terrains in the Tehri reservoir rim area. Most of the settlement areas are reflected as moderate hazard zone in the LHZ map.

High and very high landslide hazard zones are found along the side slopes adjoining the reservoir, road network, lesser proximity to drainage, lesser proximity to photo-lineament, steeper slopes and ridges.

Among the slope classes, most of the very high and high hazard zones are observed in very high and high slope angle classes. Very high and high hazard zones are also observed in high and very high relative relief classes. Southern aspect of the study area, which is receiving excessive sun radiation and high rainfall, are observed under higher hazard zones. Incidentally, a number of agricultural terraces are present on the southwest facing slopes leading to more instability. Among the secondary topographic parameters, higher hazard zones are observed in the higher TWI and SPI ranges. Very high and high hazard zones are also observed in the areas in closer proximity to drainages (drainage buffer). In case of geology classes, high and very high hazard zones are observed in the rocks belonging to Chandpur and Nagthat Formation whereas lower hazard zones are observed in rocks belonging to Blaini, Mandhali, and Deoban Formations. Alluvial soil has been observed at lower elevations along the drainage network and is not well compacted and it leads to slope failures which is manifested in the form of high hazard zone in the LHZ map. Very high and high hazard zones are observed all around the fringes of the reservoir rim owing mainly to the process of reservoir side slope settlement process. Road network and other infrastructures are observed along the reservoir rim boundary. Among the distance to road classes, high hazard zones are observed all along the areas in closer proximity to road. Combined effects of unplanned construction and reservoir side slope adjustment process results in a number of landslides during monsoon season which is reflected in the LHZ map.

4.3 Modified BIS (LHEF) Method

4.3.1 Introduction

The LHEF rating scheme is an empirical approach in engineering geological perspective but in more generalized terms, it best fits in the heuristic model. This approach was adopted by the Bureau of Indian Standard (BIS 1998) for practicing LHZ/LSZ

mapping in the hilly terrains of India at micro scale (1:25000 - 1:50000). It assumes the gross influence of six causative terrain factors: slope morphometry, lithology, structure, hydrogeological condition, relative relief and LULC and provides a rating for each factor called landslide hazard evaluation factor rating (LHEF). These fixed ratings are relative ratings (varying according to the sub-categories of factors) and it does not consider the landslide incidences. One of the important inputs to the LHEF based method is the 'uniform terrain unit called slope facet'. Slope facet is a terrain unit having similar slope characteristics and is bordered by natural features such as streams, ridges, spars, depressions etc. In general, slope facets are delineated from the topographic map. For each slope facet, nature of the six factors are determined and rated according to the LHEF rating then sum total of the six parameters are calculated which is also called total estimated hazard (TEHD). To get the relative hazard zones, the TEHD values are categorized according to the Table 4.11.

4.3.2 Methodology

In the present study, a modified BIS approach was adopted to compute landslide hazard zones. Modification involved inclusion of external factors: seismicity and rainfall along with photo-lineaments. The individual inherent causative factors considered in the present study are geology, photo-lineament density, LULC, slope morphometry (relative relief, slope angle) and hydro-geological condition whereas seismicity and rainfall are considered as external factor classes. In general, slope facets are delineated from the topographic map. In this study, facets were determined from DEM derived digital terrain model (DTM). Figure 4.6 (a-c) refers to the facet map. In this study, a number of photo-lineaments present in the each facet were considered as a substitute for structural parameters. For a large and highly rugged area with facets exceeding up to 126, it takes tremendous amount of field work to acquire all the structural data (joints, foliations, beddings etc.) needed for the LHEF rating. Photo-lineaments, as described in chapter 3, including linear features such as ridges, spars, deep dissected valleys, shear zones, faults etc., are observed from the imageries. Facet wise lineament density was calculated and normalized on the scale of 0–2 to award ratings. The entire study area was divided into 126 facets (Figure 4.6 (a-b)). One or more sub-categories of causative factors were represented in the slope facet and were awarded ratings according to their inherent characteristics (Table 4.3). TEHD for each slope facet was then calculated by adding all the rated sub-categories of the factors present in the individual facets. Relative hazard zones were

determined by categorizing TEHD values of all the slope facets. Prediction capabilities of this model were performed on the basis of cumulative percentage curve. Cumulative percentage of the TEHD value of facets were arranged in descending order on a spread sheet and in the next column of the spread sheet, cumulative percent of landslides present in the corresponding slope facet was arranged which resulted in a cumulative percentage curve. AUC value of the curve was calculated and converted into percent prediction accuracy of the model. A general methodology of this study is presented in the Figure 4.7.

4.3.3 Lithology

The lithology is an important factor in controlling the stability of rock slopes and the maximum LHEF rating of 2 is given under this category. The lithology governs the nature of the mass movement and the ratings are awarded accordingly. Under the LHEF scheme lithology is broadly classified into three categories. Type-I rocks consist of crystalline rocks (igneous and metamorphic) and massive calcareous rocks. Well and poorly cemented terrigenous sedimentary rocks belong to Type-II categories of rocks. Type-III category comprises soft argillaceous rocks and their low grade metamorphic equivalents along with well foliated gneissic rocks. Soft rocks like claystone, siltstone, mudstone, shale, slate, phyllite and other such rocks erode much faster and are easily weathered close to the surface (Chakraborty 2008). In other rocks such as slate, phyllite and schistose, rocks have well defined foliation plane along which sliding often takes place.

Provision of correction factor is also available for the weathered fresh rocks belonging to Type I and Type II in the LHEF rating system. There is also a provision for the increment of rating values of Type III rocks in extreme conditions. Table 4.4 refers to the ratings assigned to the different rock types. During the field investigations, different rock types and their weathering status have been studied. Rock formations present in the area are depicted in Figure 4.8, and their inherent litho types are referred in Table 4.4. The dominant rock types present in the study area are phyllite and quartzite. The other lithological units observed in the area are mentioned in Table 4.4. These units are quartzitewith minor bands of phyllite, phyllite with minor bands of quartzite, limestone, alternating bands of quartzite and phyllite, limestone intercalated with slates and siltstone, weathered quartzite intercalated with slate, low grade lustrous phyllite, black carbonaceous pyretic phyllite and metavolcanic rocks.

Table 4.3: Factors considered under LHEF rating based LHZ mapping

Landslide causative factors			Maximum LHEF rating
Inherent factors	Geology	1. Lithology	2.0
		2. Structure	2.0
	3. Slope parameter		2.0
	4. Land use and land cover		2.0
	5. Hydrogeological conditions		1.0
External factors	6 a) Seismicity 6 b) Rainfall		1.0 (=0.5 + 0.5)
Total			**10.0**

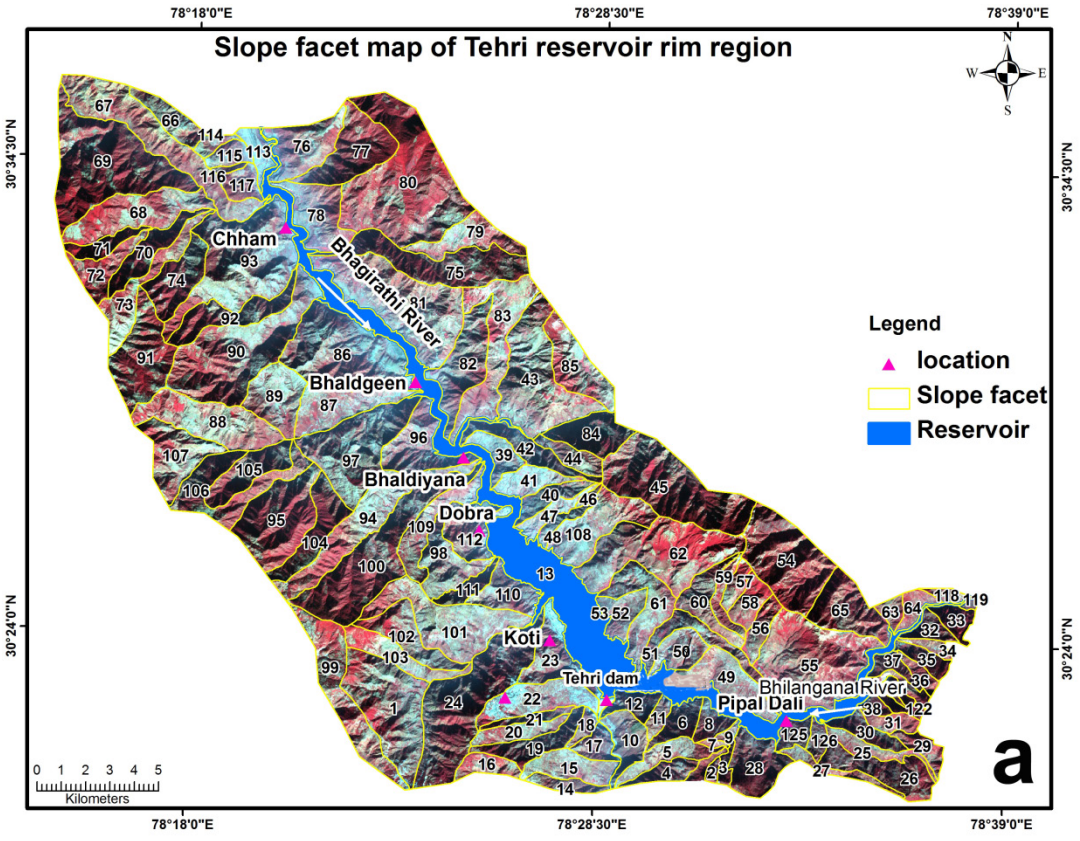

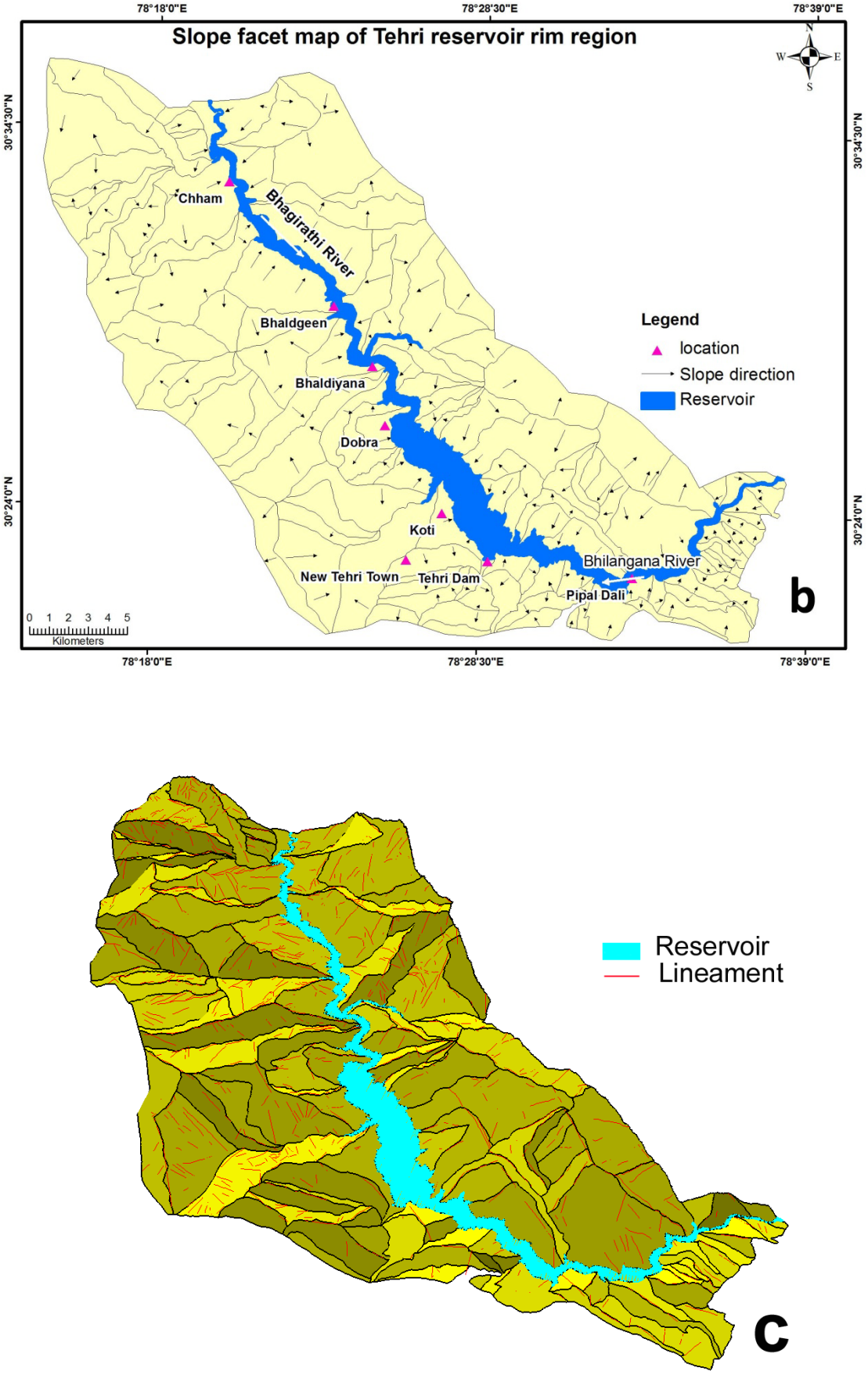

Figure 4.6 a) Slope facet map, b) slope facet map showing the direction of slope, c) Digital terrain model of the study area on the basis of which facets were demarcated.

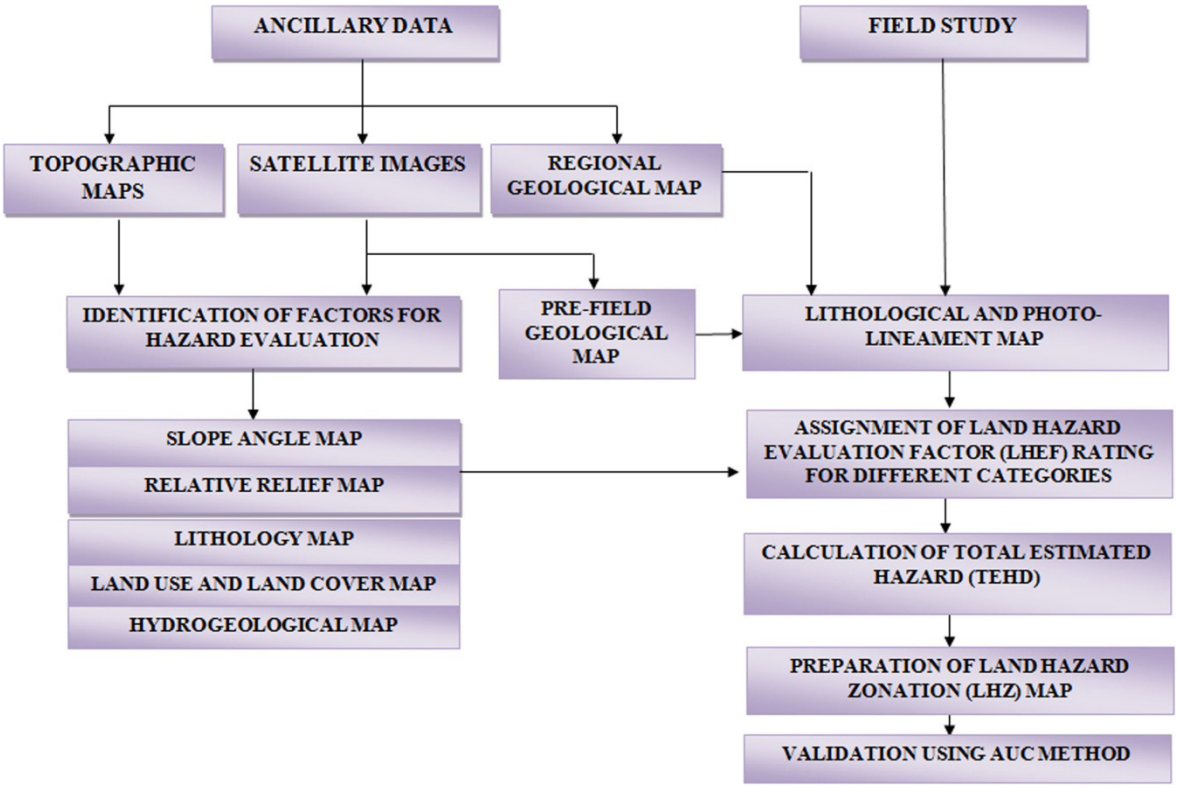

Figure 4.7 Methodology flowchart of LHZ mapping based on LHEF based rating scheme

Phyllites cover the major part of the study area and are exposed mainly on both the banks of Bhagirathi River. These rocks are generally vulnerable to the weathering and are present in the valley region. The second most dominant rock exposed in the study area is quartzites. These rocks are generally, hard, compact and form steep slopes on the higher reaches of the region. Quartzites are exposed as a thick band starting from northwest through the central region and extend up to southern part of the area. Quartzites with minor bands of phyllites are weak in comparison to quartzites. These rocks are mostly exposed in the central region of the area. Phyllites with minor bands of quartzites, mainly occupy the northern region. These rocks are also exposed on both sides of the Bhagirathi River in the south-eastern corner area. Using BIS (1998) guidelines for the ratings of the rock types, ratings were awarded and are presented in Table 4.4

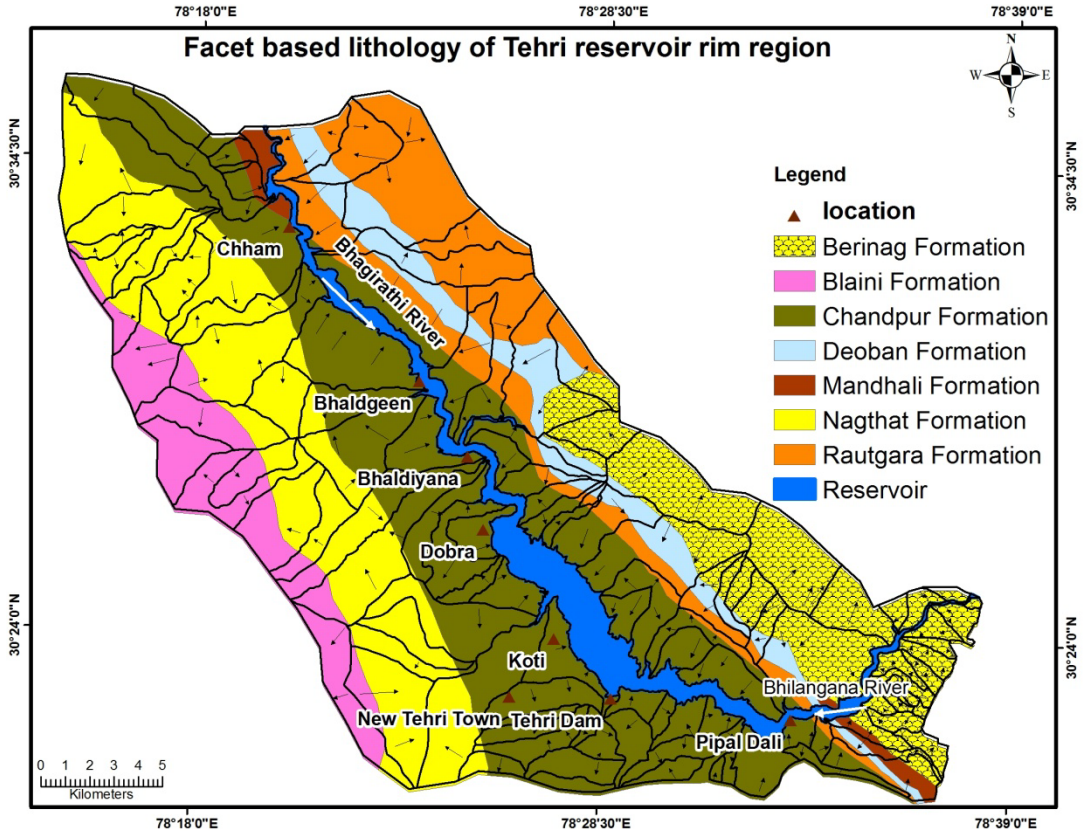

Figure 4.8 Facet based lithological map of Tehri reservoir rim region (Valdiya 1980)

Table 4.4: LHEF ratings awarded to rock types represented in Tehri reservoir rim region

S. No.	Formations	Rock type	Gross Ratings
1	Blaini Formation	Quartzite, limestone, slates, phyllites &	0.6
2	Berinag Formation	Weathered quartzite intercalated with slate	0.8
3	Nagthat Formation	Weathered quartzite intercalated with slate	1.2
4	Chandpur Formation	Low grade lustrous phyllites	1.4
5	Mandhali Formation	Black carbonaceous pyretic phyllite	0.5
6	Deoban Formation	Dolomitic limestone with phyllitic intercalations	0.8
7	Rautgara Formation	Quartzite, slate, metavolcanic rocks	1

4.3.4. Geological structure

Instability of rugged terrains consisting of *in-situ* rocks is mainly dependent on the correlation between direction of the slope and attitude of dominant discontinuities (Chakraborty 2008). Geological discontinuities include both primary and secondary discontinuities like bedding, foliation, schistosity, joints, shear zones, folds, faults etc. Translational and toppling failures are generally considered for assigning ratings to a facet. Translational failure comprises of plane and wedge failures whereas toppling failure

considers block and wedge topple. In the present study, high resolution satellite data including DEM was used to extract photo-lineaments and density of photo-lineaments within a particular facet was used as a criteria for rating under structural categories (Figure 4.6c). Lineament density was calculated by dividing the number of lineaments present in the slope facet by the area occupied by the facet. Lineaments, which were found to be overlapping in two facets, were accounted for in both the facets according to their fraction in the slope facet. As mentioned in the data preparation section, photo-lineaments were extracted from the multispectral data as well as the DEM by applying image analysis techniques. Frequency of the photo-lineaments found in different facets is depicted in Figure 4.9. Ratings were assigned by normalizing the lineament density value of the facets in a range of 0 – 2. Ratings were then categorized into very favorable, favorable, fair, unfavorable and very unfavorable classes (Figure 4.10) according to the ranges mentioned in the Table 4.5 (BIS 1998).

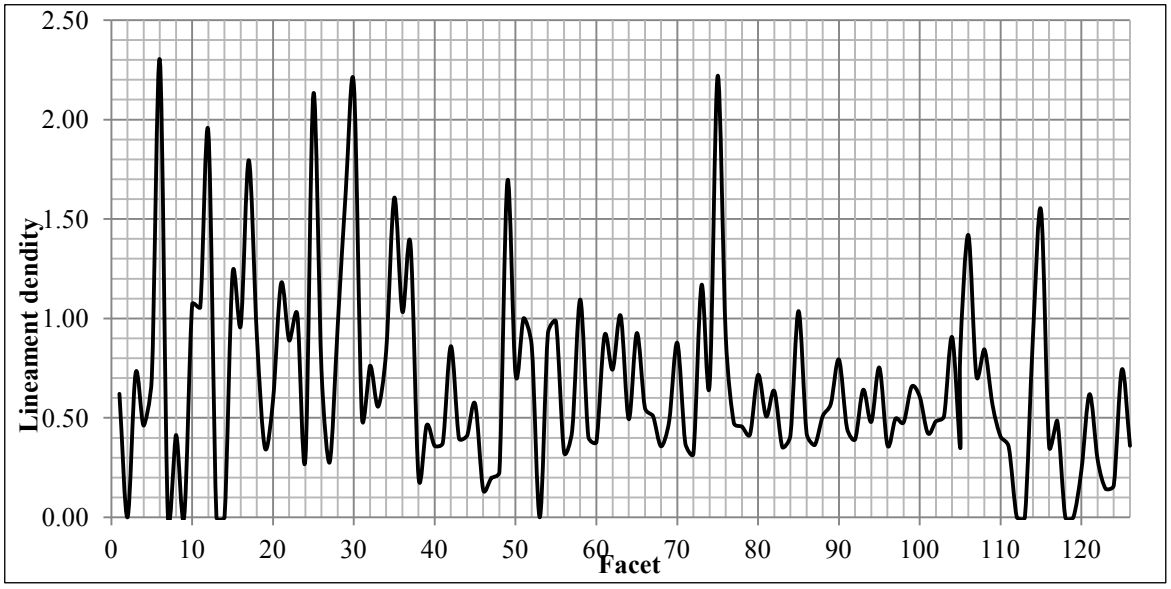

Figure 4.9 Frequency of lineament density present in each facet

4.3.5 Slope parameter

Under the LHEF rating system, slope parameter is divided into slope morphometry and relative relief and their combined maximum rating is given as 2. A matrix based system was adopted to compute the combined rating of the slope parameter category (Table 4.8).

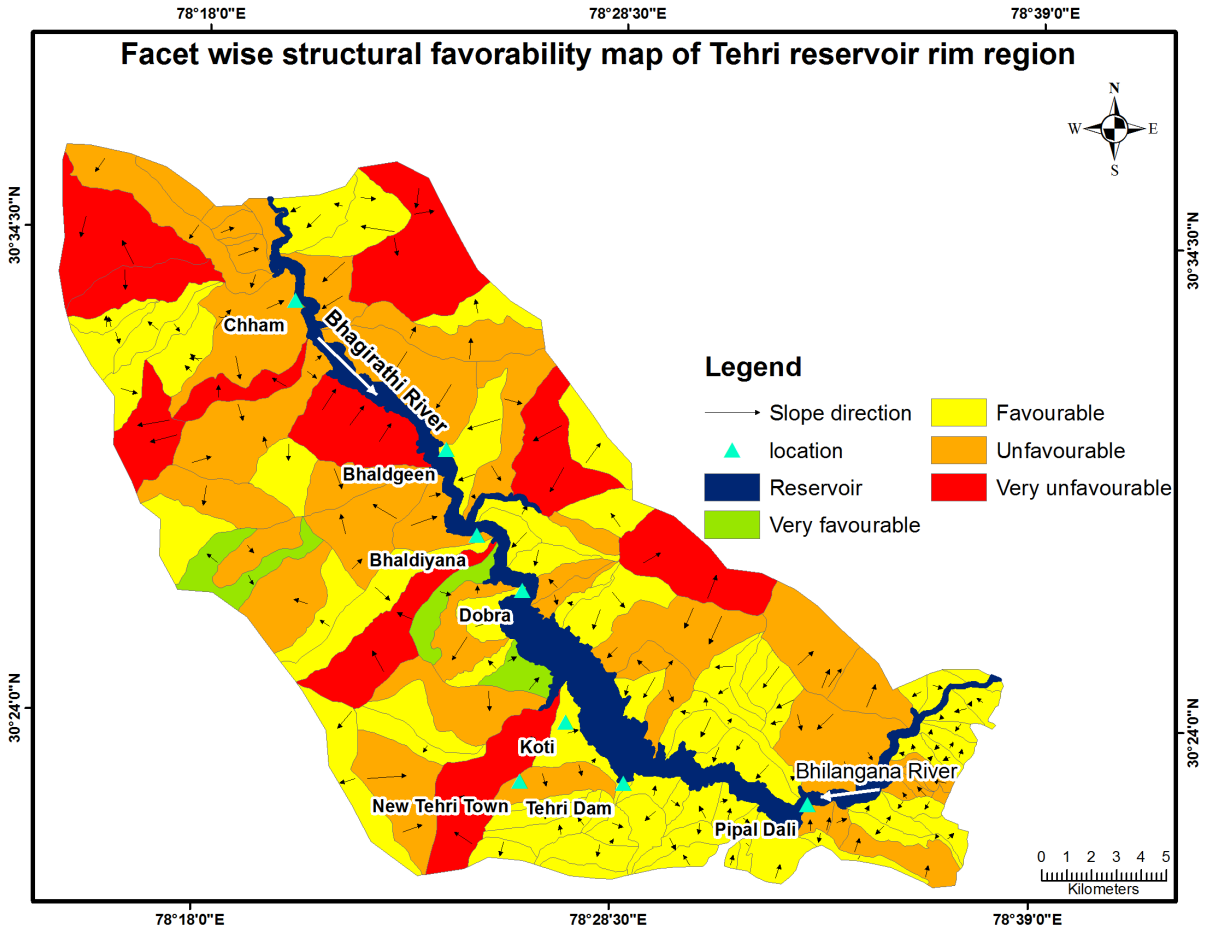

Figure 4.10 Facet wise structural favorability map of Tehri reservoir rim region

Table 4.5: Range of structural favorability adopted under LHEF rating scheme

Structure Class	LHEF rating (out of 2)	Description
I	Rating ≤ 0.7	Very Favourable
II	0.7 < Rating ≤ 1.05	Favourable
III	1.05 < Rating ≤ 1.4	Fair
IV	1.4 < Rating ≤ 1.75	Unfavourable
V	Rating > 1.75	Very Unfavourable

a) Slope morphometry

Facet wise slope map of the area was prepared covering five classes required for the LHEF rating system (Figure 4.11) (Table 4.6). This classification scheme is different from that discussed in section 3.1. DEM data was used to compute the slope category of each facet. Continuous raster slope angle data within a particular facet was averaged and the

resultant was used as slope angle parameter for the facet in question (Figure 4.11). Maximum rating of 2 is assigned for slope morphometry in LHEF system.

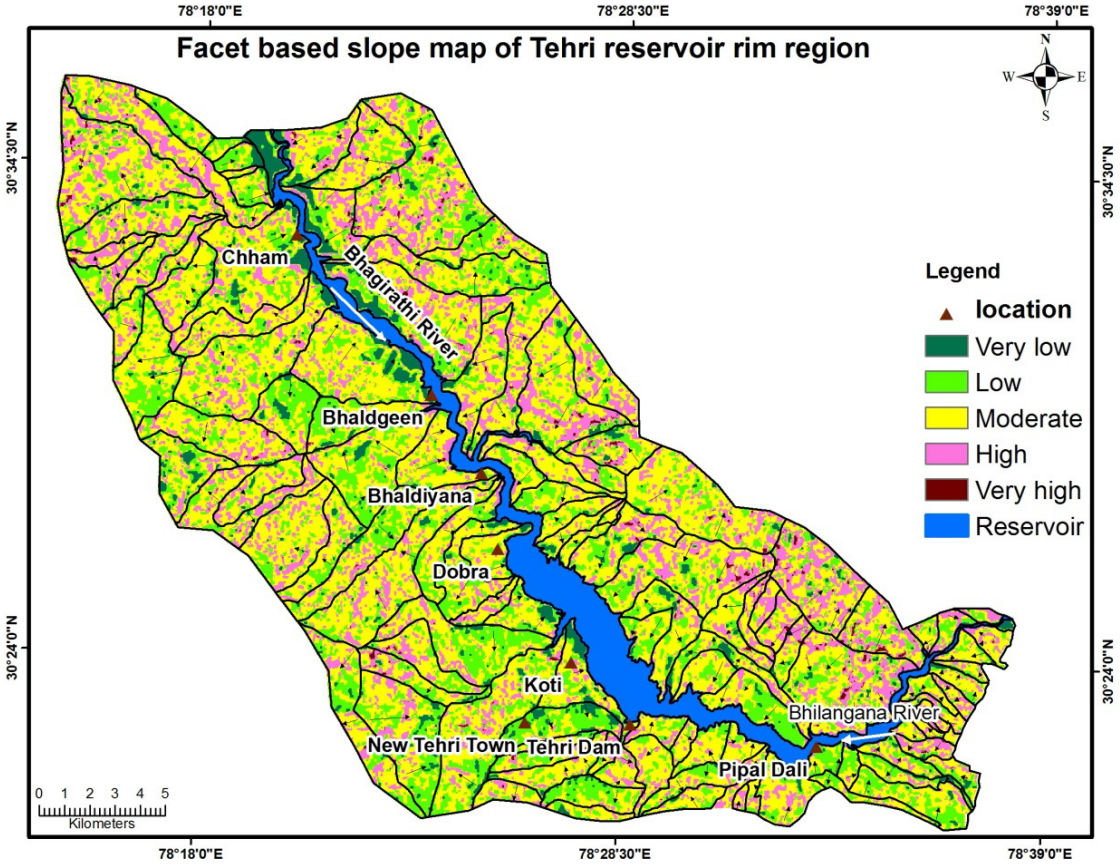

Figure 4.11 Facet based slope map of Tehri reservoir rim region

Table 4.6: Slope classification under LHEF rating scheme

Slope type	Slope Angle	Class
Very low slope	< 15°	A
Low slope	16 – 25°	B
Moderate slope	26 - 35°	C
Steep slope	36 - 45°	D
Very steep slope	>45°	E

b) Relative relief

Relative relief is the difference between the maximum and minimum elevation of the slope facet and is assigned a maximum rating of 2. Table 4.7 represents different classes of relative relief considered in the LHEF rating approach and based on that Figure

4.12 is the relative relief map of the study area. But it is different from relative relief classes mentioned in section 3.1

Table 4.7: Relative relief classification under LHEF rating scheme

Relief classes	Relative relief (m)	Class
Very low	< 50	I
Low	50 - 100	II
Medium	101 – 200	III
High	201 - 300	IV
Very high	> 300	V

The combination of slope angle and relative relief rating value was determined by setting a matrix form (5×5) in which slope morphometry was kept in rows and relative relief was kept in columns (Table 4.8). The LHEF ratings increase from left to right in rows while they decrease from top to bottom in columns. This reflects that out of the two factors, slope morphometry is given more weightage over relative relief. Following the above mentioned approach, ratings of the slope parameters were assigned and found to be varying in a range of 0.52 to 1.87 (Figure 4.13).

Table 4.8: A matrix adopted for awarding ratings to slope parameters under LHEF rating scheme

Slope parameter		a) Slope morphometry classes				
		A (< 15º)	B (16–25°)	C (26-35°)	D (36-45°)	E (> 45°)
b) Relative relief classes	I (< 50m)	0.5	0.9	1.3	1.5	1.8
	II (50 -100m)	0.6	1.0	1.4	1.6	1.9
	III (101-200m)	0.7	1.1	1.5	1.7	1.95
	IV (201-300m)	0.8	1.2	1.55	1.75	2.0
	V (> 300m)	0.9	1.3	1.6	1.8	2.0

4.3.6 Land use/land cover

Entire area was classified into five LULC classes namely, agricultural land, dense forest, scrub forest, settlement and water body (Figure 4.14). Ratings of the LULC categories were awarded on the basis of LHEF rating scheme (Table 4.9). If more than one type of LULC pattern is present in a single slope facet, the fraction area of each LULC pattern with respect to slope facet area has been calculated and multiplied by their

respective ratings and added to get the LHEF rating of the facet. Figure 4.15 shows the frequency of ratings of LULC assigned to the facets.

4.3.7 Hydrogeological condition

Ground water generally does not have uniform pattern in hilly terrain and it is usually channelized along weak planes of rocks. The observational evaluation of the ground water behaviour in hill slopes is not possible over large areas. In order to make quick appraisal, surface expression of ground water was considered for LHZ mapping. Surface indication of ground water such as flowing, dripping, wet, damp and dry were used for LHEF purpose. To assess the probability of worst hydrogeological condition, post monsoon terrain observation was considered for the rating.

In case of slope facets showing wet, damp and dry conditions, the dominant type of hydrogeological conditions were assessed and the rating awarded. The fractional ratings were calculated to get the total LHEF rating for each slope facet. Table 4.10 depicts the rating scheme adopted for the hydrogeological conditions. Three hydrogeological conditions namely, dry, dry to damp and damp were observed on the basis of their surface expressions (Figure 4.16).

Table 4.9: LHEF ratings adopted for land use/land cover classes

LULC classes	Rating
Agricultural land	0.65
Dense forest area	0.80
Scrub forest area	1.50
Settlement/ barren land	1.70

Table 4.10: Ratings adopted for hydrogeological conditions under LHEF rating scheme

Hydrogeological condition on slope	Rating
Dry	0.0
Dry to damp	0.1
Damp	0.2

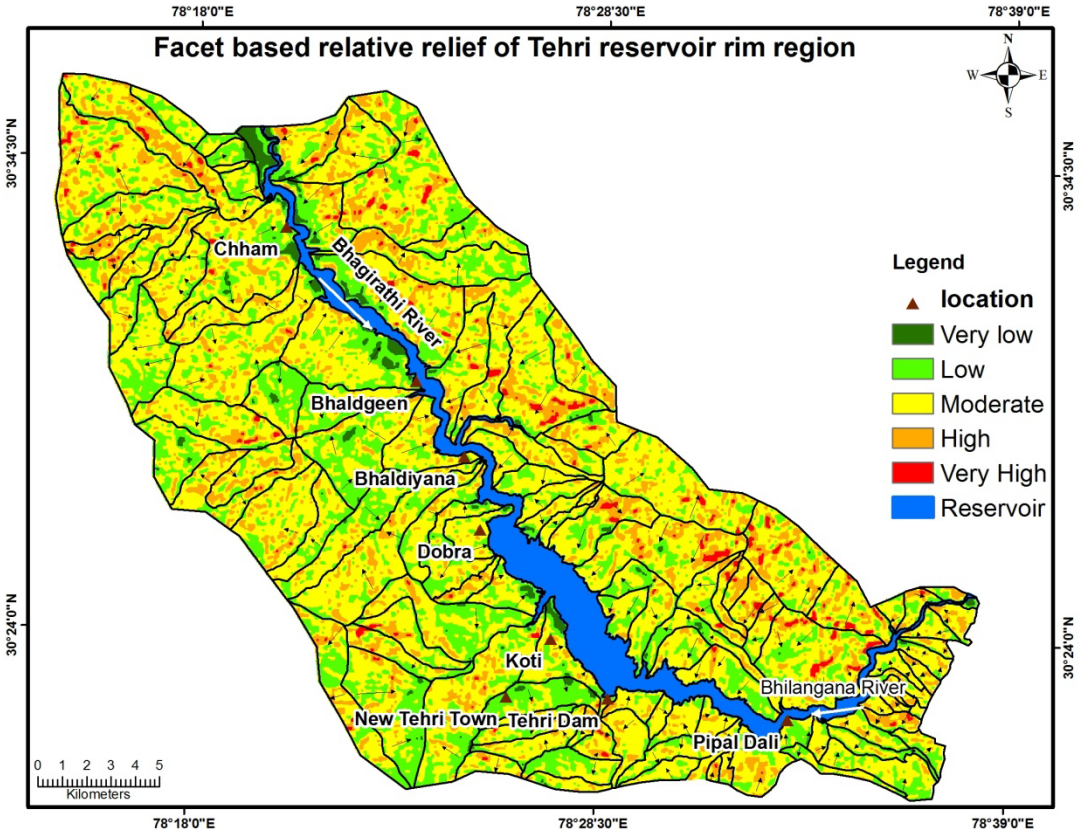

Figure 4.12 Facet based relative relief map of Tehri reservoir rim region

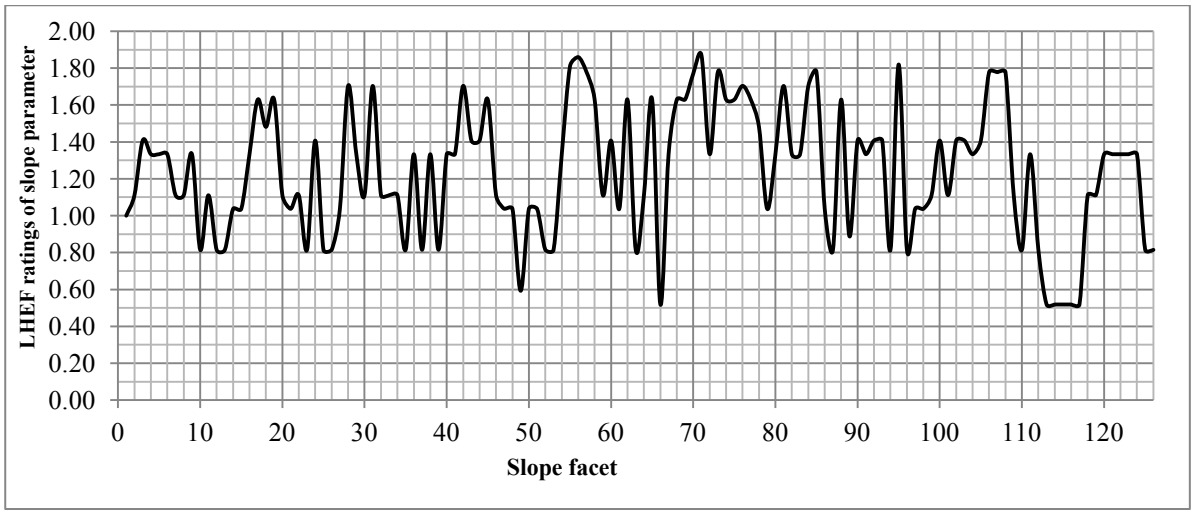

Figure 4.13 Frequency of LHEF ratings of slope parameters derived from the matrix

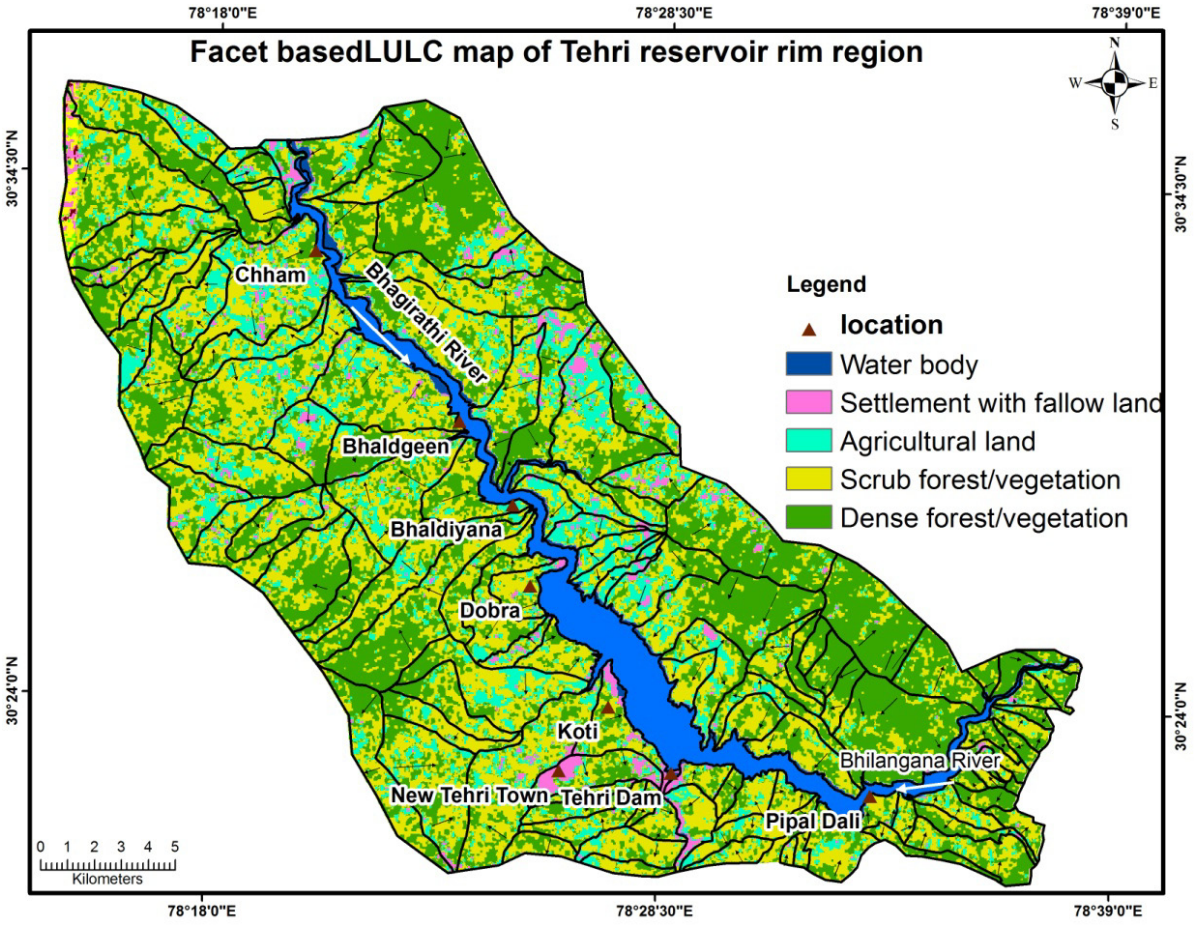

Figure 4.14 Facet based LULC map of Tehri reservoir rim region

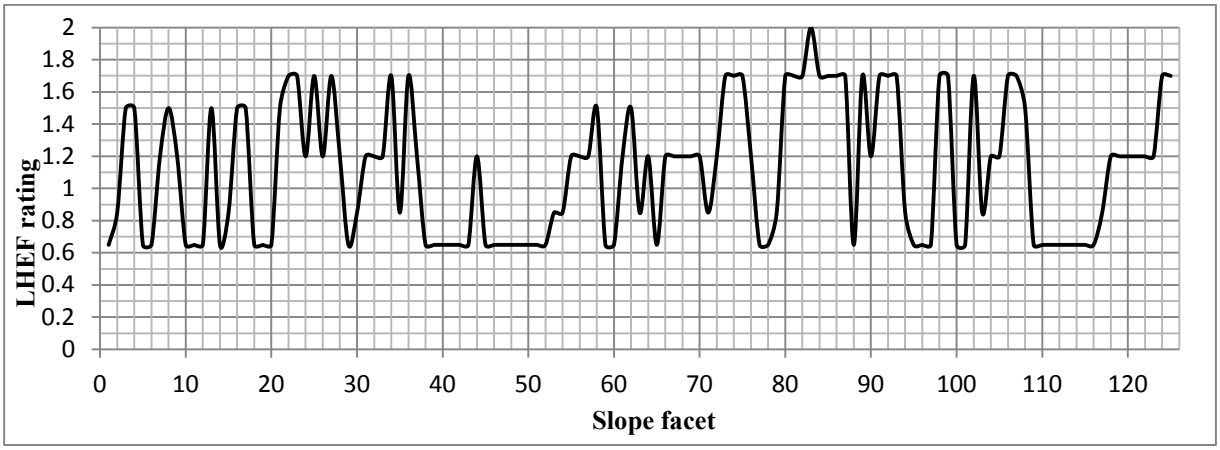

Figure 4.15 Frequency of LHEF ratings of LULC classes present in each facet

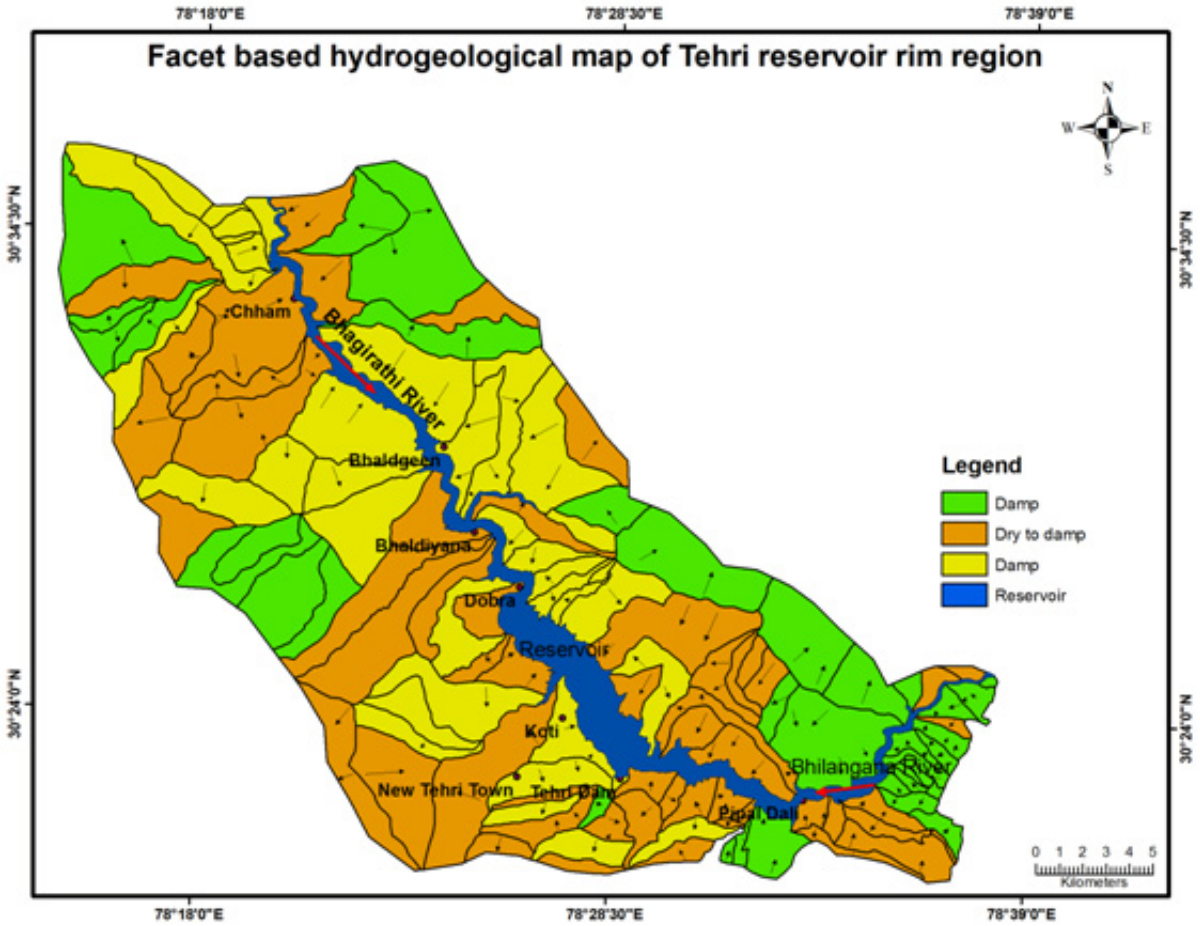

Figure 4.16 Facet based hydrogeological map of Tehri reservoir rim region

4.3.8 External factors

External factors such as earthquakes and rainfall can induce landslides and are called triggering factors. Their effect is conspicuous over a large area and it is obvious that their effect will not vary from facet to facet (Anbalagan et al. 2008). A facet which is stable under current slope situation might become instable if it falls under high earthquake prone or high precipitation zone and may result in landslide phenomenon. Following an intense precipitation, chances of abrupt increase in pore water pressure becomes inevitable. Slope facets owing to high pore water pressure may also induce landslides. It is understandable that in case of a slope facet falling in high annual precipitation zone and also high earthquake activity (as in the case of Himalaya); propensity of landslide hazard may get enhanced. Maximum rating of 1 is awarded to the external factors and is equally divided between seismicity and rainfall. The present study area falls under seismic zone-IV (BIS 2002) and also receives moderate to high precipitation uniformly throughout the area hence a rating of 0.8 was awarded to each facet.

4.3.9 Data integration and TEHD

TEHD reflects the general situation of instability of a terrain and is computed for each facet by adding the LHEF ratings of inherent parameters and external parameters. The calculated TEHD value can vary widely between different facets depending on the condition of instability of the respective facets (Anbalagan et al. 2008). In this case, TEHD values were found to be varying between 4.45 to 7.6 (Figure 4.17).

Total Estimated Hazard (TEHD) = LHEF Ratings of [(lithology + structure + slope morphometry + relative relief + LULC + hydrogeological conditions + External parameters (seismicity and rainfall)

The LHZ map of the present area is prepared on the basis of calculated TEHD values of the facets (Figure 4.18). Five relative hazard zones were assigned (Table 4.11). A LHZ map show the spatial distribution of these hazard zones and accordingly help the planners to select relatively safe areas for future development related works.

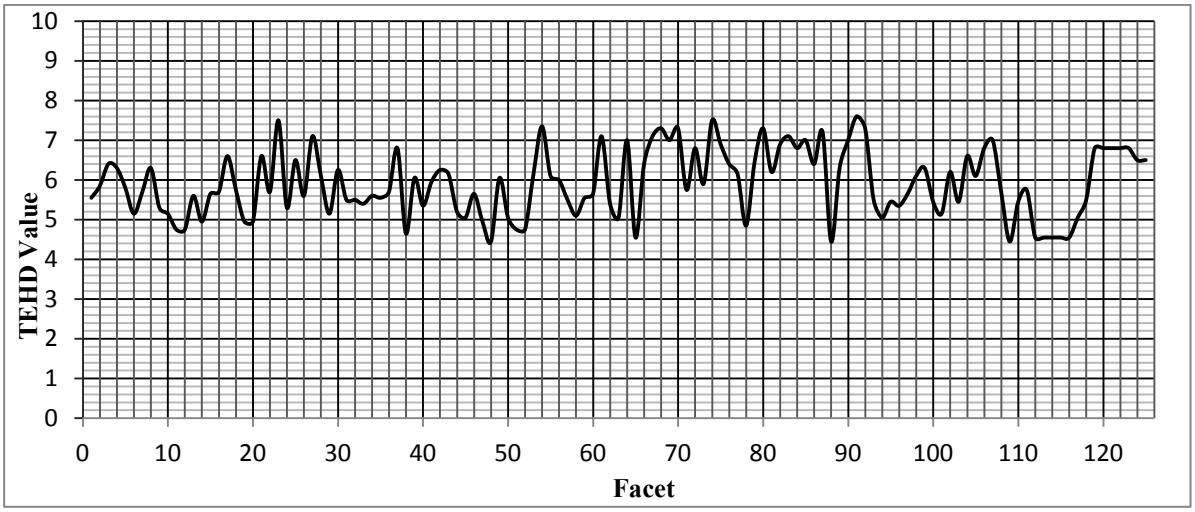

Figure 4.17 Facet wise frequency of TEHD

Table. 4.11: Landslide hazard zones based on Total Estimated Hazard values

Hazard zone	Range of corrected TEHD value	Description of zone
I	TEHD < 3.5	Very Low Hazard (VLH) zone
II	3.5 ≤ TEHD < 5.0	Low Hazard (LH) zone
III	5.0 ≤ TEHD ≤ 6.5	Moderate Hazard (MH) zone
IV	6.5 < TEHD ≤ 8.0	High Hazard (HH) zone
V	TEHD > 8.0	Very High Hazard (VHH) zone

4.3.10 Validation

Validation of this model was performed on the basis of cumulative percentage curve technique. Landslide inventory data was overlaid on the facet map containing TEHD information. Cumulative percentage of TEHD values of the slope facets were arranged in descending order and set on the vertical axis where as cumulative percentage of the landslides associated with those slope facets were set on the horizontal axis. A curve was generated showing association of TEHD and landslides (Figure 4.19). The curve in Figure 4.19 shows that 28% of the total landslides are concentrated in first 20% facets owing to high value of TEHD. Further, it shows that 22% landslides are concentrated in next 20% (20%-40%) of comparatively lower TEHD. This further shows that landslide concentration decreases with decreasing TEHD. AUC value of the curve was found to be 0.62 and it can be said that the modified BIS approach of the LHZ mapping has achieved 62% accuracy. Another way of analyzing prediction capability of the model is the comparison of landslide inventory with the relative hazard zones (Figure 4.20). It shows the association between the percentage of different LHZ and percentage of the landslides.

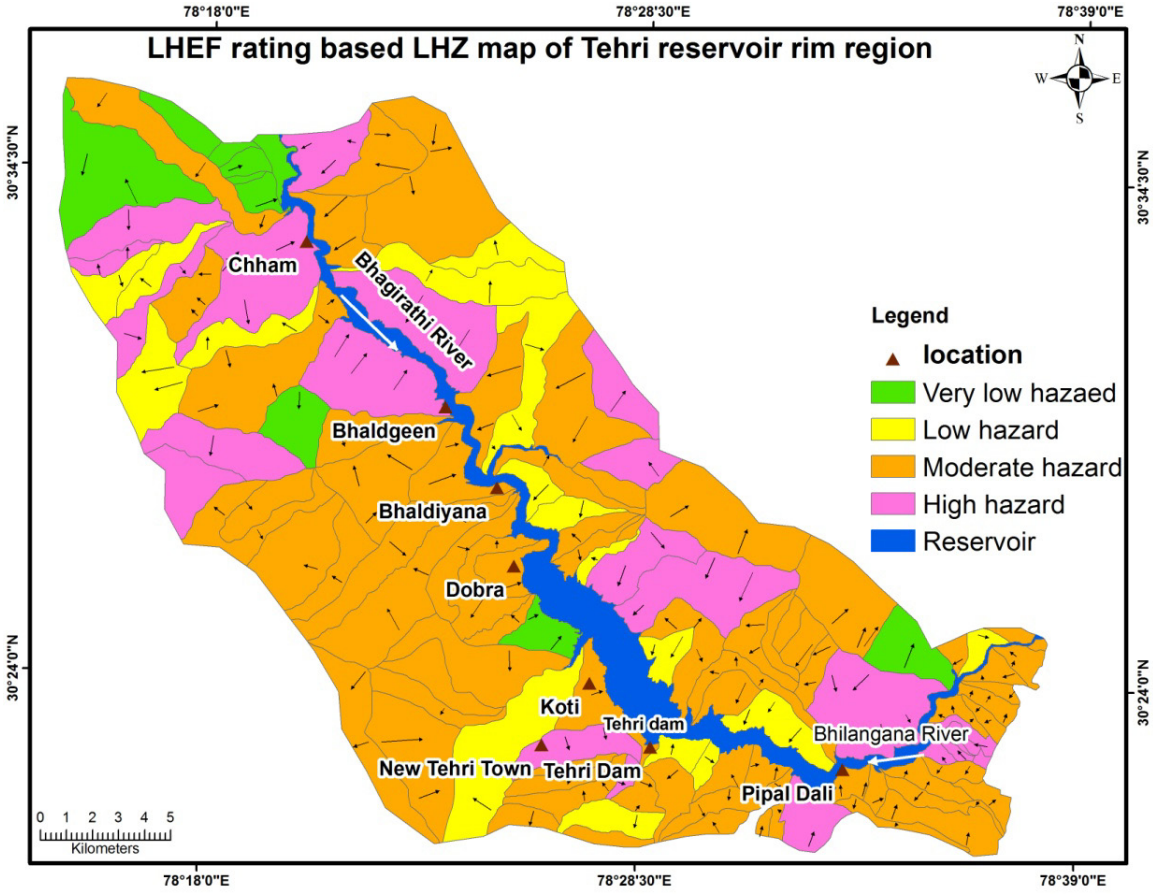

Figure 4.18 LHEF rating based LHZ map of Tehri reservoir rim region

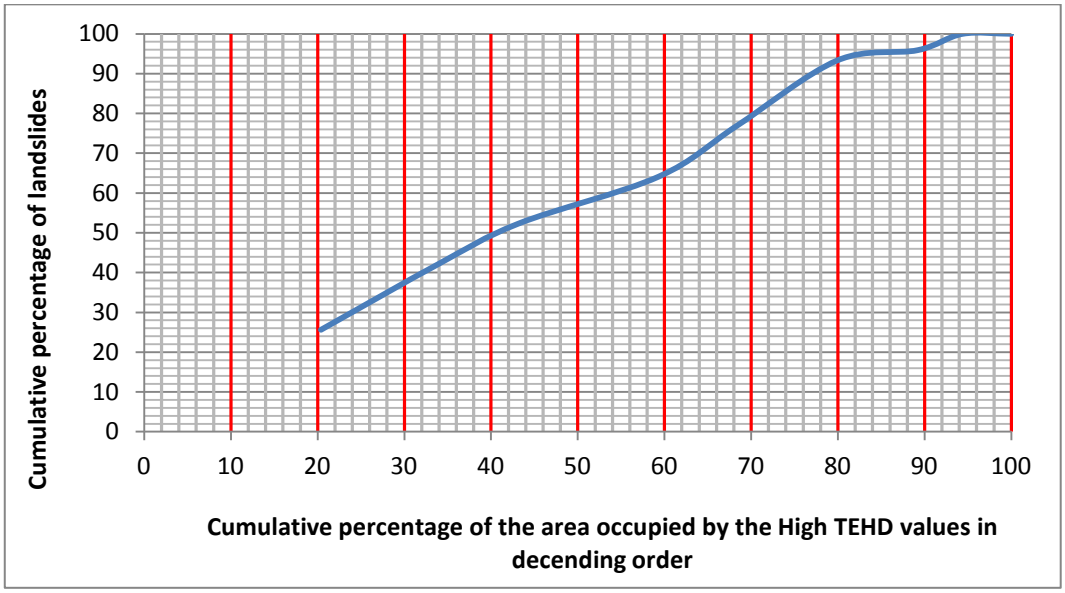

Figure 4.19 Cumulative percentage curve reflecting association of TEHD values with landslide occurrences

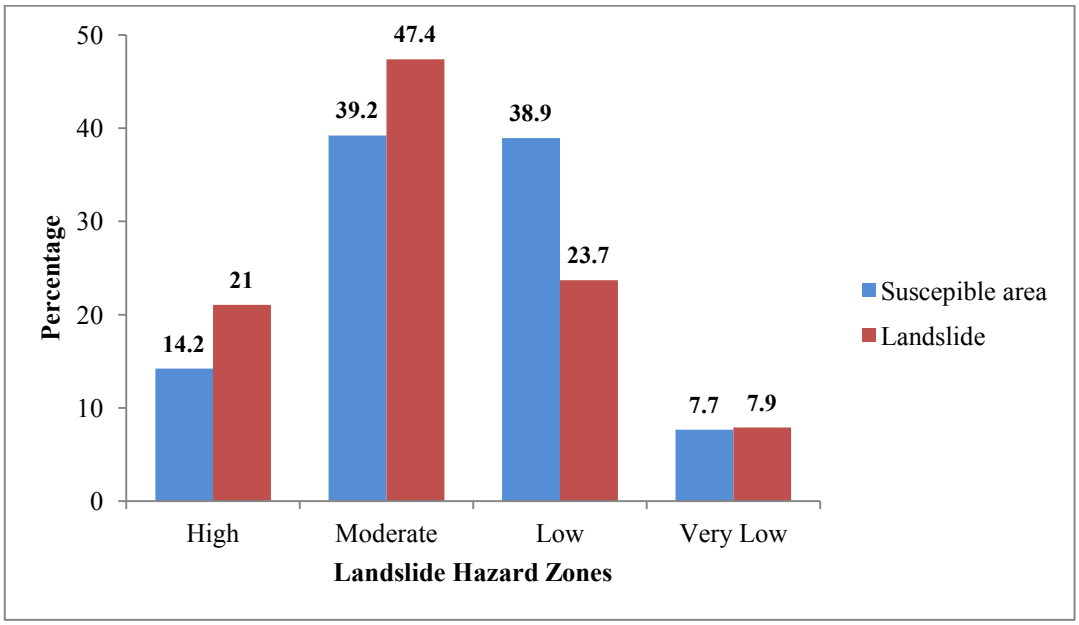

Figure 4.20 Bar diagram representing percentage domain of relative hazard zone with respect to associated percentage domain of landslide occurrences

4.3.11 Discussion

LHZ mapping based on the modified BIS approach has generally matched the ground physical conditions. Accuracy assessment, based on the cumulative percentage

curve suggests 62% landslide prediction accuracy of the LHEF based method. The bar diagram in the Figure 4.20 represents that 14.2% of the study area falls under the high hazard zone which contains 21% of the landslide inventory and it generally complies with the field conditions. Moderate hazard zone contains 39% of the entire study area and 47.4% of the landslide inventory. Low hazard zone occupies almost 40% of the study area and 23.7% of the total landslides. Such high percentage of landslides in low hazard zone reflects drawbacks of this adopted method of the LHZ mapping. Very low hazard zone occupies 7.7% of the study area and supports almost 8% of the total landslides observed. It also reflects certain degree of shortcomings of the modified BIS method. Very high hazard zone is not reflected in the LHZ map and it differs with the existing field conditions because very high number of landslides are associated with the slopes adjoining the reservoir (Figure 2.5(a-d)), road network (Figure 2.5 (e-f)) and drainage (2.5(i)).

High hazard slope facets are mostly reflected at places where the terrain is steep, relative relief is high and lithology is phyllitic in nature. These areas also supports open/scrub forest and high drainage density. Out of the 126 slope facets, 21 fall under high hazard zone category and in these 21 facets, 14 are making side slopes of the reservoir. Combined with the reservoir drawdown related failures, these 14 facets might induce a number a landslides. Moderate hazard zones are found all over the area and are associated with gentle slopes, moderate relative reliefs and agricultural areas. Slope facets, which come under low and very low hazard zones are found to be associated with the densely forested area, agricultural area, terrace and gentle talus slopes.

The Modified BIS method is based on LHEF rating and is highly subjective in nature. The fixed rating scheme of this method may induce biasness in the LHZ map. The modification in the present study includes adoption of photo-lineament at the place of structural parameter and consideration of external factors. The BIS guidelines present a detailed analysis of structural features for each slope facet in the study area which may not be feasible in the field (owing to the vastness and remoteness of the area). Photo-lineaments are extensively used in LHZ/LSZ mapping (Gupta et al. 1998; Saha et al. 2002; Arora et al. 2004; Gupta et al. 2008; Pandey et al. 2008; Ramli et al. 2010). Consideration of photo-lineament density at the place of structural favourability in each facet might result in a consistent and acceptable LHZ map. External factors such as rainfall and seismicity are mainly triggering factors. Inclusion of these external factors may enhance the prediction capability of adopted LHZ mapping method.

CHAPTER 5
LHZ MAPPING USING SEMI-QUANTITATIVE METHODS

5.1 General Introduction

Semi-quantitative methods are based on the weightings and ratings synthesised from logical tools such as analytical hierarchy process (AHP), fuzzy logic approach, combined landslide frequency ratio and fuzzy logic approach, and weighted linear combination (WLC) approach (Moon et al. 1992; Fell et al. 1996; Ercanoglu and Gokceoglu 2004; Ayalew and Yamagishi 2005; Kanoongo et al. 2006; Champatiray et al. 2007; Yalcin 2008; Pradhn and Lee 2009; Kouli et al. 2010; Mondal et al. 2012; Kayastha et al. 2013). These methods are found to be suitable for the regional scale and medium scale LHZ mapping (Guzzetti et al. 2005). These methods can be subjected to different kinds of terrain units such as grid-cell, unique-condition units; slope facets and other terrain units with good effect. Logical tools such as AHP or fuzzy logic are based on some kind of mathematical interpretation and based on those interpretations and professional experiences, weighting and ratings of terrain factors and their classes are determined. Logical interpretations can induce objectivity in a LHZ model. Two semi-quantitative approaches namely, fuzzy logic and AHP were used in the present study to carry out LHZ mapping.

5.2 Combined Fuzzy Logic and Landslide Frequency Ratio Method

Fuzzy set theory was introduced by Zadeh (1965). It facilitates analysis of non-discrete natural processes as mathematical formulae (Zimmermann 1996). According to this theory, membership value of elements (x) has varying degree of support and confidence (f(x)) in the range (0, 1) (Ercanoglu et al. 2002). A fuzzy set can be described by the formula given below:

$$A = \{x, f_A(x)\}, x \epsilon R \quad (5.1)$$

where A is a fuzzy set, x is an element of universal set R, and $f(x)$ is the fuzzy membership function. A crisp set range (0, 1) has either membership value of 1 or non-membership value of 0 whereas a fuzzy set has continuous membership in the range of (0, 1). LHZ mapping requires determination of fuzzy membership function of causative factors. Fuzzy membership function can be determined subjectively or objectively. There is no universal approach available for the determination of fuzzy membership function. A suitable and universally acceptable approach may enhance prediction capability. For LHZ mapping, several authors have used knowledge based approach for assigning fuzzy membership functions (Chung and Fabbiri 2001; Champatiray et al. 2007). Depending upon the data type (ordered or categorical), a membership function can be assigned quantitatively by using mathematical formulas. In the present study, thirteen factor (categorical) layers were considered for the fuzzy integration. Mathematical methods of fuzzy membership determination are not fit for categorical data. Therefore, in the present study, landslide factors were compared with landslide inventory and a correlation between them was quantitatively analyzed by landslide frequency ratio method (described in detail in section 3.2). Table 5.1 depicts frequency ratio and fuzzy membership value of each attribute.

Next step of fuzzy logic method is fuzzy operation. Fuzzy OR, fuzzy AND, fuzzy algebraic sum, fuzzy algebraic product and fuzzy gamma are important fuzzy operators (Chung and Fabbiri 2001). In case of fuzzy OR and fuzzy AND, only one of the contributing fuzzy set can affect the resultant value. The fuzzy algebraic sum and fuzzy algebraic product operators make the resultant set larger than, or equal to the maximum value and smaller than, or equal to the minimum value among all fuzzy sets respectively (Chi et al. 2002). Fuzzy gamma (γ) operator calculates values which range between fuzzy algebraic product and fuzzy algebraic sum. γ value has a range between 0 (no compensation) and 1(full compensation). Determination of optimum γ value is dependent on the degree of compensation between the two extreme confidence levels.

Use of the suitable fuzzy operator for data integration is required to achieve optimum result in landslide prediction studies. Choice of a fuzzy operator depends upon the type of spatial data to be integrated (Choi et al. 2000). All the thirteen factors used in the present study carry varying degrees of information. Depending upon the character of spatial data, data integration can be carried out by using several different fuzzy operators

Table 5.1: Frequency ratio and fuzzy membership values for different attributes

Factors	Classes/attributes	Frequency Ratio (Fr)	Normalized Fr/ Fuzzy membership function
Geology	Blaini Formation	0.297	0.049
	Nagthat Formation	0.790	0.131
	Chandpur Formation	1.74	0.291
	Berinag Formation	0.683	0.113
	Deoban formation	0.378	0.063
	Mandhali formation	0	0
	Rautgara formation	0.87	0.075
Soil type			
	Alluvial/sandy Loam	3.152	0.477
	Forest Soil/Black Clay	1.008	0.152
	Sandy Loam	0.108	0.016
Relative relief			
	Very low	0	0
	Low	0.09	0.013
	Moderate	0.882	0.133
	High	3.164	0.48
	Very high	2.953	0.447
Slope category			
	0°-8°	0	0
	8°-18°	0.062	0.009
	18°-30°	0.64	0.097
	30°-42°	3.996	0.605
	>42°	2.581	0.391
Lineament buffer			
	0 – 50 m	0.283	0.042
	50 – 100 m	0.66	0.099
	100 – 150 m	0.705	0.106
	150 – 200 m	2.316	0.351
	>200 m	0.9	0.136
Drainage buffer			
	0 – 50 m	2.718	0.412
	50 – 100 m	2.143	0.324
	100 – 150 m	1.628	0.246
	150 – 200 m	4.182	0.633
	>200 m	0.595	0.09
LULC Type			
	Dense forest/Vegetaion	0	0

	Scrub/Open forest	2.19	0.331
	Agricultural land	1.747	0.264
	Settlement/ Barren Land	0.985	0.149
	Water Body	0	0
Aspect			
	North	0.816	0.123
	Northwest	0.3	0.045
	West	0.629	0.095
	Southwest	0.95	0.143
	South	2.678	0.405
	Southeast	1.349	0.204
	East	0.84	0.127
	Northeast	0.476	0.072
	Flat	0	0
TWI			
	5-8	0.543	0.082
	8-12	1.353	0.205
	12-16	6.6	1
	16-19	3.882	0.588
SPI			
	1.5-3	0.603	0.091
	3-6	1.813	0.274
	6-9	1.944	0.294
	9-12	0	0
	12-15	0	0
Profile Curvature			
	Concave	0.946	.1433
	Convex	1.055	.159
Road Buffer			
	0 -50 m	6.56	1
	50 -100 m	4.136	0.62
	100-200 m	1.27	0.19
	>200 m	0.47	0.071
Reservoir buffer			
	0 - 100 m	6.17	0.93
	100 - 200 m	5.29	0.80
	200 - 300 m	2.23	0.33
	300 - 400 m	0.63	0.095
	400 - 500 m	1.07	0.162
	>500 m	0.51	0.077

separately or a combination of operators (Moon 1998). In this study, factors were grouped into the following three units: topographic, proximity and inherent units (Table 5.2). Topographic unit included slope, aspect, relative relief, profile curvature, SPI and TWI and were subjected to fuzzy OR operator using the following formula:

$$f_{OR}(x_t) = \text{MAX}\ [\ f_{slope}(x), f_{aspect}(x), f_{relative\ relief}(x), f_{profile\ curvature}(x), f_{TWI}(x), f_{SPI}(x)\ ] \quad (5.2)$$

Proximity unit included all buffer layers and inherent units included soil, LULC and geology factors. Both were subjected to fuzzy γ operation using the formula given below:

$$f_{\gamma}(x_p) = (Fuzzy\ Algebraic\ Sum)^{\gamma} \times (Fuzzy\ Algebraic\ Product)^{1-\gamma} \quad (5.3)$$

$$f_{\gamma}(x_i) = (Fuzzy\ Algebraic\ Sum)^{\gamma} \times (Fuzzy\ Algebraic\ Product)^{1-\gamma} \quad (5.4)$$

$$Fuzzy\ Algebraic\ Product = \prod_{i=1}^{n} R_i \quad (5.5)$$

$$Fuzzy\ Algebraic\ Sum = 1 - \prod_{i=1}^{n}(1 - R_i) \quad (5.6)$$

where x_i, x_p and x_t denote membership functions of inherent, proximity and topographic units respectively and also (x_i, x_p and x_t) ϵ x. R_i denotes fuzzy membership function of ith map, i = 1, 2...n. Landslide hazard index (LHI) map was prepared by subjecting results of eq. 5.2, 5.3 and 5.4 to fuzzy gamma operation. Following six γ values: 0.7, 0.75, 0.8, 0.85, 0.9 and 0.95 were chosen to prepare six different LHI maps. Another LHI map was prepared by subjecting fuzzy OR operation to the three units considered (Table. 5.2). LHI maps are ordered and continuous raster data in which each grid/cell depicts degree of landslide hazard in numerical range of 0 to 1. LHI maps were then categorized into the following five classes: very low, low, moderate, high and very high susceptibility by applying Jenk's Natural Break (ESRI 2012) classification and accordingly LHZ maps were prepared.

Quantitative prediction accuracy based on cumulative percentage curve and area under curve (AUC) technique was carried out for each LHZ map. Out of 195 landslides, 116 (60%) were used for landslide frequency ratio analysis and rest 79 (40%) were used for the accuracy assessment of the LHZ map. To carry out the accuracy of the resulting LHZ map, resulting LHI maps were sliced into twenty five LHI classes and compared with the landslide data meant for validation. Accordingly, cumulative percentage curves were

generated and the value of area under curve (AUC) was calculated using simple trapezium method. AUC was then converted into percent prediction accuracy.

Table 5.2: Different units considered for different fuzzy operations

Units considered	Factors	Fuzzy operation
Inherent Unit	LULC, soil, geology	Fuzzy gamma
Topographic Unit	Slope, relative relief, Profile curvature, aspect, TWI, SPI	Fuzzy OR
Proximity Unit	Drainage buffer, road buffer, reservoir buffer, lineament buffer	Fuzzy gamma

5.2.1. LHZ Mapping

LHZ maps were prepared by classifying LHI maps. Each cell of the LHI map contains hazard/susceptibility information in an ordered form in a range of 0 to 1. A statistical classification based on Jenk's Natural Breaks classification method was used to acquire class breaks to prepare LHZ map from the LHI maps. Natural Breaks classes are based on natural clustering inherent in the data. Jenk's Natural Breaks classification is a statistical classification of a data range in which class breaks are identified based on best group similar values which further maximize the differences between the classes (ESRI 2012). Six different LHI maps were prepared by applying fuzzy gamma operation using each gamma value mentioned in the previous section. Along with them fuzzy OR operation was used to compute a separate LHI map by integrating inherent, proximity and buffer units (Figure. 5.1 (a-g)). Table 5.3 depicts different fuzzy operations (including γ values) performed on different units considered and the resultant LHI range. For different input gamma values and different LHI range values were observed. The range of LHI is strictly an ordered value which represents degree of susceptibility and disregards its (value's) numeric meaning. Natural Breaks classification of LHI maps resulted in threshold values (Table 5.4) based on which very low, low, moderate, high and very high landslide susceptible zones were delineated. These threshold values indicate ascending tendency of

ranges as the γ value increases. Fuzzy OR operator resulted in all non-zero values. Table 5.5 shows area under susceptible classes observed for various fuzzy operations where as Figure 5.2 refers to percent area occupied by LHZ classes in LHZ maps prepared by employing different fuzzy operations.

Table 5.3: LHI range acquired for different fuzzy operations

S.N.	Fuzzy operator	Factors involved	Range
1	Fuzzy γ, γ = 0.7	Inherent unit, Proximity unit, Buffer unit	0 – 0.789
2	Fuzzy γ, γ = 0.75	Same as above	0 – 0.821
3	Fuzzy γ, γ = 0.8	Same as above	0 – 0.854
4	Fuzzy γ, γ = 0.85	Same as above	0 – 0.888
5	Fuzzy γ, γ = 0.9	Same as above	0 – 0.924
6	Fuzzy γ, γ = 0.95	Same as above	0 – 0.961
7	Fuzzy OR	Same as above	0.14– 1

5.2.2. Validation of LHZ mapping

Validation was performed to obtain the accuracy of LHZ. Accuracy of LHZ is the capability of a map to delineate landslide free and landslide prone areas. In the present study, cumulative percentage curve technique was used to validate LHZ. Cumulative percentage curves were achieved by plotting cumulative percent of LHI in descending order against cumulative percent of landslide on X and Y axis respectively. Example of the curve is given in Figure 5.3 and 5.4. Figure 5.3 indicates that 42% of the landslides fall under 100 - 90% of high LHI domains whereas 23% landslides fall under 90-80% higher LHI valued areas, and accordingly other values follow. In this way, percentage cumulative curve clearly state the accuracy of the LHZ. Further, AUC values of accuracy curves were calculated by simple trapezium method (Table 5.6). Hence, it can be said in percentage terms that 78.2% accuracy has been achieved for γ value of 0.95 and so on. Higher γ values have resulted in better accuracy whereas fuzzy OR operator has given least accuracy. Figure 5.4 refers to the comparison between cumulative percentage curves related to the LHI maps generated by fuzzy gamma operation with different gamma values.

5.2.3 Discussion

Fuzzy logic relations and fuzzy operation based LHZ have achieved satisfying results. Fuzzy membership values were determined by frequency ratio approach. To perform fuzzy operation for thirteen factors which contain varying degree of spatial information, factors were grouped into inherent, topographic and proximity units. Fuzzy γ and fuzzy OR operators were used to separately integrate factors present in these units as mentioned in methodology section. Later, these integrated units were subjected to fuzzy γ and fuzzy OR operation separately. Combined approach of fuzzy operation has enhanced the prediction accuracy.

Fuzzy gamma operators were successfully applied for the generation of LHI maps and consequent LHZ. Model suggests that higher gamma values (0.95, 0.90) yield better prediction of LHZ than low gamma values (0.8. 0.75 and 0.70), whereas fuzzy OR has given least accuracy. Results show increasing tendency of susceptibility prediction corresponding to increasing gamma values. Model accuracy was performed using cumulative percentage curves. Resulting smooth curves suggest good prediction results, whereas AUC values of curves indicate better prediction. Gamma value of 0.95 was chosen for the final LHZ map generation. Hence, it can be concluded that landslide causative factors' integration using fuzzy logic has yielded good results for the Tehri reservoir rim region.

Table 5.4: Threshold values of LSZ classes for LHI computed from different fuzzy operations

Susceptibility Class / Fuzzy operator	**Very low**	**Low**	**Moderate**	**High**	**Very high**
Fuzzy γ, γ = 0.70	0 – 0.068	0.068 – 0.186	0.186 – 0.287	0.287 – 0.424	0.424 – 0.789
γ = 0.75	0 – 0.084	0.084 – 0.218	0.218 – 0.322	0.322 – 0.457	0.457 – 0.821
γ = 0.80	0	0 – 0.271	0.271 – 0.395	0.395 – 0.542	0.542 – 0.854
γ = 0.85	0	0 – 0.313	0.313 – 0.428	0.428 – 0.571	0.571 – 0.888
γ = 0.90	0	0 – 0.376	0.376 – 0.500	0.500 – 0.641	0.641 – 0.924
γ = 0.95	0	0 – 0.437	0.437 – 0.565	0.565 – 0.712	0.712 – 0.961
Fuzzy OR	0.14 – 0.21	0.21 – 0.33	0.33 – 0.46	0.46 – 0.62	0.62 - 1

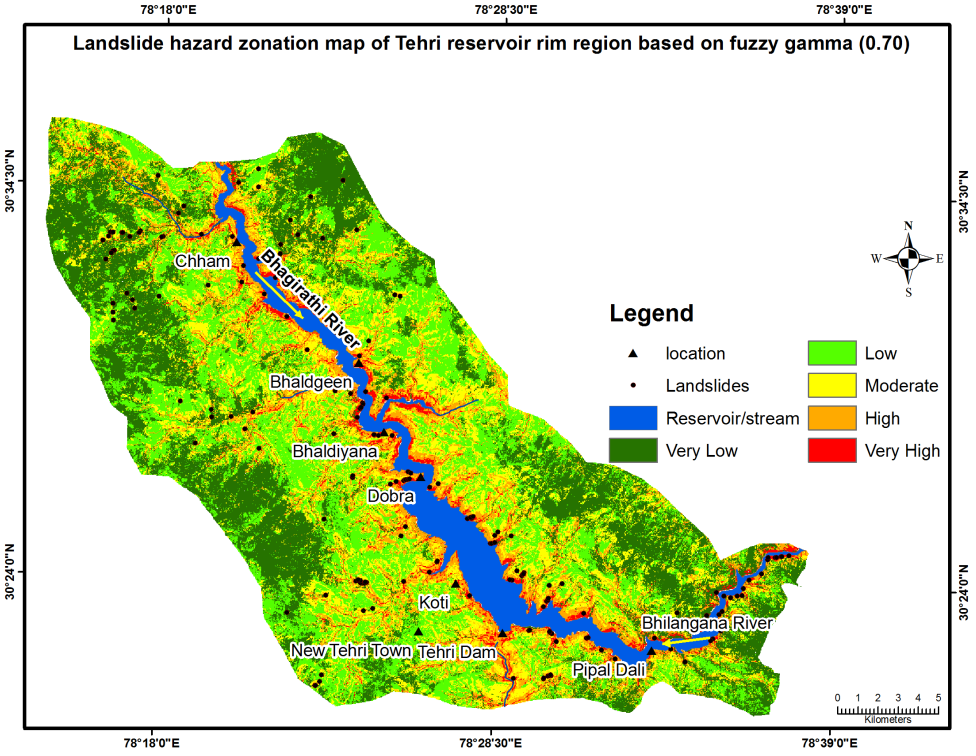

Figure 5.1a LHZ map of Tehri reservoir rim region based on fuzzy gamma (0.70)

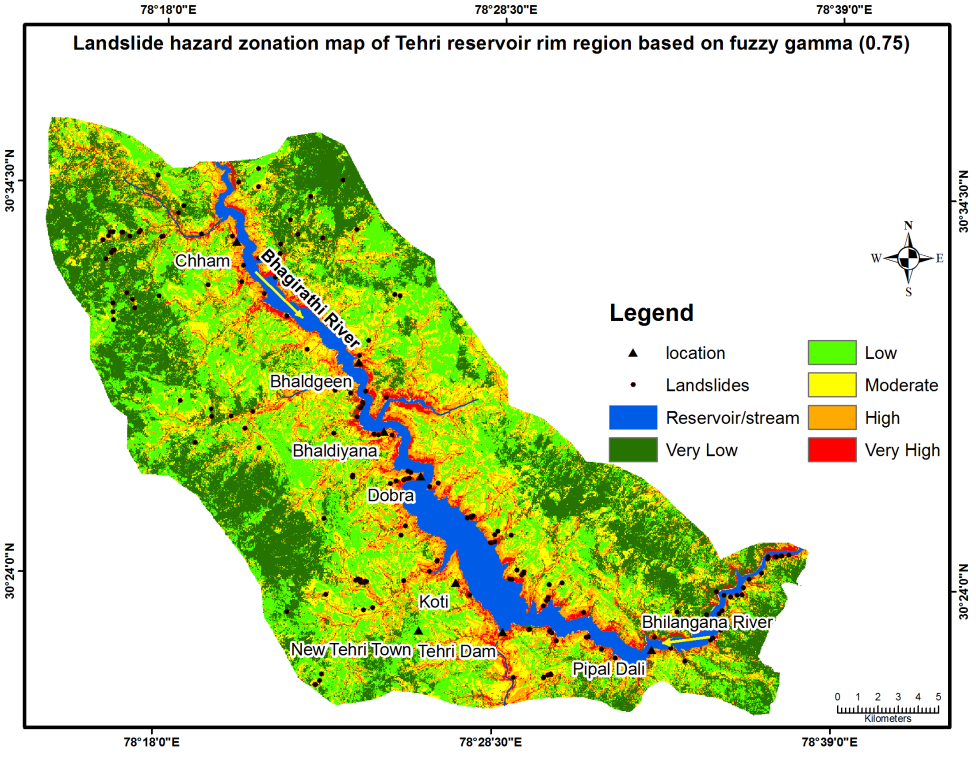

Figure 5.1b LHZ map of Tehri reservoir rim region based on fuzzy gamma (0.75)

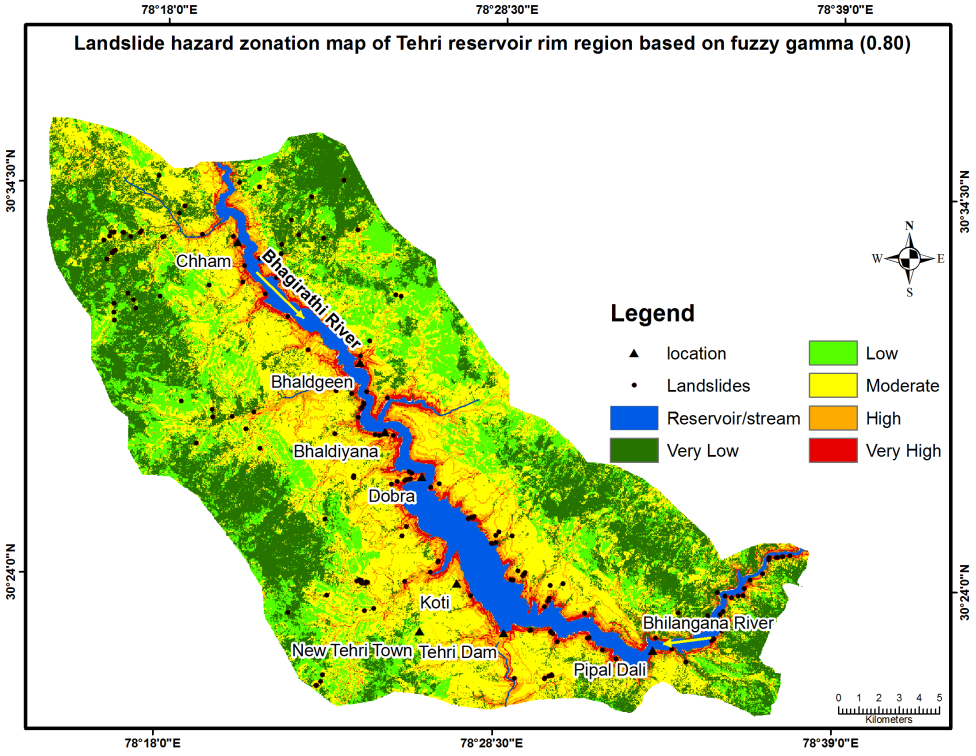

Figure 5.1c LHZ map of Tehri reservoir rim region based on fuzzy gamma (0.80)

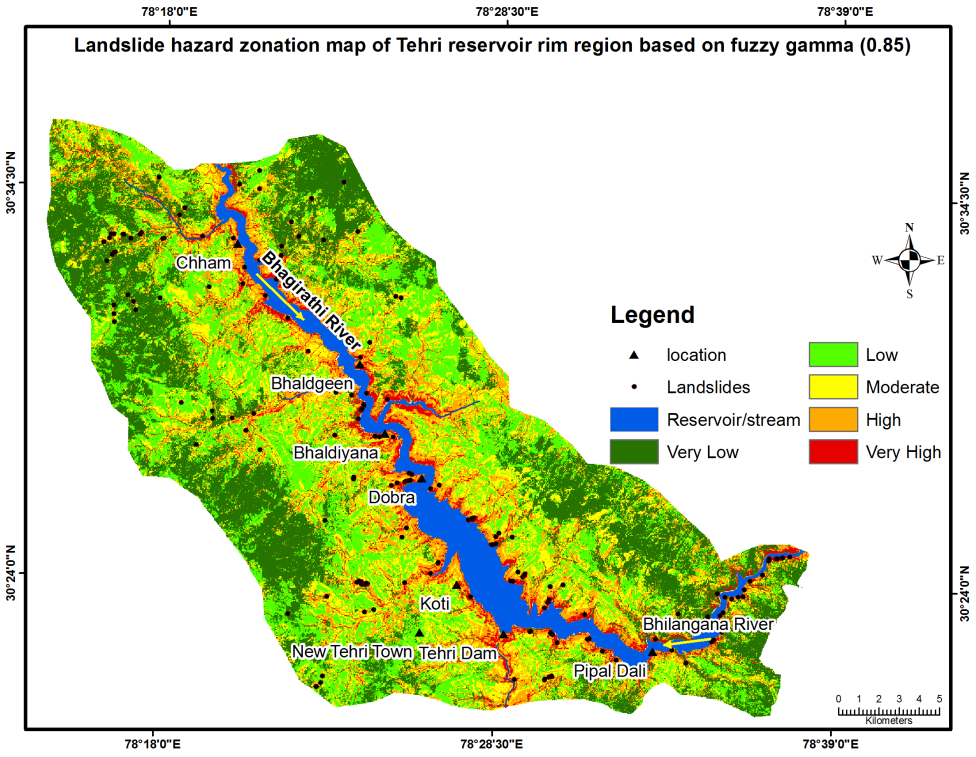

Figure 5.1d LHZ map of Tehri reservoir rim region based on fuzzy gamma (0.85)

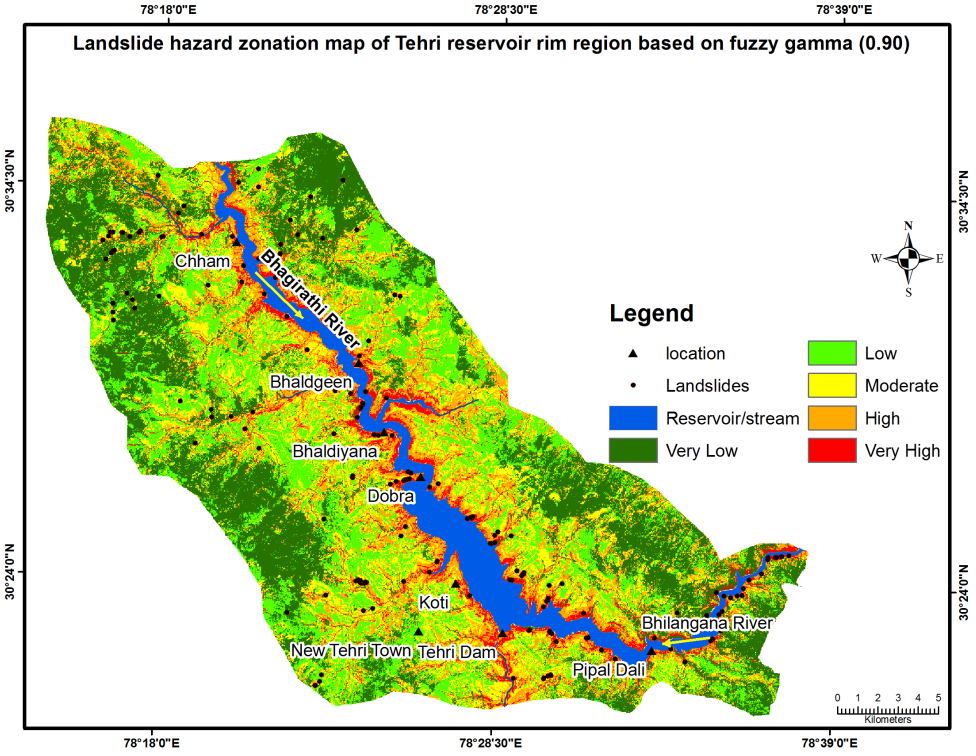

Figure 5.1e LHZ map of Tehri reservoir rim region based on fuzzy gamma (0.90)

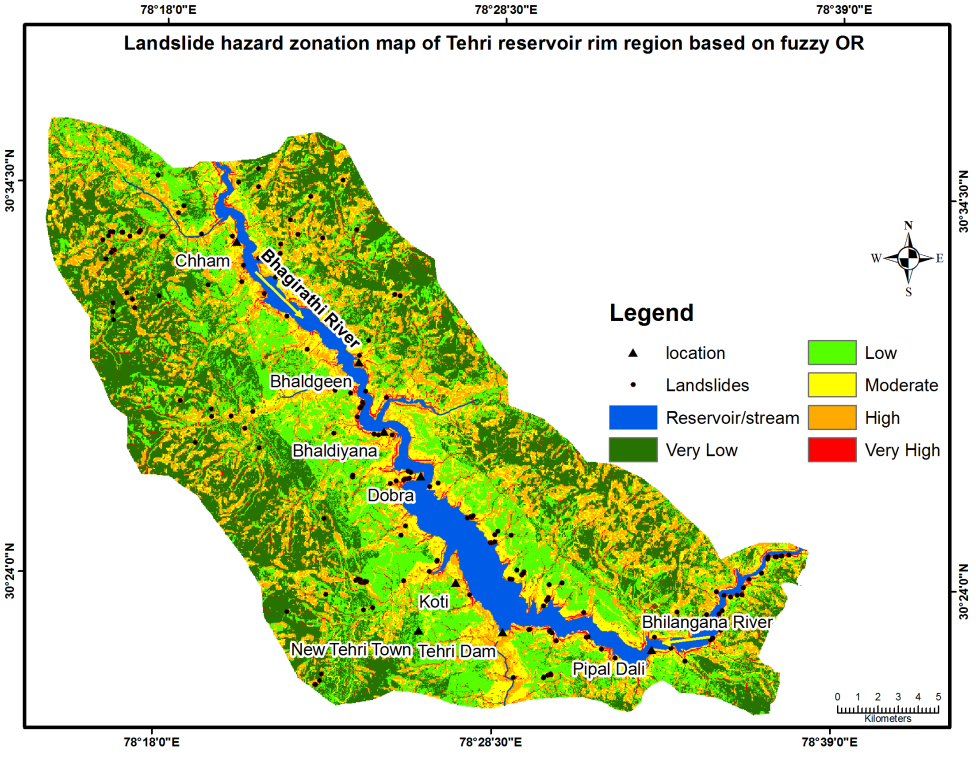

Figure 5.1f LHZ map of Tehri reservoir rim region based on fuzzy OR

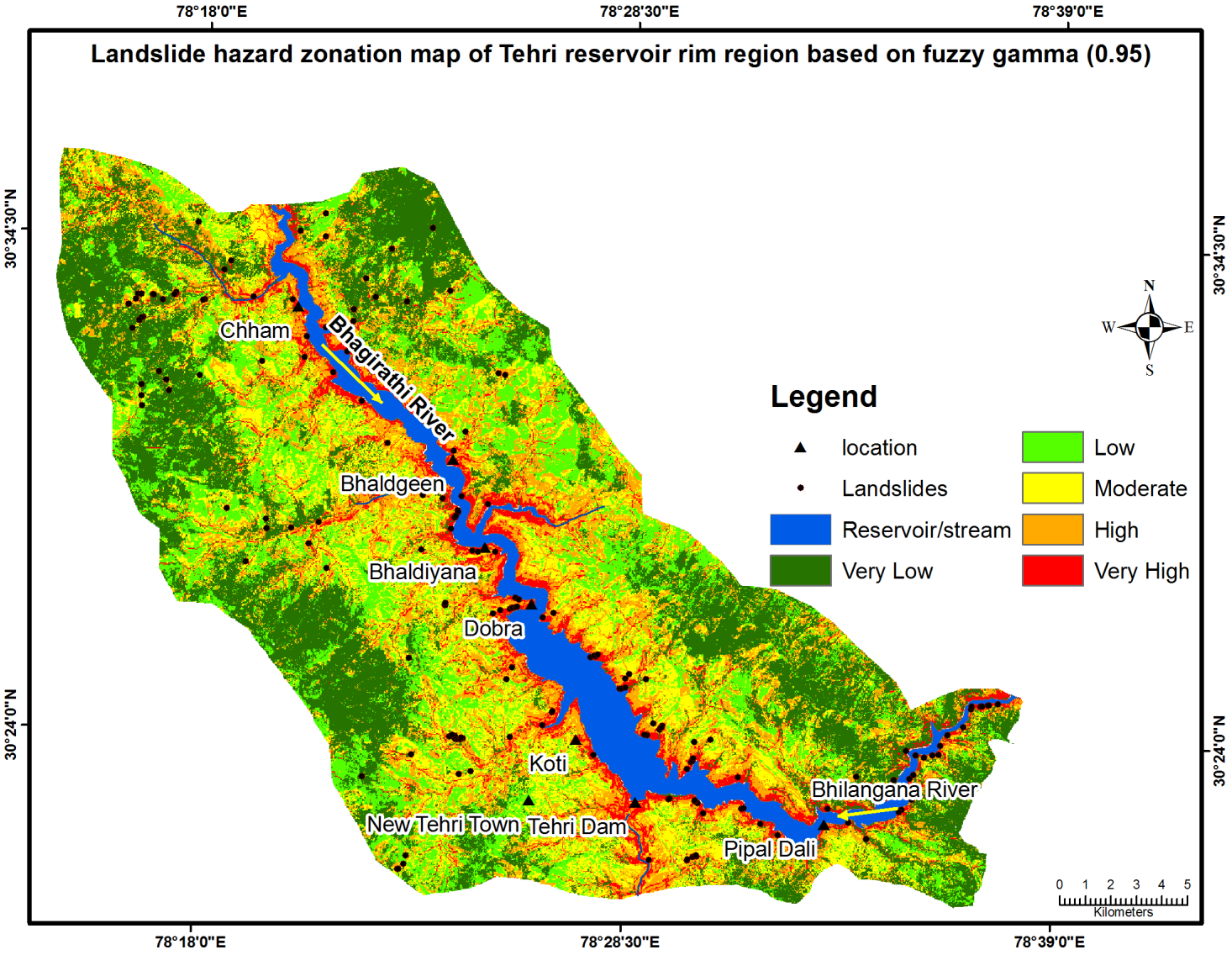

Figure 5.1g LHZ map of Tehri reservoir rim region based on fuzzy gamma (0.95)

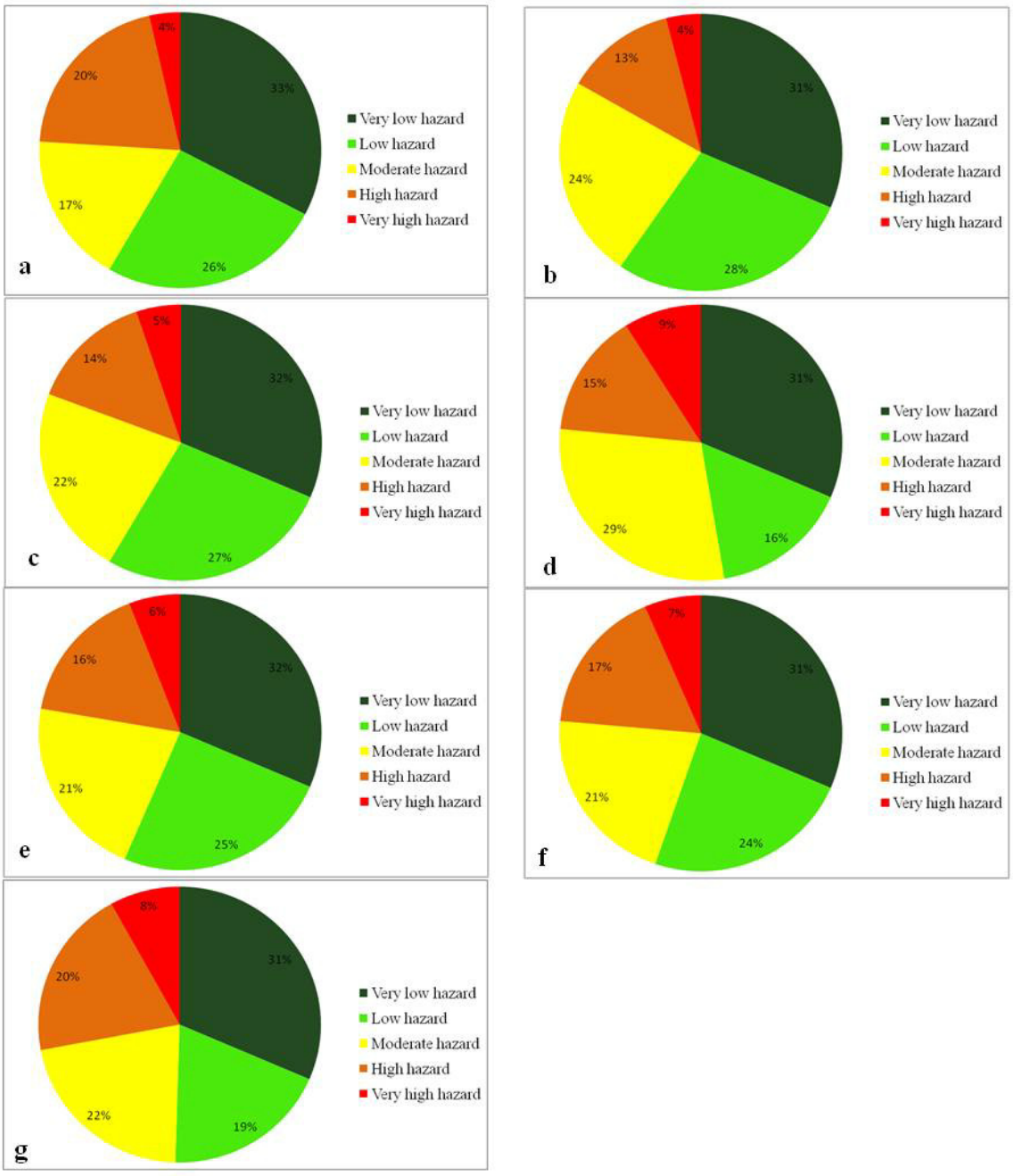

Figure 5.2 Pie charts showing the LHZ frequency computed from different fuzzy operations a) Fuzzy OR, b) Fuzzy gamma (0.70), c) fuzzy gamma (0.75), d) fuzzy gamma (0.80), e) fuzzy gamma (0.85), f) fuzzy gamma (0.90), g) fuzzy gamma (0.95)

Table 5.5: Area frequency of LHZ classes resulted from different fuzzy operations

Fuzzy operators	Fuzzy OR	γ = 0.7	γ = 0.75	γ = 0.80	γ = 0.85	γ = 0.90	γ = 0.95
LHZ							
Very low	179.51	173	172.87	172.82	172.82	172.82	172.82
Low	141.36	154.63	148.349	87.2	137.19	130.68	104.5
Moderate	96.48	129.77	122.035	160.55	116.87	116.22	118.34
High	112.3	69.85	77.723	79.58	89.99	93.77	109.33
Very high	19.59	22	28.28	49.08	32.37	35.75	44.25

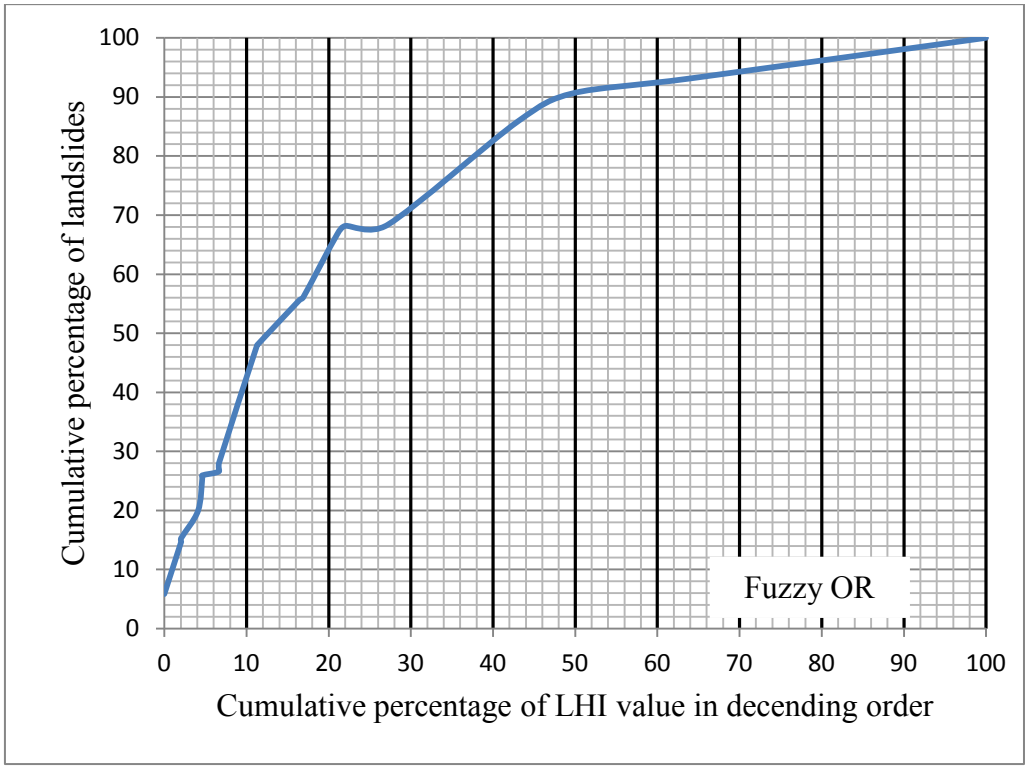

Figure 5.3 Cumulative percentage curve showing frequency of landslides in LHI map (Fuzzy OR)

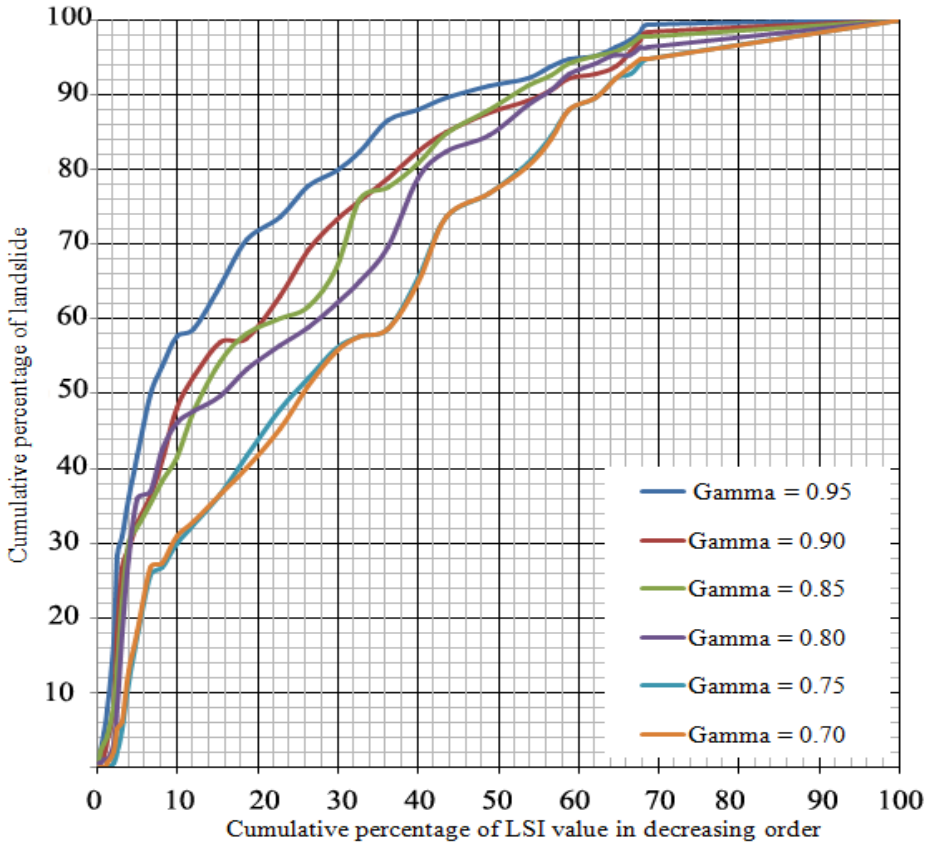

Figure 5.4 Cumulative percentage curve showing comparison of frequency of landslides in LHI maps computed from different fuzzy gamma operation

Table 5.6: AUC values and percent accuracy obtained for each LHZ map computed from fuzzy operations

Gamma (γ)	AUC values	% Accuracy
0.95	0.782	78.2
0.90	0.78	78
0.85	0.778	77.8
0.80	0.772	77.2
0.75	0.767	76.7
0.70	0.752	75.2
Fuzzy OR	0.74	74

Frequency ratio method for determination of fuzzy membership value has reduced subjectivity in the model. Based on the above discussion, it may be concluded that cumulative percentage curves method has a strong validation capability for a continuous hazard model

5.3 Analytical Hierarchy Process

AHP is a theory of measurement for dealing with quantifiable and intangible criteria that has been applied to many areas, such as decision theory and conflict resolution (Vargas 1990; Yalcin 2008). AHP is a multi-objective, multi-criteria decision-making approach which enables the user to arrive at a scale of preference drawn from a set of alternatives (Yalcin 2008). AHP is widely used in site selection, suitability analysis and LHZ mapping (Ayalew et al. 2005; Yalcin 2008; Feizizadeh and Blaschke 2013). Among the different logical and statistical techniques available for the LHZ mapping, AHP has been categorised under semi-quantitative category (Yalcin 2008; Kouli et al. 2010; Kayastha et al. 2012; Mondal et al. 2012, 2013). In view of LHZ mapping, AHP works as a logical tool for synthesising weights/ratings of geo-environmental factors/classes according to their significance in inducing landslides. Professional knowledge of experts or group of experts about the landslide conditioning factor is given as an input into the AHP model, which further makes the AHP approach subjective. It has been advocated that a certain degree of objectivity can be infused in AHP model (Yalcin 2008; Mondal et al 2012). In the present study, AHP was used to determine weights and ratings of the terrain factors and their classes by infusing landslide frequency ratio.

5.3.1 Methodology

The present study is based on the use of AHP method for synthesising weights of the factors/classes. Application of AHP method is widely used in site selection, suitability analysis and LHZ mapping (Ayalew et al. 2005; Yalcin 2008; Feizizadeh and Blaschke 2013). It is a multi-criterion decision making technique introduced by Saaty (1980) which allows subjective as well as objective factors to be considered in the decision-making process (Yalcin 2008; Feizizadeh and Blaschke 2013). AHP is based on three principles: decomposition, comparative judgment and synthesis of priorities (Malczewski, 1999; Yalcin 2008; Kayastha et al. 2013). AHP breaks complex decision making problem into a hierarchy of factors and alternatives. Factors and alternatives are assigned weights on a nine point ordinal scale (Table 5.7) by virtue of pair-wise comparison between them. Factors or their classes are arranged in the form of matrix which contains equal number of rows and columns, where scores are recorded on one side of the diagonal, while values of 1

are placed in the diagonal of the matrix (Satty 1977; Gorsevski et al. 2006). Pair-wise comparison and judgment of score is influence by professional knowledge. Source of knowledge of landslide causative factors can be subjective or it may be perceived from objective approach. Yalcin (2008) emphasized that subjective as well as objective factor to be considered in decision making process. In this study, relative value of each pair of the factors/classes were determined on the basis of professional knowledge from the field work and presence of landslides in those classes. When the factor on the vertical axis is more important than the factor on the horizontal axis, this value varies between 1 and 9 and conversely, the value varies between the reciprocals 1/2 and 1/9 (Saaty 1980; Yalcin 2008). Matrix calculation gives factor/class weights in terms of eigenvector. Calculation of maximum eigenvalue is also a part of the AHP model. Subjective decision rule can violate the transitivity rule and thus cause an inconsistency (Feizizadeh and Blaschke 2013). One of the important aspects of AHP principle is the calculation of consistency index (CI) and consistency ratio (CR). Saaty (1980) formulated consistency index as:

$$CI = \frac{(\lambda max - N)}{N-1} \tag{5.7}$$

where λ_{max} is the maximum eigenvalue and N is the number of elements present in the row/column of the matrix. CR can be calculated by ratio CI/RI, where RI stands for random index (Saaty 1980). Random index (Table 5.8) was compiled by Saaty (1980) on the basis of a number of random samples. CR value of 0.1 is the maximum threshold of consistency of the matrix. CR value >0.1 is thought to be inconsistent where as value 0 indicates perfectly consistent comparison result. Table 5.9 refers to AHP based matrix for the factors/classes showing scores awarded on ordinal scale, eigenvector, CR and maximum eigenvalue.

AHP method has its advantages in weighting/rating of factors and their classes along with some deficiencies. Relative scoring of the factors largely bank on the knowledge of a person or professional. Relative preference given to a factor by a person or professional is often not recognised by others, which a major drawback of any subjective decision making system. Nonetheless, pair wise comparison provides a simple and acceptable decision rule. In landslide studies, some factors has certain degree of

dependency in influencing landslides whereas AHP considers factors in hierarchy as an independent entity. For example, a relatively moderate slope can fail owing to increase in the moisture content of the slope forming material (TWI and SPI parameters) but in AHP system, moderate slope will be given lesser preference compared to high slope category. Overall AHP multi-criteria decision making provides a very flexible and simple decision making which can be conveniently accommodated in the GIS domain.

Next step was calculation of LHI. It was computed using weighted arithmetic sum method which can be formulated as given below:

$$\text{LHI} = \sum_{J=1}^{J=n} \text{Weight of factor } (W_J) \times \text{Weight of factor classes } (W_{iJ}) \quad (5.8)$$

where W_{Ij} denotes weight of *ith* class of factor J. LHI map was classified into very low, low, moderate, high and very high LHZ classes employing Natural Break classification methods (ESRI 2012).

Table 5.7 Ordinal scale represents preference of judgement (Saaty 1977*)*

Preference/ordinal	Degree	Remarks
1	Equally	Factors inherit equal contribution
3	Moderately	One factor moderately favoured over other
5	Strongly	Judgement strongly favour one over other
7	Very strongly	One factor very strongly favoured over other
9	Extremely	One factor favoured over other in highest
2,4,6,8	Intermediate	Compensation between weights 1,3,5,7 and 9
Reciprocals	Opposite	Refers inverse comparison

Table 5.8: Random consistency index (RI) (Saaty 1980)

N	1	2	3	4	5	6	7	8	9	10	11	12	13	14	15
RI	0	0	0.58	0.9	1.12	1.24	1.32	1.41	1.45	1.49	1.51	1.53	1.56	1.57	1.59

5.3.2 Results

LHZ mapping was performed using AHP method. AHP was used to weight factors and their classes (Table 5.9). Raster maps of each factor were assigned weight values on cell by cell basis. Integration of weighted raster maps were performed using eq. 5.8.

Integration has resulted in a LHI map, which contained numerical susceptibility information in which higher LHI values indicate high susceptibility and lower value indicate low susceptibility (Figure 5.5). LHI values are found in a range of 8.58 to 53.89 (Figure 5.5). Natural Break classifier was used to calculate class break values of the continuous LHI map (Figure 5.6) and accordingly LHI map was classified into the following five categories: Very low susceptibility, low susceptibility, moderate susceptibility, high susceptibility and very high susceptibility (Figure 5.7). 23% of the entire area is found in very low susceptibility class, 34% in low susceptibility class, 25% in moderate susceptibility class, 15% in high susceptibility class and 3% in very high susceptibility (Figure 5.8). Results have indicated that areas immediate to the reservoir banks mostly fall in high LHZ classes. Result also reflect that high susceptible classes occupy areas around the drainage network. Low LHZ classes are observed in areas having flatter terrain, dense forest cover and sparse forest cover. Settlement areas have been observed in moderate to high LHZ classes.

5.3.3. Validation

In the present study, cumulative percentage curve/success rate curve technique, which considers existing landslides, was used to validate the accuracy of the LHZ. Success rate curves were achieved by plotting cumulative percent of LHI in descending order against cumulative percent of landslide on X and Y axis respectively. Figure 5.9 is a cumulative percentage curve of the presented model. It indicates that 58% of landslides fall under 100- 90% of high susceptible classes whereas 22% landslides fall under 90-70% of high susceptible class, and accordingly other values follows. In this way, percentage cumulative curve clearly state the accuracy of the LHZ. Further, AUC value of accuracy curve was calculated by simple trapezium method. AUC value 0.80 is achieved for the present model which can be converted in terms of percent prediction accuracy of 80%. So it can be said that model has resulted in an accuracy of 80%. Nonetheless, landslide density of the susceptible classes lead to the assessment of the overall quality of the LHZ map (Sarkar and Kanungo 2004; Kayastha et al. 2012). Table 5.10 depicts the landslide density values in which it is noticeable that the landslide density for the very high susceptible class is 0.232, which is markedly larger than the other susceptible classes. It can also be

Table 5.9: AHP scores of factors/classes, eigenvector, CR and Maximum eigenvalue														
Factors and Classes														**Normalized Eigen**
	1	**2**	**3**	**4**	**5**	**6**	**7**	**8**	**9**	**10**	**11**	**12**	**13**	
FACTORS COMPARISON														
Geology (1)	1													0.0342
Soil (2)	1/3	1												0.076
LULC (3)	½	1	1											0.126
Lineament (4)	3	4	4	1										0.131
Drainage (5)	4	4	4	3	1									0.021
Slope (6)	4	4	5	3	1	1								0.077
Aspect (7)	¼	1/3	1/3	1/3	¼	1/5	1							0.065
Relative relief (8)	3	4	4	2	1/3	1/3	3	1						0.023
TWI (9)	½	1	2	1/3	¼	¼	2	1/3	1					0.21
SPI (10)	1/3	½	½	¼	1/5	1/5	2	¼	1/3	1				0.0175
Reservoir Buffer (11)	4	4	5	4	3	3	5	4	5	5	1			0.127
Curvature (12)	¼	1/3	¼	1/5	1/5	1/6	½	1/3	¼	½	1/5	1		0.0342
Road Buffer (13)	4	4	4	3	1	1	5	3	4	5	1/3	5	1	0.076
CR = 0.067, Maximum eigenvalue – 14.2														
FACTOR CLASSES COMPARISON														
Geology														
Blaini Formation (1)	**1**													0.066
Nagthat Formation (2)	4	1												0.26
Chandpur Formation (3)	5	2	1											0.345
Berinag Formation (4)	1	¼	1/5	1										0.068
Deoban Formation (6)	1	¼	1/5	1	1									0.063
Mandhali Formation (7)	1/3	1/5	1/5	1/3	½	1								0.038
Rautgara Formation (8)	4	1/3	1/3	3	3	4	1							0.160
CR = 0.0472, Maximum eigenvalue = 8.331														
Soil Cover														
Alluvial/sandy Loam (1)	1													0.636

Forest Soil/Black Clay (2)	1/5	1												0.104
Sandy Loam (3)	1/3	3	1											0.258
CR = 0.0192, Maximum eigenvalue = 3.03														
Relative relief														
Very low (1)	1													0.045
Low (2)	2	1												0.062
Moderate (3)	3	3	1											0.119
High (4)	5	5	3	1										0.242
Very high (5)	8	7	5	4	1									0.529
CR = 0.068, Maximum eigenvalue = 5.27														
Slope category														
0°-8° (1)	1													0.039
8°-18° (2)	2	1												0.057
18°-30° (3)	4	3	1											0.122
30°-42° (4)	6	5	3	1										0.241
>42° (5)	8	7	5	4	1									0.539
CR = 0.0619, Maximum eigenvalue = 5.24														
Lineament Buffer														
0 – 50 m (1)	1													0.418539
50 – 100 m (2)	½	1												0.262518
100m – 150 m (3)	1/3	½	1											0.159923
150m – 200 m (4)	¼	1/3	½	1										0.0972536
>200 m (5)	1/5	¼	1/3	½	1									0.0617666
Consistency Ratio = 0.017, Maximum Eigenvalue = 5.068														
Drainage Buffer														
0 – 50 m (1)	1													0.479
50 – 100 m (2)	1/3	1												0.267
100m – 150 m (3)	¼	1/3	1											0.128
150m – 200 m (4)	1/5	¼	½	1										0.083

>200 m (5)	1/7	1/6	¼	1/3	1									0.041
CR = 0.051, Maximum eigenvalue = 5.207														
Land use/ Land cover														
Dense forest (1)	1													0.069
Sparse forest (2)	3	1												0.149
Agricultural land (3)	4	2	1											0.243
Settlement /Fallow Land (4)	5	4	3	1										0.537
CR = 0.039, Maximum eigenvalue = 4.11														
Aspect														
North (1)	1													0.0406
Northwest (2)	3	1												0.0625
West (3)	3	2	1											0.083
Southwest (4)	4	3	3	1										0.149
South (5)	5	4	4	3	1									0.295
Southeast (6)	4	3	3	3	1/3	1								0.204
East (7)	2	2	1	1/3	¼	1/3	1							0.0791
Northeast (8)	2	1	½	1/3	¼	¼	½	1						0.0565
Flat (9)	1/3	1/3	1/3	¼	1/5	1/5	1/3	1/3	1					0.0284
CR = 0.0738, Maximum eigenvalue = 9.59														
TWI (values on natural log scale)														
5-8 (1)	1													0.068
8-12 (2)	3	1												0.134
12-16 (3)	4	3	1											0.268
16-19 (4)	5	4	3	1										0.52
5-8 (1)	1	1/3	1/4	1/5	1									0.068
CR = 0.060, Maximum eigenvalue = 4.18														
SPI (values on natural log scale)														
1.5-3 (1)	1													0.060
3-6 (2)	2	1												0.094

6-9 (3)	3	2	1											0.155
9-12 (4)	4	3	2	1										0.238
12-15 (5)	5	4	3	2	1									0.451
CR = 0.0317, Maximum eigenvalue = 5.12														
Profile Curvature														
Concave	1													0.66
Convex	1/2	1												0.33
CR = 0.0, Maximum eigenvalue = 2														
Road Buffer														
0 – 50 m (1)	1													0.558
50 – 100 m (2)	1/3	1												0.255
100m – 200 m (3)	1/5	1/3	1											0.122
>200 m (4)	1/6	¼	1/3	1										0.062
CR = 0.049, Maximum eigenvalue = 4.14														
Reservoir buffer														
0 -100 m (1)	1													0.448
100 – 200 m (2)	1/3	1												0.220
200 – 300 m (3)	1/4	1/2	1											0.142
300 – 400 m (4)	1/5	1/3	½	1										0.090
400 – 500 m (5)	1/6	¼	1/3	½	1	2								0.058
>500 m (6)	1/7	1/5	¼	1/3	½	1								0.03
CR = 0.0325, Maximum eigenvalue = 6.16														

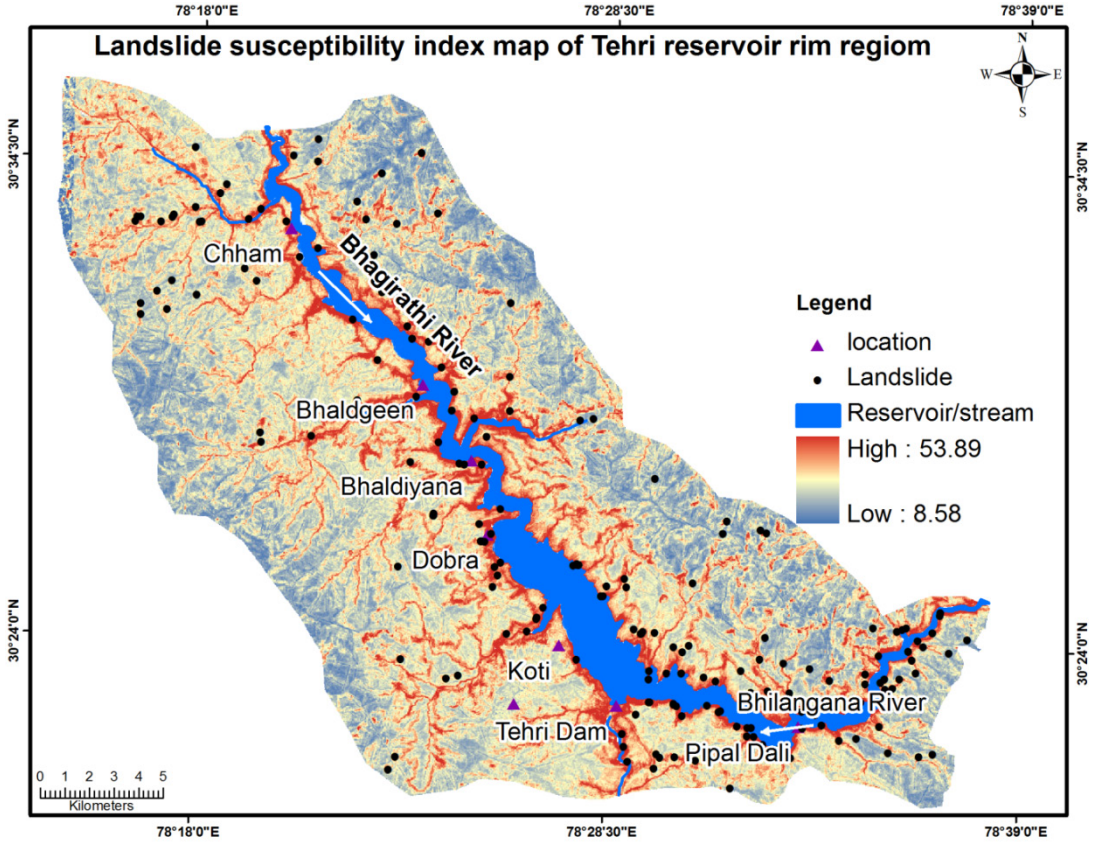

Figure 5.5 LHI map of the Tehri reservoir rim area

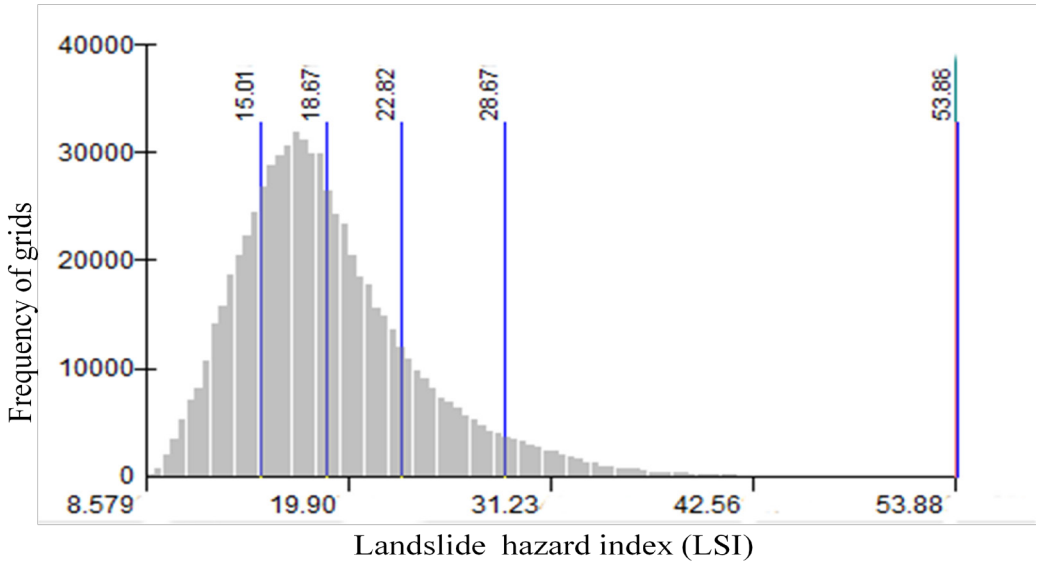

Figure 5.6 Threshold values chosen for classification of LHI map

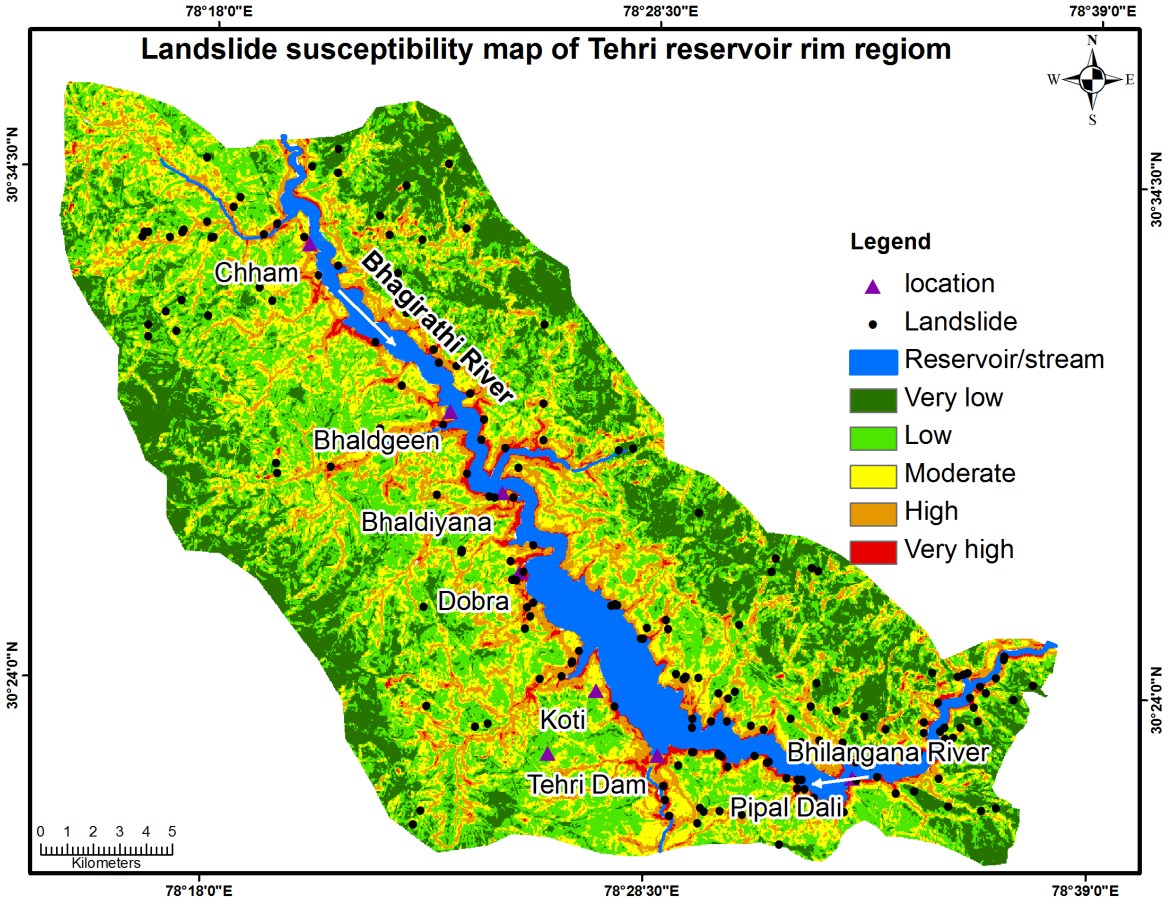

Figure 5.7 LHZ map of the Tehri reservoir rim area

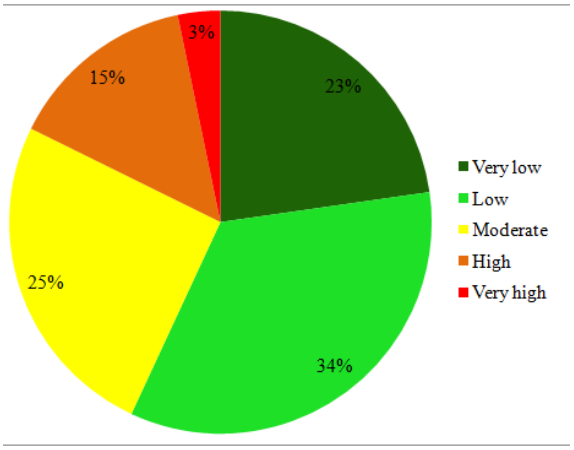

Figure 5.8 Pie chart showing density of landslide susceptible classes

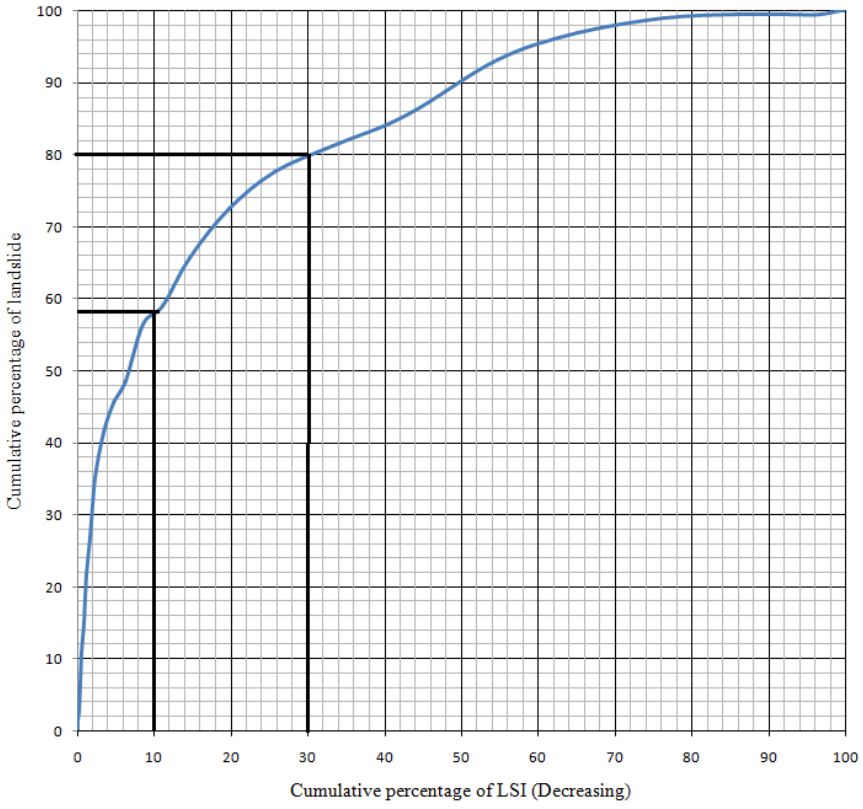

Figure 5.9. Cumulative percentage curve of decreasing LHI values

Table 5.10: Landslide density in different classes of LHZ map

Susceptibility classes	Area (km^2)	Landslide frequency (No.)	Landslide frequency density
Very low	5	0	0.000
Low	80	5	0.062
Moderate	206	13	0.063
High	198	46	0.232
Very High	61	131	2.147

observed from the Table 5.10 that there is a continuing decrease in the landslide density values from the very high to low susceptible classes. On the basis of landslide density results, it can be said that the computed LHZ classes largely comply with the field conditions.

5.3.4 Discussion

The present study provides insights into the capability of multi-criteria decision making system AHP in predicting landslide susceptible areas. AHP method was successfully used to assign weights to factors and their classes. Judgement in the pair-wise comparison matrix was motivated by the present landslides in the area. LHZ map provided critical evaluation of the factor classes present in the area.

Among the slope classes, most of the high susceptible area is observed in very high and high slope angle classes. Generally, terrain having high slope angle, the weight of the possible mobilized material under gravity will be more as compared to a moderate slope angle. Shear strength being same in both the cases, a steep slope with more mobilizing force may fail early. High susceptible area is observed in high and very high relative relief classes. High relative reliefs are surface manifestation of cliffs and ridges, which are often rendered unstable by the influence of triggering factors such as rainfall and earthquakes. Southern aspect of the study area, which is receiving excessive sun radiation and high rainfall, are observed under higher LHZ classes. Incidentally, a number of agricultural terraces are present on the southwest facing slopes leading to more instability.

Among the secondary topographic parameters, higher LHZ classes are observed in the higher TWI and SPI ranges. Higher TWI ranges are associated with the increasing water infiltration which often leads to increase in the pore water pressure and further reduces the soil strength, hence making terrain prone to slope failures. SPI indicates the erosive power of the streams and lower ranges of SPI is related to the low erosive power of the streams.

High LHZ classes are also observed in the areas in closer proximity to drainages (drainage buffer) and it can be attributed to the stream bank erosion due to the river flow such as gulling, toe cutting which further leads to landslides.

Lithology of the area belongs to different Formations and is represented by characteristic rock type, which might govern landslide incidence. High LHZ classes were observed in the rocks belonging to Chandpur and Nagthat Formation where low susceptibility classes are observed in rocks belonging to Blaini, Mandhali, and Deoban Formations. Rocks belonging to Chandpur Formation are mostly weathered phyllites which

are inherently failure prone. Rocks of Blaini, Mandhali, and Deoban Formations constitute of slate, quartzite, siltstone and carbonate rocks and are found in low LHZ classes. Alluvial soil has been observed at lower elevations along the drainage network and is not well compacted and it leads to slope failures which is manifested in the form of high hazard area in the LHZ.

High hazard zone was observed all around the fringes of the reservoir rim owing mainly to the process of reservoir side slope settlement process. Road network and other infrastructures were observed along the reservoir rim boundary. Higher LHZ classes were observed all along the areas in closer proximity to road. Impact of lineament and slope profile curvature do not show any characteristic pattern as observed from the LHZ. Combined effects of unplanned construction and reservoir side slope adjustment process results in a number of landslides during monsoon season which is reflected in the susceptibility map. Forest areas were observed in low susceptibility region of the map. Validation was performed using cumulative percentage/success rate curve technique and gave an acceptable prediction accuracy of 80%.

CHAPTER 6
LHZ MAPPING USING DATA DRIVEN METHODS

6.1 Data Driven Methods

A number of methods are practiced for the mapping of landslide hazard zones, which are based on the landslide inventory. Complete landslide inventory involves the present and historical information of landslide incidences with their types and landslide area. Incomplete landslide inventory data is not feasible for the LHZ mapping. Based on a comprehensive landslide inventory, quantitative and computational process based techniques can be applied to delineate landslide probable zones. Quantitative LHZ mapping has been discussed in chapter 1. These are landslide inventory driven techniques, in which landslide density, in factor classes, are considered, which further leads to the characterization of the factor classes pertaining to their significance in landsliding. Quantitative methods such as frequency ratio, weights of evidence (WofE), binary logistic regression and discriminant analysis vary in their conceptual models but all are based on presence or absence of landslides in factor classes. On the other hand, advancement in computation technology, data mining approaches have led to use of several approaches for the purpose of LHZ mapping and these commonly include landslide inventory information. Artificial neural network (ANN), support vector machines (SVM), decision tree (DT), Naive Bayes (NB) models and Adaptive neuro-fuzzy interface system (ANFIS) model (Samui 2008; Saito et al. 2009;Wan and Lei 2009; Pradhan et al. 2010; Yeon et al. 2010; Yilmaz 2010; Miner et al. 2010; Tien Bui et al. 2012). The main advantage of these models is that it can be used for handling large input data with fast learning capacity.

In the present study, two bivariate statistical methods namely, landslide frequency ratio and WofE along with a multivariate statistical method, binary logistic regression method (BLR) was used to produce LHZ map. Arc GIS 9.3, SPSS and Matlab 2010 software were used to perform the above mentioned analysis. Arc GIS 9.3 software in

addition to Arc-SDM extension for spatial data modeling (Bonham-Carter 1994; Kemp and others, 2001) was used for neural network analysis.

6.2. LHZ Mapping Using Frequency Ratio Method

Landslide frequency ratio, as discussed in the Chapter 3, is based on landslide density, present in each factor class (Table 3.1). The frequency ratio value of each factor class reflects their significance in landsliding. It follows the rules of conditional probability in which frequency ratio >1 is an indicative of strong relationship of factors/class in landsliding whereas <1 reflects weaker relationship of factors with landslide occurrences. A normal procedure of LHZ mapping based on landslide frequency ratio approach includes: a) rating of factor classes based on landslide frequency ratio value and b) arithmetic summation of rated factor classes to produce LHI map. But in the present study, frequency ratio value of each factor class was normalized in a range of 0 to 1 and a new tool named 'fuzzy SUM overlay' of Arc GIS 10.1 was used to integrate rated factors. Further, cumulative percentage curve was generated for the validation of the method.

6.2.1 LHZ mapping

For the LHZ mapping, normalized values in the range of 0 to 1 were used for rating to the factor classes (Table 5.1). Each factor was reclassified according to the rating values of their classes. Reclassified factor maps containing rating information were subjected to fuzzy SUM overlay. This tool is recommended for use with the result of fuzzy membership tool and it is also meant to be applied to rasters with values that range between 0 and 1 (ESRI 2012). Fuzzy sum overlay works on the principle of fuzzy SUM operator (Section 5.1). The Fuzzy SUM overlay type adds the membership values (which in this case are the frequency ratio values) of each factor class the cell location belongs to. The resulting sum is an increasing linear combination function, that is based on the number of factors entered into the analysis (ESRI 2012). As the factor ratings were in the range of 0 and 1, they fulfilled the criteria of fuzzy SUM overlay. Data integration resulted in LHI map (Figure 6.1), which was reclassified using Jenk's Natural Break classifier and class breaks were identified (Table 6.1) (Figure 6.2), which led to generation of LHZ map containing very low hazard, low hazard, moderate hazard, high hazard and very high hazard zones. Figure

6.3 depicts the LHZ map prepared on the basis of fuzzy SUM overlay, whereas Figure 6.4 reflects the percentage area occupied by different hazard zones.

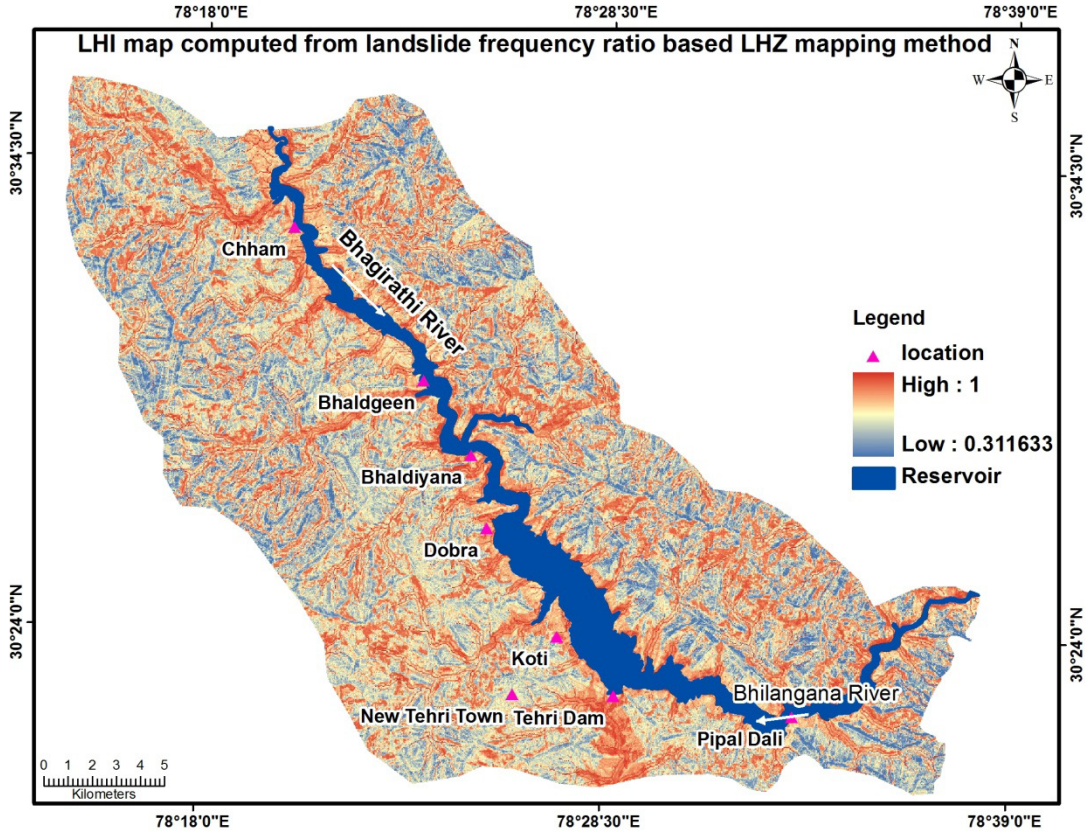

Figure 6.1 LHI map generated by applying landslide frequency ratio method for LHZ mapping

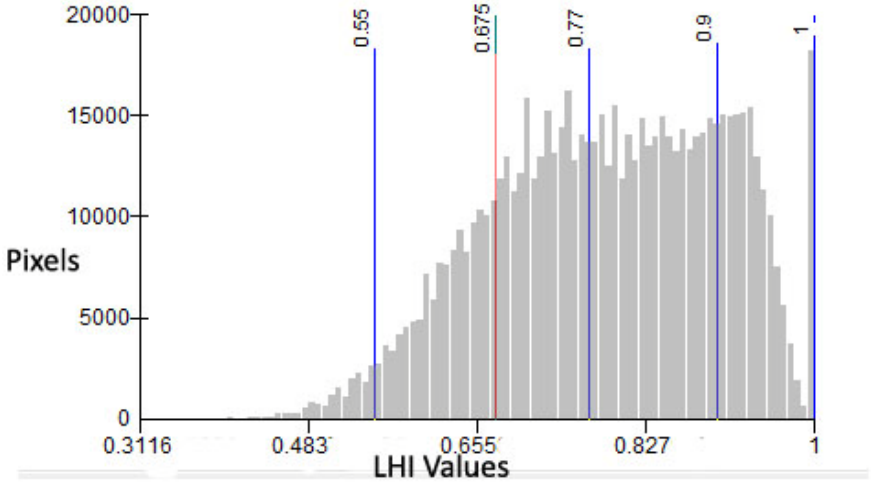

Figure 6.2 Threshold values chosen for classification of LHI map

Table 6.1: Referring range of LHI values used for LHZ mapping

LHZ	Range
Very low	0.311 – 0.55
Low	0.55 – 0.675
Moderate	0.675 – 0.77
High	0.77 – 0.9
Very high	0.9 - 1

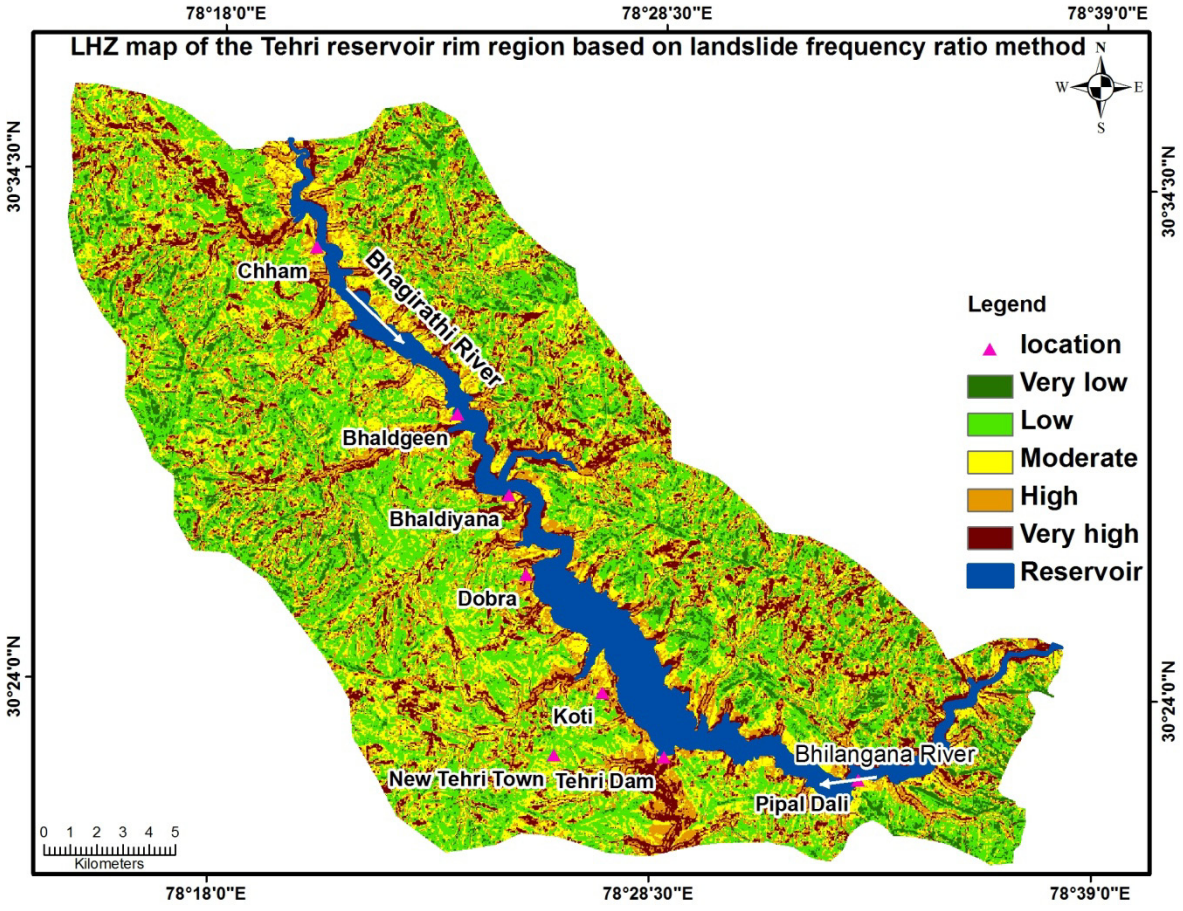

Figure 6.3 LHZ map of Tehri reservoir rim region based on landslide frequency ratio method

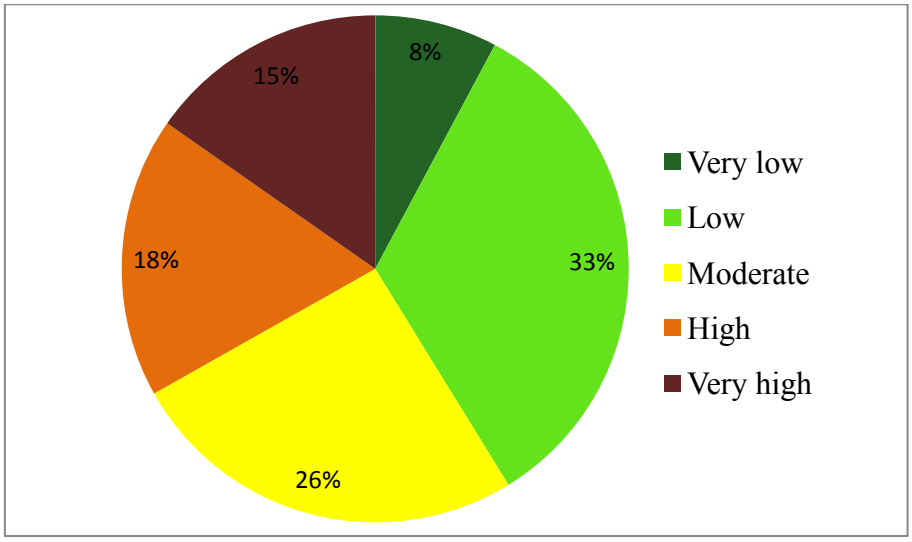

Figure 6.4 Pie chart showing percentage area occupied by different hazard zones

6.2.2 Validation

Validation was performed on the basis of cumulative percentage curve technique, procedure of which has been discussed in the previous chapter. Cumulative percentage curve was prepared using the landslide data meant for the accuracy (Total 60% landslide locations used for the landslide frequency ratio calculation and rest 40 % for the validation) (Figure. 6.5). The curve (Figure 6.5) shows that 33% of the landslides fall under the initial 10% of high LHI classes and more than 50% landslides fall under initial 20% of high LHI classes, which further indicate the prediction capability of the frequency ratio based LHZ method. Area under curve value (AUC) was calculated using the simple trapezium method, which gave a value of 0.72 for the curve in Figure 6.5. AUC value can be converted into percent prediction accuracy which in the present case is 72%. Bar chart method was also utilized in this case by using the whole landslide data. Percentage of landslides in each LHZ class was arranged along with the percent domain of LHZ classes and a bar chart was generated (Figure 6.6).

6.2.3 Discussion

Landslides cause substantial loss to property every year in the Tehri reservoir rim region. In a reservoir rim region, LHZ study delineates landslide probable zones around the reservoir boundary. Various methodologies have been used for landslide hazard/

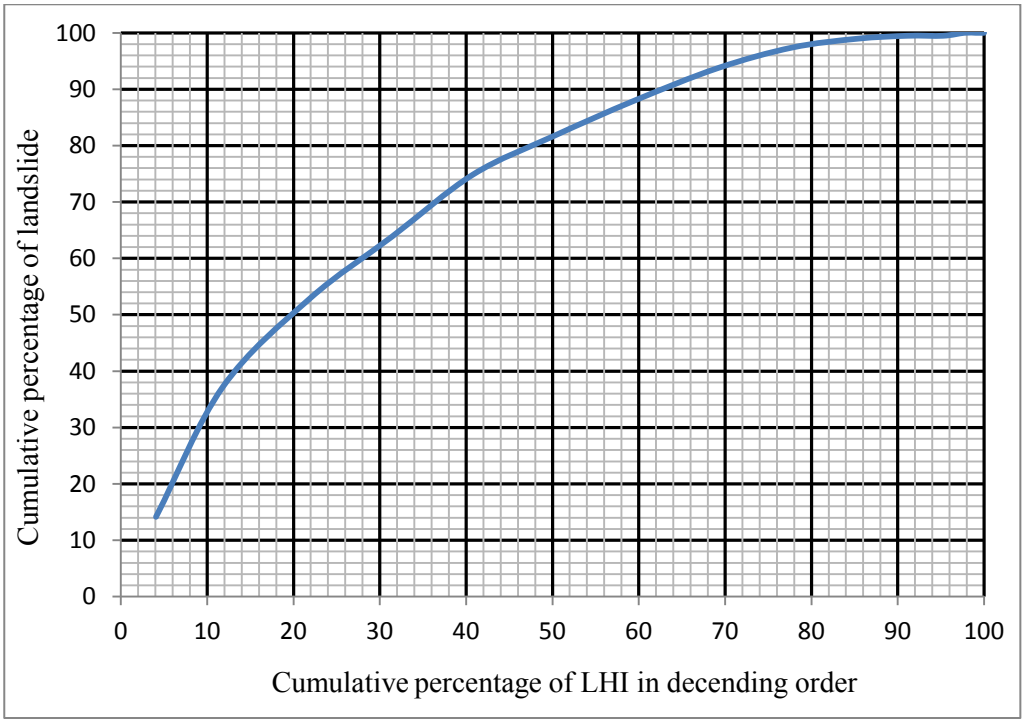

Figure 6.5 Cumulative percentage curve showing the frequency of landslide against the LHI

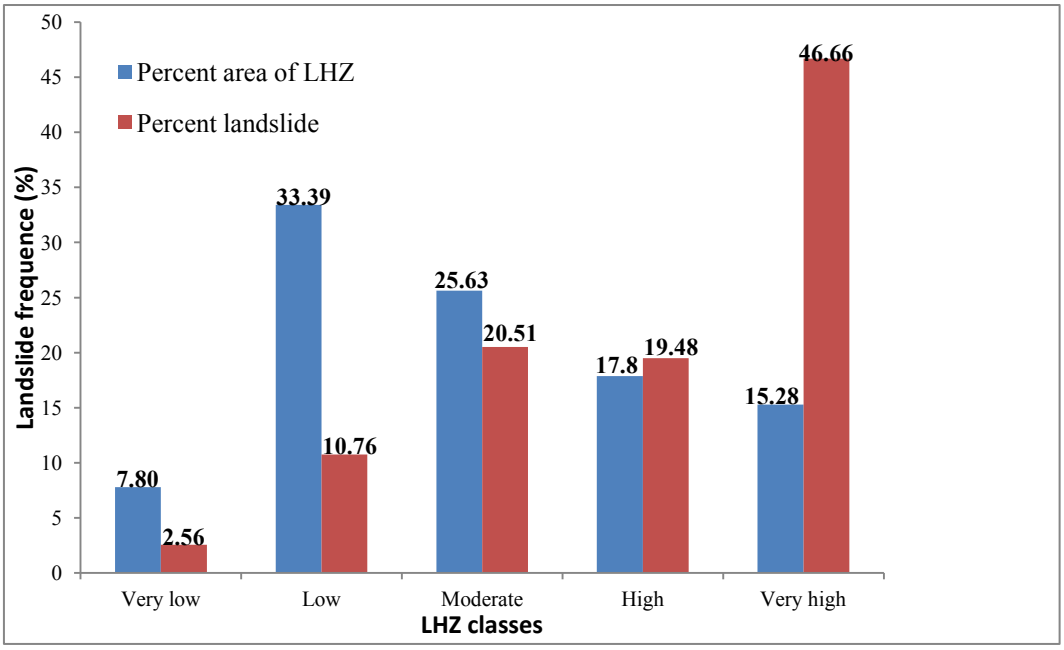

Figure 6.6 Bar chart showing landslide frequency in the LHZ

susceptibility zonation mapping. In this study, a landslide frequency ratio method for estimating landslide probable area was applied. LHZ was computed by assuming that the future landslides can be predicted by quantitative relationships among past landslides and the terrain factor classes. The statistical relationship between the terrain factors and the landslides are described in the chapter 3.

6.3. LHZ Mapping Using Weights of Evidence Method

WofE method is a Bayesian approach in a log-linear form, and it uses the prior probability of occurrence of an event such as landslide, to compute its posterior probability on the basis of the correlation between the evidential themes (factors) and landslide inventory. The objective of the study is to assess the applicability of WofE method in landslide susceptibility study of Tehri reservoir rim area. Several authors have successfully attempted WofE model in different parts of Himalaya to obtain the degree of susceptibility of terrain (Mathew et al. 2007; Dahal et al. 2008; Sharma and Kumar 2008; Ghosh et al. 2009; Kayastha et al. 2012). WofE method was originally developed for the mapping of mineral potential of an area (Bonham-Carter et al. 1988, 1989; Agterberg et al. 1993). Based on exhaustive field studies, 13 causative factors were used to generate LHZ using WofE model.

6.3.1 Methodology

WofE is a data-driven approach, which is primarily a Bayesian approach in the log-linear form using prior and posterior probability (P). WofE approach is applied, when sufficient data is available to estimate the relative importance of evidential themes by statistical means (Bonham-Carter 1994; Pradhan et al. 2010). WofE method works on the principles of conditional probability and determines the weight of a predictive pattern, B (factor/class), and given the known occurrence D (landslide) within it. Weights of the predictive pattern are synthesized on the basis of favourability of locating an occurrence of landslides given the presence and absence of the predictor (Pradhan et al. 2010). Bonham-Carter et al (1988, 1989) synthesized the mathematical formulation to deduce posterior probability of occurrence D, given the predictive pattern/factor B in terms of an odds-type formulation, where the odds, O, are defined as $O = P/(1- P)$.

$$O\{D|B\} = 0\{D\}\frac{P\{B|D\}}{P\{B|\bar{D}\}} \quad (6.1)$$

$$O\{D|\bar{B}\} = 0\{D\}\frac{P\{\bar{B}|D\}}{P\{\bar{B}|\bar{D}\}} \quad (6.2)$$

Weights for each landslide predictive pattern are computed on the basis of the presence or absence of landslides within it:

$$W^+ = \log_e \frac{P\{B|D\}}{P\{B|\bar{D}\}} \quad (6.3)$$

$$W^- = \log_e \frac{P\{\bar{B}|D\}}{P\{\bar{B}|\bar{D}\}} \quad (6.4)$$

where P denotes probability, W^+ and W^- are the weights for the presence or absence of landslides within a factor class, B refers to the presence of landslide predictive pattern, $\bar{B}$ refers to the absence of predictive pattern, D denotes the landslide occurrence and $\bar{D}$ denotes the landslide non-occurrence. The weights can be computed by cross-tabulating the observed landslide map with the landslide conditioning factor map using the equation below:

$$W^+ = \log_e \frac{\{N(B\cap D)/N(D)\}}{\{N(B\cap \bar{D})/N(\bar{D})\}} \quad (6.5)$$

$$W^- = \log_e \frac{\{N(\bar{B}\cap D)/N(D)\}}{\{N(\bar{B}\cap \bar{D})/N(\bar{D})\}} \quad (6.6)$$

Where N{A} represents number of pixels on the map when {A} occurring. For n number of predictive patterns (B_i, i = 1, 2....n) the posterior odd probability can be calculated using the formula given below and assuming that the predictive patterns are conditionally independent.

$$\log_e O\{D|B_1^s \cap B_2^s \ldots B_n^s\} = \sum_{i=1}^{n} W_i^s + \log_e O\{D\} \quad (6.7)$$

where s is positive or negative corresponding to whether the predictive pattern is present or absent respectively. Posterior odds can be converted to posterior probabilities, based on the relation $P = (O/1 + O)$ (Lee et al. 2002). The statistical significance of the weights can be

tested on the basis of their variances (S^2), which can be estimates roughly as (Bonham-Carter 1994; Kayastha et al. 2012):

$$S^2(W^+) = \frac{1}{N(B \cap D)} + \frac{1}{N(B \cap \bar{D})} \quad (6.8)$$

$$S^2(W^-) = \frac{1}{N(\bar{B} \cap D)} + \frac{1}{N(\bar{B} \cap \bar{D})} \quad (6.9)$$

A positive weight (W^+) reflects that the predictive pattern is present at the landslide locations and the magnitude of this weight is the manifestation of the positive correlation between the presence of the predictive pattern and the landslides. A negative weight (W^-) refers to the absence of the predictive pattern and shows the degree of negative correlation (Dahal et al. 2008). The contrast (C) between W^+ and W^-

$$C = W^+ - W^- \quad (6.10)$$

reflects the spatial correlation between the predictive pattern and the landslides. For a spatial association, the value of C is positive, and for disassociation, the contrast takes a negative value.

6.3.2. Analytical procedure

Initial steps involved the generation of training data set, in which a total of 134 (out of 195) landslide occasions were randomly chosen for the training and rest 61 landslides were kept for validation. To carry out WofE in the present study, Arc SDM extension of Arc GIS 9.3 software was used. The extension has several tools to compute posterior probability map along with a Grand WofE tool which computes W^+, W^- and posterior probability map etc., in a single step. All the thirteen factor maps were subjected to grand WofE tool of the Arc SDM, which resulted in a grand table (Table 6.2) containing W^+, $S^2(W^+)$ W^-, $S^2(W^-)$, $S^2(C)$, C/S(C) and C information of the each factor class using equations 6.5, 6.6, 6.8, 6.9 and 6.10. It also resulted in a posterior probability map containing information of probability (in a range of 0 to 1) of landslide occurrence on cell by cell basis by using eq. 6.7 (Figure 6.7). In general practice, some degree of conditional dependence amongst the predictor maps always exists (Bonham-Carter 1994; Mihalasky 1999; Porwal et al. 2003), which results in the artificial inflation or deflation of the

posterior probability. Henceforth, the posterior probability map should be considered largely as a *relative* ranking of landslide propensity (on cell by cell basis) rather than the corresponding posterior probability values having any direct meaning (Porwal et al. 2003; Fabbri and Chung 2008). Detailed description of W^+, W^- and C of each factor class is mentioned in the chapter 3.

6.3.3 Conditional independence test

WofE method considers conditional independence (CI) between the predictive patterns, in which each pattern induces "independent" evidence of prediction or favourability. If all evidential factors are conditionally independent, then the predicted number of occurrences will equal the observed occurrences (Agterberg and Cheng 2002). In the present research total 13 terrain factors with 65 classes were used for the WofE analysis. For the 65 classes, conditional independence test between them is an enormous work, hence it was assumed that factors and their classes are more or less conditionally independent.

6.3.4 Landslide hazard zonation

As mentioned in the section 6.3.2, the posterior probabilities should not be considered in absolute terms, but as a relative term of landslide favourability, which can be depicted by relative landslide favourable zones instead of using the actual posterior probability values. Arc-SDM's GWofE outputs a continuous raster, which represents landslide probability in a continuous scale from 0 (minimum) to 1 (maximum). In the present case, a minimum probability value of 0.00004 and a maximum of 0.997 was observed. Jenk's Natural Break method was used to classify the posterior probability map into relative LHZ map (Figure 6.8) as indicated in Table 6.3. This table also refers to the area occupied under different LHZ classes, whereas Figure 6.9 depicts percentage of area under different LHZ classes.

Table 6.2: Computed weights, contrast, standard deviation and studentized contrast for classes of various factors based on landslide occurrences

CLASS	A (km^2)	Area %	L (%)	W+	S W+	W-	S W-	C	S C	c/s
Aspect	0.046	0.008	0.00	0.000	0.000	0.000	0.000	0.000	0.000	0.000
North	18.859	3.366	3.73	0.129	0.504	-0.005	0.098	0.134	0.513	0.261
Northeast	98.793	17.633	8.96	-0.788	0.304	0.125	0.102	-0.913	0.321	-2.849
East	36.655	6.542	5.97	-0.112	0.389	0.008	0.099	-0.120	0.402	-0.298
South east	87.373	15.594	25.37	0.647	0.207	-0.150	0.110	0.798	0.234	3.409
South	83.952	14.984	27.61	0.834	0.204	-0.195	0.111	1.029	0.233	4.426
Southwest	81.435	14.534	9.70	-0.480	0.297	0.069	0.102	-0.548	0.314	-1.747
West	37.120	6.625	1.49	-1.659	0.723	0.067	0.097	-1.725	0.729	-2.365
North west	75.934	13.553	8.96	-0.492	0.309	0.065	0.101	-0.556	0.325	-1.711
North	40.123	7.161	8.21	0.172	0.341	-0.014	0.100	0.186	0.356	0.523
Drainage										
0 -50m	14.983	2.684	11.19	0.77	0.26	-0.69	0.082	1.33	0.28	4.76
50 – 100m	15.537	2.783	11.19	1.26	0.26	-0.067	0.082	1.29	0.28	4.62
100 – 150m	31.330	5.613	21.64	1.23	0.19	-0.137	0.086	1.3	0.21	6.26
150 – 200m	31.722	5.683	14.93	1.18	0.23	-0.071	0.083	0.84	0.24	3.48
>200m	464.636	83.237	64.93	-0.47	0.108	1.08	0.11	-1.55	0.158	-9.81
Geology										
Blaini Formation	48.30	8.694	0.00	0.00	0.00	0.00	0.00	0.00	0.00	0.00
Nagthat Formation	121.07	21.793	20.15	-0.08	0.19	0.02	0.10	-0.10	0.22	-0.46
Chandpur Formation	197.13	35.471	55.97	0.46	0.12	-0.38	0.13	0.84	0.17	4.82
Berinag Formation	76.80	13.826	14.18	0.03	0.23	0.00	0.09	0.03	0.25	0.12
Rautgara Formation	41.57	7.490	2.99	-0.92	0.50	0.05	0.09	-0.97	0.51	-1.91
Deoban Formation	34.69	6.235	2.99	-0.74	0.50	0.03	0.09	-0.77	0.51	-1.52
Mandhali Formation	3.91	1.264	0.00	0.00	0.00	0.00	0.00	0.00	0.00	0.00
Rautgara Formation	29.06	5.228	3.73	-0.34	0.45	0.02	0.09	-0.35	0.46	-0.78
Lineament Buffer										
0 – 50m	36.103	6.441	5.97	-0.093	0.390	0.006	0.099	-0.099	0.402	-0.247
50 – 100m	38.707	6.906	2.24	-1.275	0.596	0.061	0.098	-1.336	0.604	-2.211
100 – 150m	79.273	14.143	5.97	-0.991	0.369	0.114	0.100	-1.104	0.382	-2.890
150 - 200m	73.983	13.199	8.21	-0.561	0.321	0.070	0.101	-0.630	0.337	-1.872
>200m	332.439	59.311	77.61	0.345	0.113	-0.699	0.193	1.043	0.224	4.662

Profile Curvature										
Concave	275.544	55.240	47.01	-0.061	0.139	0.057	0.133	-0.118	0.193	-0.614
Convex	282.263	56.588	52.99	0.057	0.133	-0.061	0.139	0.118	0.193	0.614
Reservoir										
0 -100 m	13.776	2.458	14.93	1.805	0.224	-0.137	0.094	1.942	0.243	8.005
100 – 200 m	12.904	2.302	26.87	2.459	0.167	-0.290	0.101	2.749	0.195	14.092
200 – 300 m	12.256	2.187	8.21	1.323	0.302	-0.064	0.090	1.387	0.315	4.406
300 – 400 m	11.620	2.073	0.75	-1.022	1.000	0.014	0.087	-1.035	1.004	-1.031
400 – 500 m	11.141	1.988	3.73	0.630	0.447	-0.018	0.088	0.648	0.456	1.421
>500 m	498.807	88.993	45.52	-0.670	0.128	1.600	0.117	-2.270	0.174	-13.085
Road										
0 – 50 m	32.301	5.785	38.81	1.904	0.139	-0.432	0.110	2.336	0.177	13.172
50 - 100 m	27.960	5.008	5.22	0.042	0.378	-0.002	0.089	0.045	0.388	0.115
100 -200 m	46.575	8.342	5.97	-0.335	0.354	0.026	0.089	-0.360	0.365	-0.988
>200 m	451.489	80.865	50.00	-0.481	0.122	0.961	0.122	-1.442	0.173	-8.343
Relative relief										
Very low	8.405	1.499	1.49	-0.006	0.786	0.000	0.097	-0.006	0.792	-0.007
Low	145.779	26.005	8.21	-1.303	0.311	0.274	0.103	-1.577	0.328	-4.812
Moderate	316.705	56.496	58.96	0.053	0.126	-0.072	0.149	0.124	0.195	0.638
High	81.805	14.593	29.10	0.958	0.204	-0.226	0.112	1.184	0.232	5.097
Very high	7.888	1.407	2.24	0.615	0.692	-0.011	0.097	0.625	0.699	0.895
Slope										
0-8°	27.684	4.939	3.73	-0.337	0.484	0.016	0.098	-0.352	0.493	-0.714
8-18°	136.630	24.374	7.46	-1.336	0.326	0.256	0.103	-1.592	0.342	-4.658
18-30°	288.293	51.429	47.01	-0.110	0.139	0.109	0.133	-0.219	0.192	-1.136
30-42°	104.875	18.709	41.04	1.117	0.177	-0.384	0.121	1.502	0.215	7.000
>42°	3.081	0.550	0.75	0.395	1.162	-0.002	0.096	0.397	1.166	0.340
Soil										
Alluvial/sandy loam	84.092	15.003	55.97	2.354	0.216	-0.766	0.137	3.120	0.256	12.205
Forest Soil/Black clay	283.808	50.634	35.82	-0.413	0.155	0.336	0.124	-0.749	0.199	-3.766
Sandy loam	192.603	34.363	8.21	-1.597	0.309	0.434	0.105	-2.032	0.326	-6.229
SPI										
0 – 3	2.526	0.453	0.75	0.676	1.210	-0.004	0.097	0.679	1.214	0.560
3 – 6	209.757	37.623	31.34	-0.212	0.168	0.116	0.118	-0.328	0.206	-1.595
6- 9	255.445	45.817	52.99	0.193	0.135	-0.183	0.139	0.375	0.193	1.941
9 – 12	82.825	14.856	14.18	-0.048	0.254	0.008	0.104	-0.056	0.274	-0.205
12 - 15	6.978	1.252	0.00	0.000	0.000	0.000	0.000	0.000	0.000	0.000

TWI										
5-8	337.784	60.586	66.42	0.124	0.119	-0.212	0.165	0.337	0.203	1.657
8-12	189.305	33.954	32.09	-0.060	0.169	0.030	0.118	-0.090	0.206	-0.439
12-16	25.748	4.618	0.75	-1.995	1.016	0.049	0.097	-2.045	1.021	-2.004
16-19	4.693	0.842	0.00	0.000	0.000	0.000	0.000	0.000	0.000	0.000
LULC										
Water body	6.570	1.182	2	0.298	0.813	-0.004	0.097	0.302	0.819	0.369
Settlement/barren Land	37.142	6.683	23	1.413	0.294	-0.146	0.104	1.559	0.312	5.004
Agricultural land	123.805	22.276	38	0.309	0.187	-0.100	0.113	0.409	0.218	1.875
Scrub/open forest	209.616	37.715	50	-0.013	0.157	0.008	0.122	-0.021	1.199	-0.107
Dense forest/vegetation	178.648	32.144	21	-0.834	0.229	0.277	0.108	-1.111	0.253	-4.385

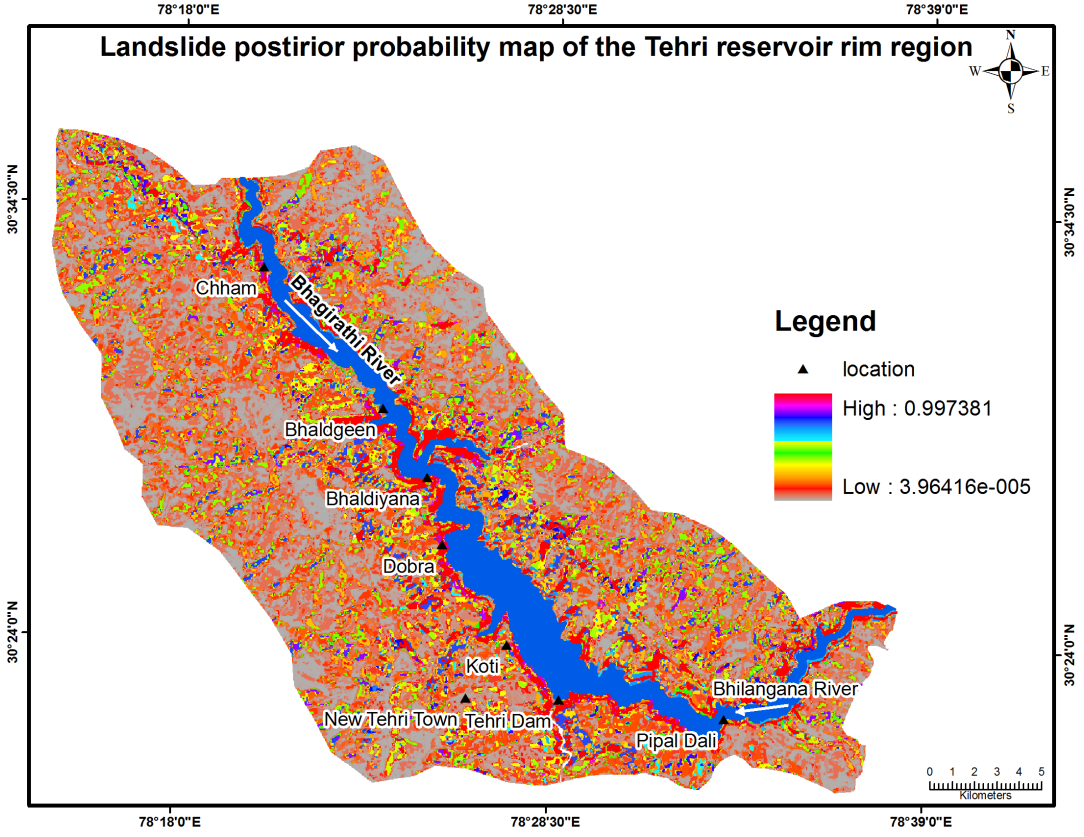

Figure 6.7 Posterior landslide probability map derived using WofE method

Table 6.3: Threshold values adopted for classifying posterior landslide probability map into relative hazard zones and area occupied in the zones

LHZ Class	Threshold value	Area occupied (km^2)
Very low	0.014	121.55
Low	0.06	164.4
Moderate	0.19	141.2
High	0.52	106.6
Very High	0.997	16.25

.

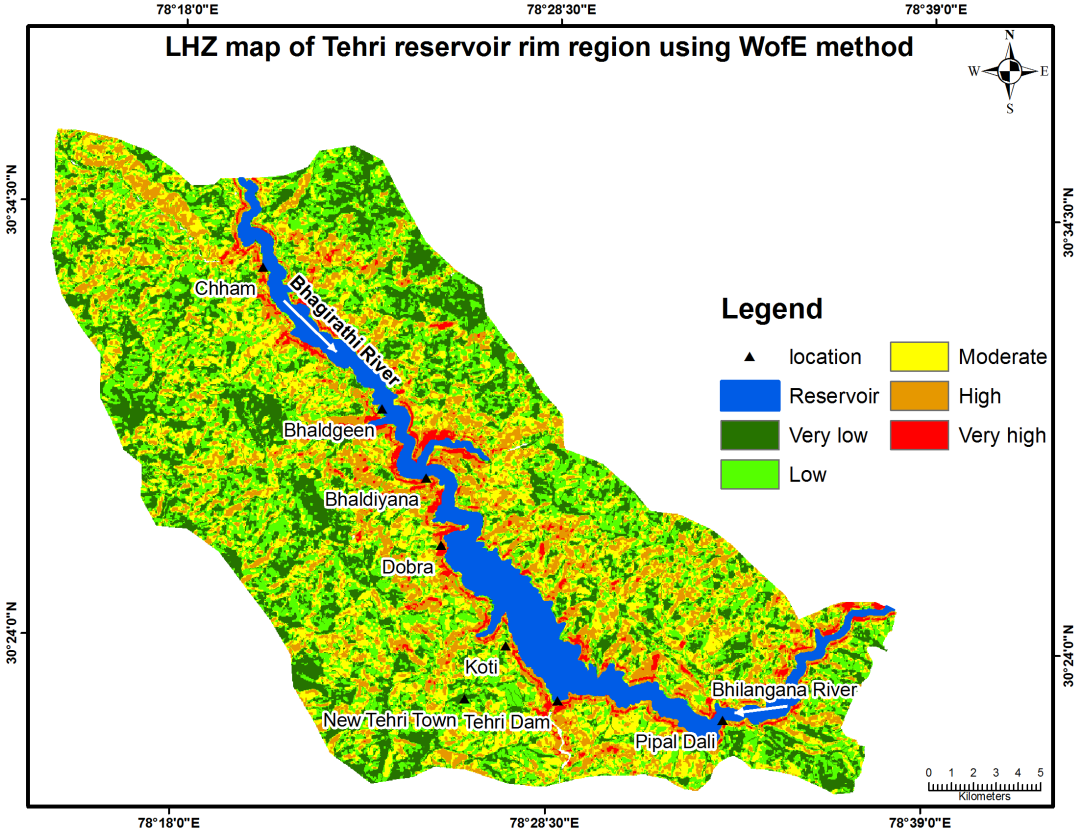

Figure 6.8 LHZ map computed by applying WofE method

6.3.5. Validation

Prediction curve was generated using the 61 landslide incidences used for the accuracy assessment. The posterior probability map was sliced into 25 classes according to the natural break thresholds and cross tabulated with the landslides present in the each sliced class in descending order of the probability classes. Cumulative percentage of the

area of sliced classes and landslide present in those were calculated to generate cumulative percentage curve (Figure 6.10). The curve shows that 60% of the landslides fall under the initial 10% of high probability classes and more than 75% landslides fall under initial 20% of high probability classes. This clearly indicates the prediction capability of the WofE based LHZ method. AUC value was calculated using the simple trapezium method, which gave a value of 0.82. AUC value can be converted into percent prediction accuracy and in the present case, it is about 82%.

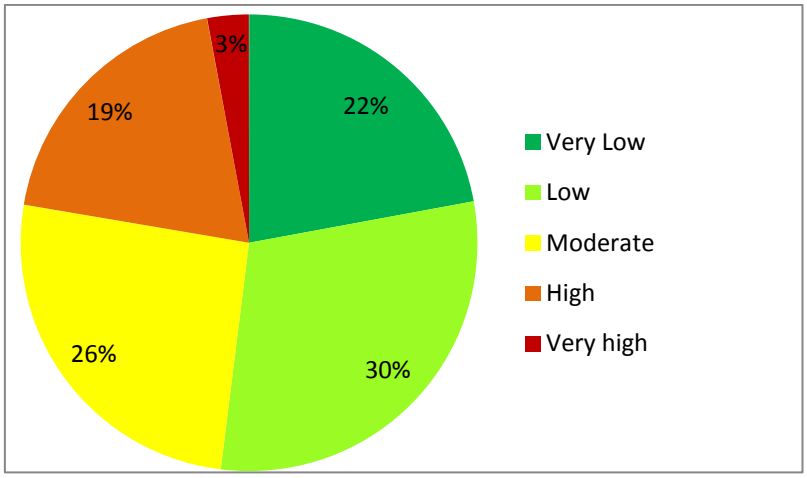

Figure 6.9 Pie chart showing percent area occupied under different LHZ classes

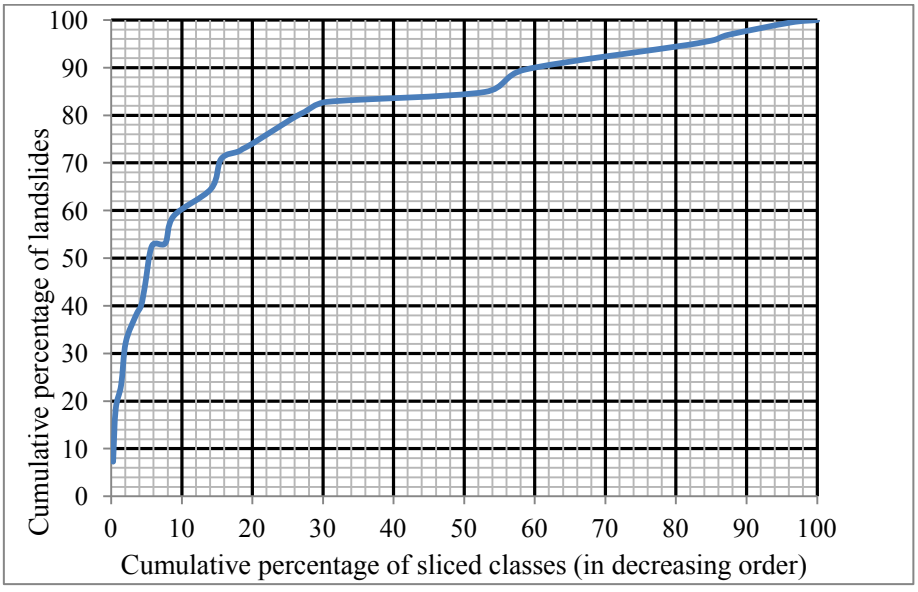

Figure 6.10 Cumulative percentage curve showing landslides in the landslide posterior probability map

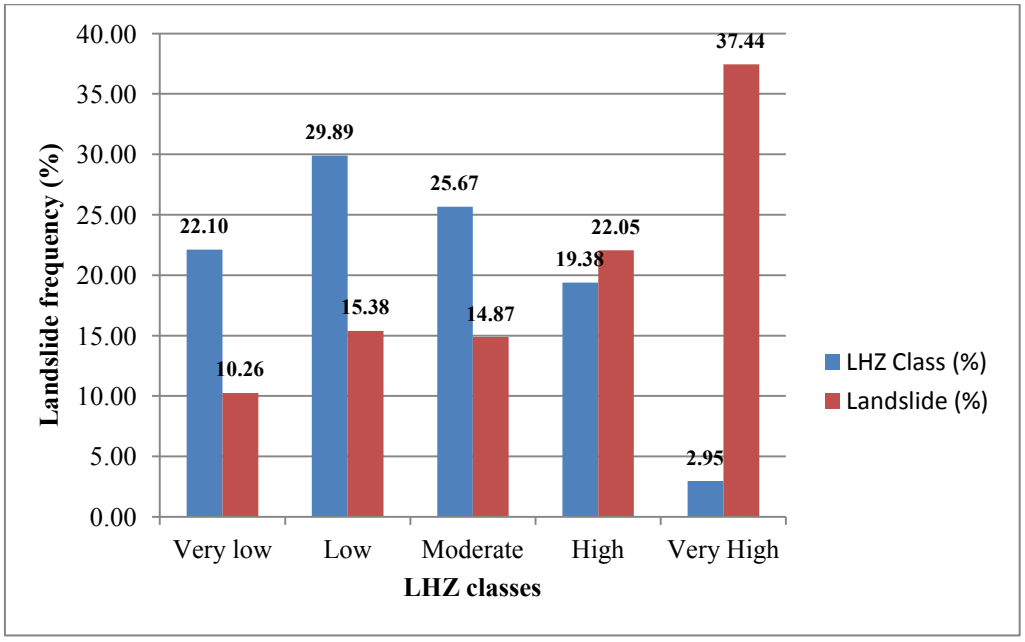

Figure 6.11 Bar chart showing percentage of landslides in each hazard zone

6.3.6. Discussion

Detailed analysis of contrast values (c) are discussed in chapter 3 to show the relationship of landslide factors with the landslide incidences. Through that analysis WofE analysis is able to identify prominent factor classes responsible for the landsliding. In this study, the resulting LHZ map (Figure 6.8) is categorised into very low, low, moderate, high and very high hazard zones in which 22.1 % of the study area has very low hazard, 29.9 % of the study area has low hazard, 25.67 % has moderate hazard, 19.38% has high hazard and the remaining 2.95 % of the study area has the very high hazard. The very high susceptible zone covers 37.44 % of the total observed landslides, whereas high, moderate and low and very low hazard zones cover 22., 14.87, 15,38 and 10.26 % of the observed landslides, respectively (Figure 6.11). Cumulative percentage curve has achieved 82% success in predicting landslides.

6.4. LHZ Mapping Using Logistic Regression Method

In the present study, estimation of LHZ was computed on the basis of binary logistic regression (BLR) method which is a multivariate method. A number of multivariate statistical methods such as linear regression, discriminant analysis and logistic regression are practiced for landslide susceptibility/hazard analysis. Linear regression method was not found to be fit for the landslide susceptibility/hazard zonation study because the coefficient varies from -∞ to +∞. Discriminant analysis can only be performed on a continuous raster data, whereas in the case of logistic regression, continuous, categorical or combination of both can be used at any scale as an independent variable. This kind of statistical analysis utilizes dependent variable (landslides) in binary form. Another advantage of logistic regression is the omission of those factors, which have no significance towards the degree of hazard (Mathew et al. 2009; Chauhan et al, 2010) In the Himalayan region, a number of authors have applied logistic regression method for the identification of landslide hazard zones and have suggested robustness and better prediction capabilities of this method. Application of the BLR model includes characterization of the selected factors, computation of the relative contribution of classes towards landslide occurrences, omission of insignificant classes and probability estimation on grid by grid basis.

6.4.1. Methodology

In this study, BLR method was used for the identification of LHZ. Procedure starts with the training phase which includes identification of the landslide incidences and non-landslide incidences. For LHZ, BLR method assumes landslide data as binary dependent variable and geo-environmental factors as independent variables (factors/classes). A total of 195 landslide incidences were covered in point vector format throughout the area, out of which 116 were considered for the BLR method and rest 79 were considered for the validation purpose. Most of the landslides were found to be shallow in nature and their dimensions more or less similar to the grids (25 m×25 m) chosen for this study, hence point vectors were appropriate for the BLR method. A binary landslide data consists of equal number of landslide occasions and non-landslide occasions. Accordingly, a spatial data consisting of 116 landslide occasion and 116 non-landslide occasions coded with 1

and 0 respectively, was prepared and arranged along with independent variables. All the training points were rasterized to 25 m × 25 m grid. For the 332 training locations, each factor class value was retrieved and arranged spatially in the coded form, which completed the training phase. BLR utilizes maximum likelihood estimation from the logit variable (transformed from the dependent variable) to measure the probability. BLR method is a generalized linear regression method, in which positive outcome of dependent variable is determined on the basis of significant independent variable and linking a function of range (0, 1) to linear regression method. For the LHZ, an important benefit of BLR method compared to other multivariate statistical techniques is that probability values lie between 0 and 1 (Ohlmacher and Davis 2003).

Independent variables/factor class (X1, X2, X3...Xn) can be of continuous, categorical or combination of both to be used in the BLR method. BLR can be quantified using the following formula:

$$P = \frac{1}{1+e^{-Z}} \tag{6.11}$$

P stands for the probability of landslide occurrence based on significant independent variable. Z is the linear combination, which has a range of -∞ to + ∞ in which -∞ to 0 indicates negative influence and 0 to + ∞ shows positive influence of independent variables towards landslide occurrence. Z can be written as:

$$Z = \alpha + \sum_{i=1}^{n} \beta_i X_i \tag{6.12}$$

where α is a constant, which refers to the intercept of the method and β_i is the coefficient of the independent variable X_i. On the basis of the presence of dependent variable in the independent variable, BLR method calculates the regression parameters α and β_i (Mathew et al. 2009; Chauhan et al. 2010; Kundu et al. 2013). Finding the best fit function and consequently computation of α and β_i are indispensible part of a BLR method. Method produces coefficients (β), which are used in the probability estimates of the concerned area on cell by cell basis.

6.4.2. Analytical results and discussion

In this study, SPSS software was used to perform the statistical analysis. It offers several methods for the stepwise selection of the best predictors to include in the method

(Mathew et al. 2013). In this study, maximum likelihood method was used for the step wise selection of the significant predictors. From the base method, which does contain only the constant, the variables have been added in successive steps, such that they cause significant changes in −2 log-likelihood (Mathew et al. 2013; Ohlmacher and Davis 2003). Total 65 independent variables belonging to 13 different classes were considered in the analysis. Forward step wise process initiated with no variables, out of 66 and terminated at seventh step retaining 25 variables. Insignificant variables owe to the significance threshold 0.05. At each successive steps, variables owing to significance threshold <0.05 were retained and >0.05 were terminated. Statistical computation achieved β_i value for each retained variable, which were statistically different from 0 (Table 6.4). To test the hypothesis β_i=0, Wald chi-square (χ^2) value at 5% significance level referring to respective degree of freedom (df) was used (Mathew et al. 2009; Chauhan et al. 2010; Kundu et al. 2013). Equation 6.13 refers to Wald chi-square test:

$$\chi^2 = \left(\frac{\beta_i}{SE}\right)^2 \tag{6.13}$$

where SE stands for the standard error, which can be given as SE=(s/$\sqrt{}$n), s refers to the standard deviation of the samples used for the input and n pertains to sample size in the input data. BLR method achieved 89.7% prediction accuracy in classifying binary training data (Table 6.5). Based on the above mentioned statistical results, a logistic regression equation was obtained which is given in Eq. 6.14

$$Z\ -0.353 + (1.409 * Flat\ aspect) - (2.504 * north\ aspect) + (0.697 * northeast\ aspect) + (1.763 * east\ aspect)(2.8 * southeast\ aspect) + (0.557 * south\ aspect) + (0.550 * southwest\ aspect) + (0.169 * west\ aspect) - (0.724 * > 500m\ DTR) + (3.32 * 100\ DTR) + (3.963 * 200\ DTR) + (2.461 * 300\ DTR12.098 * 400DTR + 6.808 * vlr + 0.413 * Low\ relief - 0.389 * Moderate\ relief + 0.305 * high\ relief - 1.9 * Alluvial\ soil + 0.250 * > 200m\ DTRO + 4.301 * 50m\ DTRO + 0.88 * 100m\ DTRO - 4.35 * VLS - 3.14 * LS - 3.04 * MS - 1.05 * HS \tag{6.14}$$

where *DTR* refers to distance to reservoir, *DTRO* for distance to road, *vlr* for very low relief, *VLS* for very low slope, *LS* for low slope, *MS* for moderate slope and *HS* for high

slope category. BLR statistics has given constant/intercept and the coefficients of the independent variables. Positive coefficient indicates that the independent variable enhances the likelihood of a landslide and the negative values reflect that the probability of landslides is negatively associated (Vanwalleghem et al. 2008; Kundu et al. 2013). Using Eq. 6.12 and Eq. 6.14 landslide probability estimate of entire study area was computed, in which probability values found to be in range of 0 to 1. Further, probability map was divided into following categories: very low susceptible, low susceptible, moderate susceptible, high susceptible and very high susceptible zones on the basis of Jenk's Natural Break classification. Figure. 6.12 depicts the LHZ map of Tehri reservoir rim region.

Coefficient values (β_i) have suggested the significance of independent variables towards the degree of landslide susceptibility. As mentioned in the previous section, positive and negative β_i values influence landslide probability accordingly, whereas insignificant independent values do not result β_i values. In this study, BLR has produced positive β for flat aspect, northeast aspect, east aspect, southeast aspect, south aspect, southwest aspect and west aspect categories. High positive coefficient values have been observed for east, south east and south aspect. It matches with the ground conditions as southern aspect of this region receives high precipitation and henceforth high probability of landslides. High positive β values are observed for the reservoir distance 100 m, 200 m and 300 m respectively and it coincides with the reservoir induced slope failure phenomenon mentioned in the introduction section (Chapter 1). Reservoir distance, of >300 m have given negative β values. Within the relative relief classes, very high positive β value is observed for the very low relief class, low relief and high relief resulted in low positive β value where as negative β is observed for moderate relief class. Overall relative relief categories have suggested mixed resemblance with ground conditions. Alluvial sandy soil class has given negative β value, which can be attributed to the fact that this kind of soil is found in the flatter topography of the area. Distance to road categories is also found to be significant contributor. Very high β value is observed for the distance up to 50 m and it does reflect the contribution of fragile cut slopes left intact after the road construction. Positive β value is also reflected for 100 m distance and >200 m distance to road and it gives the idea about the progressive slope failure phenomenon due to road cut-slopes.

Table 6.4: Significant independent variables retained in BLR method and their coefficients

Variables	β	S.E.	Wald	df	Sig.	Exp(β)
Flat aspect	1.409	1.569	.807	1	.369	4.092
North aspect	-2.504	1.419	3.111	1	.078	.082
Northeast aspect	.697	1.498	.216	1	.642	2.007
East aspect	1.763	1.210	2.124	1	.145	5.829
Southeast aspect	2.801	1.235	5.143	1	.023	16.467
South aspect	.557	1.164	.229	1	.632	1.745
Southwest aspect	.550	1.402	.154	1	.695	1.734
West aspect	.169	1.297	.017	1	.897	1.184
Distance to reservoir >500 m	-.724	.866	.699	1	.403	.485
Distance to reservoir 100 m	3.323	1.021	10.586	1	.001	27.737
Distance to reservoir 200 m	3.963	1.106	12.831	1	.000	52.615
Distance to reservoir 300 m	2.461	1.107	4.940	1	.026	11.715
Distance to reservoir 400 m	-2.098	1.546	1.841	1	.175	.123
Very low relief	6.808	2.505	7.384	1	.007	905.107
Low relief	.413	1.512	.075	1	.785	1.512
Moderate relief	-.389	1.364	.081	1	.775	.677
High relief	.305	1.402	.047	1	.828	1.357
Alluvial sandy soil	-1.905	.762	6.253	1	.012	.149
Distance to road>200 m	.250	.816	.094	1	.759	1.284
Distance to road 50 m	4.301	1.094	15.453	1	.000	73.752
Distance to road 100 m	.880	1.037	.719	1	.396	2.410
Very low slope	-4.355	1.206	13.042	1	.000	.013
Low slope	-3.142	1.074	8.553	1	.003	.043
Moderate slope	-1.042	.958	10.082	1	.001	.048
High slope	1.005	.881	1.302	1	.254	.366
Constant	-.353	1.955	.033	1	.857	.703

β = Coefficients, SE = Standard error, Wald = Wald chi-square, df = Degree of freedom, Sig. = Significance level, Exp (β) = Exponential of β value

Table 6.5: Contingency table referring to the accuracy of estimates

Observed	Predicted		Classification
	Non landslide (0)	Landslide (1)	88.8
Non landslide (0)	103	13	90.5
Observed landslide (1)	11	105	89.7

Within the slope classes, positive β is observed for high slope class, whereas very low, low and moderate classes have resulted in negative β values. All other independent variables have not found significant in BLR method.

6.4.3. Validation

Validation of LHZ maps can be based on the confusion matrix or contingency table (Bonham-Carter 1994). Confusion matrix consists of the calculation of overlap areas between the two binary maps. For confusion matrix, continuous susceptibility maps are compared with the landslide inventory map. There are two types of errors found in LHZ: 1) landslides may occur in areas that are predicted to be stable, and 2) landslides may actually not occur in areas that are predicted to be unstable (Soeters and Van Westen 1996). In the present case Validation of LHZ was performed on the basis of receiver operating characteristic (ROC) curve as well as cumulative percentage curve (Figure. 6.13, 6.14). The ROC curve technique is based on plotting method sensitivity: true positive fraction values calculated for different threshold values versus method specificity: true negative fraction values on a graph. Method sensitivity—true positive fraction is the ratio between correctly classfied presence data and all present data, while method specificity—true negative fraction is the ratio between correctly classfied grid cells without landslides and all grid cells without landslide (Pradhan 2010). Area under the ROC curve has peak value of 1 for perfect prediction, whereas value near 0.5 suggests failure of the method. The ROC curve in the present case is found to be 0.8265, which can be interpreted as having a prediction accuracy of 82.65%. The cumulative percentage curve based on the 79 landslide locations has resulted a success of 83.5% (Figure 6.14)

6.4.4. Discussion

Mechanism of slope failures due to the Tehri reservoir has been elaborated in this study. Most of the talus slopes which are generally made up of thickly compacted debris are subjected to the reservoir fluctuation related landslides. Progressive nature of these slides is major cause of concern for the settlements surrounding them. The present study provides insight about the significance of the independent variables used for the LHZ and the capability of BLR method in predicting landslide susceptible zones in the Tehri reservoir rim region. 65 independent variables belonging to 13 different classes were subjected to BLR analysis and have reflected the significance of variables in landslide

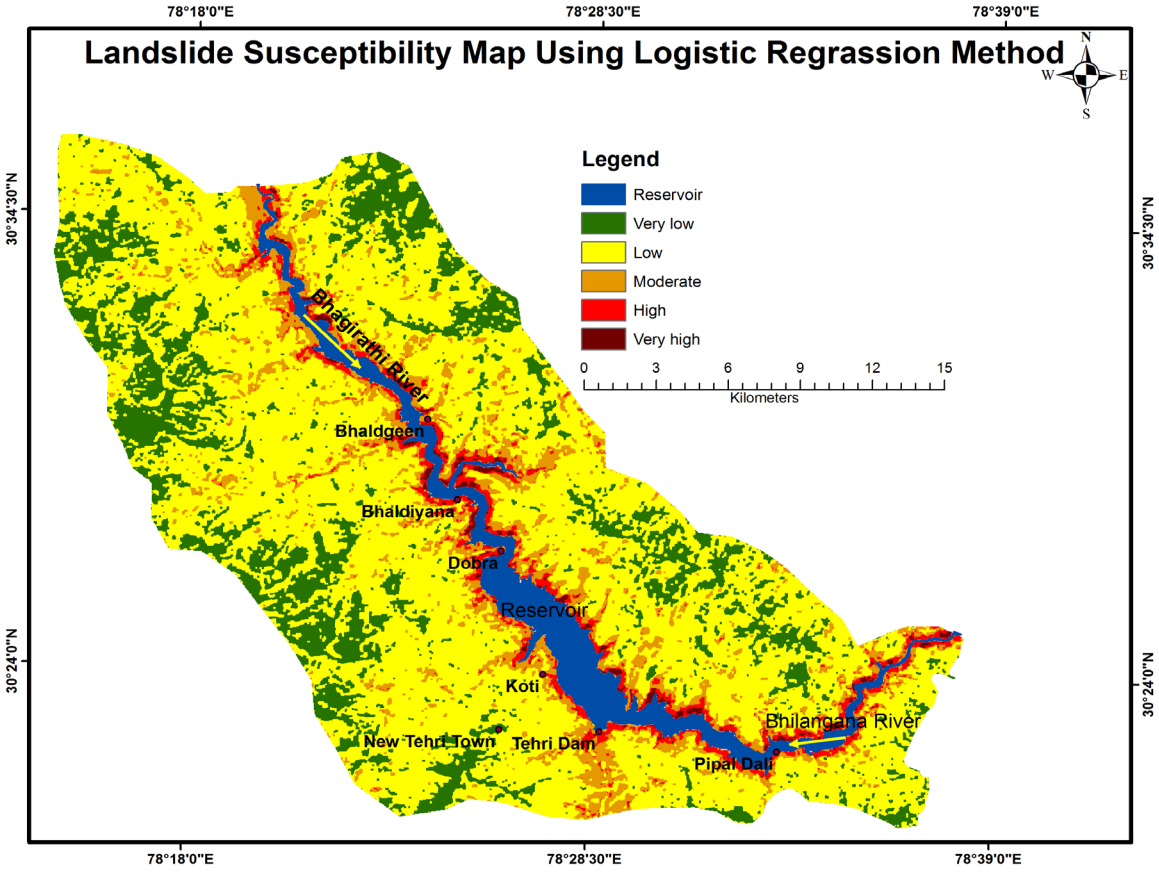

Figure 6.12 LHZ map of Tehri reservoir rim region using binary logistic regression method

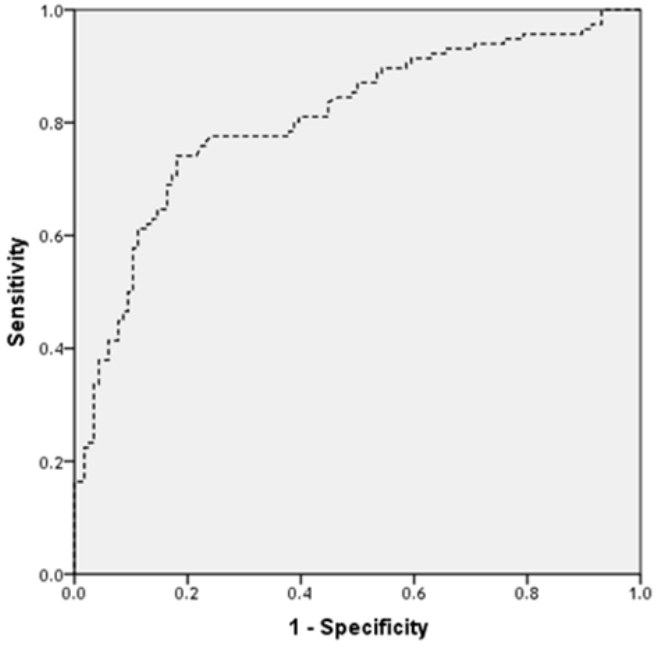

Figure 6.13 ROC curve showing prediction capability of the BLR method

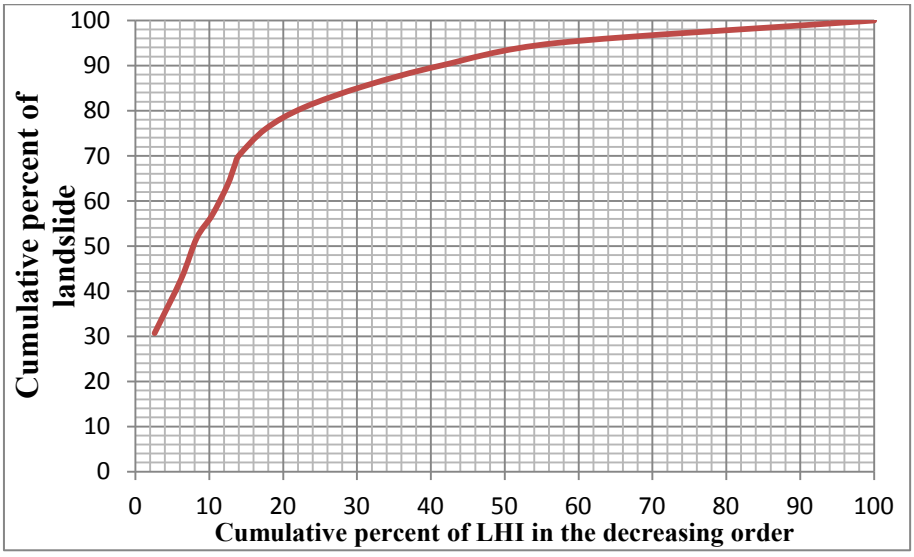

Figure 6.14 Cumulative curve showing prediction capability of the BLR method

occurrences. 25 variables are found to be significant, whereas rest are terminated. Based on these significant variables LHZ map was prepared. The LHZ map has provided critical evaluation of the regions surrounding the reservoir in view of the slope instability. High hazard zone zone has been observed all around the fringes of the reservoir rim. Road network and other infrastructures are observed along the reservoir rim boundary. Combination of unplanned infrastructure development around the reservoir rim region and reservoir side slope adjustment process results in a number of landslides during the monsoon season, which is reflected in the LHZ map. Forested regions are observed in low hazard zone. Validation was performed using ROC curve technique which gave an acceptable prediction accuracy of 82.65%. and cumulative percentage curve technique which resulted 83.5% accuracy

CHAPTER 7
COMPARASION OF LHZ METHODS AND CONCLUSIONS

Tehri dam is one of the major dams located in southeast Asia and is one of the unique dam of its type (5th biggest in the world) with a height of 260.5 meters and reservoir exceeding 42 km in Bhagirathi valley and 25 km in Bhilangana valley. Apart from the dam, there is an underground powerhouse associated with the dam having a capacity of 1000 MW (in first stage). The reservoir has a dead storage level (DSL) at El ± 740 m and the full reservoir level (FRL) at El ± 830 m and thus the gross and live storage of the reservoir is approximately 3540 million m^3 and 2615 million m^3 respectively. The dam lies in the Lesser Himalayan region. A prominent tectonic feature, the NAT lie 5 km north of the dam site and it crosses Bhagirathi at Chham village. Phyllites of Chandpur Formation of Jaunsar Group and quartzites along with limestones and patches of metabasics are exposed along the reservoir spread. Seismically the area falls in Zone IV.

Because of the reservoir water fluctuation, wetting and drying of valley slopes occurs and it results in minor to major landslides. The unstable slope tends to get affected with the functioning of reservoir. Number of villages is situated on both the valley slopes of reservoir. Due to natural process of toe cutting, many settlements (villages) are submerged into the reservoir along with a huge area of farm land. Even though population living in close proximity of reservoir are compensated monetarily, yet the ongoing slope settlement process is continuously damaging the valuable land. The natural reservoir slope stabilization processes combined with the inherent causative factors of slope failure (slope, relative relief, hydro-geological condition, lithology, structural discontinuity) are causing a number of landslides in the reservoir rim region. Reservoir filling might have impacted the hydro-geological conditions of the region which might be a factor for the increased number of slope failure phenomenon reported from the upper reaches of side slopes of the reservoir. Study of the general slope stabilization characteristic of the entire reservoir area is undertaken mainly to understand stable and unstable slopes. For these purposes, remote sensing data along with ancillary data led to the utilization of different methods of LHZ mapping to delineate landslide probable zones.

This research intended to utilize different LHZ methods to delineate landslide probable zones that can be effectively used in the framework of existing terrain conditions and can approximate the relationship between a set of landslide causative terrain factors and the landslide incidences using GIS. In the absence of a universally acceptable method to quantify the relationship between the landslide incidences and the terrain factors, landslide frequency ratio values and WofE derived contrast values were alternatively hypothesized to achieve the relationship. The performance of the LHZ models are analytically compared in this chapter in order to draw conclusions regarding their (a) efficacy in approximating the relationship between landslide incidences and terrain factors, and (b) prediction capability of the different methods on the basis of cumulative percentage curves and landslide density techniques. Here, a best fit method is also proposed for the LHZ mapping in the Tehri reservoir rim region.

7.1. Relationship of the Terrain Factors with the Landslides

Geo-environmental factors responsible for the landsliding are discussed in different literatures, Keeping in view those geo-environmental factors, exhaustive field surveys and interpretation of ancillary data were conducted to select thirteen terrain factors: lithology, soil, LULC, slope, aspect, relative relief, profile curvature, TWI, SPI, road buffer, drainage buffer, photo-lineament buffer and reservoir buffer. Secondary topographic attributes such as TWI and SPI along with a local terrain factor- distance to reservoir (reservoir buffer)- was considered complying with the field conditions. Use of other terrain factors incorporated in this research are indispensible to any LHZ mapping method.

Relationship of all the 13 factors with the landslides was achieved on the basis of landslide frequency ratio and WofE derived contrast value. Summary of the relationship results are listed below:

1. Landslide frequency ratio values, which follow the principle of conditional probability, resulted in significance of the factor classes in landsliding. Among the geological classes, rocks belonging to Chandpur Formation and Nagthat Formation were found to be having strong relationship with landslide probability, whereas other classes showed weak relationship. Settlement with barren land and agricultural land class of LULC type were found to have strong relationship for landslide probability. Alluvial sandy loam soil class shows strong relationship among the soil types. Among the topographic factors, high slope angle, very high slope angle, high relative relief and very high relative relief classes were

found to have strong relationship to landsliding. South, south-east aspect among aspect classes, higher TWI ranges and lower SPI ranges were found to be having strong relationship with the landslide probability. Profile curvature classes show weak relationship. Among the buffer classes, in general, lesser distances classes were found to be having strong relationship with landslide probability for example 0-50 m distance to reservoir, 0 -50 m distance to road, 0-50 m distance to road showed stronger relationship with landslide probability. Relationships progressively became weaker as the distance increased.

2. WofE derived contrast values (C) are a measure of the spatial association between landslides and the factor classes, in which positive value of C indicates positive association and negative value of C indicates negative association. Positive association was observed in Chandpur Formation, Nagthat Formation, alluvial sandy loam, scrub/open forest and agricultural land factor classes. Among the primary topographic factor classes, very high slope angle, high slope angle, moderate relief, high relative relief, very high relative relief, north aspect, southeast aspect and south aspect were found to be positively associated with landslide occurrences. Positive contrast values were observed for the lowest range of TWI and SPI classes. Among the buffer layers, 0-50 m, 50-100 m, 100-150 m and 150-200 m distance to drainage resulted in positive association to landslide. 0-50 m, 50-100 m distance to road, 0-100 m, 100-200 m, 200-300 m distance to reservoir and >200 m distance to lineament classes were found to be positively associated with landslide incidences. Rest other factors were found to be disassociated pertaining to null value of contrast or negatively associated with landslide incidences.

7.2. Comparison of LHZ Models Used in this Study

In this study, seven different LHZ mapping methods belonging to three broader groups- qualitative/heuristic, semi quantitative and quantitative methods were applied for the Tehri reservoir rim area. Heuristic approaches are based on the subjective judgement of an expert for the weighting/rating of the terrain factors. In the present case, a GIS based weighted overlay approach and modified BIS approach was adopted for the LHZ generation. A certain degree of objectivity was brought into the GIS based weighted overlay model by considering landslide frequency ratio value in awarding weights and ratings. A BIS based model is completely subjective in nature. As this method did not utilize the training landslide data, their validation was performed using cumulative

frequency diagram/curve. Two semi-quantitative methods namely, AHP method and combined fuzzy logic and frequency ratio method were used for the LHZ modelling and their validation was performed using cumulative percentage curve. Quantitative methods used in the present study included, frequency ratio approach, WofE approach and logistic regression approach, which utilize landslide inventory data. Cumulative percentage curves were obtained for the validation of the quantitative LHZ method.

For comparison of these methods, landslide density and cumulative percentage curves were analyzed and their descriptions are given below.

7.2.1. Landslide density method

The landslide frequency of each LHZ class is required to compute the landslide density, which is the ratio of number of landslides in a LHZ class to the area of that LHZ class (Sarkar and Kanungo 2004; Kayastha et al 2013). The results are given in Table 7.1. A perfect LHZ map should have the highest landslide density for the very high LHZ class and there should be a decreasing trend of landslide density values successively from the very high to the low LHZ classes (Gupta et al. 2008; Kayastha et al. 2013). From the table, it can be observed that the landslide density for the very high LHZ class is 10, 2.09, 1.22, 1.06, 4.49 and 5.2 respectively for the GIS based weighted overlay method, AHP, fuzzy logic, frequency ratio, WofE and logistic regression methods repsectively, which are distinctly larger than for the other LHZ classes. Furthermore, there is a gradual decrease in density values from very high to low LHZ class and there is also a considerable difference in landslide density values between the LHZ classes. Very high hazard zone is not observed for the modified BIS based LHZ map. Hence, it can be inferred that the LHZ reflect the physical conditions of the ground. The regions that are devoid of landslides in the very high and high LHZ classes indicate potential future failures.

7.2.2. Comparison using the cumulative percentage curve method

Prediction rate curves can be generated by overlaying the landslide data (which was not used to train the model) on the LHI maps. In previous chapters, model validation was performed on the basis of the prediction rate curves (Figure 4.4, 4.19, 5.4, 5.9, 6.5, 6.10 and 6.12) along with the descriptions of those curves and their AUC values. The AUC represents the strength percentage of the model. Variation from 0.9 to 1.0 is the ideal situation (Podiyal et al. 2010). AUC value can be converted to percent prediction accuracy.

Table 7.1 Observed landslide density in the different LHZ classed of LHZ maps

LHZ	Area (km^2)	Landslide frequency (No.)	Landslide frequency density
Weighted overlay			
Very low	30	5	0.17
Low	252	49	0.20
Moderate	239	34	0.14
High	28	97	3.46
Very High	1	10	10
Modified BIS method			
Very low	42.35	15	0.35
Low	213.95	45	0.21
Moderate	215.6	90	0.42
High	78.1	45	0.58
Very High	0	0	0
AHP			
Very low	5	1	0.2
Low	80	5	0.06
Moderate	206	13	0.06
High	198	48	0.24
Very High	61	128	2.09
Fuzzy			
Very low	172.82	13	0.07
Low	104.5	24	0.23
Moderate	118.24	43	0.36
High	109.33	60	0.55
Very High	45.01	55	1.22
Frequency Ratio			
Very low	44	5	0.11
Low	183.7	19	0.10
Moderate	140.8	40	0.28
High	99	43	0.43
Very High	82.5	88	1.06
WofE			
Very low	121.55	20	0.16
Low	164.4	30	0.18
Moderate	141.2	29	0.21
High	106.6	43	0.40
Very High	16.25	73	4.49
Logistic Regression			
Very low	99	9	0.09
Low	363	32	0.09
Moderate	60.5	36	0.59
High	22	68	3.09
Very High	5.5	50	9.09

Table 7.2: AUC values and percentage accuracies of cumulative percentage curves obtained for different landslide hazard methods

LHZ method	AUC	Percent Accuracy
GIS weighted overlay	0.74	74
BIS	0.62	62
Fuzzy logic combined with frequency ratio	0.782	78.2
AHP	0.8	80
Frequency ratio	0.72	72
WofE	0.82	82
Logistic regression	0.835	83.5

In the present research, AUC values of the seven different models were compared to analyze the capabilities of those models in predicting landslide incidences in Tehri reservoir rim region. Table 7.2 depicts the area under curve value calculated from the prediction curves of different LHZ mapping methods. The AUC values are 0.74, 0.782, 0.80, 0.78, 0.82 and 0.835 for GIS based overlay, combined fuzzy logic with frequency ratio, which means that the overall success rates are 72.42%, 75.78% and 75.04% for the heuristic, statistical index and landslide susceptibility maps respectively. These results also validate the LHZ maps with the existing slope instability conditions, and indicate that the maps obtained by the bivariate methods are qualitatively similar and slightly better than the heuristic methods. Modified BIS (LHEF) rating method resulted in least prediction accuracy and it can be said that the modification incorporated in the method has reduced the prediction accuracy. It can also be said that BIS method is a completely field based method which requires extensive field data to produce a LHZ map. Highest accuracy was achieved in the case of logistic regression method with a prediction accuracy of 83.5%.

Based on the comparison between the prediction rate curves, it can be observed that the high prediction accuracy can be achieved from semi-quantitative, bivariate and multivariate methods of LHZ mapping. The peak prediction accuracy can be achieved from the multivariate LHZ mapping technique.

7.3 Concluding Remarks

In the mountainous region like Himalaya, reservoir develops at the place of river valley and generally adjoined by slopes made up of thick debris and river borne material. Water fluctuation between FRL and DSL is associated with reservoir processes. When the water level is at FRL, valley slopes immediate to reservoir periphery are submerged, though the weight of the rocks get reduced due to the uplift pressure of the water, the lateral thrust of the standing water prevents the sliding tendency of the slope. If there is a sudden significant draw-down, it causes increase in the weight of the slope material considerably, while the shear strength gets reduced causing favourable conditions for slope instability. On the other hand, if the reservoir operation is carefully planned so as to avoid sudden draw-down conditions, the stability conditions of the rim may not get changed rapidly. However, the reservoir operations with fluctuating water between FRL and DSL, the side slope stability is invariably affected and the nature of the instability of the reservoir rim area increases gradually with time. During this period, the unstable slopes may tend to fail causing damages to the infrastructure located in the upper levels. A systemic study involving LHZ mapping of the rim area will help to identify the unstable zones so that suitable precautionary measures can be adopted.

REFERENCES

1. Agterberg, F. P. and Cheng, Q. (2002) Conditional independence test for weights of evidence modeling. *Nat. Resour. Res*., v.11, pp. 249–255.
2. AHEC report for Uttarakhand government (2008) Impact of Tehri dam lessons learnt; www.iitr.ernet.in/centers/AHEC/pages/index.html
3. Akgun A., Dag, S. and Bulut, F. (2008) Landslide susceptibility mapping for a landslide-prone area (Findikli, NE of Turkey) by likelihood-frequency ratio and weighted linear combination models. *Environ. Geol.,* v.54, pp. 1127-1143.
4. Aleotti, P. and Chowdhury, R. (1999) Landslide hazard assessment: summary review and new perspectives. *Bull. Engg. Geol. Environ*., v.58, pp. 21–44.
5. Anbalagan, R. (1992) Landslide hazard evaluation and zonation mapping in mountainous terrain. *Engg. Geol.,* v.32, pp. 269–277.
6. Anbalagan, R., Chakraborty, D. and Kohli, A. (2008) Landslide hazard zonation (LHZ) mapping on meso-scale for systematic town planning in mountainous terrain. *J. Sci. Indus. Res*., v.67, pp. 486–497.
7. Anbalagan, R., Kumar, R., Lakshmanan, K., Parida, S. and Neethu, S. (2014) Remote Sensing and GIS Based Landslide Susceptibility Mapping Using Frequency Ratio and Fuzzy Logic Approach. *Int. J. Emerging Tech. .Adv. Engg.*, v.4, pp. 431-441.
8. Arora, M. K., Das Gupta, A. S. and Gupta, R. P. (2004) An artificial neural network approach for landslide hazard zonation in the Bhagirathi (Ganga) Valley, Himalayas. *Int. J. Remote Sens.,* v.25, pp. 559–572.
9. Ayalew, L. and Yamagishi, H. (2005) The application of GIS-based logistic regression for landslide susceptibility mapping in the Kakuda–Yahiko Mountains, Central Japan. *Geomorphology*, v.65, pp. 15 – 31.
10. Ayalew, L., Yamagishi, H. and Ugawa, N. (2004) Landslide susceptibility mapping using GIS-based weighted linear combination, the case in Tsugawa area of Agano River, Niigata Prefecture, Japan. *Landslides*, v.1, pp.73–81
11. Ayalew, L., Yamagishi, H., Marui, H. and Kanno, T. (2005) Landslides in Sado Island of Japan: Part II. GIS-based susceptibility mapping with comparisons of results from two methods and verifications. *Engg. Geol*., v.81, pp. 432–445.
12. Begueria, S. (2006) Validation and evaluation of predictive models in hazard assessment and risk management. *Nat. Hazards,* v.37, pp. 315-329.

13. BIS (1998) Preparation of landslide hazard zonation maps in mountainous terrains-Guidelines, Bureau of Indian Standards (BIS) IS 14496 (Part-2).
14. BIS (2002). criteria for earthquake resistant design of structures: General provisions and buildings, Bureau of Indian Standards (BIS) IS 1893:2002 (Part-1).
15. Bonham-Carter, G. F. (1994) Geographic Information System for Geoscientists: Modelling with GIS, Pergamon/Elsevier Science Ltd, pp. 8.
16. Bonham-Carter, G. F, Agterberg, F. P. and Wright, D. F. (1989) Weights of evidence modelling: A new approach to mappingmineral potential. In: Agterberg, F. P. and Bonham-Carter, G. F. (eds.) Statistical applications in the Earth Sciences. Geological Survey of Canada, pp. 171-183.
17. Brabb, E. E. (1984) Innovative approaches to landslide hazard mapping. In: *Proc. 4th Int. Sym. on Landslides*, Toronto, v.1, pp. 307–324.
18. Carrara, A., Cardinali, M., Guzzeti, F. and Reichenbach, P. (1995) GIS technology in mapping landslide hazard; In: Carrara, A. and Guzzetti, F. (eds), *Geographical Information Systems in Assessing Natural hazards*, Kluwer Academic Publishers, Dordrecht, The Netherlands, pp. 135–175
19. Chakraborty, D. and Anbalagan, R. (2008) Landslide hazard evaluation of road cut slopes along Uttarkashi – Bhatwari road, Uttaranchal Himalaya**.** *J. Geol. Soc. India,* v.71, pp. 115-124.
20. Champatiray, P. K., Suvarna, D., Lakhera, R. C. and Sati, S. (2007) Fuzzy based method for landslide hazard zonation in active seismic zone of Himalaya. *Landslides*, v.5, pp. 101–111.
21. Chauhan, S., Sharma, M., Arora, M. K. and Gupta, N. K. (2010) Landslide susceptibility zonation through ratings derived from Artificial Neural Network. *Int. J. Appl. Earth Observ. Geoinf.,* v.12, pp. 340–350.
22. Chi, K. H., Park, N. W. and Lee, K. (2002) Identification of Landslide Area using Remote Sensing Data and Quantitative Assessment of Landslide Hazard. In: *Proc. IEEE Int. Geosci. Rem. Sens. Symp.* 19 July Toronto, Canada.
23. Choi, S. W., Moon, W. M. and Choi, S. G. (2000) Fuzzy logic fusion of W-Mo exploration data from Seobyeog-ri, Korea. *Geosci. J.*, v.4, pp. 43-52.
24. Chung, C. F. and Fabbri, A. G. (1999) Probabilistic prediction models for landslide hazard mapping. *Photogramm. Engg. Rem. Sens.,* v.65, pp. 1389 – 1399.

25. Chung, C. F. and Fabbri, A. G. (2001) Prediction model for landslide hazard using a Fuzzy set Approach. In: M. Marchetti and V. Rivas (eds), *Geomorphology and Environmental Impact Assessment,* Balkema, Rotterdam, pp. 31–47.
26. Chung, C. F. and Fabbiri, A. G. (2002) prediction models for landslide hazard Zonation using a fuzzy set approach. In: Marchetti, M. and Rivas, V. (eds), *Geomorphology & Environmental Impact Assesment,* Balkema Publishers, pp. 31-47.
27. Chung, C. J. and Fabbri, A. G. (2003) Validation of spatial prediction models for landslide hazard mapping. *Nat Hazards*, v.30, pp. 451–472.
28. Clerici, A., Perego, S., Tellini, C. and Vescovi, P. (2002) A procedure for landslide susceptibility zonation by the conditional analysis method. *Geomorphology,* v.48, pp. 349–364.
29. Dahal, R. K., Hasegawa, S., Nonomura, A., Yamanaka, M., Dhakal, S. and Paudyal, P. (2008) Predictive modelling of rainfall-induced landslide hazard in the Lesser Himalaya of Nepal based on weights-of-evidence. *Geomorphology*, v.102, pp. 496-510.
30. Dahal, R. K., Hasegawa, S., Nonomura, S., Yamanaka, M., Masuda, T. and Nishino, K. (2009) GIS-based weights-of-evidence modelling of rainfall-induced landslides in small catchments for landslide susceptibility mapping. *Environ. Geol.,* v.54, pp. 314–324.
31. Dai, F. C. and Lee, C. F. (2002) Landslide characteristics and slope instability modeling using GIS Lantau Island, Hong Kong. Geomorphology, v.42, pp. 213 – 238.
32. Dai, F. C., Lee, C. F. and Ngai, Y. Y. (2002) Landslide risk assessment and management: an overview. *Engg. Geol.,* v.64, pp. 65–87.
33. Dai, F. C., Lee, C. F., Li, J. and Xu, Z. W. (2001) Assessment of landslide susceptibility on the natural terrain of Lantau Island, Hong Kong. *Environ. Geol.,* v.40, pp. 381–391.
34. Das, I., Sahoo, S., Van Westen, C. J., Stein, A. and Hack, R. (2010) Landslide susceptibility assessment using logistic regression and its comparison with a rock mass classification system, along a road section in the northern Himalayas (India). *Geomorphology*, v.114, pp. 627–637.
35. Das, I., Stein, A., Kerle, N. and Dadhwal, V. K. (2012) Landslide susceptibility mapping along road corridors in the Indian Himalayas using Bayesian logistic regression models. *Geomorphology,* v.179, pp. 116-125.

36. Deleo, J. M. (1993) Receiver operating characteristic laboratory (ROCLAB): software for developing decision strategies that account for uncertainty. In: *Proc. 2nd Int. Sym. uncertainty modelling and analysis.* Computer Society Press, College Park, pp. 318–325
37. Dhobal, D. P., Gupta, A. K., Mehta, M. and Khandelwal, D. D. (2013) Kedarnath diaster: Facts and plausible causes. *Curr. Sci*., v.105, pp. 171-174.
38. Ercanoglu, M. and Gokceoglu, C. (2002) Assessment of landslide susceptibility for a landslide-prone area (north of Yenice, NW Turkey) by fuzzy approach. *Environ. Geol*., v.41, pp. 720–730
39. Ercanoglu, M. and Gokceoglu, C. (2004) Use of fuzzy relations to produce landslide susceptibility map of a landslide prone area (West Black Sea Region, Turkey). *Engg. Geol*., v.75, pp. 229–250.
40. ESRI FAQ. (2012) What is the Jenks optimization method? http://support.esri.com/en/ knowledgebase/techarticles/detail/26442.
41. Feizizadeh, B. and Blaschke, T. (2013) GIS-multicriteria decision analysis for landslide susceptibility mapping: comparing three methods for the Urmia lake basin, Iran. *Nat. Hazards*, v.65, pp. 2105–2128
42. Fell, R., Corominas, J., Bonnard, C., Cascini, L., Leroi, E. and Savage, W. Z. (2008) Guidelines for landslide susceptibility, hazard and risk zoning for land-use planning. *Engg. Geol*., v.102 (3–4), pp.99–111.
43. Fell, R., Finlay, P. J. and Mostyn, G. R. (1996) Framework for assessing the probability of sliding of cut slopes. In: Senneset, K. (ed.) *Landslides, Proc.7th Int. Sym. landslides,* A. A. Balkema, Rotterdam, pp. 201-208.
44. Fritz, H. M. et al. (2012). The 2011 Japan tsunami current velocity measurements from survivor videos at Kesennuma Bay using LiDAR. *Geophys. Res. Letters*, v. 39, pp. L00G23, doi:10.1029/2011GL050686.
45. Ghosh, S., Carranza, E. J. M., Van Westen, C. J., Jetten, V. and Bhattacharya, D. N. (2011) Selecting and weighting spatial predictors for empirical modeling of landslide susceptibility in the Darjeeling Himalayas (India). *Geomorphology,* v.131, pp.35-56.
46. Ghosh, S., Van Westen, C. J., Carranza, E. J. M., Ghoshal, T. B., Sarkar, N. K. and Surendranath, M. (2009) A quantitative approach for improving the BIS (Indian) method of medium-scale landslide susceptibility. *J. Geol. Soc. India,* v.74, pp. 625-638.

47. Gokceoglu, C. and Aksoy, H. (1996) Landslide susceptibility mapping of the slopes in the residual soils of the Mengen region (Turkey) by deterministic stability analyses and image processing techniques. *Engg. Geol*., v.44, pp. 147–161.
48. Gorsevski P. V., Jankowski P. and Gessler, P. E. (2006) An heuristic approach for mapping landslide hazard by integrating fuzzy logic with analytic hierarchy process. Control. *Cybern.*, v.35, pp. 21–141
49. Gupta, P. (1996) Landslide hazard zonation mapping, considering geoenvironmental conditions, of parts of Bhagirathi river valley, U.P. India. Unpublished Doctoral Dissertation, University of Roorkee, India.
50. Gupta, P. and Anbalagan, R. (1997) Landslide hazard zonation (LHZ) and mapping to assess slope stability of parts of the proposed Tehri dam reservoir, India. *Quart. J. Engg. Geol*., v.30, pp. 27-36.
51. Gupta, R. P. and Joshi, B. C. (1990). Landslide Hazard Zonation using the GIS Approach - A case Study from the Ramganga Catchment, Himalayas. *Engg. Geol*. v.28, pp. 119-131.
52. Gupta, R. P., Kanungo, D. P., Arora, M. K. and Sarkar, S. (2008) Approaches for comparative evaluation of raster GIS-based landslide susceptibility zonation maps. *Int. J. App. Earth. Obs*. *Geoinformation*, v.10, pp. 330-341.
53. Gupta, R. P., Saha, A. K., Arora, M. K. and Kumar, A. (1999) Landslide hazard zonation in a part of Bhagirathy Valley, Garhwal Himalayas, using integrated Remote Sensing & GIS. *J. Him. Geol.,* v.20, pp. 71-85.
54. Guzetti, F., Carrara, A., Cardinali, M. and Reichenbach, P. (1999) Landslide hazard evaluation: a review of current techniques and their application in a multi-scale study, central Italy. *Geomorphology*, v.31, pp. 181–216.
55. Guzzetti, F., Reichenbach, P., Ardizzone, F., Cardinali, M. and Galli, M. (2006) Estimating the quality of landslide susceptibility models. *Geomorphology*, v.81, pp. 166–184.
56. Guzzetti, F., Reichenbach, P., Cardinali, M., Galli, M. and Ardizzone, F. (2005) Probabilistic landslide hazard assessment at the basin scale. *Geomorphology*, v.72, pp. 272–299.
57. Hasegawa, S., Dahal, R. K., Yamanaka, M., Bhandary, N. P., Yatabe, R. and Inagaki, H. (2009) Causes of large scale landslides in the Lesser Himalaya of central Nepal. *Environ. Geol.,* v.57, pp. 1423–1434.

58. Hutchinson, J.N. (1995) Landslide hazard assessment. In*: Proc. VI Int. Sym. landslides*, Christchurch, v.1, pp. 1805–1842.
59. Ives, J. D. and Messerli, B. (1989) The Himalayan Dilemma- Reconciling development and conservation. The United Nations University. Routledge, London-New York, pp. 295.
60. Jain, A. K. (1987) Kinematic of the transverse lineaments, regional tectonics and holocene stress field in the Garhwal Himalaya. *J. Geol. Soc. India*, v.30, pp. 169-186.
61. Joint Expert committee report (2011) Study of damages to different villages after filling in reservoir of Tehri dam above elevation 830 m. Government of Uttarakhand, Dehradun, India.
62. Kanungo, D. P., Arora, M. K., Sarkar, S. and Gupta, R. P. (2006) A comparative study of conventional, ANN black box, fuzzy and combined neural and fuzzy weighting procedures for landslide susceptibility Zonation in Darjeeling Himalayas. *Engg. Geol*., v.85, pp. 347–366.
63. Kanungo, D. P., Arora, M. K., Sarkar, S. and Gupta, R. P. (2009a) Landslide Susceptibility Zonation (LSZ) Mapping – A Review. *J. South Asia Disaster Studies*, v.2, pp. 81-105.
64. Kanungo, D. P., Arora, M. K., Sarkar, S. and Gupta, R. P. (2009b) A Fuzzy Similarity Concept Based Rating Determination and Fuzzy Gamma Operator Based Thematic Maps Integration for Landslide Susceptibility Zonation. *Georisk*, v.3, pp. 30-40.
65. Kayastha, P., Dhital, M and De Smedt, F. (2012) Landslide susceptibility mapping using the weight of evidence method in the Tinau watershed, Nepal. *Nat Hazards*, v.63, pp.479–498
66. Kayastha, P., Dhital, M., De Smedt, F. (2013) Application of the analytical hierarchy process (AHP) for landslide susceptibility mapping: a case study from the Tinau watershed, west Nepal. *Comp. Geosci.,* v.52, pp. 398–408.
67. Kirschbaum, D., Adler, R., Hong., Y., Hill, S. and Lerner-Lam, A. (2010). A global landslide catalog for hazard applications: method, results, and limitations. *Nat. Hazards*, v.52, pp. 561-575.
68. Kleianbum, D. G. (1994) Logistic regression: A self learning text. Springer, New York, pp. 282.
69. Kouli, M. et al. (2010) Landslide hazard zonation in high risk areas of Rethymno Prefecture, Crete island, Greece. *Nat. Hazards*, v.52, pp. 599-621.

70. Kumar, G. and Dhoundiyal, J. N. (1976) Stratigraphy and structure of Garhwal synform, Garhwal and Tehri Garhwal districts, Uttar Pradesh, An appraiser. *J. Himalayan Geol*., Part-1, v.9, pp. 18-39.
71. Kumar, R and Anbalagan, R. (2013) Pixel based terrain analysis for Landslide Hazard Zonation, a case study of Tehri reservoir region, Uttarakhand, India. In*: Int. Geos. Remote Sens. Sym. (IGARSS), IEEE,* pp. 2868-2871
72. Kundu, S., Saha , A. K., Sharma, D. C. and Pant, C. C. (2013) Remote Sensing and GIS Based Landslide Susceptibility Assessment using Binary Logistic Regression Model: A Case Study in the Ganeshganga Watershed, Himalayas. *J. Ind. Soc. Remote Sens.,* v.41(3), pp. 697-709.
73. Lee, S. (2005). Application of logistic regression model and its validation for landslide susceptibility mapping using GIS and remote sensing data. *Int. J.. Remote Sens*., v.26 (7), pp. 1477–1491.
74. Lee, S. and Choi, J. (2004) Landslide susceptibility mapping using GIS and the weight-of-evidence model. *Int J Geogr Inf Sci,* v.18, pp. 789–814.
75. Lee, S., Choi, J. and Min, K. (2002) Landslide susceptibility analysis and verification using the Bayesian probability model. *Environ. Geol.,* v.43, pp. 120–131.
76. Lee, S. and Pradhan, B. (2007) Landslide hazard mapping at Selangor, Malaysia using frequency ratio and logistic regression models. *Landslides*, v.4, pp. 33-41.
77. Lee, S. and Sambath, T. (2006). Landslide susceptibility mapping in the Damrei Romel area, Cambodia using frequency and logistic regression models. *Environ. Geol.,* v.50, pp. 847–856.
78. Lee, S. and Talib, J. A. (2005) Probabilistic landslide susceptibility and factor effect analysis. *Environ. Geol*., v.47, pp. 982-990.
79. Malczewski, J. (1999) GIS and multi criteria decision analysis. Wiley, New York. ISBN: 978-0-471-32944-2, pp. 408
80. Mandal, S. and Maiti, R. (2013) Assessing the triggering rainfall-induced landslip events in the Shivkhola watershed of Darjiling Himalaya, West Bengal. *European J Geog*., v.4.
81. Mathew, J., Jha, V. K. and Rawat, G. S. (2007) Weights of evidence modelling for landslide hazard zonation mapping in part of Bhagirathi valley, Uttarakhand. *Curr. Sci.,* v.92, pp. 628–638.

82. Mathew, J., Jha, V. K. and Rawat, G. S. (2009) Landslide susceptibility zonation mapping and its validation in part of Garhwal Lesser Himalaya, India, using Binary Logistic Regression analysis and receiver operating characteristic curve method. *Landslides,* v.6, pp. 17-26.
83. Mondal, S. and Maiti, R. (2012) Landslide susceptibility analysis of Shiv-Khola watershed, Darjiling: A remote sensing & GIS based Analytical Hierarchy Process (AHP). *J. Ind. Soc. Remote Sens.*, v.40, pp. 483–496.
84. Mihalasky, M. J. (1999) Mineral potential modelling of gold and silver mineralization in the Nevada Great Basin-: a GIS-based analysis using weights of evidence. *Unpublished Doctoral Dissertation,* Univ. Ottawa.
85. Miner, A. S., Vamplew, P., Windle, D. J., Flentje, P. and Warner, P. (2010) A comparative study of various data mining techniques as applied to the modeling of landslide susceptibility on the Bellarine Peninsula, Victoria, Australia. In: Geologically Active, Williams, A. L., Pinches, G. M., Chin, C. Y. and McMorran, T. J. (eds.), CRC Press, New York, NY, USA, pp. 352.
86. Moon, A.T., Olds, R.J., Wilson, R.A., and Burman, B.C. (1992) Debris flow zoning at Montrose, Victoria. In: Bell, D. H. (ed.) *Landslides, Proceedings of the 6th International Symposium on Landslides*, A. A. Balkema, Rotterdam, v.2, pp. 1015–1022.
87. Moon, W. M. (1998) Integration and fusion of geological exploration data: a theoretical review of fuzzy logic approach. *Geosci. J.*, v.2, pp. 175-183.
88. Nagarajan, R., Mukherjee. A., Roy. A and Khire, M. V. (1998) Temporal remote sensing data and GIS application in landslide hazard zonation of part of Western Ghat, India. *Int. J. Remote Sens.*, v.19, pp. 573–585
89. Nagarajan, R., Roy, A., Vinod Kumar, R., Mukherjee, A. and Khire, M. V. (2000) Landslide hazard susceptibility mapping based on terrain and climatic factors for tropical monsoon regions. *Bull. Eng. Geol. Environ*. v.58, pp. 275 – 287.
90. NDMA (2009) Management of landslides and snow avalanches. National Disaster Management Authority (NDMA), Government of India, New Delhi, pp. 144.
91. Nilsen, T. H. and Brabb, E. E. (1977) Slope stability studies in the San Francisco Bay region, California. Geological Society of America, *Rev. Engg. Geol.,* v.3, pp. 235–243.
92. OFDA/CRED (2010) EM-DAT International Disaster Database- www.em-dat.net. Universite Catholique de Louvain, Brussels, Belgium.

93. Ohlmacher, C. G. and Davis, J. C. (2003) Using multiple logistic regression and GIS technology to predict landslide hazard in northeast Kansas, USA. *Engg. Geol.,* v.69, pp. 331–343.
94. Pachauri, A. K., Gupta, P. V. and Chander, R. (1998) Landslide zoning in a part of the Garhwal Himalayas. *Environ. Geol*., v.36, pp. 325–334.
95. Pachauri, A. K. and Pant, M. (1992) Landslide hazard mapping based on geological attributes. *Engg. Geol.,* v.32, pp. 81–100.
96. Pandey, A., Dabral, P. P., Chowdary, V. M. and Yadav, N. K. (2008). Landslide hazard zonation using remote sensing and GIS: a case study of Dikrong river basin, Arunachal Pradesh, India. *Environ. Geol*., v.54, pp. 1517–1529.
97. Pardeshi, D. S., Autade, E. S. and Pardeshi, S. S. (2013) Landslide hazard assessment: recent trends and techniques. *Environ. Earth Sci.,* v.2, doi:10.1186/2193-1801-2-523
98. Porwal, A., Carranza, E. J. M. and Hale, M. (2003) Knowledge-driven and data-driven fuzzy models for predictive mineral potential mapping. *Nat. Resour. Res*., v.12, pp. 1-25.
99. Poudyal, C. P., Chang, C., Oh, H. and Lee, S. (2010) Landslide susceptibility maps comparing frequency ratio and artificial neural networks: a case study from the Nepal Himalaya. *Environ. Earth Sci.,* v.61, pp. 1049–1064.
100. Pourghasemi, H. R., Goli Jirandeh, A., Pradhan, B., Xu, C. and Gokceoglu, C. (2013) Landslide susceptibility mapping using support vector machine and GIS. *J. Earth Syst. Sci.*, v.122, pp. 349–369.
101. Pradhan, B. (2010) Remote sensing and GIS-based landslide hazard analysis and cross-validation using multivariate logistic regression model on three test areas in Malaysia. *Adv. Space. Res.*, v.45, pp. 1244-1256.
102. Pradhan, B. and Lee, S. (2010) Delineation of landslide hazard areas on Penang Island, Malaysia, by using frequency ratio, logistic regression, and artificial neural network models. *Environ. Earth. Sci.*, v.60, pp. 1037-1054.
103. Pradhan, B., Lee, S. and Buchroithner, M. F. (2010) A GIS-based back-propagation neural network model and its cross application and validation for landslide susceptibility analyses. *Comp. Environ. Urban Sys.,* v.34, pp. 216–235.
104. Ramani, S. E. , Pitchaimani, K. and Gnanamanickam, V. R. (2011) GIS based landslide susceptibility mapping of Tevankarai Ar sub-watershed, Kodaikkanal, India using binary logistic regression analysis. *J. Mt. Sci*., v.8, pp. 505–551.

105. Saaty, T. L. (1977) A scaling method for priorities in hierarchical structures. *J. of Math. Psycho*., v.15, pp.234–281.

106. Saaty, T. L. (1980) The analytic hierarchy process: planning, priority setting, resource allocation. McGraw-Hill International Book Company, New York.

107. Saha, A. K., Gupta, R. P. and Arora, M. K., (2002) GIS-based landslide hazard zonation in the Bhagirathi (Ganga) valley, Himalayas. *Int. J. Remote Sens*., v.23 (2), pp. 357–369.

108. Saha, A. K., Gupta, R. P., Sarkar, I., Arora, M. K. and Csaplovics, E. (2005) An approach for GIS-based statistical landslide susceptibility zonation with a case study in the Himalayas. *Landslides*, v.2, pp. 61-69.

109. Saito, H. Nakayama, D. and Matsuyama, H. (2009) Comparison of landslide susceptibility based on a decision-tree model and actual landslide occurence: the Akaishi mountains, Japan. Geomorphology, v.109, pp. 108-121.

110. Saklani, P. S. (1979) Folded rocks of northern Tehri Garhwal Himalaya. *Str. Geol. Himalaya*, pp. 1012-1112.

111. Samui, P. (2008) Slope stability analysis: A support vector machine approach. *Environ. Geol*., v.56, pp. 255-267.

112. Sarkar S. (1996) Landslide hazard zonation and slope stability assessment techniques: Applications to Srinagar-Rudraprayag, Garhwal Himalaya. Unpublished Doctoral Dissertation, University of Roorkee, India.

113. Sarkar, S. and Kanungo, D. P. (2004). An integrated approach for landslide susceptibility mapping using remote sensing and GIS. *Photo. Engg. Remote Sens.,* v.70, pp. 617-625.

114. Sarkar, S., Kanungo, D.P. and Mehrotra, G. S. (1995) Landslide hazard zonation : A case study in Garhwal Himalaya, India. *J. Mountain Res. Dev*., U.S.A,.v.15, pp. 301-309,

115. Sarkar, S., Kanungo, D. P., Kumar, P. and Patra, A. K. (2008) GIS based spatial data analysis for landslide susceptibility mapping. *J. Math. Sci*., v.5, pp. 52–62.

116. Sharma, S., Raghuvanshi, T. and Anbalagan, R. (1994) Plane failure analysis of rock slopes. *Int. J. Geotec. Geol. Engg.,* v.13, pp. 105-111.

117. Singh, T. N., Gulati, A., Dontha, L. K. and Bharadwaj V. (2008) Evaluating cut slope failure by numerical analysis—a case study. *Nat Hazards,* v.47, pp. 263–279.

118. Soeters, R. and Van Westen, C. (1996) Slope stability: recognition, analysis and zonation. In: Turner, A. and Shuster, R. (eds), *Landslides: investigation and mitigation,* National Academy Press, Washington, D. C., pp. 129-177.

119. Suzen, M. L. and Doyuran, V. (2004) Data driven bivariate landslide susceptibility assessment using geographical information systems: a method and application to Asarsuyu catchment, Turkey. *Engg. Geol.,* v.71, pp. 303–321.

120. Tien Bui, D., Pradhan, B., Lofman, O. and Revhaug, I. (2012) Landslide susceptibility assessment in Vietnam using support vector machines, decision tree, and Naive Bayes models. *Mathematical Prob. Engg*., v.12, pp. 1-26.

121. Thakur, V. C. and Kumar, S. (1995) Seismotectonic of the 20th October 1991 Uttarkashi Earthquake in Garhwal Himalaya, New Delhi, India. *Memoir, Geol. Soc. India,* v.30, pp. 101-108.

122. Valdiya, K. S. (1980) Geology of Kumaun Lesser Himalaya. Dehradun: Wadia Institute of *Himalayan Geology. Interim. Report*, pp. 291

123. Valdiya, K. S. (1983) Lesser Himalayan Geology, Crucial problems and controversies. *Curr. Sci.,* v.52, pp. 839-857.

124. Valdiya, K. S. (2001) Reactivation of terrane-defining boundary thrusts in central sector of the Himalaya: implications. *Curr. Sci.,* v.81, pp. 1418–1431.

125. Van Westen, C. J., Rengers, N. and Soeters, R. (2003) Use of geomorphological information in indirect landslide susceptibility assessment. *Nat Hazards*, v.30, pp. 399–419.

126. Van Westen, C. J., Van Asch, T. W. J. and Soeters, R. (2006) Landslide hazard and risk zonation— why is still so difficult? *Bulletin. Engg. Geol. Environ*. V.65, pp. 167–184.

127. Vanwalleghem, T., Van Den Eeckhaut, M., Poesen, J., Govers, G. and Deckers, J. (2008) Spatial analysis of factors controlling the presence of closed depressions and gullies under forest: Application of rare event logistic regression. *Geomorphology,* v.95, pp. 504–517.

128. Vargas, L.G., (1990) An overview of the analytic hierarchy process and its applications. *Eur. J. Opr. Res.*, v.48, pp. 2−8.\

129. Varnes, D. J. (1984) Landslide Hazard Zonation: A Review of Principles and Practice, Commission on Landslides of the IAEG, UNESCO, Paris, France, pp. 63.

130. Wan, S. and Lei, T. C. (2009) A knowledge-based decision support system to analyze the debris-flow problems at Chen-Yu-Lan river, Taiwan. Knowledge-Bases Sys., v.22, 580

131. Watershed Management Directorate, Dehradun (2009) Report on Uttarakhand State perspective and strategic planning 2009-2027. file:///D:/For%20review/UTTARAKHAND%20SOIL.pdf

132. Wilson, J. (2011) Digital terrain modelling. *Geomorphology*, v.5, pp. 269–297.
133. Wilson, J. P. and Gallant, J. C. (2000) Terrain Analysis: Principles and Applications. John Wiley & Sons Ltd., New York, USA, pp. 1–27,
134. www.digitalglobe.com/8bandchallenge - (2010) Acquisition of Worldview – 2 data.
135. http://pubs.usgs.gov/of/2006/1052/pdf/ofr-2006-1052.pdf
136. Yalcin, A. (2008) GIS-based landslide susceptibility mapping using analytical hierarchy process and bivariate statistics in Ardesen (Turkey): comparisons of results and confirmations. *Catena* v.72, pp. 1–12.
137. Yeon, Y.-K., Han, J.-G. and Ryu, K.H., (2010) Landslide susceptibility mapping in Injae, Korea, using a decision tree. *Engg. Geol.,* v.116, pp. 274–283.
138. Yesilnacar, E and Topal, T. (2005) Landslide susceptibility mapping: a comparison of logistic regression and neural networks methods in a medium scale study, Hendek region (Turkey). *Engg. Geol.,* v.79(3–4), pp. 251–266.
139. Yilmaz, I. (2009) Landslide susceptibility mapping using frequency ratio, logistic regression, artificial neural networks and their comparison: a case study from Kat landslides (Tokat-Turkey). *Comp. Geosci.*, v.35, pp. 1125–1138.
140. Zadeh, L. A. (1965) Fuzzy sets. *Inf. Control,* v.8, pp. 253–338
141. Zimmerman, M., Bichsel, M. and Kienholz, H. (1986) Mountain hazards mapping in the Khumbu Himal, Nepal, with prototype map, scale 1:50,000. *Mountain Res. Dev.,* v.6, pp. 29–40.
142. Zimmermann, H. J. (1996) Fuzzy set theory and its applications. (Kluwer Academic Publishers) pp. 435